

GE-NE-523-148-1193
DRF 137-0010

BWR CORE SHROUD EVALUATION

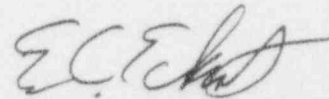
April 1994

Prepared for the
BWR Owners' Group

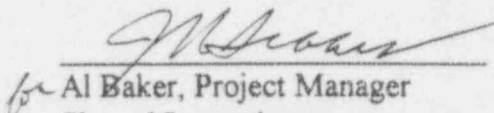
Prepared by:



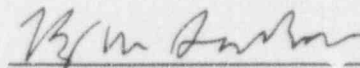
Marcos L. Herrera, Principal Engineer
Structural Mechanics Projects



Gene Eckert, Principal Engineer
Power Uprate Projects

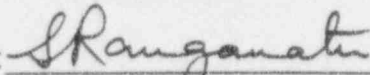


for Al Baker, Project Manager
Shroud Inspections

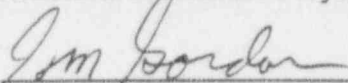


Barry Gordon, Project Manager
Corrosion Technology

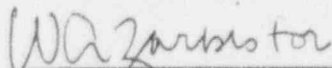
Approved by:



Dr. Sampath Ranganath, Manager
Structural Mechanics Projects



Dr. Gerald Gordon, Chief Technologist
BWR Technology



Steven J. Stark, Projects Manager
BWR Owners' Group Projects

GE Nuclear Energy
San Jose, CA

9404080189 940405
PDR TOPRP EMVGENE
B PDR

**IMPORTANT NOTICE REGARDING
CONTENTS OF THIS REPORT**

Please Read Carefully

The only undertaking of the General Electric Company (GE) respecting information in this document are contained in the Task Authorization (TA) between the participating utilities of the BWR Owners' Group (BWROG) and GE, and nothing contained in this document shall be construed as changing the TA. The use of this information by anyone other than the participating utilities of the BWROG, or for any purpose other than that for which it is intended under the TA is not authorized; and with respect to any unauthorized use, GE makes no representation or warranty, and assumes no liability as to the completeness, accuracy, or usefulness of the information contained in this document, or that its use may not infringe privately owned rights.

BWROG Core Shroud Evaluation

Table of Contents

EXECUTIVE SUMMARY

1.0 INTRODUCTION.....	1
2.0 CORE SHROUD DESIGN INFORMATION.....	6
3.0 SCREENING CRITERIA	10
4.0 MITIGATION OF CORE SHROUD IGSCC	48
5.0 OPERATIONAL SYMPTOMS.....	70
6.0 INSPECTION STRATEGY	80
7.0 SUMMARY	91

APPENDIX A - BASIS FOR THE CRACK GROWTH RATE
APPENDIX B - LIST OF PARTICIPATING UTILITIES

EXECUTIVE SUMMARY

Cracking has been observed in the vicinity of core shroud welds at six boiling water reactors (BWRs). Of the six BWRs where cracking was observed, three are domestic plants. Visual (VT) and ultrasonic (UT) test examinations of the shroud weld areas have shown both circumferential and axial indications, mostly associated with the heat affected zone of the shroud welds. This report contains a discussion of various aspects of the shroud cracking issue and provides the generic tool which utilities may use to address shroud cracking concerns. These issues include: screening criteria, mitigation actions, operational symptoms, and inspection strategy.

The screening criteria were developed to determine the acceptability of any indications. The criteria consist of a graded approach in screening indications. There are three major steps in the screening approach. These are:

- Acceptance Standard
- Visual Screening Criteria
- UT Screening Criteria

The acceptance standard is similar to the ASME Code Section XI IWB-3500 approach to acceptance of indications. Indications which meet this criteria do not require further evaluation. The visual screening criteria are used when an indication does not meet the acceptance standard criterion. The visual screening criteria include several significant conservatisms. These include using the maximum stress at any location in the shroud for all shroud locations, and assuming that all indications are positioned to result in lower allowable flaw sizes. In addition, the screening criteria include the consideration of potential growth of two neighboring indications into one indication, and the interaction of two neighboring indications with respect to linear elastic fracture mechanics (LEFM). If the indications meet the screening criteria, then the indications are considered to be acceptable for at least one additional fuel cycle without further evaluation. If the indications do not meet the screening criteria, guidance is presented for the performance of a more detailed evaluation assuming through-wall indications.

The UT screening criteria can be used when part through-wall characterization of indications has been obtained. With this criteria, the position of the indications in the

shroud (azimuthal) and remaining through-wall ligament can be used to obtain added structural margin.

Information regarding mitigation of core shroud cracking is presented. This includes discussion of hydrogen water chemistry, water conductivity control, and noble metal plasma spray coating. The recent incidences of cracking have demonstrated the advantage of taking early precautions to lessen the potential and extent of intergranular stress corrosion cracking (IGSCC). Water chemistry history, fabrication technique, and material have been identified as being significant contributors to the potential for cracking.

Operational symptoms are discussed to address the potential situation if unexpected significant crack growth occurs during plant operation. The potentially affected plant operational parameters are identified, as well as the modes of reactor operation that are most likely to show these symptoms if the shroud has degraded to the point that significant, through-wall leakage can occur.

Information for use by utilities to assess the shroud condition and level of inspection is also presented. The inspection strategy presented is designed to meet the intent of Service Information Letter (SIL) 572, Rev. 1 while responding to utility specific needs.

1.0 INTRODUCTION

Boiling water reactors (BWRs) are designed with a core shroud. The core shroud is a stepped cylinder which directs flow through the core. The core shroud rests on the shroud support legs (in most cases) and the shroud support plate. The steam separators, shroud head, top guide, and core plate rest on the shroud. The shroud does not support the weight of the fuel (except for a limited number of peripheral fuel bundles). The design configuration of the core shroud differs from plant to plant depending on the fabricator and BWR product line. The shroud is primarily made of Type 304 or Type 304L stainless steel of various carbon levels. The shroud support cylinder and flange is typically made from Alloy 600 material. The residual stresses due to welding, oxidizing core environment and fabrication practices create the potential for intergranular stress corrosion cracking (IGSCC). Figure 1-1 shows a schematic of a typical shroud.

In 1990, cracking was found near the circumferential seam weld at the core beltline area of the shroud in a GE BWR/4 located outside the United States. The crack indications, initially observed at three locations on the inside surface of the shroud, are confined to the heat-affected-zone (HAZ) of the circumferential seam weld.

GE RICSIL No. 054 provided interim recommendations. All owners of GE BWR plants were requested to review fabrication records for the type of material used in their plants' shroud and determine the weld locations. For plants with shrouds made of high carbon stainless steel, GE recommended visual examinations of the accessible areas of the seam welds and HAZs on the inside and outside surfaces of the shroud at the next scheduled outage.

Metallurgical samples removed from the overseas GE BWR/4 shroud revealed that the stress corrosion cracking (SCC) occurred in Type 304 stainless steel material from a relatively low carbon heat (0.045% carbon), and cracking was located in a region of high neutron fluence (8×10^{20} nvt, $E > 1$ MeV). The SCC mechanism appears to be irradiation assisted stress corrosion cracking (IASCC) with propagation promoted by residual stresses and likely helped by corrosion oxide wedging stresses.

As a result of In-Vessel Visual Inspection (IVVI) performed per RICSIL 054, cracking was subsequently observed at Brunswick Unit-1 in July 1993. Cracking was observed on

the inside diameter (ID) surface of the top guide support ring near the H3 weld. The cracking is 360° around the circumference, originating on the ID, in a material with carbon content of about 0.06%. The fluence at this location was estimated at 1.8×10^{20} nvt ($E > 1$ MeV).

A boat sample was taken from the H3 weld inside surface. A second sample containing a portion of a second outer shroud surface crack near the H4 weld was also removed for evaluation. This crack is axial in orientation and appears to initiate in the circumferential weld HAZ. Two additional boat samples were removed to verify UT sizing.

In addition to the initially observed cracking at the boat sample locations, additional crack-like indications (axial and circumferential) at the H1, H2, H4, H5, H6A weld (at core plate) and at the eccentric alignment pin, shroud head bolt lugs and the bottom of the top guide were observed.

As a result of the Brunswick Unit-1 shroud cracking, GENE SIL 572, Rev. 1 was issued which provided recommendations to address the potential for shroud cracking. The recommendations addressed the following areas:

- Plant fabrication and operational history
- Non-destructive examination (NDE) actions
- Destructive analysis
- Structural margin analysis
- Corrective action

As a result of inspections in response to SIL 572, Rev. 1, crack-like indications were observed at Peach Bottom Unit-3 in October 1993. Indications were seen on the shroud barrel inside surface in the plate side HAZ of the H3 weld; and at the H4 weld. The indications at the H3 weld differed from that at Brunswick Unit-1 because indications were not observed in the ring. It is believed that the ring did not crack due to the fact that it is a forged component.

This report provides the methodology and procedure for the evaluation of shroud indications which can be applied on a plant-specific basis. A graded approach is presented which includes comparison of the indications with an acceptance standard, visual screening criteria (assumed through-wall indications), and UT screening criteria (part through-wall indications). In addition, information is provided regarding potential mitigation actions, inspection program strategy, and operational symptoms if significant cracking were to occur.

1.1 Cause of Cracking

The extent and density of cracks associated with the H4 and H5 welds at Brunswick Unit-1 which were observed in September 1993, were found to have some correlation with regions of higher neutron fluence. On the basis of the results of the metallurgical evaluation of the boat sample, the current understanding of the root causes of cracking at the top guide support ring and higher flux H4 weld at the Brunswick plant are as follows:

1. The cracking in the HAZ on the top guide support ring side of the H3 weld was caused by IGSCC in the weld sensitized HAZ of high carbon stainless steel with apparent acceleration from:
 - Neutron fluence
 - Cold worked surface layer (approximately 0.01 inch deep) resulting from machining operations during fabrication
 - Possibly elongated inclusions or stringers because of exposure of surfaces oriented in the short transverse direction
 - Highly oxidizing environment at the weld location
2. The cracking in the H4 weld in the beltline region of the shroud at the outer surface was caused by IGSCC in weld sensitized material, with propagation by an IASCC mechanism, with:
 - Apparent acceleration of crack initiation caused by:
 - ◆ Circumferential weld HAZ
 - ◆ HAZ from apparent "repair weld"

- ♦ Possible localized high weld residual stresses, including the effect of "repair weld"
- Possible effects of localized surface grinding associated with the "repair weld"
 - ♦ Apparent promotion of crack propagation caused by:
 - Moderate sensitization associated with "repair weld"
 - Neutron fluence

On the basis of the pattern of observed cracking, it is believed that many of the conditions leading to the cracking observed in two boat samples are also present at the other observed crack locations in the core shroud. In addition, it is known that temporary welded attachments were used during both shroud fabrication and installation of the shroud in the vessel. Removal of these welded attachments could result in localized areas exhibiting heavy grinding as well as potential weld sensitization, and could lead to some SCC initiation in regions remote from the seam welds.

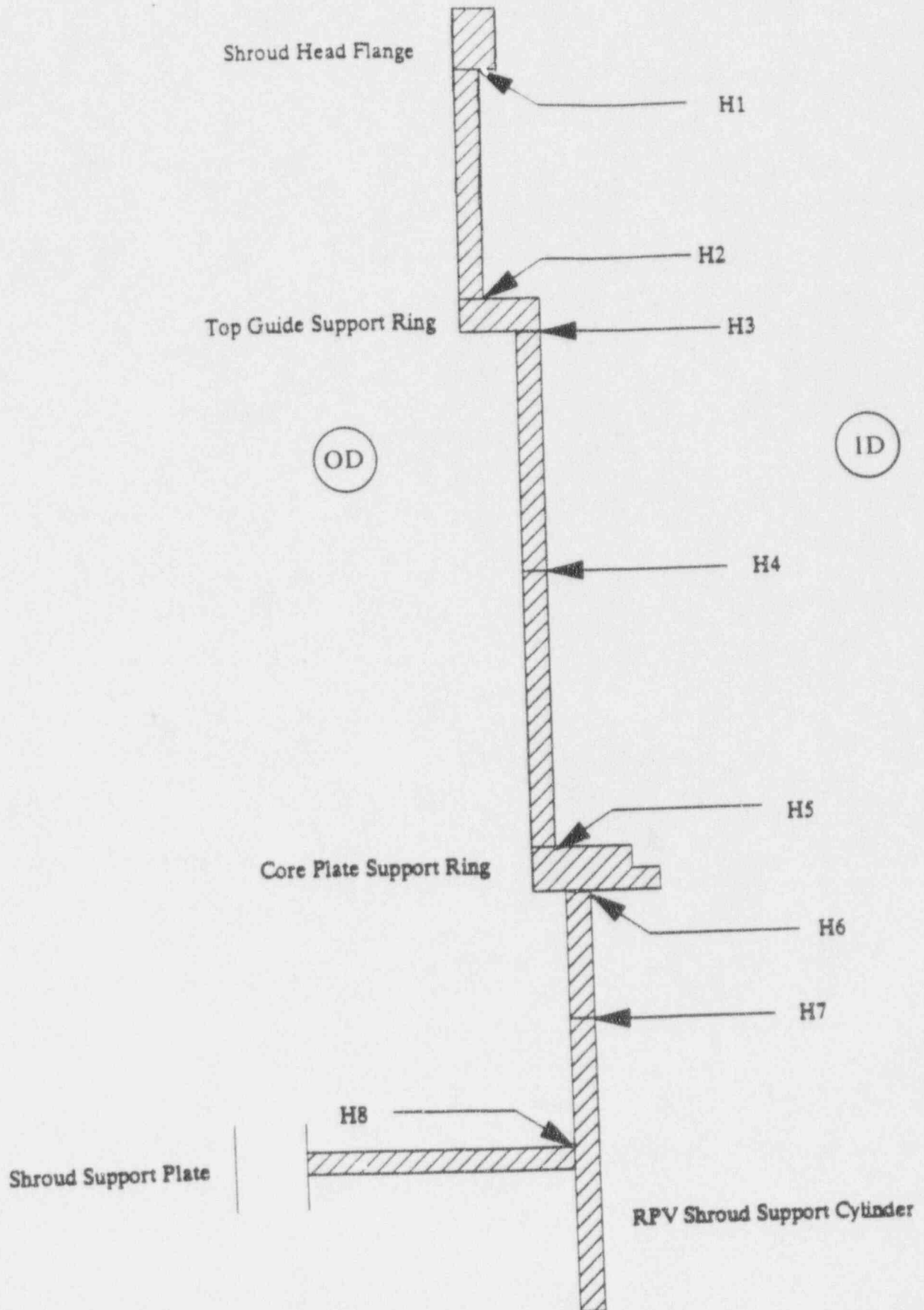


Figure 1-1 Example of Core Shroud (Design is plant specific)

2.0 CORE SHROUD DESIGN INFORMATION

The core shroud is typically composed of three cylindrical shell sections and three rings. The three rings are the shroud head flange, top guide support ring and core plate support ring. The top cylindrical shell connects the shroud head flange to the top guide support ring. The largest cylindrical portion connects the top guide support ring to the core plate support ring. The bottom cylindrical shell connects the core plate support ring to the shroud support cylinder which is typically made from Alloy 600 material. The shroud support legs are located at the bottom edge of the shroud support cylinder (a few plants do not have support legs).

Some of the significant differences between core shroud designs are:

- Diameter of shroud (diameter varies in some plants)
- Thickness of shroud wall (in some cases varying thickness along shroud height)
- Number of horizontal welds in the core beltline
- Number of vertical welds connecting the cylindrical shells
- Material (Type 304 vs. 304L)
- Carbon content
- Fabrication of rings (single piece forging vs. segmented welded plate pieces)
- Tapered lower cylindrical shell vs. straight lower cylindrical shell

Figure 2-1 and 2-2 illustrate two examples of the core shroud design. In Figure 2-1, there are two core beltline horizontal welds (H4 and H5). The thickness of the shroud wall is 1.5". In Figure 2-2, the shroud wall thickness is 2.0" and there is only one horizontal weld in the core beltline (H4). There are other variations to the two designs shown (e.g., BWR/2); however, the information provided in this report is applicable to all designs.

Based on a review of some plant records, in some plants the rings are made from single-piece forged material with low carbon ($\cong 0.035\%$). Carbon content for Type 304 shrouds varies from 0.045% to 0.074%. Hardness ranges vary from Rockwell B hardness of 90 for Type 304 and Rockwell B hardness of 92 for Type 304L.

The horizontal and vertical welds are typically submerged arc automatic welding. Weld filler material is Type 308 or Type 308L. The weld between the lower cylinder and the

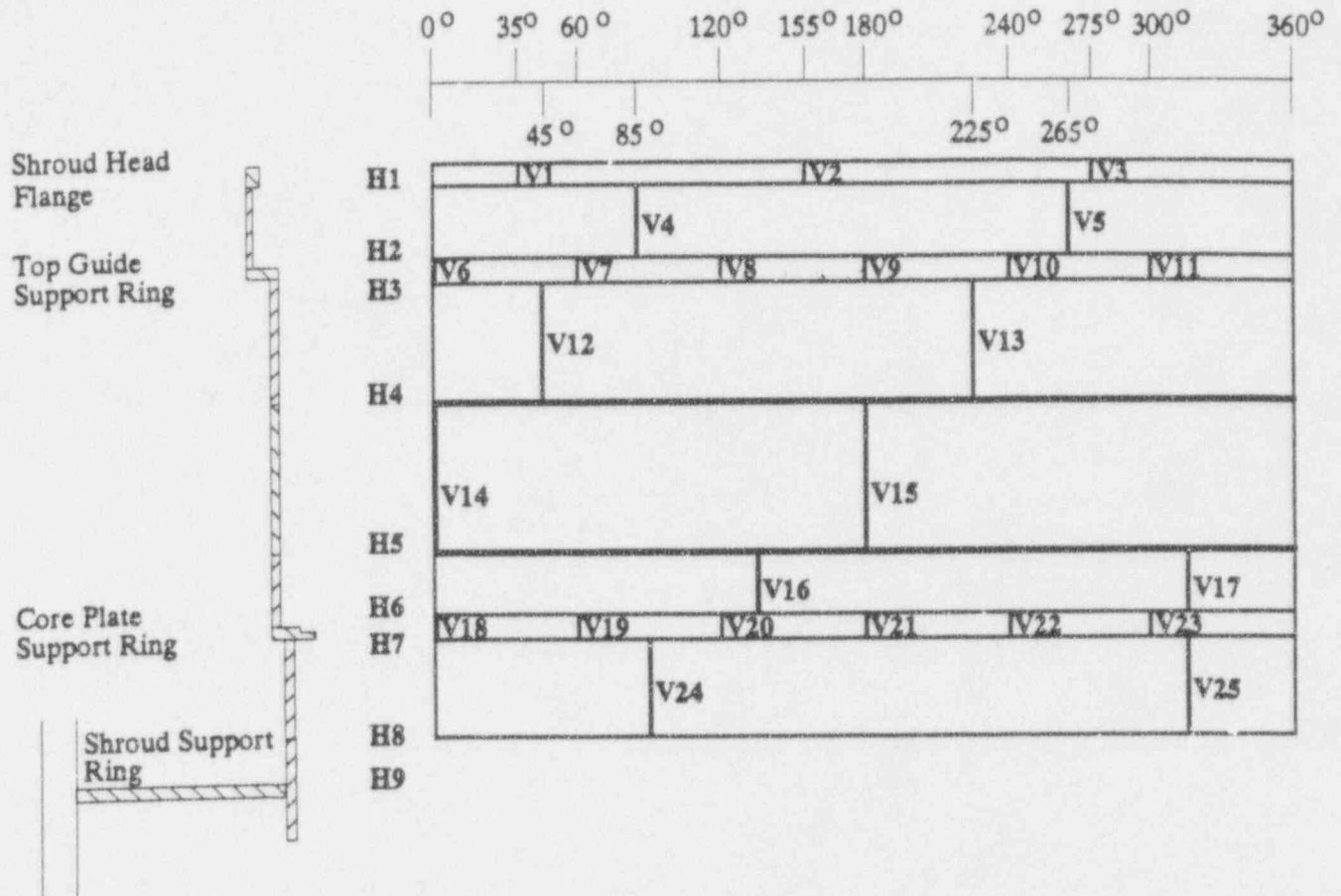
RPV shroud support cylinder is typically Alloy 182. The weld prep is typically single beveled with or without a backing ring.

Typically, weld prep surfaces of the base metal were prepared by machining. The backside of the groove welding was prepared by grinding or gouging, followed by liquid penetrant inspection. Final surfaces of the welds were inspected by liquid penetrant examination.

The austenitic stainless steel material is typically purchased in solution annealed condition. No solution annealing is performed after welding of the various shroud parts.

General practices during assembly and shipment of the core shroud, bracing, jacks, temporary welds, and supports are used to help in meeting design geometric tolerances. Sometimes, there is no recorded documentation of these practices. However, it is likely that they did occur. These actions can result in local effects on material behavior and stress. For example, temporary welding results in local areas of high residual stress, and grinding results in local areas of cold working. If these local effects were to contribute to cracking, it is likely that the cracking would be of lesser concern than cracking at horizontal seam welds.

The design considerations discussed in this section are included in the development of the screening criteria. For example, the shroud thicknesses and diameter are considered in the determination of the stress, and a bounding crack growth rate is used which applies to all materials present in any of the shroud designs.



NOT TO SCALE

Figure 2-1 - Sketch Showing Typical Welds in Core Shroud (Example)

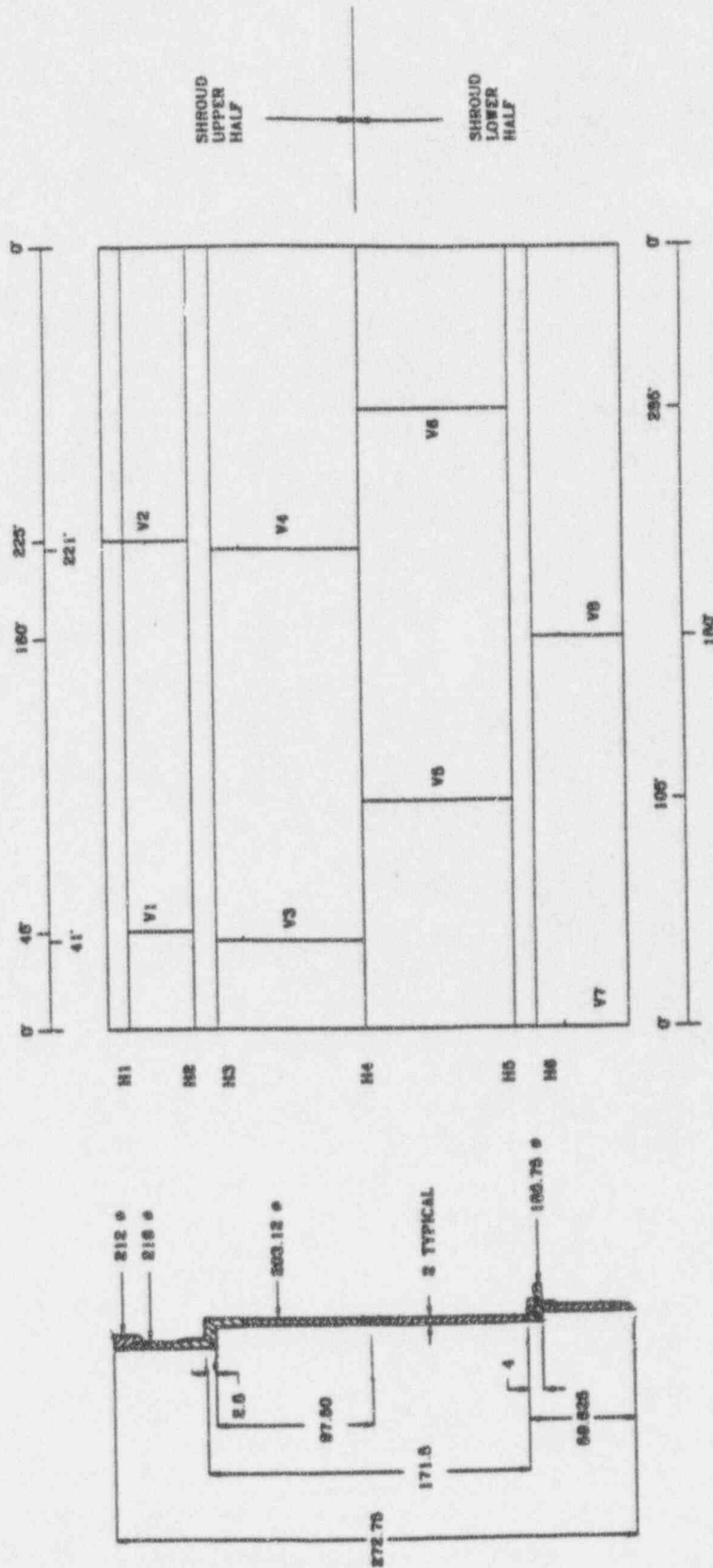


Figure 2-2 Schematic Showing Typical Welds in Core Shroud (Example 2)

3.0 SCREENING CRITERIA

This section provides the methodology and procedure which can be used to evaluate indications found by Non-Destructive Examination (NDE, e.g., ultrasonic testing (UT) or visual techniques (VT)). The screening criteria is presented as a graded procedure. The criteria is comprised of three major steps. These steps (in the order of application) are:

- Acceptance Standard
- Visual Screening Criteria
- UT Screening Criteria

The first step is to compare any indications with the acceptance standard. If the indications meet the acceptance standard, further evaluation of the indications is not required. Note that this approach is similar to that in ASME Code Section XI Subarticle IWB-3500.

The second step, performed if the indication does not meet the acceptance standard, is to compare the indication with the visual screening criteria. These criteria include several conservatisms and are intended to be a first-cut evaluation of the indications. The major assumption in this step is that all indications seen by IVVI are assumed to be through-wall. If UT is performed, this simpler method can be first applied (by assuming all flaws are through-wall) for rapid disposition of the indications.

The third step is to use UT through-wall characterization and the specific azimuthal location of the indications in the evaluation for structural acceptability. The evaluation is similar to that used for the visual screening criteria except for the through-wall and location aspects of the flaw mentioned above.

3.1 Acceptance Standard

This first step in the evaluation is to compare the observed indications to the acceptance standard. This approach is similar to that stated in ASME Code Section XI Subarticle IWB-3500 for acceptability of flaws without further evaluation. If the indications meet the acceptance standard, then further evaluation of the indications is not required.

3.1.1 Determination of Effective Flaw Length for Acceptance Standard

The ASME Code Section XI Subarticle IWA-3300 (1989 edition) proximity rules must be applied to the indications prior to comparing with the acceptance standard. Section IWA-3300 specifies how flaws are to be combined depending on the location and orientation of the indications found by volumetric examination. Briefly, the flaws are combined lengthwise if the distance between the crack tips is less than 2 times the depth of the deepest indication and the crack planes lie within 0.5 inches (perpendicular distance between the crack planes). However, for this acceptance standard, the Section XI proximity criteria are modified by increasing the 0.5 inches to 2 times the shroud wall thickness. Thus, two indications are combined lengthwise if,

$$S \leq 2B$$

where S = distance between indications

B = depth of deepest indication if depth of flaw known (for UT)

B = shroud thickness (for IVVI)

If UT data are available, the application of the proximity criteria should use the ASME Code Section IWA-3300 method based on the depth of the deepest indication. If IVVI information is the only information available, then the depth of the deepest indication should be taken as the thickness of the shroud. It can be seen that UT data may result in fewer flaw combinations due to the smaller required ligament between flaw tips.

3.1.2 Basis for Acceptance Standard

The acceptance standard was arrived at by evaluating information from several shroud analyses. In addition, an allowable length was desired which could also be related to the ASME Code margins. Based on shroud evaluations which represent a wide range of shroud designs and after application of a safety factor of 2.8 on stress, an acceptance standard was developed and is shown in the following table.

Acceptance Standard

Circumferential		Axial
<u>LEFM</u>	<u>Limit Load</u>	<u>LEFM and Limit Load</u>
15"	15" in any 90° quadrant	15"

Any flaw which meets the acceptance standard shown above is acceptable without further evaluation. It should be noted that the value of 15" is approximately one-tenth the length of a shroud quadrant.

3.2 Visual Screening Criteria

In the visual screening criteria, all indications are considered to be through-wall (consideration of UT sizing is discussed in Section 3.3). This screening criteria for evaluation of the shroud indications is based on the ASME Code Section XI procedures. This is considered conservative since most core shrouds were not originally designed using the ASME Code nor is it a primary pressure boundary component. In fact, the original design of the shroud included consideration of fabrication requirements. For example, the shroud thickness was made relatively thick (≥ 1.5 ") to avoid deformation during fabrication and shipping.

The limiting parameter is the allowable through-wall flaw size, which already includes the ASME Code Section XI safety factors. If all of the detected indications are assumed to be through-wall, then the longest flaws, or combination of flaws, would have the limiting margin against the allowable through-wall flaw size. In reality, the indications are likely not through-wall (which can be confirmed by UT), and therefore the criteria and methods presented in this report are conservative.

The result of this procedure will be the determination of the effective flaw lengths which will be compared against the allowable flaw size and selection of indications for more detailed evaluation. The determination of effective flaw length is based on ASME Code, Section XI, Subarticle IWA-3300 (1989 Edition) UT proximity criteria. These criteria provide the basis for the combination of neighboring indications depending on various geometric dimensions. Crack growth over a subsequent cycle is factored into the criteria.

The proximity rules described here also conservatively assume that there is interaction between two perpendicular flaws. It is assumed that circumferential and axial indications could increase the effective flaw length depending on the unflawed distance between them. This effective circumferential flaw length must be compared against the allowable circumferential flaw length. The axial flaw would be compared against the allowable axial flaw length.

Flaws are considered in the same plane if the perpendicular distance between the planes is within two times the shroud thickness or less ($2T$, where T =shroud thickness). Any flaws which lie at an angle to the horizontal plane should be separated into a circumferential and axial component. These components can then be used separately in the determination of effective flaw lengths.

The selection of indications for further investigation can be performed by evaluating the resulting effective flaw lengths. **Indications with effective flaw lengths greater than the allowable flaw sizes would require more detailed analysis or further characterization by NDE** (which is used as input to the UT screening criteria, Section 3.3). The procedure described here is conservative since all of the indications are assumed through-wall and are being compared against the allowable through-wall flaw size. More detailed evaluation of the indications can include using the location specific stress. Details of the more specific evaluation are described in Section 3.2.6.

This section describes the following steps:

- Determination of effective flaw length including proximity criteria for adjacent flaws.
- Determination of allowable flaw sizes based on both linear elastic fracture mechanics (LEFM) and limit load criteria.
- Visual screening criteria.

The procedure uses the limiting stresses for all the shroud welds. Therefore, the screening criteria developed here cover all shroud weld indications. A list of conservatisms used in this evaluation is summarized in Table 3-1.

Table 3-1 - Conservatisms Included in Visual Screening Criteria

1. All surface indications were assumed to be through-wall for analysis.
2. The visual screening criteria limit one-fourth of allowable circumferential flaw to any arbitrary 90° sector.
3. All indications are assumed to be grouped together for the limit load calculation and no credit is taken for the spacing between indications.
4. ASME Code Section XI primary pressure boundary safety margins were applied even though the shroud is not a primary pressure boundary.
5. ASME Code, Section XI proximity rules were applied.
6. An additional proximity rule which accounts for fracture mechanics interaction between adjacent flaws was used.
7. The highest stress computed for any single location was used for all locations.
8. Both LEFM and limit load analysis were applied, even though LEFM underestimates allowable flaw size for austenitic materials and is not required per ASME Code Section XI procedures.
9. The bounding crack growth estimated for the next fuel cycle was included in flaw lengths used for evaluation (See Appendix A).
10. A proximity rule to account for perpendicular flaws was applied, although not required by Section XI.

3.2.1 Determination of the Effective Flaw Length

The effective flaw lengths are based on ASME Code, Section XI proximity criteria as presented in Subarticle IWA-3300. The procedure addresses both circumferential and axial flaws. Indications are considered to be in the same plane if the perpendicular distance between the planes is less than two times the shroud thickness (2T). All flaws are considered to be through-wall. Therefore, indications on the inside and outside surface should be treated as if they are on the same surface. When two indications are close to each other, rules are established to combine them based on proximity. These rules are described here.

Proximity Rules

The flaw combination methodology used here is similar to the ASME Code, Section XI proximity rules concerning neighboring indications. Under the rules, if two surface indications are in the same plane (perpendicular distance between flaw planes <two times the shroud thickness, 2T) and are within two times the depth of the deepest indication, then the two indications must be considered as one indication.

In Figure 3-1, two adjacent flaws L1 and L2 are separated by a ligament S. Crack growth would cause the tips to be closer. Assuming a conservative crack growth rate (see Appendix A) of $g=5 \times 10^{-5}$ in/hr, crack extension at each tip is the crack growth rate multiplied by the number of hot operating hours above 200°F for the next fuel cycle. The crack growth at each tip is thus, gt . Therefore, combining the crack growth and proximity criteria, the flaws are assumed to be close enough to be considered as one continuous flaw if the ligament is less than $(2gt + 2T)$. If the ligament is less than $(2gt + 2T)$, the effective length is $(L1+L2+S+2gt)$. Note that the addition of $2gt$ is to include crack growth at the other (non-adjacent) end of each flaw (See Figure 3-2).

If the ligament is greater than $(2gt + 2T)$, then the effective flaw length is determined by adding the projected tip growth to each end of the flaw.

$$L1_{\text{eff}} = L1 + 2gt$$

$$L2_{\text{eff}} = L2 + 2gt$$

A similar approach is used to combine flaws when a circumferential flaw is close to an axial flaw (See Figure 3-3). If the ligament between the flaws is less than $(2T + gt)$, then the effective flaw length for the circumferential flaw is $L_{eff} = L1 + S + gt$ (the bounding ligament for these cases). If the ligament is greater than $(2T + gt)$, then the flaws are treated separately.

After the circumferential and axial flaws have been combined per the above criteria, a map of the effective flaws in the shroud can be made, and the effective flaw length can be used for subsequent fracture mechanics analysis.

To demonstrate the proximity criteria, three examples are shown in Table 3-2 and described below.

Table 3-2 Flaw Combinations Considered in Proximity Criteria

Case	Circumferential Flaw	Axial Flaw
A	Yes	No
B	Yes	Yes
C	No	Yes

Case A: Circumferential Flaw - No Axial Flaw

This case applies when two circumferential indications are considered. Figure 3-2a shows this condition. If the distance between the two surface flaw tips is less than $(2T + 2gt)$, the indications must be combined such that the effective length is (see Figure 3-2b):

$$L_{eff} = L1 + S + L2 + 2gt$$

where: L1 = length of first circumferential indication
 L2 = length of second circumferential indication
 S = distance between two indications

If the distance between the two tips is greater than $(2\Gamma + 2gt)$, the effective flaw lengths are (See Figure 3-2c):

$$\begin{aligned} L1_{\text{eff}} &= L1 + 2gt \\ L2_{\text{eff}} &= L2 + 2gt \end{aligned}$$

Case B: Circumferential Flaw - Axial Flaw

This case applies when both a circumferential and an axial flaw are being considered. Figure 3-3a demonstrates this condition. For this case, only growth of the circumferential flaw is considered. If the distance between the circumferential indication tip and the axial indication is less than $(2T + gt)$, then the effective circumferential flaw length is (see Figure 3-3b):

$$L_{\text{eff}} = L1 + S + gt$$

where: $L1$ = length of circumferential indication
 S = distance between the circumferential tip and axial flaw.

and the effective axial length is (Figure 3-3b):

$$L_{\text{eff}} = L2 + 2gt$$

where: $L2$ = length of axial indication

If the distance between the circumferential indication tip to the axial indication is greater than $(2T + gt)$, then the flaws are not combined (see Figure 3-3c) and the effective lengths are:

$$\begin{aligned} L1_{\text{eff}} &= L1 + 2gt \quad (\text{for circumferential flaw}) \\ L2_{\text{eff}} &= L2 + 2gt \quad (\text{for axial flaw}) \end{aligned}$$

Case C: No Circumferential Flaw - Axial Flaw

This case applies to when only axial flaws are being considered. The effective length is determined in a manner similar to that used for case A for circumferential flaws.

Application of Effective Flaw Length Criteria

The application of the effective length criteria is applied to two adjacent indications at a time. Figure 3-4 is a schematic which illustrates the process. For example, using the 0° azimuth as the starting location for a circumferential weld or plane, the general procedure would be as follows:

- Moving in the positive azimuthal direction, the first indication encountered is indication 1.
- The next indication is indication 2.
- Apply proximity rules to the pair of indications (indications 1 and 2). Combine the flaws if necessary (L_1+L_2+S). If the flaw is combined, the flaw becomes indication 2.
- Continue along positive azimuthal direction until the next indication is encountered. This becomes indication 3.
- Apply proximity rules to new indications 2 and 3.
- Continue proximity rule evaluation until all indications along the subject weld or plane have been considered.

3.2.2 Structural Analysis

The preceding section of this report described the determination of effective flaw lengths from the NDE results for use in the visual screening criteria. These effective flaw lengths have to be compared to the allowable flaw lengths to assess the structural integrity of the shroud. This section describes the details of the structural analysis to determine the allowable flaw lengths. The structural analysis consists of two steps: the determination of axial and circumferential stress magnitudes in the shroud, and the calculation of the allowable flaw lengths. Both the fracture mechanics and limit load methods are used in the calculation of allowable flaw lengths.

Applied Loads and Calculated Stresses

The applied loads on the shroud consist of internal differential pressure, weight and seismic. All other stresses are negligible in comparison. The seismic loads consist of a horizontal shear force at the top of the shroud and an overturning bending moment. The shear force produces a shear stress of insignificant magnitude, and is not considered. The bending moment stress at a shroud cross-section varies as a function of its vertical distance from the top of the shroud. Because of the inherent ductility of the material, residual stresses and other secondary stresses do not affect structural margin. Thus, they need not be considered in the analysis.

The magnitudes of the applied loads are obtained from the currently applicable seismic stress analysis and system information reports. The nominal shroud radius and thickness, R and T , are used to calculate the stresses from the applied loads. The stresses are essentially based on the strength of materials formulas. Since the bending stress due to seismic shear force varies with the elevation of a location, two conservative values of this stress can be calculated: one applicable to shroud sections above the core plate and the other for sections below the core plate. Figures 2-1 and 2-2 show the weld designation and relative locations for two of the shroud designs.

The seismic stress magnitudes for both the upset and faulted conditions must be calculated using the applied loads. The appropriate pressure differences for the normal and faulted conditions must also be obtained. The normal and faulted condition pressure drop across the shroud head and upper shroud, and core plate support ring and lower shroud are

required to obtain the appropriate stress due to pressure. Note that for below the core plate, the effective pressure difference for circumferential indications (axial stress) is:

$$\Delta P_{\text{below core plate}} = \Delta P_{\text{sh}} + \Delta P_{\text{cp}}$$

where: ΔP_{sh} = Pressure difference across shroud head + upper shroud

ΔP_{cp} = Pressure difference across core plate support ring and lower shroud

The structural analysis for the indications uses two methods: linear elastic fracture mechanics (LEFM) and limit load analysis. Both the limit load and the LEFM methods are used in determining the allowable flaw sizes in the shroud. Since the limit load is concerned with the gross failure of the section, the allowable flaw length based on this approach may be used for comparison with the sum of the lengths of all the flaws at a cross-section. On the other hand, the LEFM approach considers the flaw tip fracture toughness and thus, the allowable flaw length based on this approach may be used for comparison with the largest effective flaw length at a cross-section. The technical approach for the two methods is described below.

Fracture Mechanics Analysis

The shroud material (austenitic stainless steel) is inherently ductile and it can be argued that the structural integrity analysis can be performed entirely on the basis of limit load. In fact, J-R curve measurements (Figure 3-5) made on a core shroud sample taken from an overseas plant having a fluence of 8×10^{20} n/cm² showed stable crack extension and ductile failure when tested. The ASME Code recognizes this fact in using only limit load techniques in Section XI, Subsubarticle IWB-3640 analysis. Nevertheless, a conservative fracture mechanics evaluation can be performed using an equivalent K_{Jc} corresponding to the material J_{Ic} . The K_{Jc} for the overseas plant shroud was approximately 150 ksi $\sqrt{\text{in}}$. Use of this equivalence is considered conservative since the J-R curves show J_{max} values well above the J_{Ic} , confirming that there is load capability well beyond crack initiation (See Figure 3-5).

The allowable K_I is obtained by applying the appropriate safety factor for normal and upset or faulted conditions to the K_{Jc} obtained from the test specimens described above. For the analysis presented here, the LEFM analysis is confined to the welds above the core

plate support ring (not including the core support plate ring welds). The fluence corresponding to welds at and below the core plate elevation is an order of magnitude lower and the associated fracture toughness is comparable to that of the unirradiated material. For those locations, only limit load analysis is used.

An additional consideration that applies only to the fracture mechanics analysis is the question, "When is a flaw independent of an adjacent flaw?". The ASME Code proximity rule described in Section 3.2.1 considers how flaws can link up and become a single flaw as a result of proximity. However, even when two flaws are separated by a ligament that exceeds $(2T + 2gt)$, they may not be considered totally independent of each other. That is, the flaw tip stress intensity factor may be affected by the presence of the adjacent flaw. This can be accounted for by using the finite width correction factor for a flaw in a finite plate. For a through-wall flaw in an "infinite" plate, the stress intensity factor is:

$$K = \sigma\sqrt{\pi a}$$

For a finite plate, the K value is higher as determined by the finite width correction factor, F . In this screening evaluation it is assumed that the plate is "infinite" if the correction factor F is less than 1.1. As seen in Figure 3-6, if the width of the plate exceeds $2.5L$ (or a/b less than 0.4), then there would be little interaction (less than 10% since $F \approx 1.1$) due to plate end edge effects. If this same condition is applied to two neighboring flaws, then there will be no interaction between the two indications if the tips are at least $0.75(L1+L2)$ apart. If the distance between indications is greater than $0.75(L1+L2)$, then they may be considered as two separate flaws. If however, they are closer, for the purpose of fracture analysis, the equivalent flaw length is the sum of the two individual flaws.

Limit Load Analysis

A through-wall circumferential flaw was assumed in this calculation. Limit load calculations were conducted using the approach outlined in Subsubarticle IWB-3640 and Appendix C of Section XI of the ASME Code. The flow stress was taken as $3S_m$. The S_m values for the shroud material are 16.9 ksi and 14.4 ksi for Type 304 and Type 304L, respectively, at the normal operating temperature of 550°F.

Safety factors similar to that used in the ASME Code (for normal and upset and emergency and faulted conditions) are used in the analysis. The highest seismic stress is used for the limit load calculations. Similarly, the highest axial pressure stress corresponding to the lower shroud is used. Thus, the analytical results are applicable for all welds since limiting values are used.

3.2.3 Allowable Through-Wall Flaws

Allowable through-wall flaw sizes are determined using both fracture mechanics and limit load techniques for both circumferential and axial flaws. It should be emphasized that the allowable through-wall flaws are based on many conservative assumptions (e.g., using the limiting stress for all welds) and are intended for use only in the visual screening criteria. More detailed analysis can be performed to justify larger flaws (both through-wall or part through when measured flaw depths are available). However, since the intent of the screening criteria is to determine when additional evaluation or NDE characterization is needed, a conservative bounding approach is utilized.

Allowable Through-Wall Circumferential Flaw Size

Both the LEFM and limit load methods are used to evaluate the allowable through-wall flaws. Above the core plate, the limiting location for through-wall cracking is the lowest weld above the core plate (e.g., H5 for the shroud design in Figure 2-1, and H4 for the shroud design in Figure 2-2). The weld between the lower shroud cylinder and core support cylinder involves Alloy 600, which has higher S_m values and therefore higher limit load capability, and is bounded by the allowable flaw size based on calculations assuming stainless steel.

Fracture Mechanics Analysis

The total axial pressure and seismic stress corresponding to the upset condition and faulted conditions are calculated based on simple strength of materials solutions. Using the ASME Code safety factors for fracture analysis, it must be determined which condition governs, faulted or normal and upset conditions. This is determined by multiplying the total normal plus upset stress by 2.8 and the faulted stress by 1.4. The condition with the highest resulting stress is considered the limiting condition.

To determine the allowable flaw size based on LEFM methods, the conservatively estimated irradiated material fracture toughness K_{Ic} value of 150 ksi $\sqrt{\text{in}}$ was used. Applying a safety factor of 2.8 for the upset condition or 1.4 for faulted conditions, the allowable K_I of 53.5 ksi $\sqrt{\text{in}}$ for normal and upset and 107 ksi $\sqrt{\text{in}}$ for faulted is obtained. The allowable flaw size is calculated using the following equation:

$$K_I = G_m * \sigma * \sqrt{(\pi a)}$$

where G_m is a curvature correction factor as defined in Figure 3-7 (Reference 3-1), σ is the axial stress, and 'a' is the half flaw length. The allowable through-wall circumferential flaw length (2a) is calculated by determining the crack length where the applied stress intensity factor equals the fracture toughness limit.

Limit Load Analysis

The stresses for the limit load analysis consist of an axial force stress and a bending moment stress. These stresses are calculated for both the normal and upset and faulted conditions. The allowable flaw length is then calculated using the approach in Subsubarticle IWB-3640 and Appendix C of Section XI of the ASME Code.

Allowable Through-Wall Axial Flaw Size

Fracture Mechanics Analysis

The allowable axial flaw size is governed entirely by the pressure hoop stress. Similar to the circumferential flaw case, the allowable axial flaw size is determined assuming a through-wall flaw. For a through-wall flaw of length 2a in the shroud, the applied stress intensity factor is given by:

$$K = M * \sigma_h * \sqrt{(\pi a)}$$

where M is the curvature correction factor as defined in Figure 3-8 (Reference 3-1). M is given by:

$$M = G_m + G_b$$

In the above expression, the allowable flaw length $2a$ can be determined by equating the calculated K to the fracture toughness divided by the safety factor of 3 or 1.5 depending on which condition is limiting, normal and upset or faulted. Comparison of the applied stress intensity factor with the allowable fracture toughness defines the allowable through-wall flaw length, $2a$.

Limit Load

An alternate approach to determining the allowable flaw size is to use limit load techniques. The allowable flaw length is given by the equation:

$$\sigma_h = \sigma_f / (M_1 * SF)$$

where M_1 is a curvature correction factor (which is a function of the flaw length (Reference 3-2)), $\sigma_f = 3S_m$ is the flow stress, SF is the safety factor of 3.0 for upset conditions or 1.5 for faulted, and σ_h = the hoop stress corresponding to the upset or faulted ΔP . The allowable flaw length is determined satisfying the equation shown above. The allowable flaw size is the limiting length determined from either the limit load or LEFM calculation.

3.2.4 Visual Screening Criteria

The determination of the allowable through-wall flaws has been described in Section 3.2.3. The objective was to use the allowable flaw size as the basis for the screening criteria. Since the screening rules represent the first step in the evaluation, they are by definition conservative. If the criteria are exceeded, the option of doing further detailed evaluation or performing additional NDE remains.

A conservative approach in developing the screening rule is to include both the LEFM and limit load analysis.

For circumferential flaws the LEFM based limit for a single flaw is not sufficient since there could be several flaws (each less than the allowable) in a circumferential plane that cumulatively add up to greater than the allowable circumferential flaw size based on limit load analysis. Thus, the cumulative flaw length should be less than that determined using

limit load analysis. While this fully assures the ASME Code margins, a significant conservatism has been included in the screening. **That is: the cumulative flaw length cannot be more than one-fourth of the limit load allowable flaw length in any 90° sector of the shroud.** This is a conservative restriction that assures that long continuous flaws are not admissible without additional inspection or analysis. With the provision that the cumulative flaw length cannot exceed one-fourth of the limit load allowable flaw length in any 90° sector of the shroud, this criterion may become more limiting than the fracture mechanics limitation. The approach used here for the one-fourth of the limit load allowable flaw length limitation for circumferential flaws is to assume a template with a moving window equal to the 90° sector. The cumulative length of flaws that appear in the window should be less than one-fourth of the limit load allowable flaw length. This is shown graphically in Figure 3-9. A similar restriction based on limit loads is not needed for axial flaws since they are associated only with circumferential welds and are unlikely to be aligned in the same plane.

The additional requirement of one-fourth of the limit load allowable flaw length can be revised if actual inspection demonstrates that there is significant uncracked ligament around the entire circumference of the shroud assuring the absence of long indications. This assures that all the indications are not concentrated in one part of the shroud section. If observed flaws are not long and continuous, a technical justification can be made to demonstrate structural integrity when the one-fourth limit is exceeded.

It should be noted that when considering LEFM based evaluations, the crack interaction criteria described in Section 3.2 must be applied in comparing against the allowable lengths. For example, for adjacent flaws where the spacing S is less than $0.75(L_1 + L_2)$, the length $L = L_1 + L_2$ is used for comparison with the LEFM based allowable flaw length.

3.2.5 Summary of Visual Screening Criteria

The visual screening criteria is schematically shown in Figure 3-10. The first step is to map the flaw indications observed by NDE. Next the proximity rules are applied to the flaw map to develop effective flaw lengths. The results of the effective flaw lengths are also mapped.

For axial flaws aligned in a vertical plane, two neighboring flaws must be summed if $S < 0.75(L_1 + L_2)$. If the longest resulting combined flaw is less than the limiting allowable axial through-wall flaw (LEFM), then the screening limit is met for axial flaws. Similarly, the effective flaw length for axial flaws must be compared against the limit load allowable for through-wall axial flaws.

For circumferential flaws, all flaws are summed in any 90° sector using a template. The total flaw length in the 90° window must be less than one-fourth of the limit load allowable through-wall flaw to meet the screening criteria. The next step is the LEFM based comparison using the interaction criteria. If $S < 0.75(L_1 + L_2)$, then the length $L = L_1 + L_2$ should be compared with the LEFM limit for circumferential flaws.

3.2.6 Detailed Evaluation of Indications

The visual screening criteria summarized in Section 3.2 is based on several conservative assumptions as noted in Table 3-1. If indications are found which exceed the visual screening criteria, more detailed analysis may be performed to evaluate the indication acceptability. Following are some of the modifications to the visual screening criteria which provide a more detailed evaluation for specific indication locations:

<u>Visual Screening Criteria</u>		<u>Detailed Analysis</u>
Use limiting stress for all locations.	⇒	Use location specific stress.
Assume all indications located to provide limiting results. Includes 90° limit applied to allowable circumferential flaw.	⇒	Knowing actual location of indications, reduce 90° limit if remaining ligament evenly distributed around circumference.
Limit load performed assuming flaws located in limiting configuration.	⇒	Perform limit load evaluation for known indication locations.
Use bounding crack growth rate.	⇒	Determine crack growth rate based on SCC predictive modeling.
Use LEFM and limit load analysis.	⇒	Perform elastic-plastic fracture mechanics analysis.
Assume through-wall indications.	⇒	Perform screening criteria with actual UT data to obtain contribution of remaining through-wall ligament. (See Section 3.3).

3.3 UT Screening Criteria

This section provides the methodology and procedure for the evaluation of indications based on UT information. In this procedure, the through-wall depth and location of the indication(s) (relative to the shroud) must be known. The visual screening criteria described in Section 3.2 uses the assumption that all indications are through-wall. This is a very conservative assumption and the use of flaw depth information provides a more realistic evaluation of the shroud structural margin.

Figure 3-11 can be used to demonstrate the difference in the flaw geometry assumed for the visual and UT screening criteria limit load analysis. The first figure shows an example flaw map of indications found during a UT inspection. The second figure shows how the flaw is modeled in the visual screening criteria. As can be seen, the flaw used to determine the allowable flaw size is assumed to be a single flaw located at the limiting location in terms of seismic overturning moment. The third figure shows how the flaw is treated in the UT screening criteria. The indications, once combined using the proximity criteria to determine effective flaw depth, are evaluated considering the actual location and flaw depth. Typically, significant added margin can be gained by considering the remaining ligament and actual location of the indication.

The methodology and procedure for the UT screening criteria is the same as that for the visual screening criteria described in Section 3.2 except for the following two major exceptions:

1. Flaw depth information regarding indications are used. Credit taken for the remaining ligament (after accounting for crack growth over one cycle).
2. Shroud azimuthal location of indications considered.

The result of this procedure is the determination of effective flaw lengths which, along with the flaw location and flaw depth, will be used to compare against the allowable flaw size. The determination of effective flaw length is based on the ASME Code, Section XI, Subarticle IWA-3300 (1989 Edition) proximity criteria. These criteria provide the basis for the combination of neighboring indications depending on various geometric dimensions. Crack growth over a subsequent cycle is factored into the criteria.

Flaws are considered in the same plane if the perpendicular distance between the planes is within two times the shroud thickness or less. Any flaws which lie at an angle to the horizontal plane should be separated into a circumferential and axial component. These components can then be used separately in the determination of effective flaw lengths.

Indications which do not satisfy the allowable flaw sizes based on the UT screening criteria would require further detailed analysis or repair of the shroud may be needed. More detailed evaluation of the indications can include using the location specific stress.

This section describes the following steps:

- Determination of effective flaw length including proximity criteria for adjacent flaws.
- Determination of allowable flaw length based on linear elastic fracture mechanics (LEFM) and determination of safety margin using limit load analysis.
- UT screening criteria

The UT screening criteria is similar to that used for the visual screening criteria. The conservatisms used in the visual screening criteria, except for the first three given in Table 3-1, are used in the UT screening criteria.

3.3.1 Determination of the Effective Flaw Length

The effective flaw lengths are based on ASME Code, Section XI proximity criteria as presented in Subarticle IWA-3300. Note that in the UT screening criteria, the position of the indication in the shroud (both through-wall depth and azimuthal location) is needed.

Similar to the visual screening criteria, rules are included to combine flaws based on proximity.

Proximity Rules

The flaw combination methodology is similar to that described in Section 3.2.1 for the visual screening criteria. The difference between the UT and visual criteria is that credit is taken for the part-through-wall flaw depth.

In Figure 3-1, two adjacent flaws, L1 and L2, are separated by a ligament S. Crack growth would cause the tips to be closer. Assuming a conservative crack growth rate of 5×10^{-5} in/hr (See Appendix A), crack extension at each tip is the crack growth rate multiplied by the number of hot operating hours above 200°F for the next cycle. The crack growth at each tip is thus, gt . Likewise, the flaw depth would become $a_1 = a_1 + gt$ and $a_2 = a_2 + gt$. Therefore, combining the crack growth and proximity criteria, the flaws are assumed to be close enough to be considered as one continuous flaw if the ligament is less than $(2gt + 2a')$, (where a' =deepest of the two indications considered). If the ligament is less than $(2gt + 2a')$, the effective length is $(L1+L2+S+2gt)$. Note that the addition of $2gt$ is to include crack growth at the other (non-adjacent) end of each flaw. Also, the crack depth of the combined flaw becomes $a_{eff} = a' + gt$ (a' =depth of deepest indication).

If the ligament is greater than $(2gt + 2a')$, then the effective flaw length is determined by adding the projected tip growth to each end of the flaw.

$$L1_{eff} = L1 + 2gt$$

$$L2_{eff} = L2 + 2gt$$

The crack depth is also modified to:

$$a1_{eff} = a_1 + gt$$

$$a2_{eff} = a_2 + gt$$

A similar approach is used to combine flaws when a circumferential flaw is close enough to an axial flaw (See Figure 3-3). If the ligament between the flaws is less than $(2a' + gt)$, then the effective flaw length for the circumferential flaw is $L_{eff} = L1 + S + gt$, and the crack depth is equal to the depth of the circumferential or axial flaw, whichever is greater. If the ligament is greater than $(2a' + gt)$, the flaws are treated separately.

After the circumferential and axial flaws have been combined per the above criteria, a map of the effective flaws in the shroud (which includes flaw depth and azimuthal location) can be made, and the effective flaw length can be used for subsequent fracture mechanics analysis.

Examples of the application of the combination of effective flaws for the UT screening criteria is similar to that for the visual screening criteria methods described in Section 3.2.1 except that the governing ligament is $(2a' + 2gt)$ instead of $(2T + 2gt)$.

Application of Effective Flaw Length Criteria

The application of the effective flaw length criteria is the same as that presented in Section 3.2.1 for the visual screening criteria. It should be noted that the flaw depths are now considered in this application.

3.3.2 Structural Analysis

The structural analysis of the shroud is similar to that used in the visual screening criteria described in Section 3.2. This section describes the analysis methodology and how it differs from that used in the visual screening criteria.

The methodology for the applied loads and resulting stresses and fracture mechanics analysis is identical to that described in Section 3.2. It should be noted that although part-through-wall credit is taken in the UT screening criteria, the interaction between crack tips (for LEFM analysis) still uses the shroud thickness instead of the depth of the deepest indication.

Limit Load Analysis

In the UT screening criteria limit load analysis, the part-through-wall depth, length and shroud azimuthal position are used to determine the acceptability of the flaws. Limit load calculations can be conducted using a similar approach to that outlined in Subsubarticle IWB-3640 and Appendix C of Section XI of the ASME Code. The flow stress was taken as $3S_m$. The S_m values for the shroud material are 16.9 ksi and 14.4 ksi for Type 304 and Type 304L, respectively, at the normal operating temperature of 550°F.

Safety factors similar to that used in the ASME Code are used in the analysis. The highest seismic stress is used for the limit load calculations. Similarly, the highest axial pressure stress corresponding to the lower shroud is used. Thus, the analytical results are applicable for all welds since limiting values are used. As an option, location specific stresses may be used in this evaluation.

3.3.3 Allowable Part Through-Wall Flaws

Allowable part through-wall flaws are determined using both fracture mechanics and limit load techniques for circumferential and axial flaws.

Allowable Part Through-Wall Circumferential Flaws

Both LEFM and limit load methods are used to evaluate the specific pattern of indications at a particular cross section. Above the core plate, the limiting location is the lowest weld above the core plate (e.g., H5 for the shroud design in Figure 2-1, and H4 for the shroud design in Figure 2-2). The weld between the lower shroud cylinder and core support cylinder involves Alloy 600, which has higher S_m values and therefore higher limit load capability, and is bounded by the allowable flaw size based on calculations assuming stainless steel.

Fracture Mechanics Analysis

The total axial pressure and seismic stress corresponding to the upset condition and faulted conditions are calculated based on simple strength of materials solutions. Using the ASME Code safety factors for fracture analysis, it must be determined which condition governs, faulted or normal and upset conditions. This is determined by multiplying the total normal and upset stress by 2.8 and the faulted stress by 1.4. The condition with the highest resulting stress is considered the limiting condition.

To determine the allowable flaw size based on LEFM methods, the conservatively estimated irradiated material fracture toughness K_{Ic} value of 150 ksi $\sqrt{\text{in}}$ was used. Applying a safety factor of 2.8 for the upset condition or 1.4 for faulted conditions, the allowable K_I of 53.5 ksi $\sqrt{\text{in}}$ for normal and upset and 107 ksi $\sqrt{\text{in}}$ for faulted is obtained. The allowable flaw size is calculated using the following equation from Section XI of the ASME Code:

$$K_I = \sigma_m M_m \sqrt{\pi} \sqrt{(a/Q)} + \sigma_b M_b \sqrt{\pi} \sqrt{(a/Q)}$$

Where σ_m = membrane stress

σ_b = bending stress

M_m = correction factor for membrane stress from Figure A-3300-3
from ASME Code, Section XI

M_b = correction factor for bending stress from Figure A-3300-5
from ASME Code, Section XI

a = crack depth

Q = flaw shape parameter from Figure A-3300-1 of ASME Code
Section XI.

Note that the flaw depth and length must include consideration for crack growth over the next cycle (gt for flaw depth, and 2gt for flaw length). Comparison of the applied stress intensity factor with the allowable fracture toughness determines if the flaw is acceptable.

Limit Load

Applying the limit load concept to the specific flaw configuration will result in a safety margin against collapse. Figure 3-12 shows an example of a flaw configuration. Similar to that performed in the visual screening criteria, the equations which can be used to determine the structural margin against collapse are derived by requiring equilibrium between an unflawed section of the shroud and the particular section of interest. Since the resulting equations are dependent on the particular crack configuration, a general expression cannot be determined prior to obtaining the actual UT results.

Prior to applying the equilibrium condition to a flaw pattern, the orientation of the axis (which defines the seismic moment direction) must be determined. This may be obtained on an iterative procedure until the limiting location is found.

Allowable Part Through-Wall Axial Flaws

Fracture Mechanics Analysis

The allowable axial flaw size is governed entirely by the pressure hoop stress. The applied stress intensity factor can be obtained using the same methodology presented for the

circumferential flaw LEFM determination. In this case, the axial stress (σ_h) is neglected. Comparison of the applied stress intensity factor with the allowable fracture toughness defines the allowable through-wall flaw length.

Limit Load

An alternate approach to determining the allowable flaw size is to use limit load techniques. The allowable flaw length is given by the equation:

$$\sigma_h = \sigma_f / (M_1 * SF)$$

where M_1 is a curvature correction factor (Reference 3-2), σ_f is the flow stress, SF is the safety factor of 3 for upset conditions or 1.5 for faulted, and σ_h = the hoop stress corresponding to the upset or faulted ΔP . The allowable flaw length is determined by satisfying the equation shown above.

3.3.4 UT Screening Criteria

The determination of flaw acceptability was described in Section 3.3.2. The UT screening criteria is summarized below.

For circumferential flaws, the effective flaw lengths (after application of proximity criteria) must be evaluated using the limit load method. In this method, a safety factor greater than 1.0 against the actual limit load must be shown to assure structural integrity. In addition to the limit load evaluation, the flaws must also be evaluated based on LEFM. This includes consideration of crack tip interaction, and subsequently compared with the allowable single flaw length for the given depth.

The effective axial flaw lengths can also be compared against the allowable LEFM length and the allowable limit load length.

It should be noted that when considering LEFM based evaluations, the crack tip interaction criteria must be applied in comparing against the allowable lengths. For example, for adjacent flaws where the spacing S is less than $0.75(L_1 + L_2)$, the length $L = L_1 + L_2$ is used for comparison with the LEFM based allowable flaw length.

3.4 References

- 3-1 Rooke, D.P. and Cartwright, D.J., "Compendium of Stress Intensity Factors," The Hillingdon Press (1976)
- 3-2 Ranganath, S., Mehta, H.S., and Norris, D.M., "Structural Evaluation of Flaws in Power Plant Piping," ASME PVP Volume No. 94 (1984)

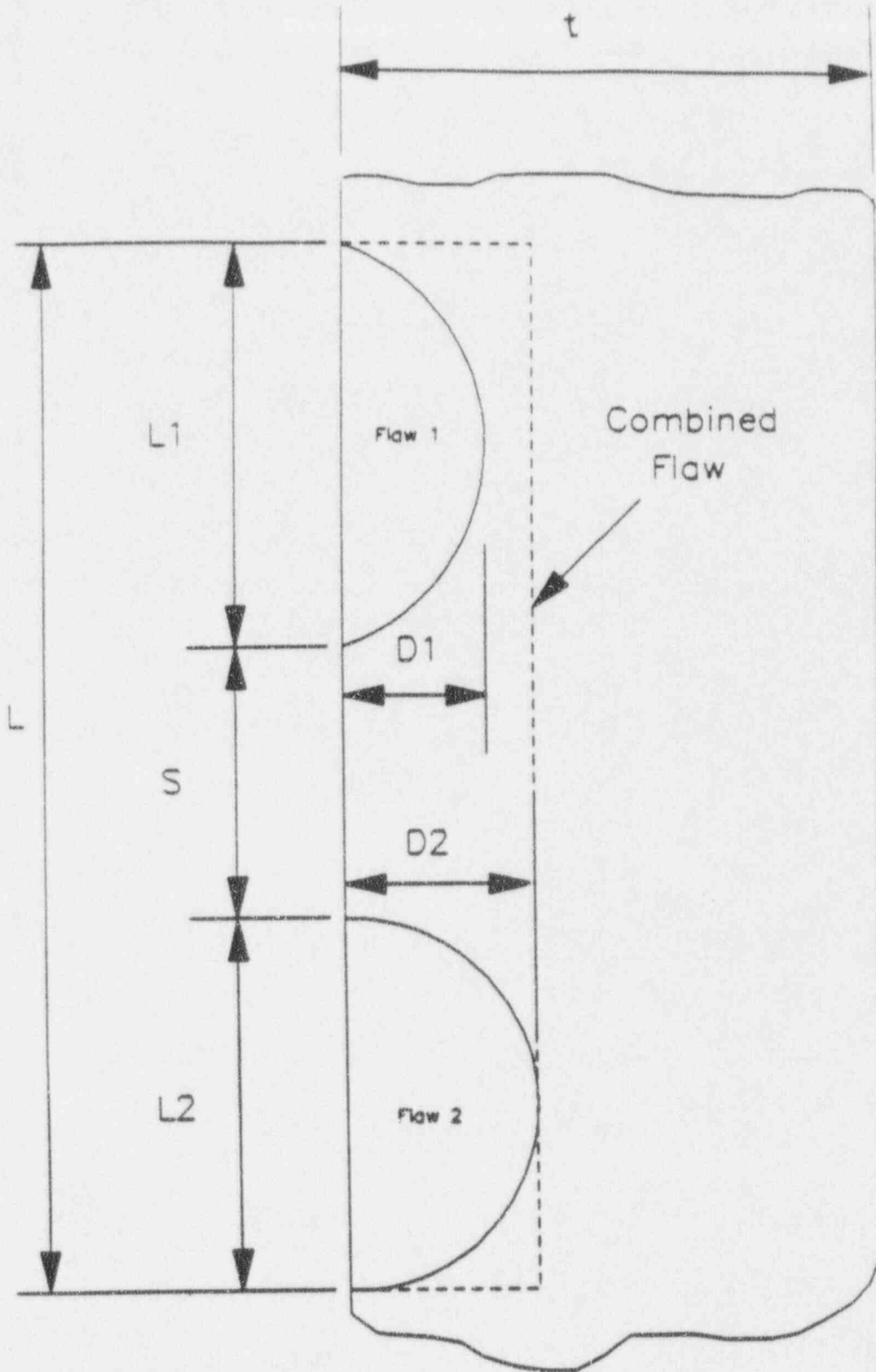


Figure 3-1 ASME Code Proximity Criteria

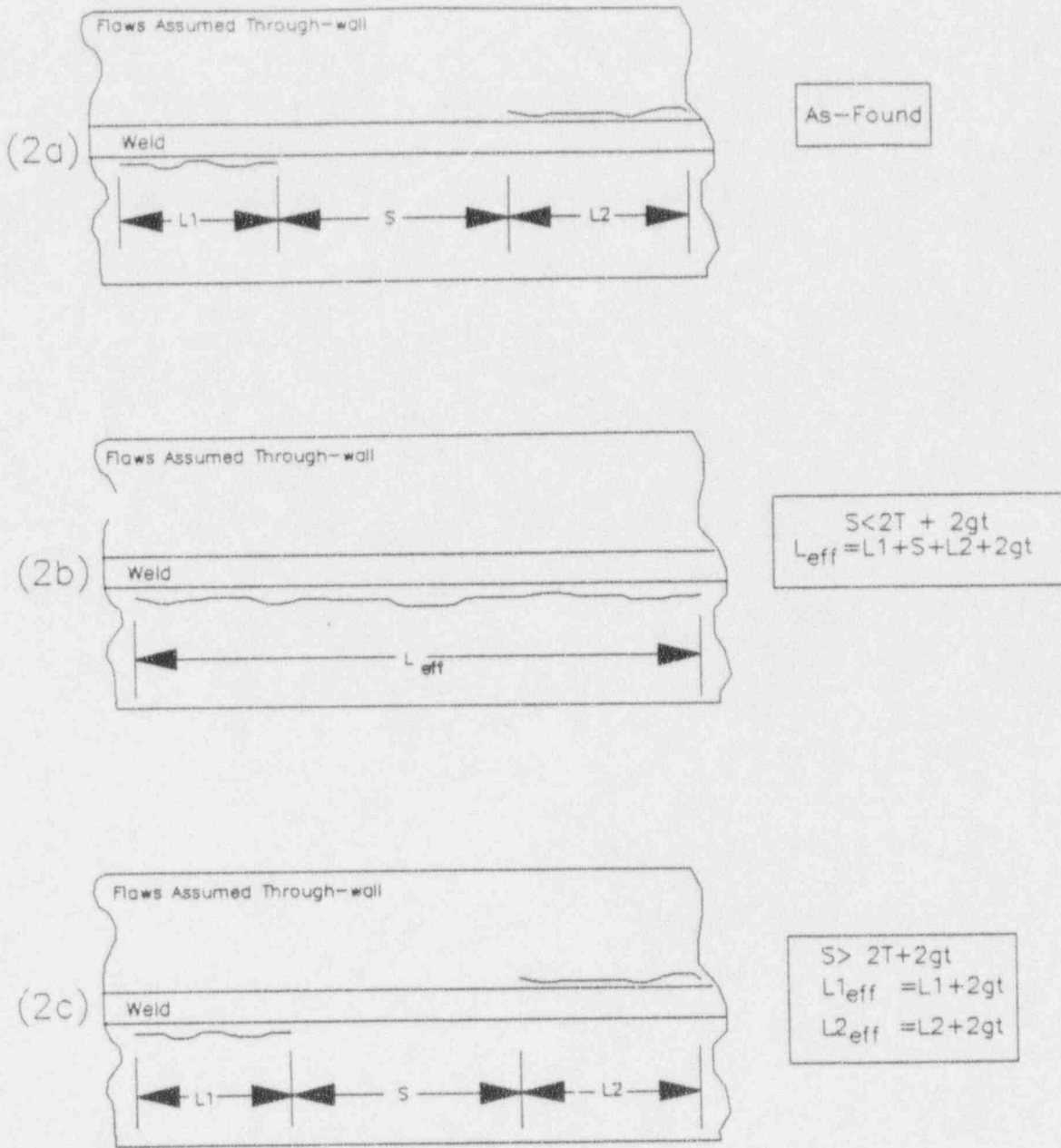


Figure 3-2 Application of Proximity Procedure to Neighboring Circumferential Flaws

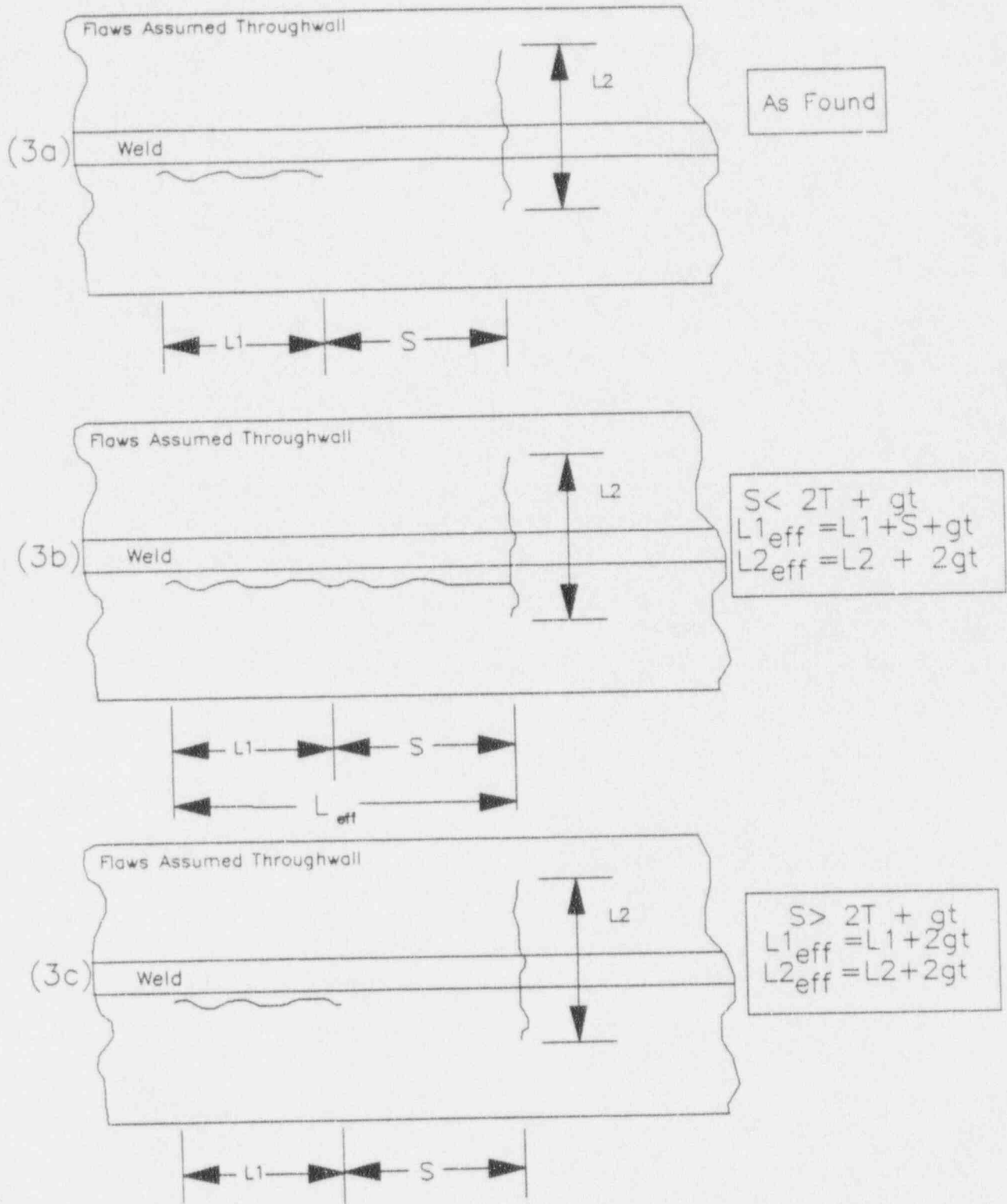


Figure 3-3 Application of Proximity Procedure to Neighboring Axial and Circumferential Flaws

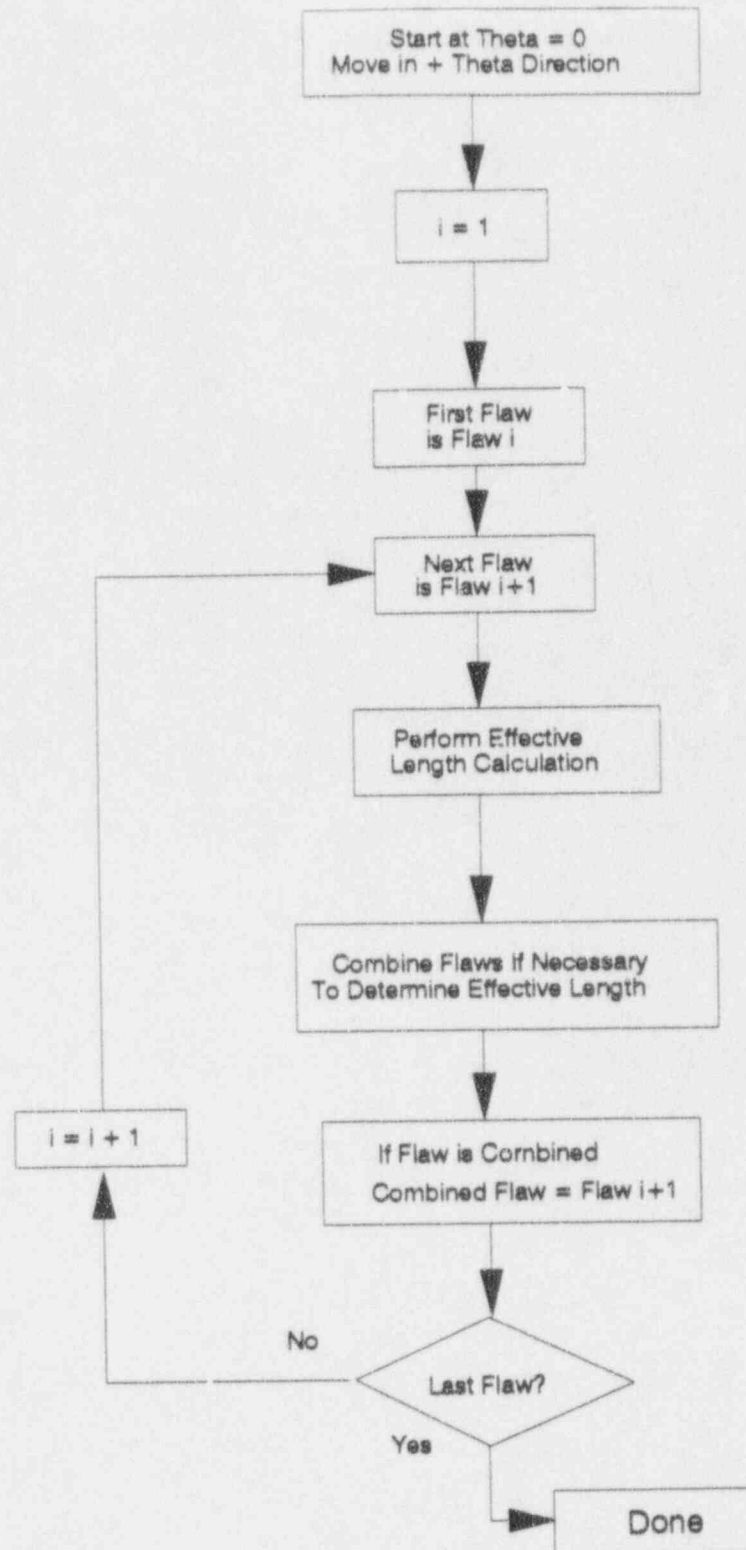


Figure 3-4 Process For Determining Effective Circumferential Flaw Length

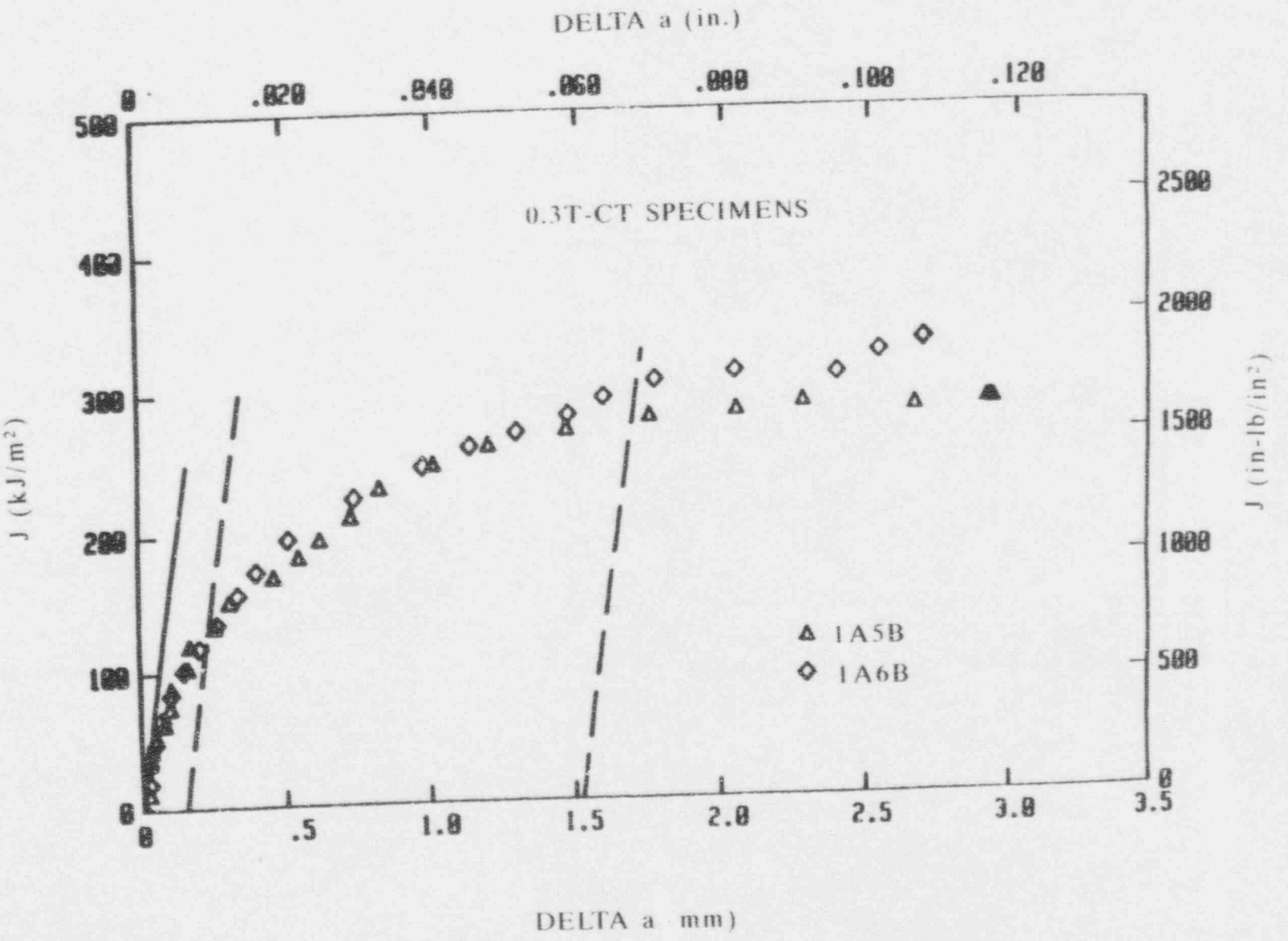


Figure 3-5 Comparison of J-R Curves For Two Irradiated Stainless Steel Specimens

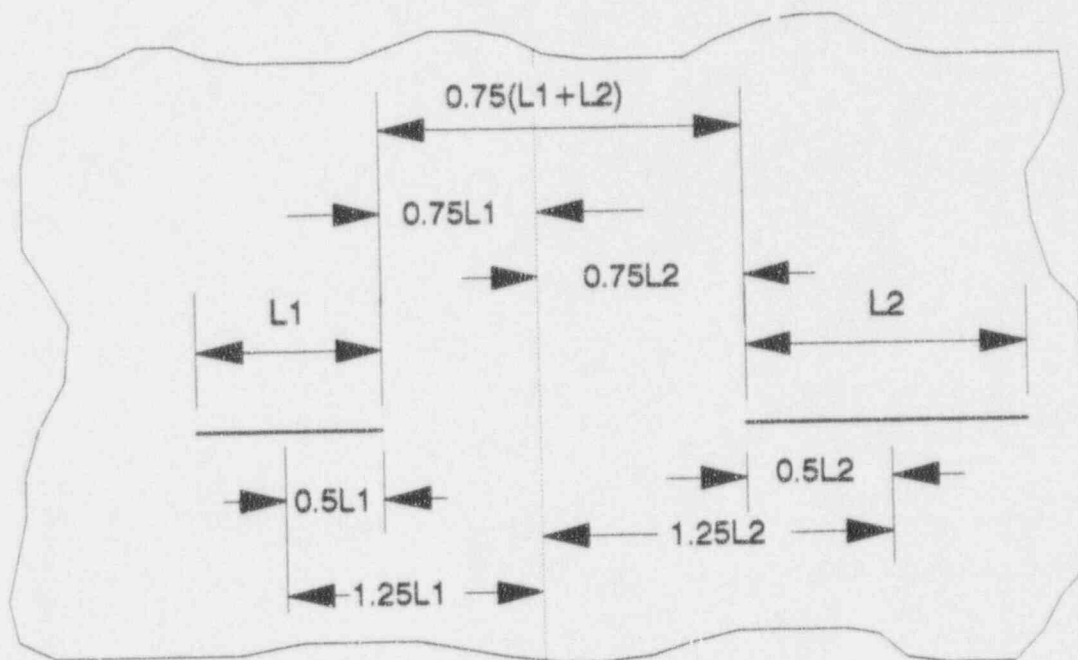
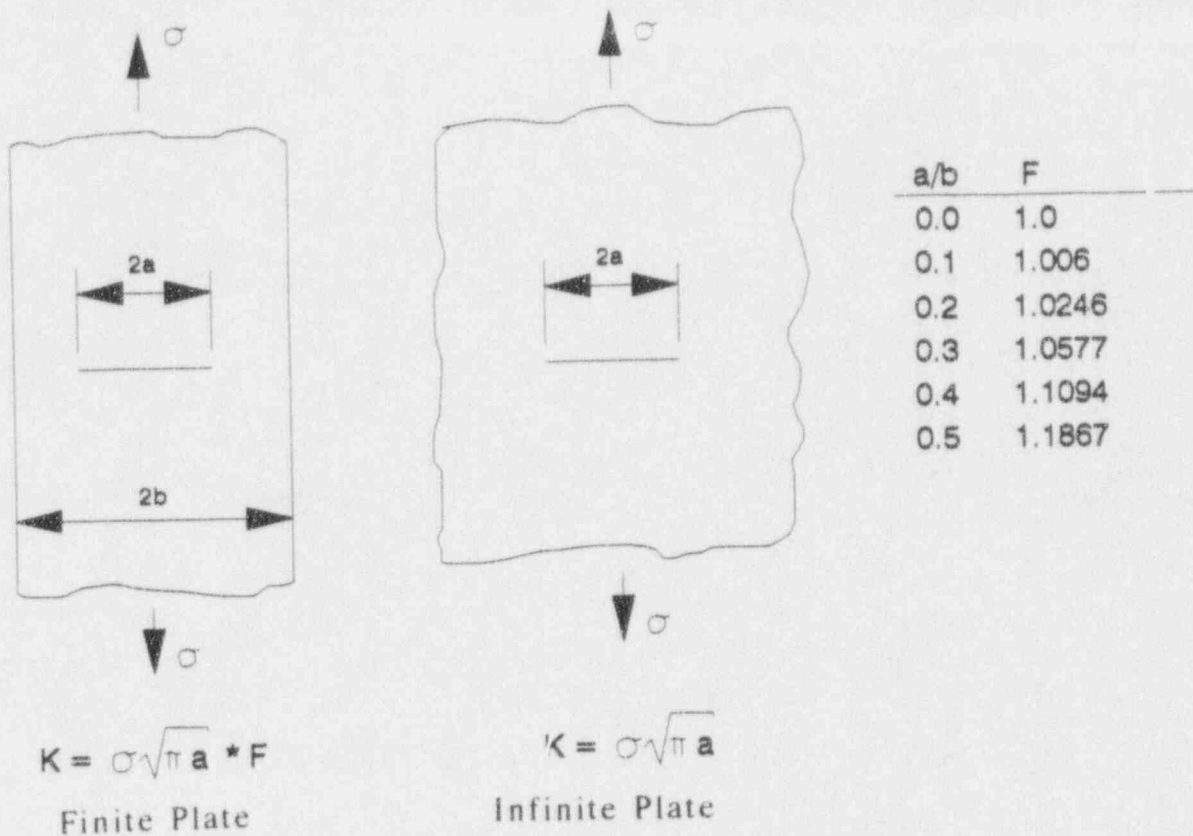


Figure 3-6 Schematic Illustrating Flaw Interaction

42

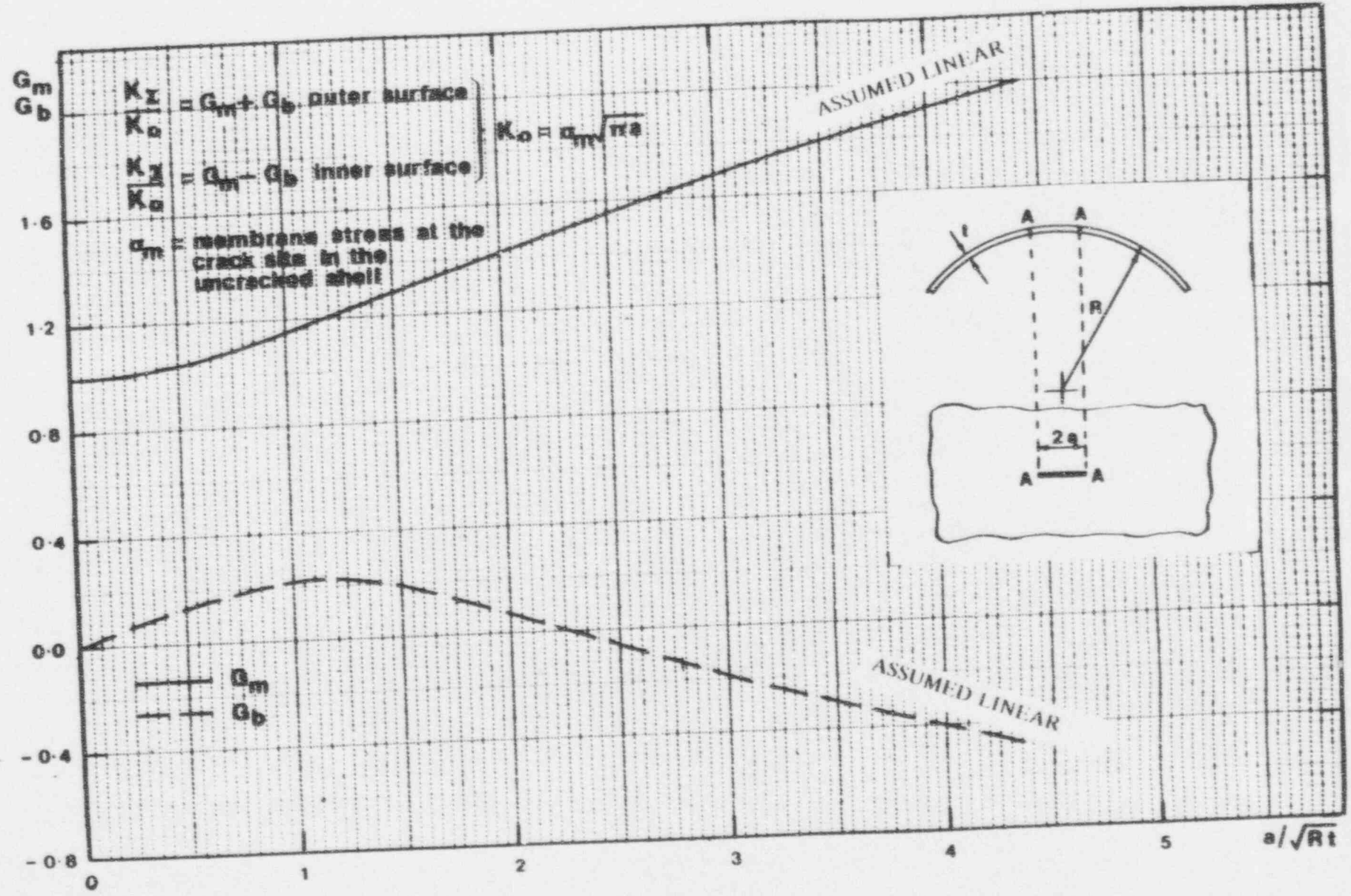


Figure 3-7 KI for Point A of a Circumferential Crack in a Cylindrical Shell Subjected to a Uniform Membrane Stress

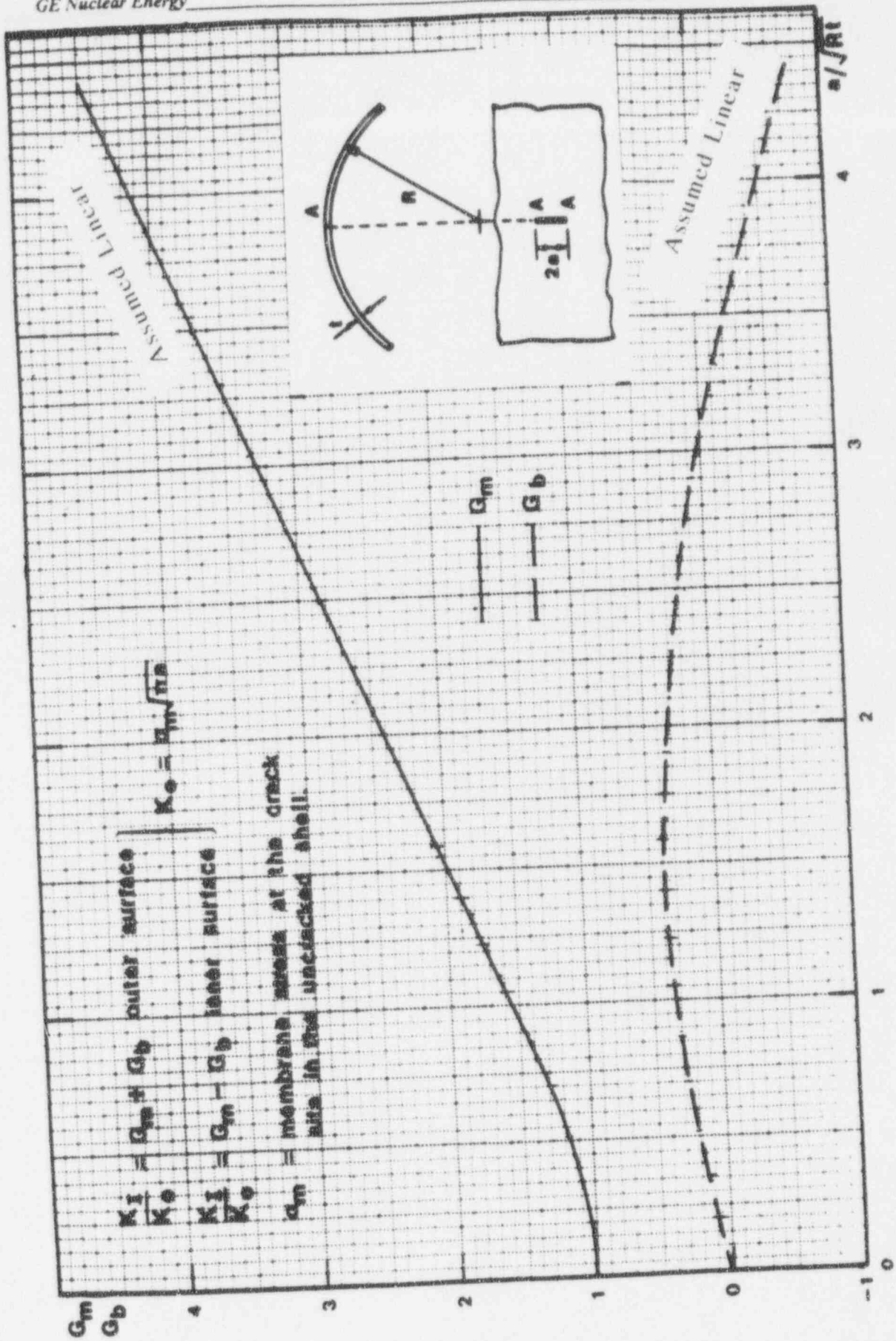
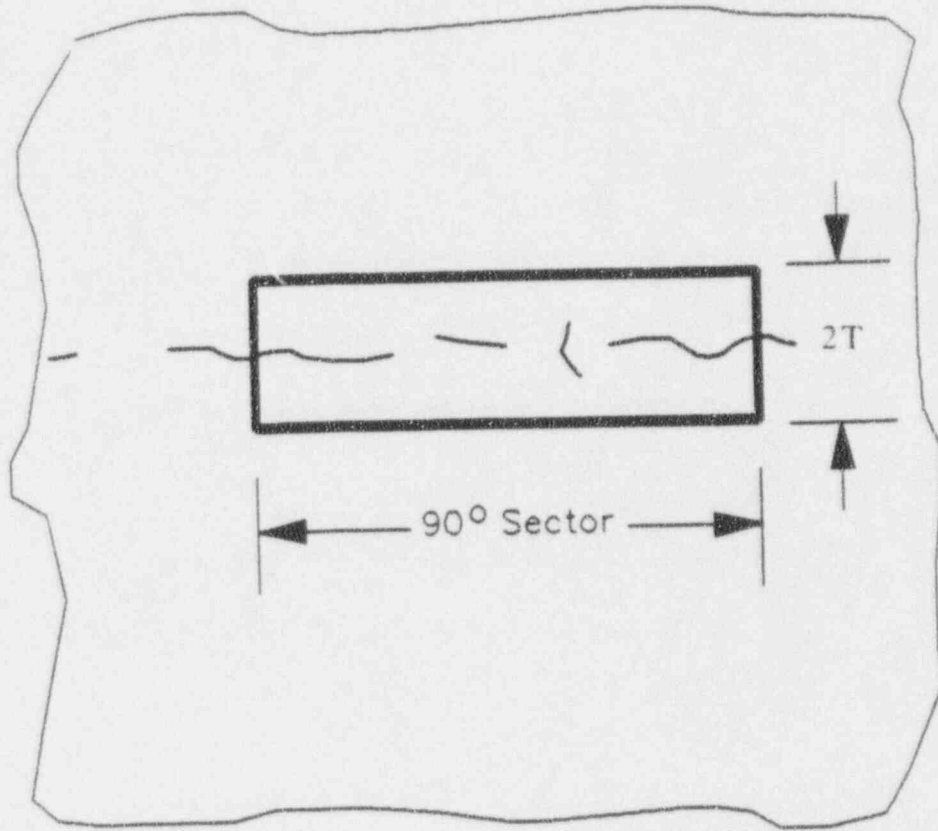


Figure 3-8 KI for Point A of a Longitudinal Crack in a Cylindrical Shell Subjected to a Uniform Membrane Stress



Not to Scale

Figure 3-9 Schematic Illustrating Cumulative Effective Flaw Criterion

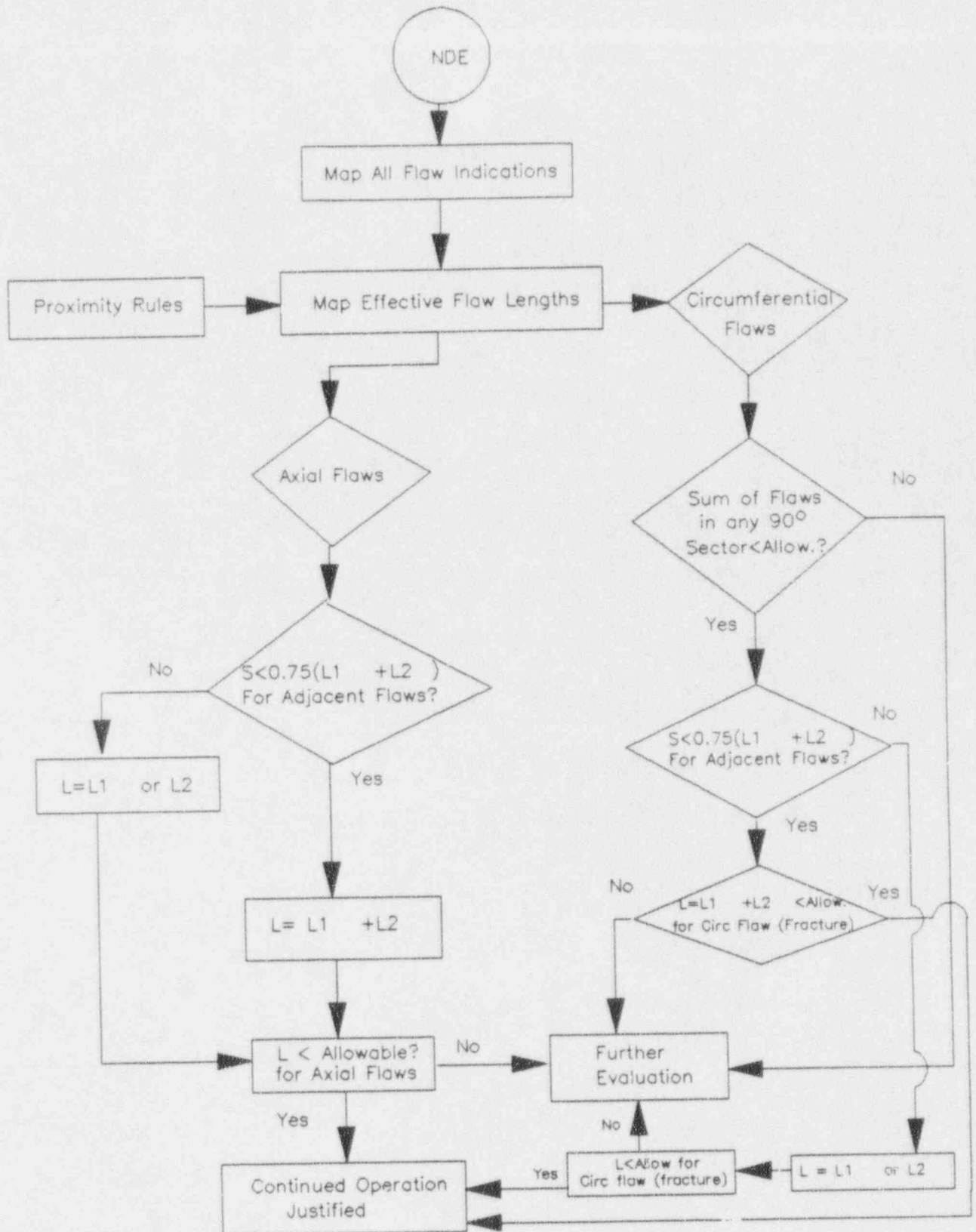


Figure 3-10 Schematic of Screening Criteria

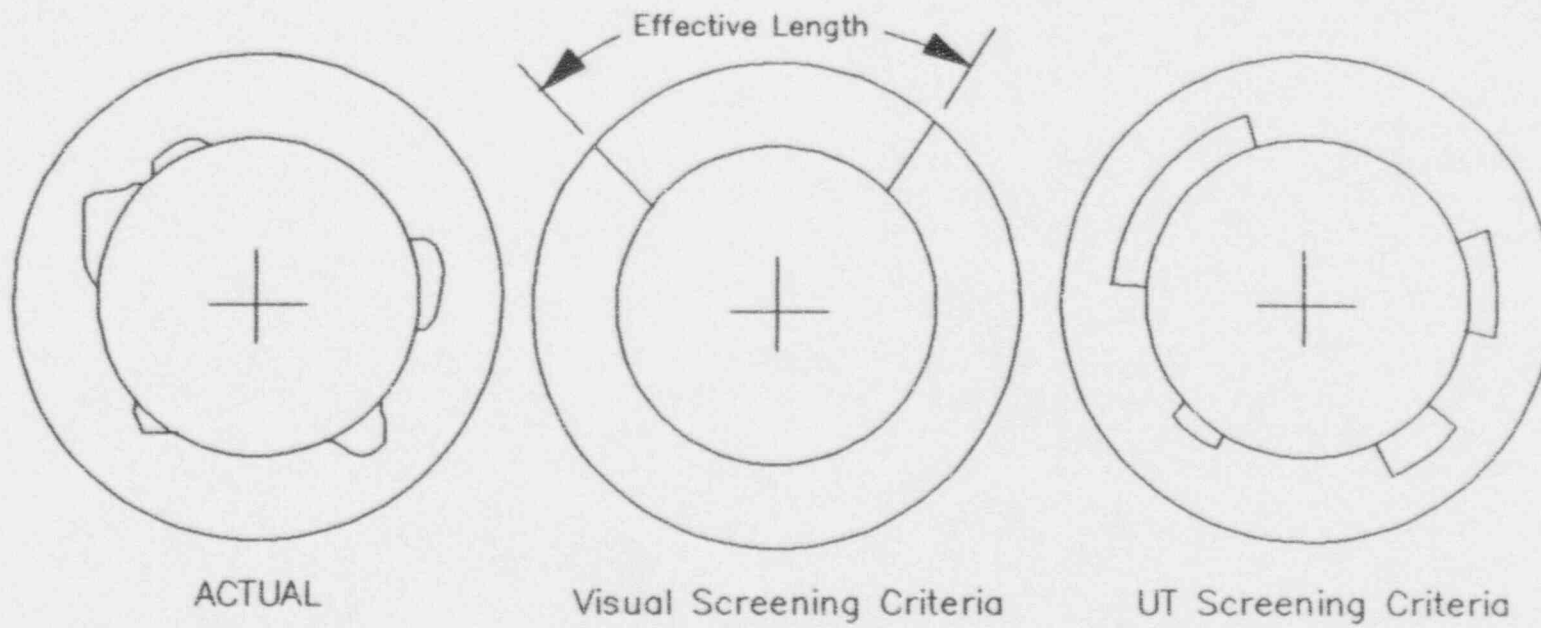


Figure 3-11 Flaw Geometry Assumption Used in Screening Criteria
(For Limit Load Evaluation)

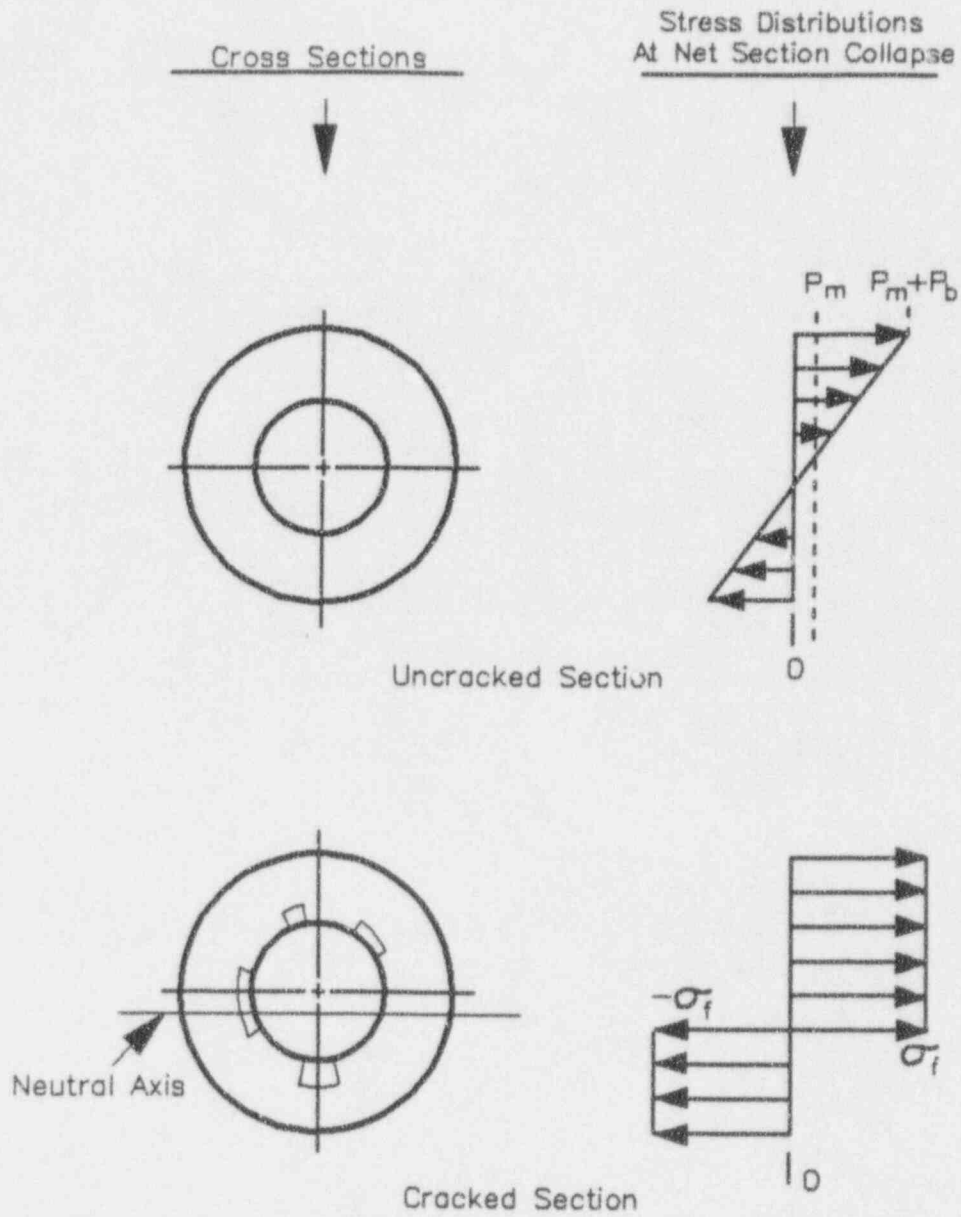


Figure 3-12 Limit Load Schematic for UT Screening Criteria

4.0 MITIGATION OF CORE SHROUD IGSCC AND IASCC

4.1 Introduction

This section provides information regarding mitigation of core shroud cracking. The recent incidences of cracking have demonstrated the advantage of taking early precautions to lessen the potential and extent of intergranular stress corrosion cracking (IGSCC) and irradiation assisted stress corrosion cracking (IASCC).

It is well documented that the BWR recirculation coolant's $\cong 200$ ppb dissolved oxygen is more than sufficient to provide the electrochemical driving force for IGSCC of BWR structural materials. This concentration of dissolved oxygen (and other oxidizing species) generates an electrochemical potential (ECP) in the austenitic stainless steel piping system of $\cong 100$ mV(SHE) that is above the ECP threshold for IGSCC of sensitized stainless steel and nickel based alloys. The more oxidizing core of the BWR is characterized by a higher ECP of $\cong +250$ mV(SHE). Finally, the conductivity of the BWR coolant is sufficiently high to allow these corrosion phenomena to occur.

Over a decade of laboratory and in-reactor investigations have revealed that lowering the ECP of sensitized stainless steel to < -230 mV(SHE) by injecting hydrogen gas into the BWR feedwater, and reducing coolant conductivity to < 0.3 μ S/cm by better BWR water chemistry operational practices, would mitigate IGSCC of BWR piping (Reference 4-1). For IASCC of non-thermally sensitized stainless steel, the threshold ECP is $\cong -140$ mV(SHE) (Reference 4-2). Since this process, hydrogen water chemistry (HWC), reduces the "corrosiveness" of the entire BWR coolant, it is considered a potential "blanket" IGSCC/IASCC mitigation technique. The results of extensive testing have clearly demonstrated that HWC mitigates environmental cracking in numerous BWR structural materials and has no insuperable materials deleterious effects (Reference 4-1).

However, some BWRs may not be able to implement HWC on a timely basis. For this category of plants, the strict control of conductivity can still provide dramatic IGSCC benefits, albeit not total IGSCC/IASCC mitigation.

4.2 Core Shroud IGSCC Mitigation with HWC

Although IGSCC/IASCC of reactor internals to date has been limited due to their typically low tensile stress levels, and the impact has been manageable, IGSCC of reactor internals is an increasing concern as the BWR fleet ages. In the short term, continued operation of an overseas BWR-4 plant and Peach Bottom Unit-3 with core shroud indications are being supported by analysis. The Brunswick Unit-1 shroud has been repaired for the limiting locations and analysis is being used to disposition cracking at other weld locations.

Due to the complete lack of sensitization (chromium carbides at the grain boundaries) of the relatively low carbon (0.045%) stainless steel shroud, the cracking at the overseas BWR-4 appears to be strictly IASCC. For the Brunswick Unit-1 shroud, the nature of the cracking, (i.e., shroud ID surface with grain cracking envelopment, thicker oxides and extensive crack branching and OD surface with more pipe-like SCC characteristics) suggests that the total SCC phenomenon appears to be a synergistic combination of thermal sensitization IGSCC and IASCC.

Recent reactor internal cracking incidences suggest that the "blanket" IGSCC remedy, HWC, may be necessary to protect the reactor internals. However, to provide sufficient environmental protection in the highly oxidizing core region (O_2 plus H_2O_2) with HWC would require, in many instances, such large injection rates of hydrogen that burdensome radiation (increased N-16 during operation and increased shutdown radiation levels) penalties could occur. At most plants, this N-16 dose rate could be increased by factors of 4 to 6 or higher, and require additional shielding and modified operational practices to reduce personnel and site boundary exposures to acceptable levels.

Because of the highly oxidizing nature of the coolant within and above the core, even with HWC at moderate (1.0 to 1.6 ppm) to high (2.0 to 2.6 ppm) hydrogen addition levels, the upper shroud H1 and H2 welds are not protected on the outside diameter surface for plants with Type 304 stainless steel shrouds (Figure 4-1). In addition, at moderate levels, the inside of the shroud beltline welds H3, H4 and H5 (some plants only have H4 beltline weld) are not protected. Fortunately, as will be discussed in Section 4.3, the use of noble metal coatings (NMCs) in conjunction with HWC looks

promising for use in the future to provide SCC protection for these specific shroud welds.

4.3 "Low Impact" HWC and Internal Noble Metal Coatings/Alloys

A perhaps more timely shroud IGSCC/IASCC mitigation option for some plants that can make HWC more efficient while minimizing radiation penalties is the use of Noble Metal Coatings (NMCs). This technology is currently under development and qualification, and is being continuously evaluated by the BWROG. This approach would consist of depositing dilute NMCs on the shroud to lower the local ECP below the IGSCC/IASCC thresholds with near stoichiometric ratios of hydrogen and oxygen, i.e., with little excess hydrogen injection.

As noted above, due to the BWRs core's highly oxidizing nature ($\cong +250$ mV[SHE]), more hydrogen is required for an equivalent shift in ECP to provide protection against IGSCC/IASCC in the core region. However, since noble metals have long been recognized as recombination catalysts for oxygen and hydrogen dissolved in water, it is possible to use NMCs to assist in-core recombination. It has been determined that the ECP of a surface containing only small amounts of noble metals decreased to very low values when hydrogen was present in stoichiometric amounts (or greater), even in the absence of complete volume recombination of oxygen and hydrogen in the water (Reference 4-3).

Figure 4-2 presents the effect of Pd in 285°C (545°F) water containing 300 ppb oxygen and various hydrogen concentrations (Reference 4-3). While the nominal Type 316 stainless steel demonstrates little change in ECP, the palladinized electrode exhibits a dramatic drop in ECP from $\cong 100$ mV (SHE) to approximately -500 mV (SHE) below a molar ratio of 2. This hydrogen concentration ($\cong 24$ ppb) is less than stoichiometrically required for 300 ppb oxygen (37.5 ppb) due to the higher diffusivity (1.83x) of hydrogen versus oxygen in the water boundary layer. The above results clearly indicate that a catalyzed surface can reduce the ECP of stainless steel with significantly less hydrogen than is required in the absence of a catalyst. Subsequent studies have replicated these coating results and have also demonstrated identical beneficial results with Pd microalloyed stainless steel (Reference 4-4).

Constant extension rate tests (CERT) were conducted on welded plus low temperature sensitized (500°C/24h) Type 304 stainless steel to directly evaluate the effect of Pd coatings on IGSCC. The results are summarized in Table 4-1 and Figure 4-3 (Reference 4-3). As anticipated, the measured ECPs for Type 304 stainless steel were similar to those obtained for Type 316 stainless steel described above. It is uniformly observed that the stainless steel autoclave is characterized by ECPs above the protection potential since it was not palladinized.

The dissolved oxygen levels in all the CERT tests were maintained at significantly higher levels than would be observed in a HWC environment. In addition, the first two CERTs, which included the unpalladinized control specimen, were performed at high hydrogen-to-oxygen molar ratios. The remainder of the CERTs had hydrogen-to-oxygen molar ratios at the sample surface close to the stoichiometric value for the formation of water of 2:1, with consideration for the differences in diffusion coefficients. When the molar ratio exceeded 2.0, the ECPs of the palladinized specimens was considerably below the IGSCC protection potential even with coatings as thin as 0.03 μm . When the molar ratio was less than 2.0, the ECPs of the specimens were above the IGSCC (and in most cases the IASCC) protection ECP. Subsequent scanning electron microscopy (SEM) examinations of the fracture surfaces confirmed that only the unpalladinized specimens suffered IGSCC.

Since a few shrouds have SCC, crack propagation studies on Pd coated specimens are particularly relevant (Reference 4-5). Figure 4-4 presents the crack growth results of a furnace sensitized Type 304 stainless steel specimen that was noble metal coated under water with 0.42% Pd Type 309L stainless steel weld metal using the high velocity oxy-fuel (HVOF) technique. The high stress intensity (33 $\text{MPa}\sqrt{\text{m}}$ [30 $\text{ksi}\sqrt{\text{in}}$]) fracture mechanics specimen was exposed to both stoichiometrically excess oxygen (H_2/O_2 molar ratio < 2) and excess hydrogen environments (H_2/O_2 molar ratio > 2). When the specimen was exposed to the excess oxygen environment (180 ppb O_2 , 9.6 ppb H_2 , $\text{H}_2/\text{O}_2 = 0.85$), the crack propagation rate is 1.46 $\mu\text{m}/\text{h}$ (503 mpy). However, when the hydrogen concentration is increased to create a stoichiometrically excess hydrogen (150 ppb O_2 , 24 ppb H_2 , $\text{H}_2/\text{O}_2 = 2.56$) environment, the crack propagation rate dramatically decreases two orders of magnitude to only 0.01 $\mu\text{m}/\text{h}$ (3.5 mpy).

4.4 Conductivity Control to Reduce IGSCC Susceptibility

The benefit of good water purity in reducing IGSCC susceptibility has been recognized for several years, and the average water conductivity of the entire BWR fleet has improved dramatically in recent years.

An example of the effects of conductivity (sulfate) on crack initiation in uncreviced material is presented in Figure 4-5 (References 4-6 through 4-9). It is clear that an increase in sulfate/conductivity results in an acceleration in crack initiation as measured by CERT. A specific example of an acceleration in crack propagation rate on creviced material with sulfate is shown in Figure 4-6. Figure 4-6 displays June 1986 Peach Bottom 3 on-line reversing DC potential drop crack monitoring data for sensitized Type 304 stainless steel. The results clearly illustrate the change in crack growth observed after two closely linked water chemistry transients of 4-5 $\mu\text{S}/\text{cm}$, i.e., increases in water conductivity due to intrusions of demineralizer resin material (Reference 4-10). This figure demonstrates the dramatic increase in crack growth rate (2X) with conductivity. Similar on-line crack monitoring results with sulfate have also been documented in the laboratory, Figure 4-7 (Reference 4-11). Other anions such as chloride, fluoride, silicate, phosphate, etc., have similar kinetic effects on IGSCC initiation and propagation (References 4-12 and 4-13).

This high conductivity crack initiation and propagation acceleration factor is consistent with the relatively high incidence of IGSCC in creviced Alloy 600 shroud head bolts and access hole covers. Additional documentation on the strong correlation of IGSCC susceptibility with actual BWR plant water chemistry history for creviced BWR components has been published (Reference 4-14).

4.4.1 IGSCC Modeling

Finally, the effect of conductivity and ECP on crack propagation has also been quantified at the GE Research and Development Center based on a "first principles" model of crack advance known as the film rupture/slip dissolution model (Reference 4-15). Predictions from PLEDGE (Plant Life Extension Diagnosis by GE) model have been extensively compared with laboratory and field data and have provided validation of the technique. For example, PLEDGE predicts the crack growth rate in stainless steel and low alloy steel within a factor of approximately two for a 70% statistical

confidence over a range in observed crack growth rate of more than six orders of magnitude. Likewise, it provides a very reasonable mean value and can accurately bound the observed crack growth rate in stainless piping and other components. Aside from piping predictions, PLEDGE has been successfully used for predicting in-reactor on-line compact tension specimen crack growth monitoring data and incorporating this data into the model for refinement. In a more practical application, the PLEDGE modeling approach was used to avoid a mid-cycle plant shutdown safe end inspection. Non-sensitized (stabilized) stainless steels and reactor internals such as the core shroud, top guide, access hole cover and in-core monitor housing have also been successfully modeled with PLEDGE.

Finally, the PLEDGE Model of IGSCC and, more recently, IASCC (Reference 4-16) clearly indicate the strong effect of conductivity on crack growth rate and, by inference, crack initiation. Figure 4-8 presents a schematic estimation of Peach Bottom 2 and 3 sensitized Type 304 stainless steel crack growth rates as a function of conductivity using the PLEDGE model. Crack growth rates based on actual conductivity averages for the first ten years (Unit-2: 0.593 $\mu\text{S}/\text{cm}$, Unit-3: 0.752 $\mu\text{S}/\text{cm}$) were compared to those averages for the last two years. A value of 200 mV(SHE) was used for the ECP in these calculations. As noted in Figure 4-8, a factor of improvement (FOI) of approximately twenty (20) decrease in crack growth rate is obtained with Unit-2's decrease in conductivity. The FOI for Unit-3 is eleven (11).

4.5 Shroud IGSCC/IASCC Mitigation Factors of Improvement

Table 4-2 summarizes the estimated FOIs for reactor internals, based on relative crack propagation rates. The ECPs for the top of the core (Brunswick 1 shroud flange IGSCC) and bottom of the core (access hole cover) were estimated from FitzPatrick data, Figure 4-9 (Reference 4-17). The ECP of noble metals was derived from data from Duane Arnold, Figure 4-10 (Reference 4-18). The benefits of conductivity (only) improvement as based on PLEDGE model calculations are also included.

4.6 An Additional Potential IGSCC/IASCC Mitigation Technique

Although it has been demonstrated that there is a clear crack growth rate reduction benefit with zinc injection and HWC (References 4-19 and 4-20), the latest synergistic

depleted zinc oxide (DZO)/HWC laboratory studies indicate that the amount of crack growth reduction is highly variable with uncertain reproducibility, especially for Alloy 182. Since it has been observed that the material response time is much slower than that obtained with high hydrogen (HWC) levels alone, it requires considerably longer time to establish the lower bound crack growth rates. Although there is insufficient data to establish a BWR water chemistry specification with predictably reliable results, testing will continue to quantify the benefit at low DZO levels (10 ppb) since this may provide a future cost saving by allowing somewhat lower hydrogen addition rates to achieve HWC protection. The BWR Owners' Group will continue to monitor the progress of this activity.

4.7 Core Shroud IGSCC/IASCC Mitigation Options

The above discussion reveals the following options for addressing the degradation of the BWR core shroud:

1. HWC. This "blanket" IGSCC/IASCC remedy lowers the ECP of the core shroud and mandates a lower coolant conductivity. However, achieving such in-core protection can result in high radiation levels during operation and shutdown.
2. "Low Impact" HWC and NMCs. This technique utilizes the catalytic nature of noble metals to increase HWC efficiency and minimize radiation penalties. Although this concept has been clearly proven in the laboratory, technological application details are under development and qualification.
3. Conductivity Control. This universally sound approach would only delay the initiation of cracking and reduce crack propagation rates. It is not sufficient to mitigate SCC in the BWR.
4. DZO/HWC. This is a potential "low impact" HWC technique where an operating specification relationship could be developed between DZO and hydrogen additions to minimize SCC and radiation penalties. Additional testing of this technique is required.

It is obvious that the above SCC mitigation options are characterized by either detrimental side effects (HWC) or inadequacy (conductivity only), or they have not been fully qualified (HWC/NMCs and DZO/HWC). Therefore, the optimum core shroud SCC mitigation approach will vary from plant to plant and will require a complete specific evaluation of these and future options.

4.8 References

- 4.1. B. M. Gordon et al, "Hydrogen Water Chemistry for BWRs-Materials Behavior-Final Report," EPRI TR-100304, Palo Alto, CA, February 1992.
- 4.2. M. E. Indig et al, "Investigation of the Protection Potential Against IASCC," paper #71 presented at Corrosion 92, NACE, Nashville, April 1992.
- 4.3. L. W. Niedrach, "Effect of Palladium Coatings on the Corrosion Potential of Stainless Steel in High Temperature Water Containing Dissolved Hydrogen and Oxygen," Corrosion, Vol. 47, No. 3, p. 162, March 1991.
- 4.4. Y. Kim et al, "The Application of Noble Metals in Light-Water Reactors," Journal of Metals, p. 14, April 1992.
- 4.5. P. L. Andresen, "Effect of Pd-coating and Pd-alloying on the Stress Corrosion Cracking of Stainless Steel," PMWG-G-627, August 1992.
- 4.6. W. J. Shack, et al, "Environmentally Assisted Cracking in Light Water Reactors: Semiannual Report April - September 1985," NUREG/CR-4667, ANL-86-31, June 1986.
- 4.7. W. J. Shack, et al, "Environmentally Assisted Cracking in Light Water Reactors: Annual Report October 1983 - September 1984," NUREG/CR-4287, ANL-85-33, June 1985.
- 4.8. L. G. Ljungberg, D. Cubicciotti and M. Trolle, "Effects of Impurities on the IGSCC of Stainless Steel in High Temperature Water," Corrosion, Vol. 44, No. 2, February 1988.
- 4.9. W. E. Ruther, W. K. Soppet and T. F. Kassner, "Effect of Temperature and Ionic Impurities at Very Low Concentrations on Stress Corrosion Cracking of Type 304 Stainless Steel," paper 102 presented at Corrosion 85, Boston, MA, NACE, March 1985, published in Corrosion, Vol. 44, No. 11, November 1988.
- 4.10. D. A. Hale and C. G. Diehl, "Real Time Monitoring of Environmental Crack Growth in BWRs," paper 455 presented at Corrosion 88, St. Louis, MO, NACE, March 1988.
- 4.11. B. M. Gordon, "Corrosion and Corrosion Control in BWRs," NEDE-30637, p. 6-22, December 1984.

4.8. References (continued)

- 4.12. R. B. Davis and M. E. Indig, "The Effect of Aqueous Impurities on the Stress Corrosion Cracking of Austenitic Stainless Steel in High Temperature Water," paper 128 presented at Corrosion 83, Anaheim, CA, NACE, April 1983.
- 4.13. P. L. Andresen, "A Mechanism for the Effects of Ionic Impurities on SCC of Austenitic Iron and Nickel Base Alloys in High Temperature Water," paper 101 presented at Corrosion 85, Boston, MA, NACE, March 1985.
- 4.14. K. S. Brown and G. M. Gordon, "Effects of BWR Coolant Chemistry on the Propensity for IGSCC Initiation and Growth in Creviced Reactor Internals Components," paper presented at the Third Int. Symp. of Environmental Degradation of Materials in Nuclear Power Systems-Water Reactors, Traverse City, MI, August 1987, published in proceedings of same, TMS-AIME, Warrendale, PA, 1988.
- 4.15. F. P. Ford et al, "Prediction and Control of Stress Corrosion Cracking in the Sensitized Stainless Steel/Water System," paper 352 presented at Corrosion 85, Boston, MA, NACE, March 1985.
- 4.16. P. L. Andresen and F. P. Ford, "Modeling of Irradiation Effects on Stress Corrosion Cracking Growth Rates," paper 497 presented at Corrosion 89, New Orleans, LA, NACE, April 1989.
- 4.17. R. A. Head and M. Siegler, "In-Core Response to Hydrogen Water Chemistry at J. A. FitzPatrick," EP89-32, January 1992.
- 4.18. W. D. Miller, R. A. Head and M. E. Indig, "Measurement of In-Core and Recirculation Response to Hydrogen Water Chemistry at the Duane Arnold Energy Center," EPRI TR-102310 April 1993.
- 4.19. P.L. Andressen and T.P. Diaz, "Effects of Zinc Additions on the Crack Growth Rate of Sensitized Stainless Steel and Alloys 600 and 182 in 288°C Water," Paper #72 presented at the 6th International Conference on Water Chemistry of Nuclear Reactor Systems, October 1992.
- 4.20. W.J. Shack et al, "Environmentally Assisted Cracking in Light Water Reactors: Semiannual Report, April - September 1986," NUREG/CR-4667 Vol. III, ANL-87-37, September 1987

Table 4-1. Results of Constant Extension Rate Tests
Sensitized Type 304 Stainless Steel

CERT No.	Pd			Molar Ratio		ECP		Time to	
	Thick (μm)	H ₂ (ppb)	O ₂ (ppb)	H ₂ :O ₂ (a)	(b)	CERT (mV)	Auto (mV)	Failure (h)	IGSCC (%)
1	0.00	161	95	27.1	49.6	-102	31	70	26
2	0.77	161	104	24.8	45.3	-535	-110	124	0
3	0.77	16	196	1.3	2.4	-515	-100	125	0
4	0.77	9	196	0.7	1.3	50	-102	76	33
5	0.07	19	251	1.2	2.2	-490	-150	118	0
6	0.03	20	263	1.2	2.2	-400	-110	126	0

Test Conditions:

287°C

0.3×10^{-6} M H₂SO₄

Conductivity: 0.3 $\mu\text{S}/\text{cm}$

Strain rate: $1 \times 10^{-6}/\text{s}$

(a) Molar ratio in water = 16 x ppb H₂/O₂

(b) Molar ratio at surface = 1.83 Molar ratio in water
where 1.83 is the ratio of the diffusion coefficients
for H₂ and O₂ in water

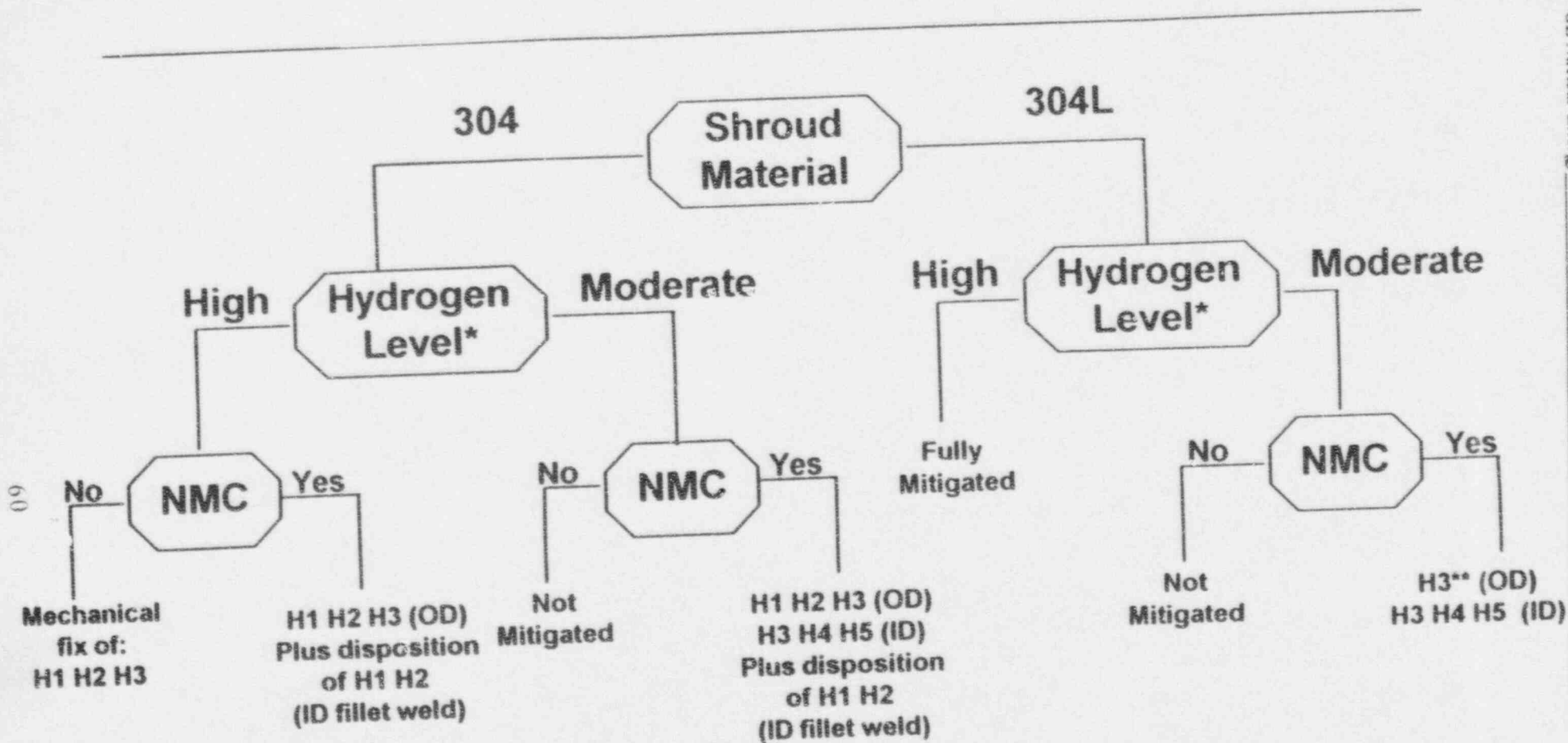
Auto = autoclave

Table 4-2. Shroud Estimated IGSCC Factors of Improvement (FOI)¹

	<u>Top of Core</u>			<u>Bottom of Core</u>		
H2 SCFM	0	12	20	0	12	20
T 304 ECP	225	200	140	140	75	-40
Pd ECP	225	-220	-310	140	-345	-435
HWC FOI	1	1.5	3	1	2	8
Pd FOI	1	100	60	1	30	7
Conductivity 0.3 to 0.06 μ S/cm (only)	5			5		

1. Assumes that all FOIs are multiplicative. Separate conductivity FOI.

Figure 4-1 Shroud SCC Mitigation Options



* High H₂ range is 2.0 to 2.7 ppm in feedwater. BOP flow assisted corrosion evaluation and fuel surveillance recommended by EPRI/BWROG Water Chemistry Guidelines (currently under revision).
Moderate H₂ range is 1.0 to 1.6 ppm in feedwater.

** NMC if end of life fluence exceeds 5x10²⁰ nvt
NMC (Noble Metal Coating)

61

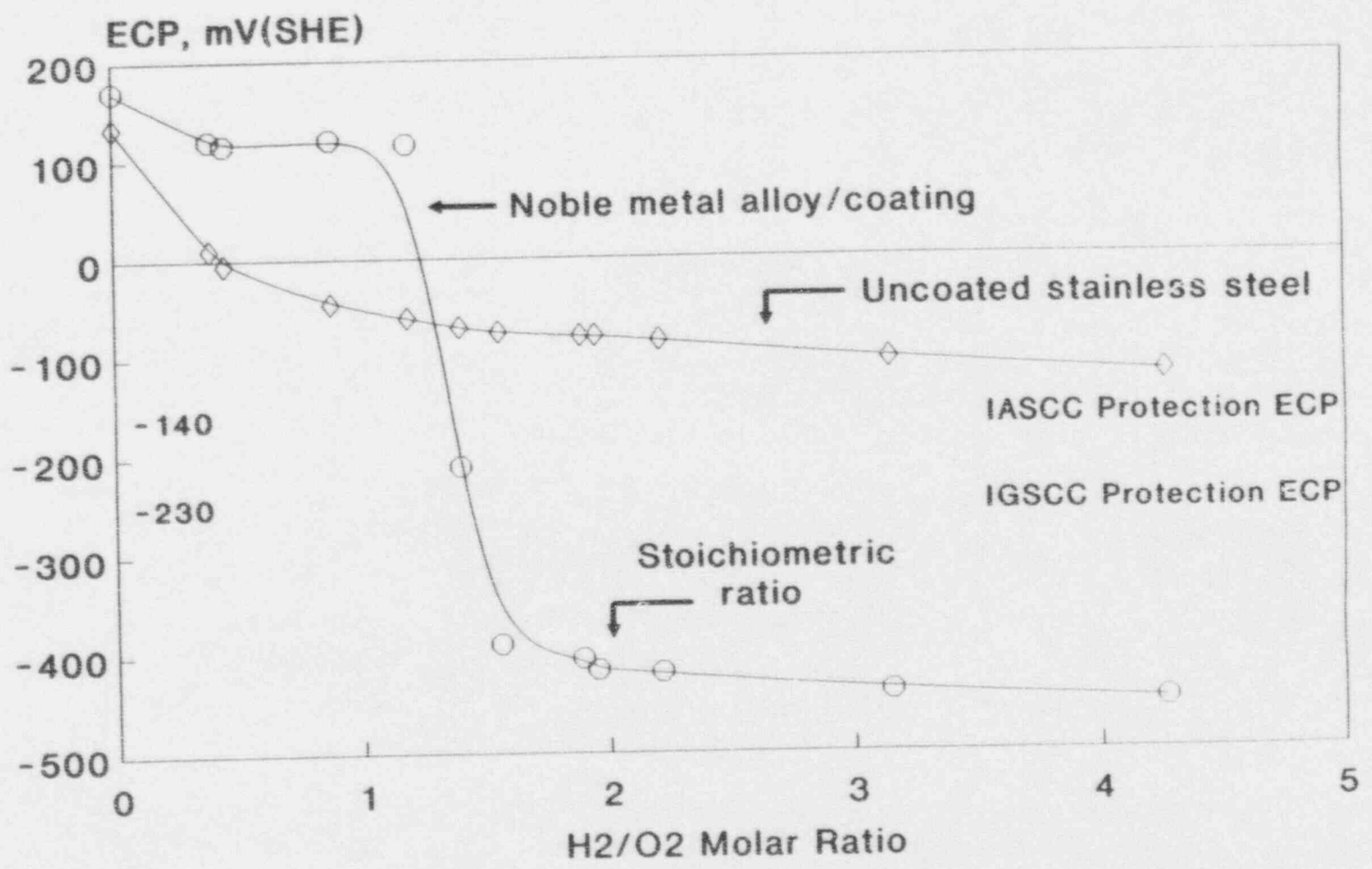
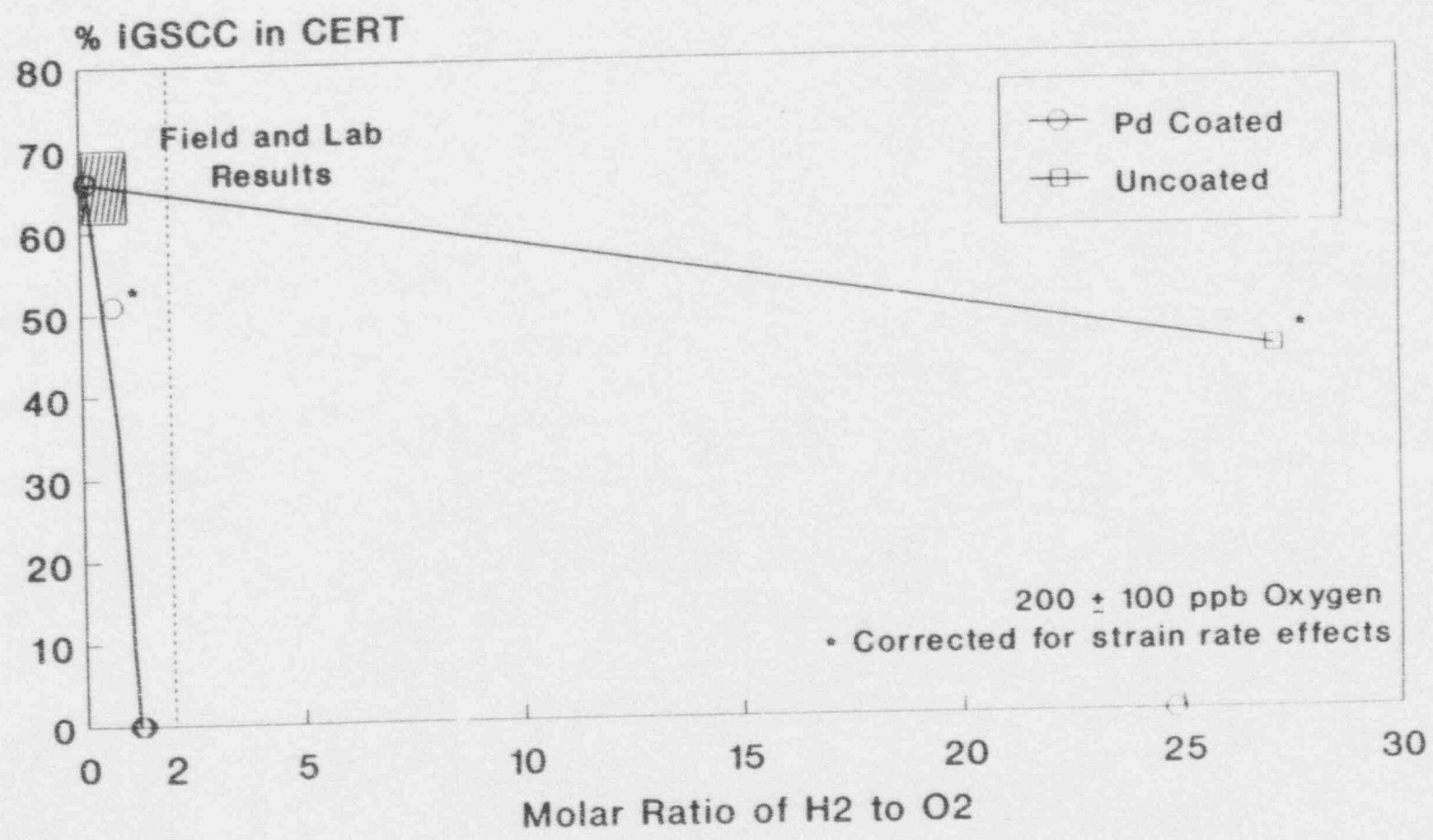


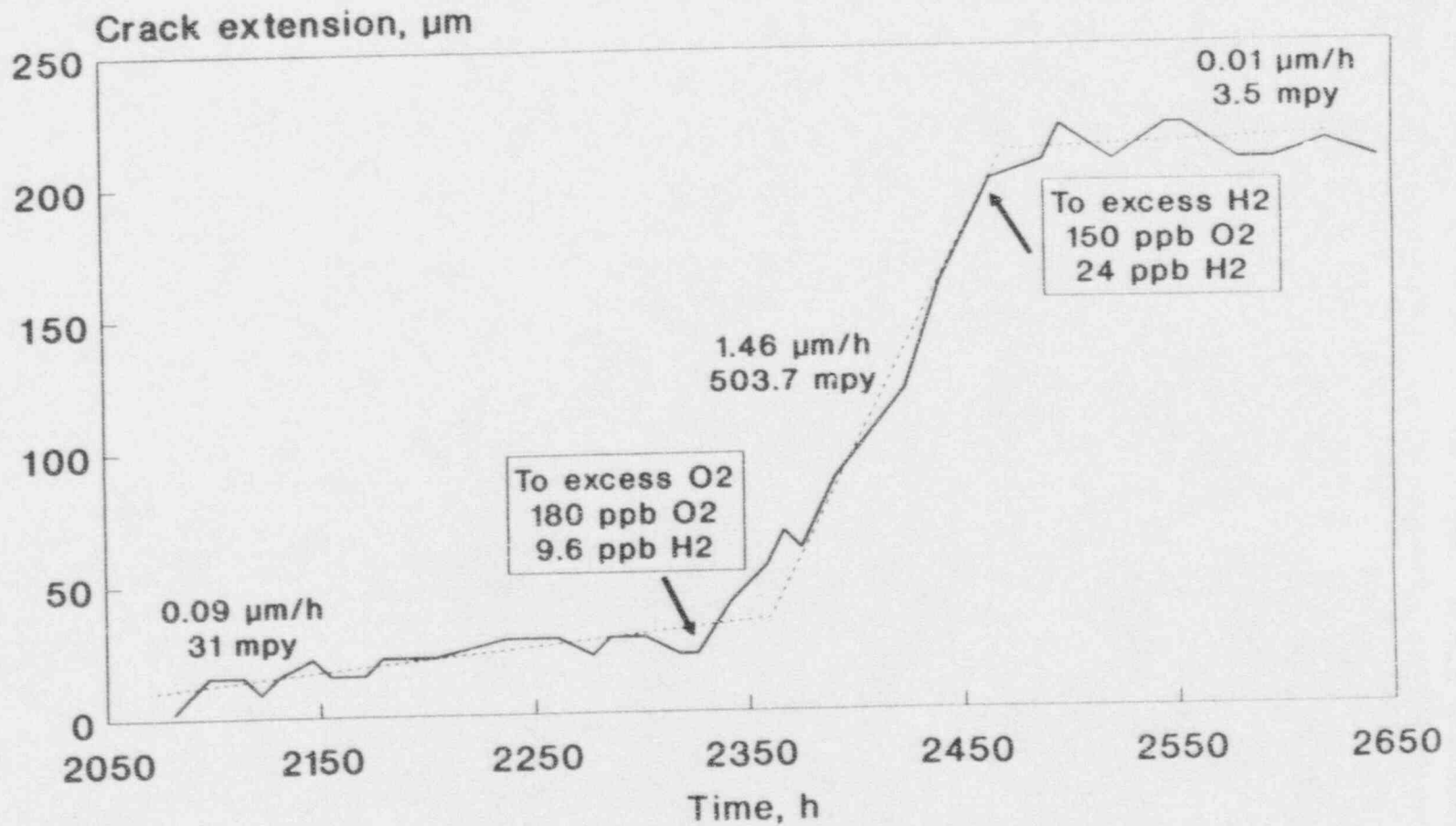
Figure 4-2 - ECPs of Pd-coated Type 316 SS in 300 ppb Oxygenated Water at 282C



62

Figure 4-3 - Effect of Hydrogen/Oxygen Molar Ratio on IGSCC of Pd Coated and Uncoated FS Type 304 in CERT at 288C

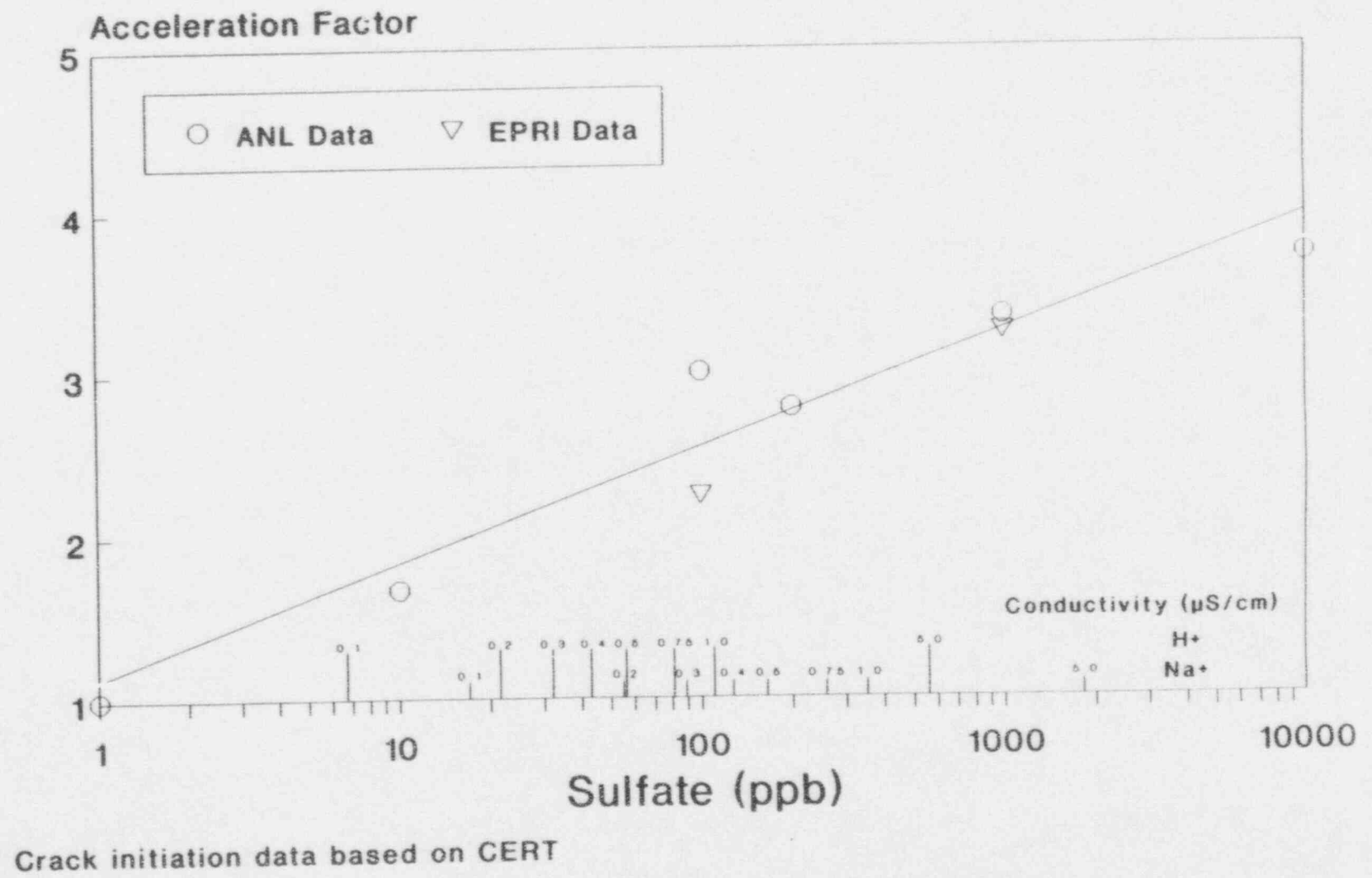
63



Coated in shallow water by HVOF/T309L SS
 K = 33MPa√m, R = 0.7, 0.01 Hz after 200s
 0.435 µS/cm H₂SO₄

Figure 4-4 - Effect of 0.42% Pd Coating on Crack Propagation in FS Type 304

64



Crack initiation data based on CERT
Figure 4-5 - Effect of Concentration and Conductivity on FS Type 304 IGSCC Initiation

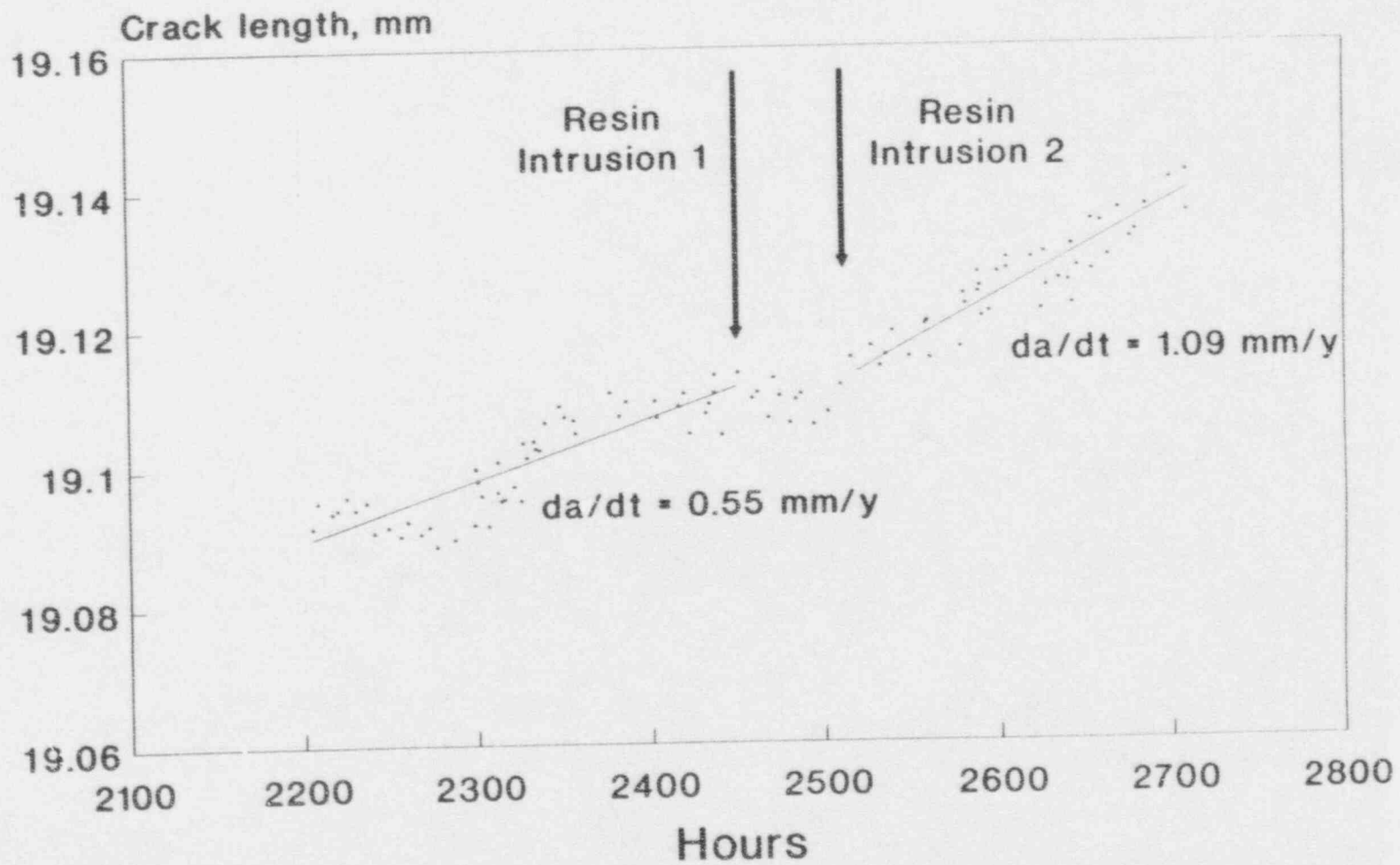


Figure 4-6 - Peach Bottom 3 Response to June 1986 Water Chemistry Transient

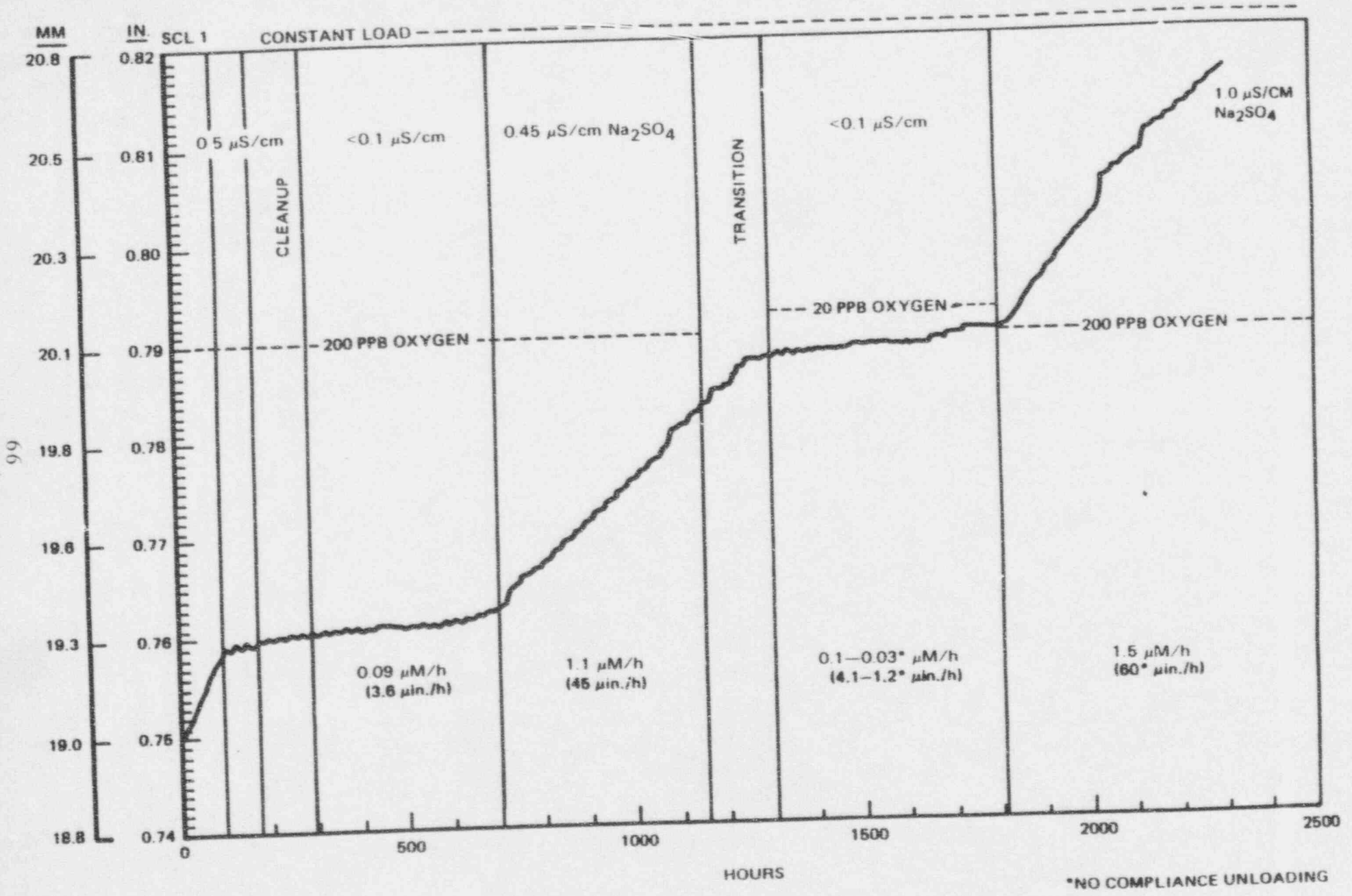
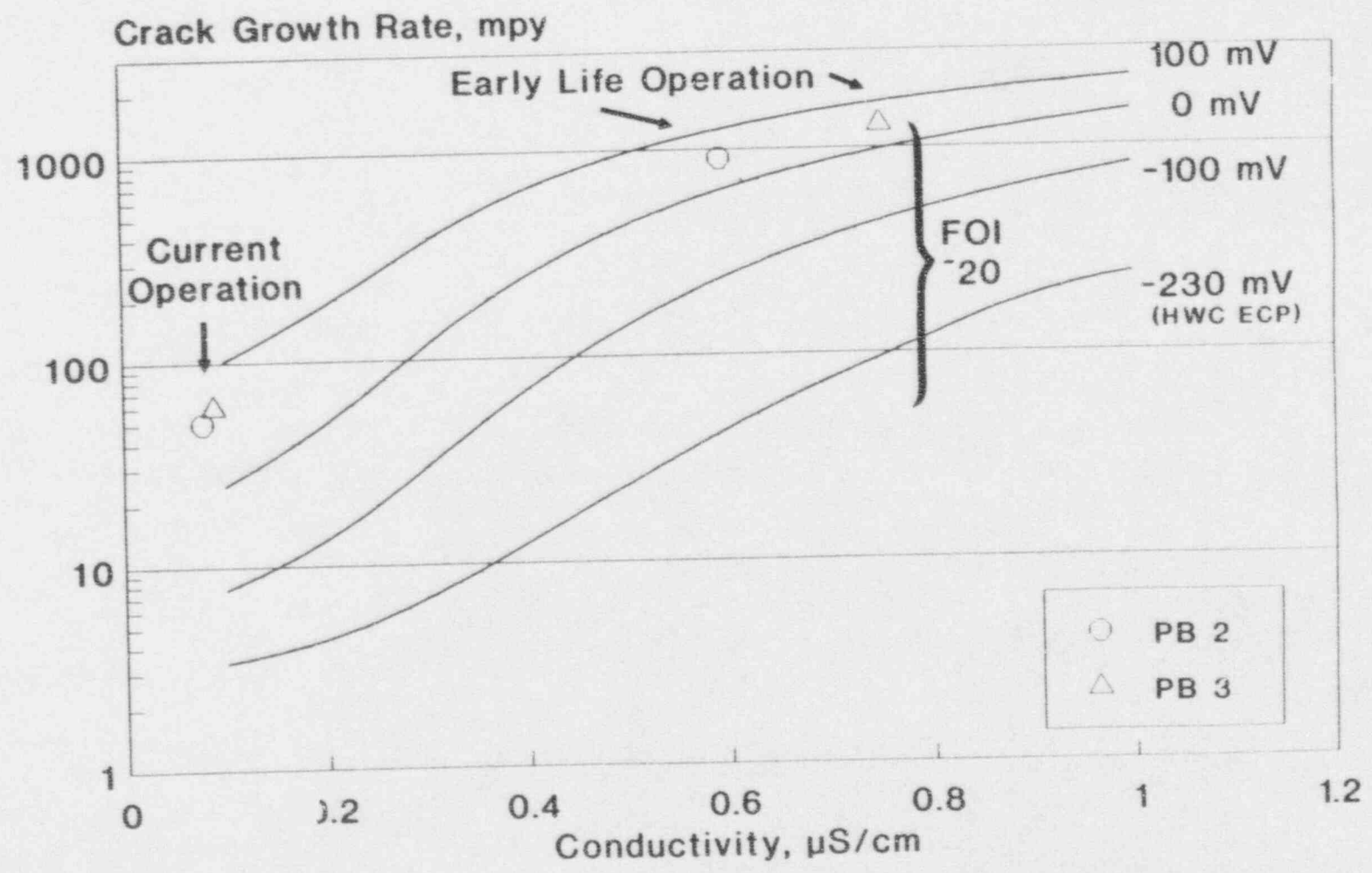


Figure 4-7 Crack Length vs. Time, Sensitized Type 304 Stainless Steel 286C Oxygenated Water Environment
 $K = 28.5$ to $30.5 \text{ MPa}/\sqrt{\text{m}}$ (26 - $28 \text{ ksi}/\sqrt{\text{in}}$)

67

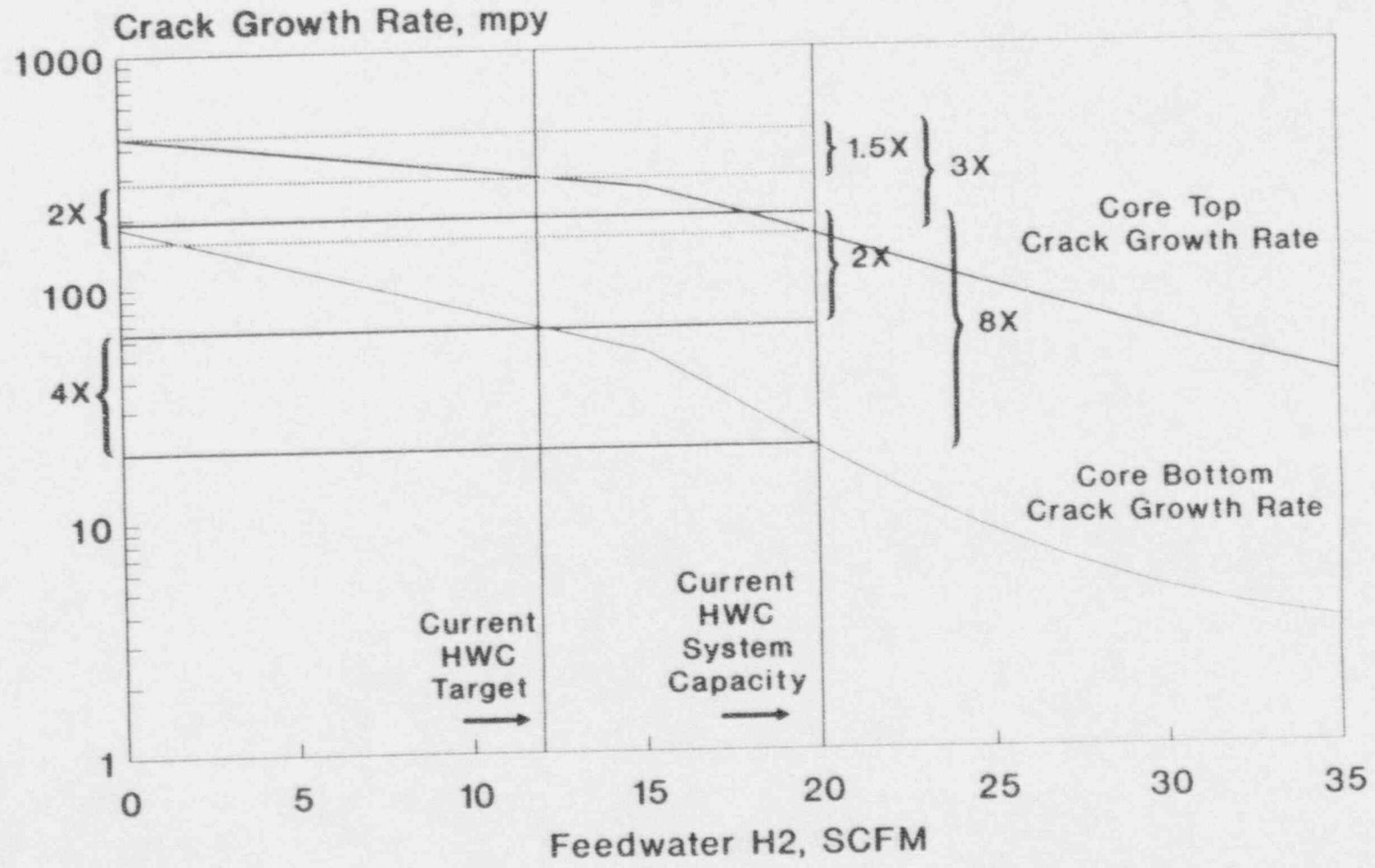


Estimated CGRs for ECP 0-100 mV[SHE]

PLEDGE: 15 C/cm², 25ksi/in

Figure 4-8 - GENE PLEDGE Model Prediction for Peach Bottom Type 304 Crack Growth

68

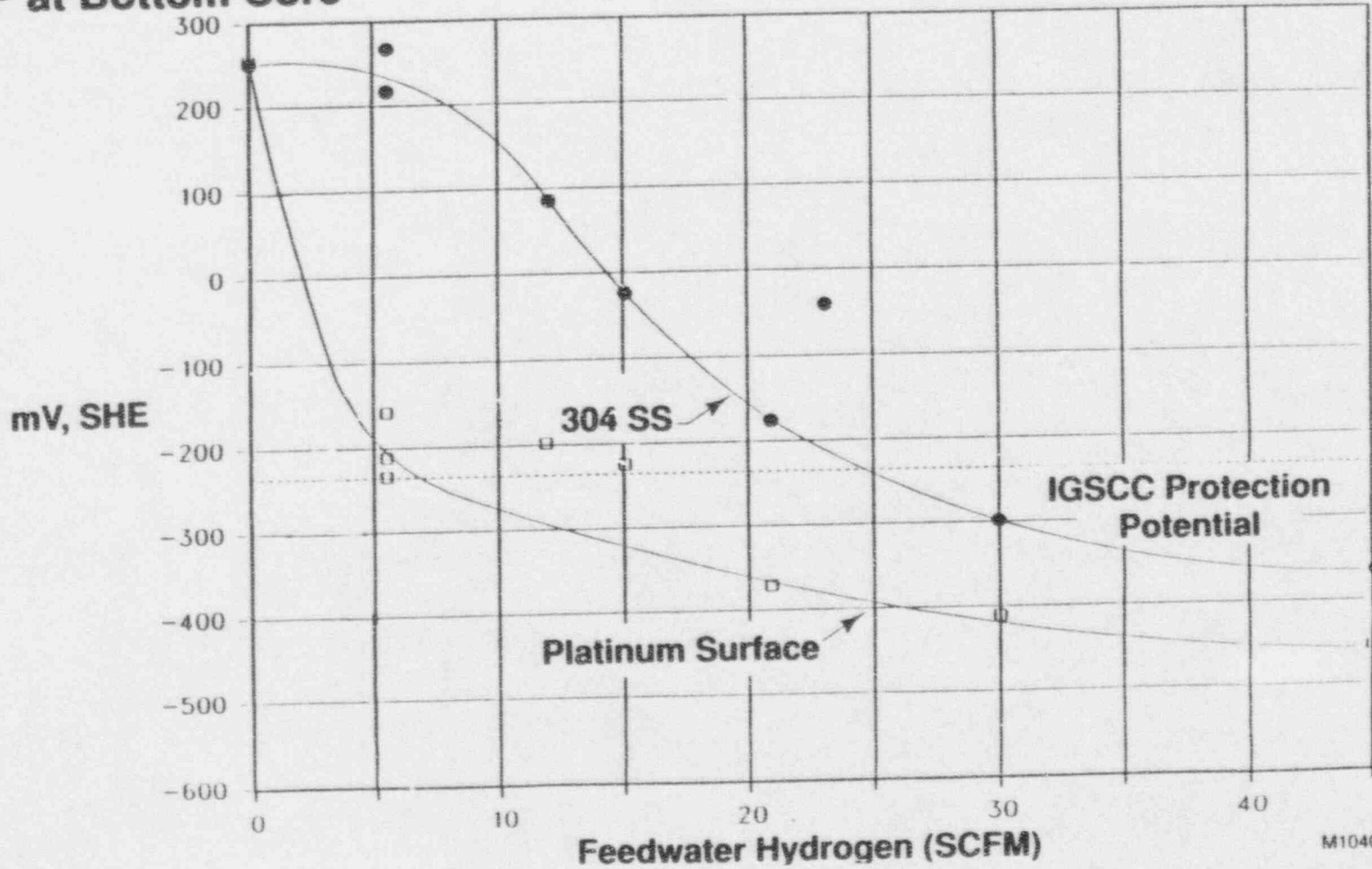


PLEDGE: 25 ksi√in, 15 C/cm², 0.12 μS/cm

ECP based on FitzPatrick

Figure 4-9 - Effect of H₂ Injection Rate on Calculated IGSCC Rate for Brunswick 1

ECP at Bottom Core



69

M10407 13

Figure 4-10 - Comparison of ECP for 304 SS and Platinum Surfaces vs. Hydrogen Addition Rate for BWR 4

5.0 OPERATIONAL SYMPTOMS

This section on operational symptoms is included to address the potential situation if unexpected significant crack growth occurs during plant operation. The potentially affected plant operational parameters are identified, as well as the modes of reactor operation that are most likely to show these symptoms if the shroud has degraded to the point that significant, through-wall leakage can occur.

5.1 Functional Effects of Significant Leakage in the Upper Shroud

The primary abnormal effect of significant leakage through the top portion of the core shroud assembly is that a portion of the steam-liquid flow leaving the core will bypass the steam separators. The bypass leakage will instead flow directly into the vessel annulus region.

The left side of Figure 5-1 shows the normal flow and fluid enthalpy pattern for a typical BWR unit. A postulated situation with some shroud leakage is shown on the right side of Figure 5-1. Several fluid paths are mixing in this bulkwater/annulus region of the vessel. The normal mixing process involves the combination of the following flow paths (typical full power values are given for a BWR/4 218 inch vessel plant):

- Downward liquid flow from the separators (66.2×10^6 lbm/hr)
- Carryunder steam flow ($.0025 \times \text{sep. liquid flow} = 0.17 \times 10^6$ lbm/hr)
- Drain flow (liquid) from the dryers ($\sim 1\%$ of steam flow = 0.1×10^6 lbm/hr)
- Feedwater flow (10.5×10^6 lbm/hr)

The subcooled feedwater flow (420°F, 398 Btu/lbm) mixes with the other, saturated flow paths, normally producing a downcomer enthalpy that is about 527 Btu/lbm (below saturation [subcooled] by about 18.7 Btu/lbm).

The right side of Figure 5-1 shows the same parameters, but assumes, for example, that significant leakage is occurring equivalent to 6% of the total core flow. This is approximately the amount of leakage that would occur with an equivalent crack height (Leakage area / Circumference of the shroud) of about 1/2 inch.

An initial calculation was made assuming that the power and core flow remained at the rated values. Subsequent calculational iterations were performed to adjust the power/flow for the new parameters. The results for the different flow paths are:

- Downward liquid flow from the separators (63.8×10^6 lbm/hr)
- Carryunder steam flow ($0.0025 \times \text{sep. liquid flow} = 0.148 \times 10^6$ lbm/hr)
- Drain flow (liquid) from the dryers ($\sim 1\%$ of steam flow = 0.1×10^6 lbm/hr)
- Feedwater flow (9.45×10^6 lbm/hr)
- Liquid leakage flow (4.1×10^6 lbm/hr)
- Leakage steam flow (0.15 quality in plenum above core gives 0.6×10^6 lbm/hr)

The subcooled feedwater flow (417°F, 395 Btu/lbm) still mixes with the saturated flow paths from the separators and dryers. However, the leakage flow increases the effective carryunder fraction to about 5 times normal. This raises the downcomer, recirculation loop, and core enthalpy to about 532 Btu/lbm, however, it remains below saturation [subcooled] by about 11.8 Btu/lb.

The change in subcooling (from about 19 to 12 Btu/lbm in this example) would not impact the recirculation system significantly because the net pump suction head (NPSH) margins remain adequate. However, the shroud leakage does change four other basic reactor parameters:

- The warmer recirculation water will become evident in the recirculation loop temperature monitors. For this example, the temperatures would be about 4°F above normal.
- The reduced core inlet subcooling will reduce reactor power. For this example, a power reduction of about 11% is expected.
- The leakage path essentially reduces the pressure drop in the flow path from the core upper plenum to the downcomer. This effect will produce a slight increase in the total core flow (assuming that the recirculation drive loop flow remains constant). For this example, a core flow increase of only about 1.5% is expected.
- The core flow effect will raise power about 1%, so that the overall power reduction will be from 100% to about 90%. Clearly this is the strongest indicator of the presence of leakage

For reasonable ranges of hypothesized effective crack size and resulting leakage, the power level signal is the strongest indication of an abnormal condition of the shroud. Figure 5-1 (right side) shows the approximate operating conditions with the 10% power decrease and the slight core flow increase.

The example case only produced a small change in the recirculation loop temperature. Close monitoring would be needed to identify this change. The temperature difference between the loops and the vessel dome (saturation) temperature is reduced to about 11°F, very close to the setpoint of the subcooling monitors on those units that have them.

If leakage develops on one side more than another, the symptoms may also include indications of non-symmetry: greater changes for one recirculation loop than the other(s). This asymmetry may also be seen in local core power (one side reduced more than the other).

If a larger leakage flow path is postulated, the downcomer subcooling could be reduced to the point where recirculation system cavitation is experienced. At about four times more leakage (leakage about ten times the normal amount of steam carryunder from the separators), the recirculation pump NPSH margin approaches zero. Plants with jet pumps would also approach cavitation at the jet pump suction and nozzle areas. Under these conditions, the recirculation system efficiency is reduced rapidly, and significant indications of low recirculation drive loop flow, low core flow, and additionally reduced power can be experienced. These signals may also show noisy and erratic behavior.

One other characteristic would be observed if a through shroud wall crack developed abruptly while the unit was at high power, steady state conditions. The rapid creation of leakage flow into the annulus region of the vessel could potentially cause an observable increase in the water level. This sequence of events could even raise the water level so that a high water level trip could be initiated. In the more probable case that the water level transient is not enough to reach the trip points, reactor operation will change to conditions displaying the other symptoms previously identified.

5.2 Specific Operational Parameters for Upper Shroud Leakage

The following monitored parameters will provide indication of abnormal conditions to the reactor operating staff. They are presented in the approximate order in which the indication would become significant as upper shroud leakage developed.

- (1) Reactor thermal power will be suppressed below its normal value for the selected rod pattern and core flow. A good way to observe this anomaly is to compare the power ascension trajectory versus core flow (as in Figure 5-2).

The process computer trend output information will clearly be helpful in these comparisons to normal. It is recommended that a baseline trajectory for these parameters should be established (if it does not already exist) in a useful format. This will enable utilities to perform this type of comparison to expected performance at each reactor startup.

The experiences observed at two BWRs (in 1984 and in 1991) used this type of comparison (between expected and observed power versus core flow) to discover problems associated with loose shroud head bolts. In those cases, physical motion of the shroud head occurred as the pressure drop became large enough to lift the upper shroud/separator assembly. At that power-flow condition (about 80% power and 85% core flow), leakage began. In these cases, the motion of the shroud head and induced leakage was restricted by the bolts that were in place.

For upper shroud leakage without significant shroud motion, there will not be such a distinct characteristic change at a particular power-flow condition. Power will be suppressed over the whole power versus flow range. If some motion is postulated (e.g., only one side is intact, and the other tends to open further when the power-flow conditions exceed the point of lifting pressure drop), then some of the distinctive characteristics of the loose bolts case may be experienced. This case (shroud lifting) is quite remote because it takes such a small amount of remaining ligament (even on one side) to maintain shroud integrity and geometry.

- (2) Those plants that have recirculation loop cavitation instrumentation could reach those setpoints if large leakage flow occurs from the upper shroud. All plants would be able to observe the increase in recirculation drive loop temperature

above normal. If cavitation conditions are actually encountered, the loop flow, jet pump diffuser flow, pump head, and vibration monitoring instruments may display noisy, erratic signals.

It is recommended that baseline characteristics of normal recirculation loop temperature versus power and flow conditions be established so that an abnormal pattern can be detected. Figure 5-3 shows a typical pattern for recirculation loop temperature during the upper portion of the ascension to full power. The differences calculated for the example case of shroud leakage are also shown.

- (3) The characteristic that a slight increase in core flow may be observed due to the reduced pressure loss in the shroud/separator region can also be monitored. This anomaly can be discovered by comparing the core flow to drive loop flow (in a jet pump plant), or by comparing core flow to couplet scoop tube position or pump speed (for all MG set plants). Figure 5-4 shows a typical relationship between core flow and drive flow, and the type of anomaly that may be observed. This sensitivity is not very strong for potential equivalent crack sizes up to the 1/2 inch upper shroud leakage example shown here.

The baseline relationship of these parameters along the rated flow control rod line should be established for use in detecting abnormal operation.

- (4) If bypass leakage develops on one side of the upper shroud more than another, the symptoms may also include indications of non-symmetry in the core power (one side reduced more than the other), or greater changes for one recirculation loop than the other(s).
- (5) In the unlikely case that upper shroud leakage develops abruptly during normal steady state operation, a rising water level transient would be created. Such a transient could reach the high water level trip setpoints. If the unit does not trip on high water level, it will shift to operating conditions with the characteristics described in the previous items.
- (6) The discussion of these symptoms is most applicable to the upper shroud area associated with weld areas H1 and H2. These areas see the full, two-phase mixture being discharged from the core. The H3 weld area is below the fuel top

guide. It is primarily exposed to the bypass region flow which is heated, but the mixture quality is lower than the core exit. A significant leak in this area would draw some two-phase flow from the plenum above the core in addition to the heated water. However, the symptoms would be smaller than if the cracking developed higher in the shroud.

5.3 Functional Effects of Leakage in Beltline or Lower Shroud Areas

If large cracking occurs lower on the shroud, in the beltline zone or lower, it does not produce observable symptoms. The fluid that would leak through the shroud wall would be partially heated water from the outer bypass region outside the fuel bundles. It would only produce a very small change in the temperature of the recirculation and core inlet flow, and no detectable change in power or loop temperature is expected. At the bottom of the shroud, the bypass region water is the same temperature as the recirculation flow in the vessel annulus and recirculation loops.

It is concluded that no detectable symptoms would accompany larger than expected cracking in the middle and lower shroud. All indications found so far are well below the allowable criteria, and no leakage has occurred through the shroud (in the upper, middle, or lower region of the shroud). Safe operation is assured for all areas by regular inspection of the shroud.

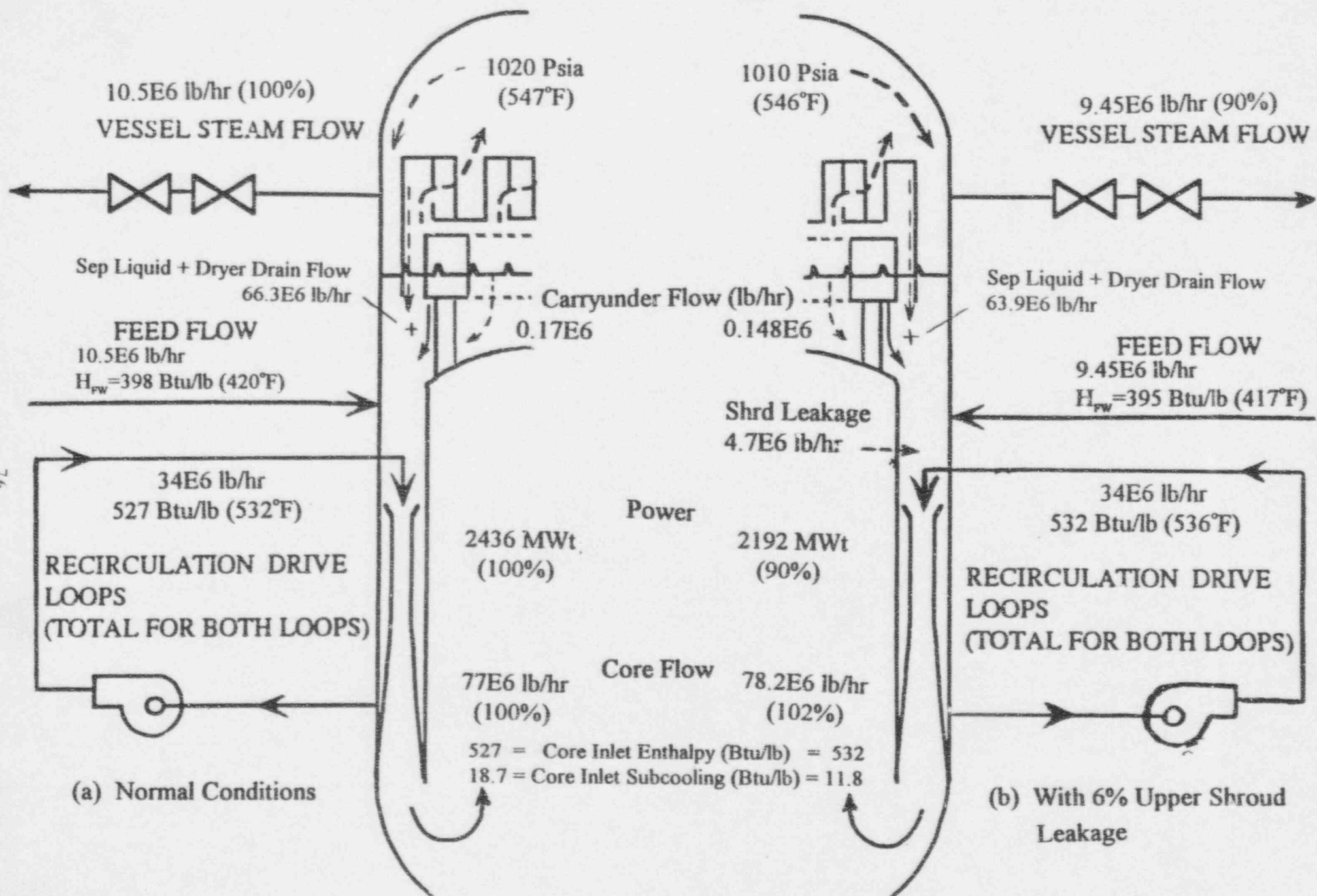


Figure 5-1 Typical Reactor Flow and Enthalpy Conditions Normal (Left) and With 6% Upper Shroud Leakage (Right)

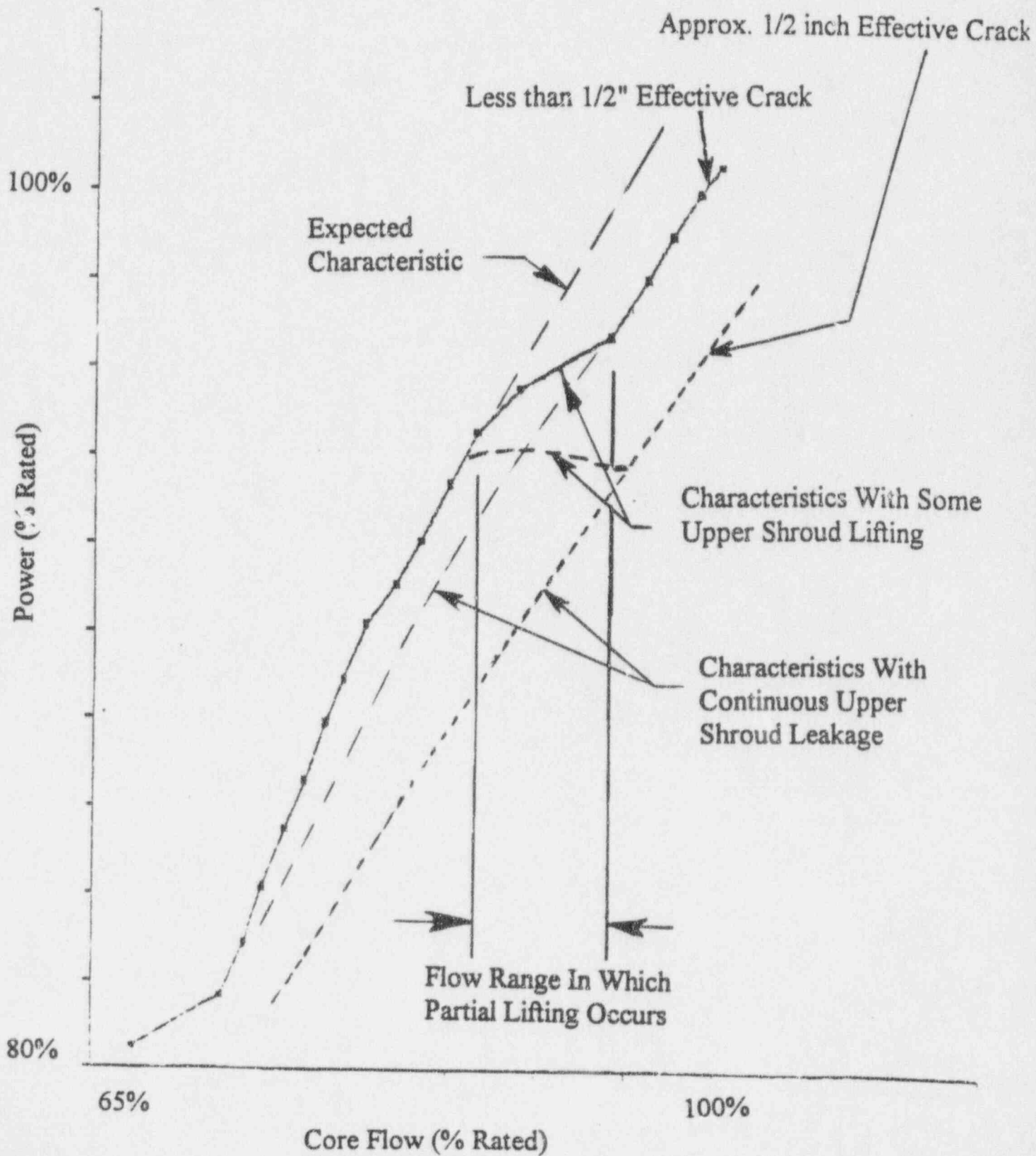


Figure 5-2 Typical Plant - Core Power vs Core Flow

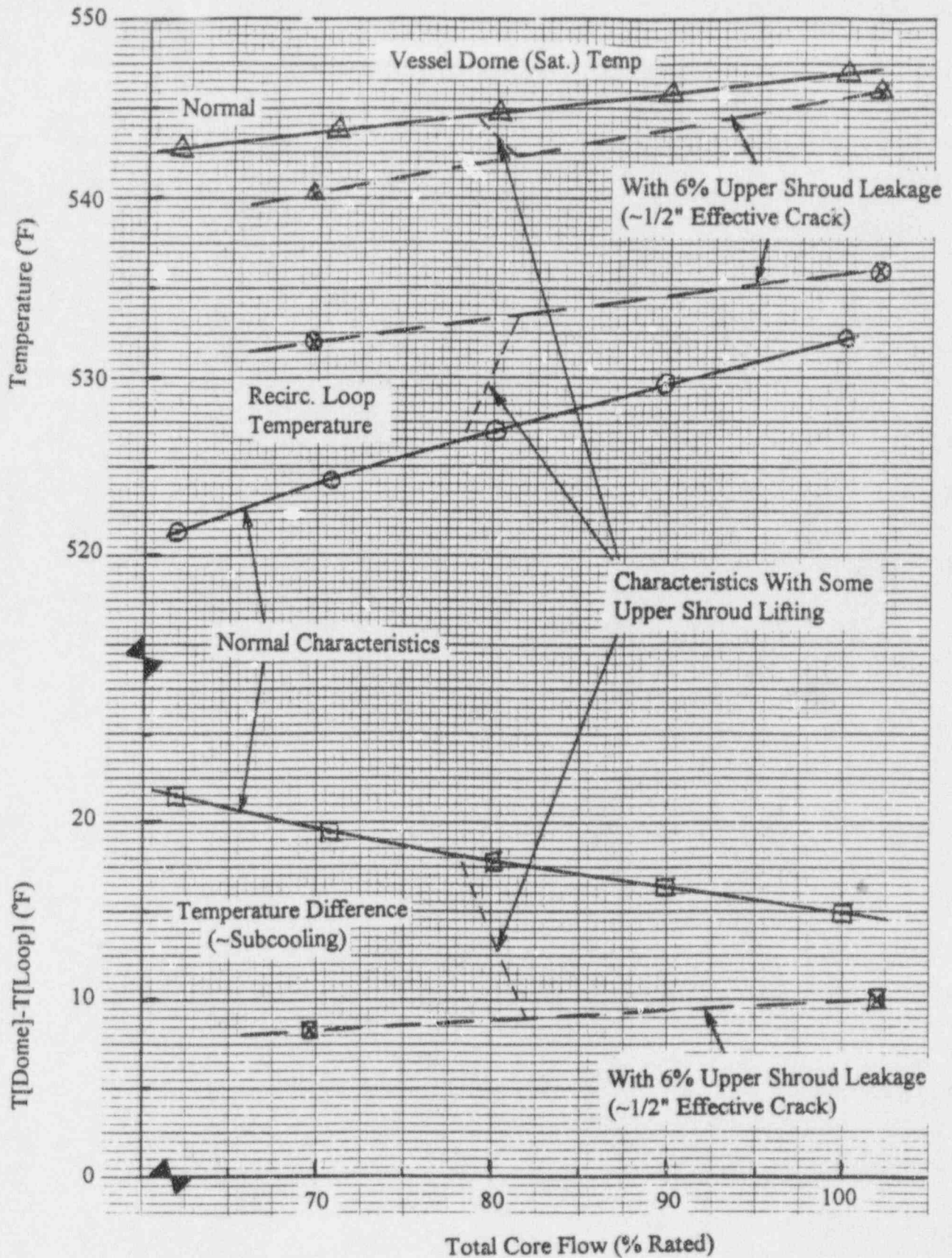


Figure 5-3 Typical Plant - Recirculation Loop Temperature and Vessel Dome (Saturation) Temperature vs Total Core Flow (100% Flow Control/Rod Line)

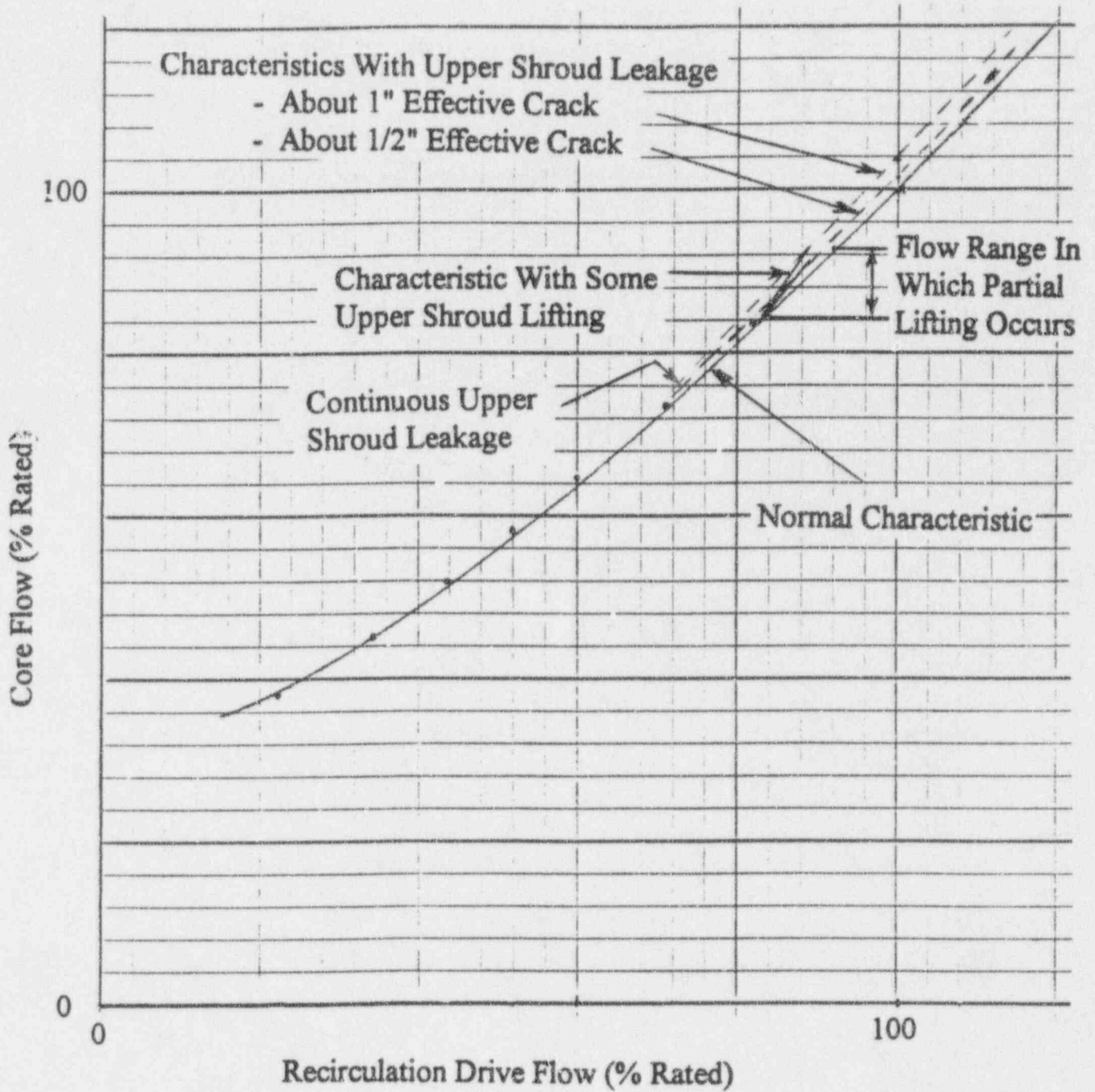


Figure 5-4 Typical Plant - Total Core Flow versus Recirculation Drive Flow (100% Flow Control/Rod Line)

6.0 INSPECTION STRATEGY

This section describes a strategy and integrated plan for shroud inspections. This program is designed to meet the intent of SIL 572 Rev. 1 while responding to utility specific needs. This discussion is based on shroud inspections to date and current available inspection equipment. The information in this section may require modification as new inspection equipment becomes available.

This strategy and recommendations are provided based on current knowledge of the shroud issue and experience at various plants. As more inspections are performed, some of these recommendations may change. The recommendations provided here are not mandatory, but provided to utilities as a guide in developing their plant-specific inspection plans. For example, the selection of VT or UT and consideration of inspecting for sufficient material to confirm structural margin could result in a modified inspection plan. Thus, the plant specific inspection plans may vary from those provided in this section.

The inspection recommendations provided here are considered applicable to all BWR's and exceed the requirements of ASME Code Section XI (where applicable, e.g., for BWR/6).

The specific goals of this inspection plan are to:

- Provide an integrated shroud inspection philosophy that:
 1. Meets the intent of the inspection recommendations in SIL 572 Rev. 1
 2. Meets utility requirements
 3. Contains a defensible basis, and
 4. Can be applied uniformly and consistently from plant to plant
- Provide a strategy to minimize the impact of the shroud inspections on the overall outage.

6.1 Susceptibility Factors

SIL 572 Rev. 1 recommends a review of shroud fabrication records and operating history for each plant. The purpose of this review is to determine the relative degree of shroud susceptibility to cracking. This will affect the decision process to determine what types

and to what extent inspections should be performed. In some situations a repair contingency package may be applicable.

The susceptibility evaluations involve a combination of absolute and relative comparisons to other information and data and can be quite subjective. As new information becomes available the perceived susceptibility of the plant to shroud cracking may change.

In considering the relative susceptibility of one BWR plant versus another, there are several key parameters that must be evaluated. These include materials, fabrication, water chemistry, neutron fluence, and IGSCC/IASCC history of other in-reactor components.

1. Materials: Material composition, in general, and carbon content more specifically, can have a major affect on shroud IGSCC susceptibility. Bimetallic welds utilizing Ni-Cr-Fe material (Alloy 182) have higher susceptibility than stainless materials. Laboratory tests and field experience conclude that components with a higher carbon content are more susceptible to cracking than a lower carbon equivalent.

The primary effect of carbon content is to increase the degree of sensitization in the as-welded condition, which is related to the minimum chromium content of the chromium depleted regions at the material grain boundaries, and thus the IGSCC susceptibility. A series of time to failure tests versus percent carbon have been performed in the GE pipe test labs for 304 stainless steel in 288°C oxygenated water. In general, based upon the results of the pipe tests and field experience, it appears that those plants with materials containing above 0.05% carbon are in the highest susceptibility category, those with 0.04% to 0.049% are in the intermediate category, and those with less than 0.04% are in the most resistant category.

2. Fabrication: The fabrication processes and weld designs affect IGSCC susceptibility. Examples of higher susceptible fabrication techniques include designs containing crevices, welds utilizing backing rings, high weld residual stress from fitup, and the orientation of plate materials that result in the laminations exposure to the oxidizing environment (presence of surface cold work, cool down rate from solution heat treatment temperature, weld repair, fit-up stresses, etc.).
3. Water chemistry: Water chemistry can be divided into steady state and transients. Steady state involves maintaining/sustaining proper chemistry such as low conductivity. Transients are short term events such as seawater and resin intrusions. Transients and poor water chemistry have been shown to increase IGSCC susceptibility. A significant contributor to shroud condition is plant conductivity

history (early life vs. overall operation, presence of severe potentially damaging transients, etc.).

GE has performed a considerable amount of laboratory testing and analytical modeling of material susceptibility to IGSCC as a function of conductivity. Based upon this data, it was observed that a plant operated early in life with a conductivity of about $0.5 \mu\text{S}/\text{cm}$ has about a five to tenfold increase in IGSCC propensity when compared to a plant that has operated at $0.1\text{-}0.2 \mu\text{S}/\text{cm}$. Field data has, in general, supported this conclusion. As a measure of ranking, the most susceptible category would be for those plants that have operated for the first five operating cycles with conductivity above $0.5 \mu\text{S}/\text{cm}$. The next most susceptible category would be those plants that have operated between 0.3 and $0.5 \mu\text{S}/\text{cm}$, and the least susceptible category would be those plants that operated below $0.3 \mu\text{S}/\text{cm}$ consistent with the EPRI Water Chemistry Guidelines Action Level 1 values.

4. **Fluence:** The shroud fluence distribution is a function of core design/configuration and operating power history. The threshold fast neutron fluence ($E > 1\text{mev}$) for initiation of IASCC (Irradiated Assisted Stress Corrosion Cracking) is approximately $5 \times 10^{20} \text{ n}/\text{cm}^2$ based upon test data. IASCC has been observed to occur below the predicted initiation threshold if classic IGSCC is also present. This observation is based upon metallurgical evaluations of a boat sample of a core shroud whose fluence was approximate $3 \times 10^{20} \text{ n}/\text{cm}^2$. Based upon this data, plants with shrouds having fluences above $5 \times 10^{20} \text{ n}/\text{cm}^2$ are considered susceptible to IASCC. Plants with fluences below $3 \times 10^{20} \text{ n}/\text{cm}^2$ are not considered susceptible to IASCC.

In addition, the plant specific cracking history is an indicator of shroud susceptibility. The presence of previous cracking in other components of a plant such as shroud head bolts, access hole covers, recirculation piping, and core spray spargers/piping would suggest a greater susceptibility for shroud cracking. It is also useful to review/compare inspection results from other plants with similar shroud susceptibility factors when known.

6.2 Inspection Plan

Figure 6-1 is a graphic representation showing the relationship between SIL 572 Rev. 1 (top level document containing the bases for the inspection recommendations) and the site specific inspection strategy, tools and procedures.

The first step to generating a plant specific inspection plan consists of reviewing SIL 572 Rev. 1 for applicability. The factors affecting shroud susceptibility to cracking are then

evaluated. The inspection plan is developed by utilizing the susceptibility factors in combination with the utility specific input. The utility specific input includes outage and inspection specific goals as well as the integration of the shroud inspection with other site activities.

6.2.1 Inspection Strategy

Inspection Recommendation Summary

The following is a summary of the key inspection recommendations:

- Inspect at the appropriate refueling outage as indicated by SIL 572, Rev. 1 criteria, susceptibility factors, etc.,
- Perform either an Enhanced VT-1 or UT inspection. Decision of UT vs. VT is dependent on a plant specific evaluation (i.e., time cost/benefit, history, susceptibility)
- Determine the extent of cleaning required, and perform as appropriate,
- Perform inspection on a significant statistical sampling based upon perceived susceptibility to cracking, and
- Re-examine every second outage if no cracking is observed.

The strategy invoked to accomplish this is to perform a susceptibility evaluation of the shroud and to characterize its susceptibility to cracking as either low, medium, or high. Then, each utility should compare the benefits of each type of exam (UT or VT) such as minimum sample size prior to selecting the exam technique.

Inspection Philosophy

The inspection philosophy is to start with the smallest data set that will provide justification for continued operation in the absence of cracking. If the inspections were performed visually on a limited data set, then the data set must be expanded if cracking is observed. One domestic utility inspected for 8 weeks with a combination of VT and UT to fully map out the cracking. An alternative is to use UT to simultaneously detect and characterize the cracking. This may be very cost effective as a proactive inspection alternative if substantial cracking is anticipated.

The two welds initially targeted for the inspection are the H3 and H4 welds. The H3 weld (shroud to top guide support ring) is susceptible to IGSCC due to the highly oxidizing environment. Some plants additionally have shrouds with top guide support rings that have been fabricated in a manner that may make it more susceptible to IGSCC. The H4 or beltline weld is the most susceptible to IASCC since it is located in the high flux region and thus has the highest fluence.

It is believed that the H3 and H4 weld are the most susceptible welds to IGSCC and IASCC, respectively. Therefore, the initial examination data set should be based upon these two welds. The recommended initial UT inspection for all risk plants (High, Medium, Low) is full inspection of the H3 and H4 welds.

Inspection Plan 1: Low Risk Plants

A low risk plant is not expected to experience shroud cracking at this time. Therefore, the strategy is for a minimum visual inspection. In general, low risk plants have had good water chemistry, low fluence, have shrouds made of low carbon materials and do not have substantial fabrication anomalies (e.g., weld repairs) and have no reported IGSCC of other in-reactor components. A recommended strategy involves:

- Limited enhanced VT-1 inspection. Surface preparation is considered by comparing cleaned and non cleaned surface resolutions.
- Minimum number of weld locations selected.
- OD or ID depending on weld location.

A typical inspection plan for a low risk plant would include:

- Weld H3 - Examine 4 cell locations, preferably at highest neutron flux azimuths.
- Mid plane weld - Examine 4 cell locations, preferably at highest neutron flux azimuths.
- Shroud to shroud support weld - Examine 10% of weld length on OD at azimuths where access hole covers are located.

Alternative Plan 1 inspection: Use UT approach to establish baseline for future inspections. A complete UT with no findings may support a longer cycle prior to a reinspection.

Inspection Plan 2: Medium Risk Plants

A medium risk plant may have some limited shroud cracking. The screening criteria (flaw evaluation) can be utilized with other information to determine in advance the amount of inspection required for each weld. Identified shroud anomalies, such as weld repairs, areas with ground off lifting lugs, etc., should be inspected. Significant indications may result in "crack chasing" and/or UT for crack characterization. Performing UT initially in lieu of VT may be cost effective option. The inspection strategy for a medium risk plant is similar to the low risk plant.

A typical inspection plan for a medium risk plant would include:

- Weld H3 - Examine 8 cell locations, preferably at highest neutron flux azimuths
- Mid plane weld - Examine 4 cell locations, preferably at highest neutron flux azimuths
- Vertical weld - Examine 1 weld if cell already vacated
- Shroud to shroud support weld - Examine 10% of weld length on OD at azimuths where access hole covers are located
- Expand sample set if cracking is observed

Alternative Plan 2 inspection: Use UT approach to establish baseline for future inspections. A complete UT with no findings may support a longer cycle prior to a reinspection.

Inspection Plan 3: High Risk Plants

In general, high risk plants have had below average water chemistry, high fluence, have shrouds made of high carbon materials and may have some fabrication anomalies. Shroud cracking is expected for a high risk plant. The inspection strategy for a high risk plant should consider UT in lieu of VT as an alternative.

To summarize, for high risk plants:

- Weld H3 - Examine 8 cell locations, preferably at highest neutron flux azimuths

- Mid plane weld - Examine 8 cell locations, preferably at highest neutron flux azimuths
- Vertical weld - Examine 1 weld if cell already vacated
- Shroud to shroud support weld - Examine 10% of weld length on OD at azimuths where access hole covers are located
- Expand sample set if cracks are found

Alternative Plan 3 inspection: One plant with shroud cracking spent 8 weeks mapping and characterizing the cracks. Another domestic BWR took about 3 weeks to perform enhanced VT-1 on the original and expanded data set. UT is suggested for consideration as a proactive cost beneficial alternative to visual inspections. One overseas utility inspected 180 degrees of the shroud beltline weld in 8 hours using UT. The inspection was performed from the shroud OD, thus requiring no cell disassembly, and the cracking was detected and characterized simultaneously.

6.3 Inspection Techniques

The following is a brief discussion of the available shroud inspection techniques.

6.3.1 Visual Inspection

The enhanced VT-1 examination is the recommended technique for visual inspections. Visual examinations are typically performed from the refueling bridge. As a result, no other refuel activities are performed in parallel since the bridge cannot be moved. The following four major steps are involved:

1. Vacate fuel cells as applicable
2. Clean examination areas, if required
3. Inspect areas (ID and OD)
4. Evaluate results against screening criteria, then depending on results
 - No action required,
 - Expand VT sample set, or
 - Perform UT sizing

If no indications are observed, then the examination is complete and no further actions are required. If indications are present, then the sample set may need to be increased. In

addition, an ultrasonic examination may also be required (depending on results of screening criteria application) as a visual examination cannot fully characterize the crack.

6.3.2 Ultrasonic Examinations

Ultrasonic inspections have been performed on the shroud from the OD and ID at two plants.

A localized UT scanner was utilized on an overseas plant to characterize cracking on the beltline weld from the shroud ID. A second examination using a more sophisticated device was performed on a 180° segment of the beltline weld from the shroud OD. In this instance no fuel was removed since the inspection was performed from the OD. The ID and OD measurements were compared at the applicable area with good correlation.

A domestic utility performed ultrasonic measurements of some shroud cracking from the ID and the OD depending on location. Two boat samples were obtained from the H2 weld and the crack depth was physically measured which validated the UT technique.

6.3.3 UT/VT Comparison

This section is a comparison of VT and UT shroud examination. This is based on current available inspection equipment, and shroud inspection experience to date. This comparison should be reviewed and modified if needed as new inspection equipment becomes available.

VT and UT: Advantages & Disadvantages**Visual****Ultrasonic****Advantages**

Equipment readily available
Large experience base
Utilized for ID and OD
Images can be digitized and enhanced

Most exams from OD
No surface preparation
No cell disassembly
Detection/sizing performed simultaneously
Minimum impact on other vessel work
Faster than VT
Consistent and repeatable

Disadvantages

Surfaces may need cleaning
Indications may be missed
Fuel cells must be disassembled (ID)
Welds difficult to locate
Refuel bridge required
No through wall sizing
Frequent camera changeouts
Low repeatability
Subjective evaluation

More personnel required
New technology
Higher equipment costs

6.4 Recommendations

The following is a summary of BWROG recommendations relative to shroud:

- Susceptibility Investigation; Each utility should determine its relative susceptibility to shroud cracking.
- Screening criteria; The utility should perform flaw size evaluations in advance of the inspection to establish acceptance criteria.
- Plant specific objectives; The inspection goals must be established to determine the most effective inspection technique; short term and long term goals and philosophies should be considered.
- Integrate inspection plan into refuel floor activities; the shroud inspection should be incorporated into the refuel floor activities to optimize productivity and ,minimize outage length.
- Contingency repair package as appropriate; in cases where the shroud has been evaluated as having high susceptibility factors for cracking, the utility should have a contingency repair package in place.

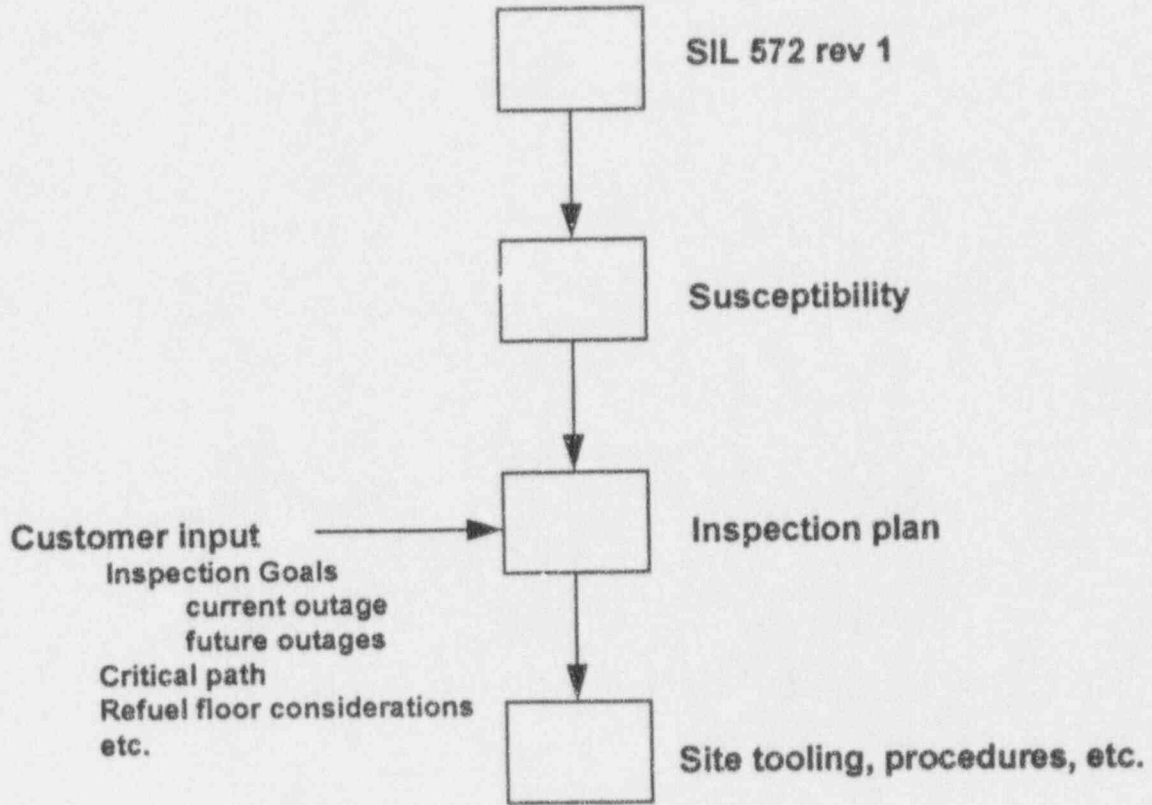


Figure 6-1 Shroud Inspection Plan Approach

7.0 SUMMARY

This report was prepared in response to recent cracking observed in the vicinity of core shroud welds at four boiling water reactors (BWRs). This report contains a discussion of various aspects of the shroud cracking issue and provides the generic tool which utilities may use to address shroud cracking concerns. These issues include: screening criteria, mitigation actions, operational symptoms, and inspection strategy.

The graded screening criteria was developed to provide the procedure for the evaluation of any indications. The screening criteria includes three steps, 1) acceptance standard, 2) visual screening criteria, and 3) UT screening criteria. If the indications meet the screening criteria, then the indications are considered to be acceptable for at least one fuel cycle without further evaluation. If the indications do not pass a particular level of the graded approach, the next level may be applied. For example, if the indications do not meet the acceptance standard, then the visual screening criteria may be applied. If the indications do not meet the UT screening criteria, then repair of the shroud may be required.

Information regarding mitigation of core shroud cracking was presented. This includes discussion of hydrogen water chemistry, water conductivity control, and noble metal plasma spray coating. The recent incidences of cracking have demonstrated the advantage of taking early precautions to lessen the potential and extent of IGSCC. Water chemistry, fabrication techniques, and material have been identified as being significant contributors to the potential for cracking.

Operational symptoms were discussed to address the potential situation if unexpected significant crack growth occurs during plant operation. The potentially affected plant operational parameters are identified, as well as the modes of reactor operation that are most likely to show these symptoms if the shroud has degraded to the point that significant, through-wall leakage can occur.

An integrated plan and strategy for shroud inspections was also presented. This program was designed to meet all the recommendations of SIL 572 Rev. 1 while responding to utility specific needs. The purpose of the inspection plan is to provide the link between SIL 572, Rev. 1 and the plant specific shroud inspection.

APPENDIX A - BASIS FOR THE CRACK GROWTH RATE

The basis for the crack growth rate used in the screening criteria is provided in this section. The shroud cylinder was fabricated from roll formed Type 304 or Type 304L stainless steel plate. Therefore, the weld heat-affected-zone (HAZ) is likely sensitized. The shroud is also subjected to neutron fluence during the reactor operation which further increases the effective degree of sensitization. The other side effect of neutron fluence induced irradiation is the relaxation of weld residual stresses. The slip-dissolution model developed by GE quantitatively considers the degree of sensitization, the stress state and the water environment parameters, in predicting a stress corrosion cracking (SCC) growth rate. The crack growth rate predictions of this model have shown good correlation with laboratory and field measured values.

A.1 Slip-Dissolution Model

Figure A-1 schematically shows the GE slip-dissolution film-rupture model (Reference A-1) for crack propagation. The crack propagation rate V_t is defined as a function of two constants (A and n) and the crack tip strain rate, ϵ'_{ct} .

$$V_t = A \epsilon'_{ct}{}^n \quad (\text{A-1})$$

$$\begin{aligned} \text{where } \epsilon'_{ct} &= CK^4 \quad (\text{for constant load}) \\ A &= 7.8 \times 10^{-3} n^{3.5} \quad (\text{from Reference A-2}) \\ n &\text{ is defined in Reference A-2} \\ K &= \text{stress intensity factor (units of MPa}\sqrt{\text{m)}} \end{aligned}$$

The constants are dependent on material and environmental conditions. The crack tip strain rate is formulated in terms of stress, loading frequency, etc. When a radiation field, such as the case for the shroud, is present, there is additional interaction between the gamma field and the fundamental parameters which affect intergranular stress corrosion cracking (IGSCC) of Type 304 stainless steel (see Figures A-2 and A-3).

The increase in sensitization (i.e., Electrochemical Potentiokinematic Reactivation, EPR) and the changes in the value of constant A as a function of neutron fluence (>1MeV) is given as the following:

$$\text{EPR} = \text{EPR}_0 + 3.36 \times 10^{-24} (\text{fluence})^{1.17} \quad (\text{A-2})$$

where, EPR is in units of C/cm^2 , fluence is in units of n/cm^2 and the calculated value of EPR has an upper limit of 30.

The constant C is defined as the following:

$$\text{for fluence} \leq 1.4 \times 10^{19} \text{ n/cm}^2: C = 4.1 \times 10^{-14} \quad (\text{A-3a})$$

$$\begin{aligned} \text{for fluence} > 1.4 \times 10^{19} \text{ n/cm}^2 \text{ but } \leq 3 \times 10^{21} \text{ n/cm}^2, \\ C = 1.14 \times 10^{-13} \ln(\text{fluence}) - 4.98 \times 10^{-12} \end{aligned} \quad (\text{A-3b})$$

$$\text{for fluence} \leq 3.0 \times 10^{21} \text{ n/cm}^2: C = 6.59 \times 10^{-13} \quad (\text{A-3c})$$

A.2 Calculation of Parameters

The parameters needed for the crack growth calculation by the GE model are: stress state and stress intensity factor, effective EPR, water conductivity, and electro-chemical corrosion potential (ECP).

The stress state relevant to IGSCC growth rate is the steady state stress which consists of weld residual stress and the steady applied stress. Figure A-4 shows observed through-wall weld residual stress distribution for large diameter pipes. This distribution is expected to be representative for the shroud welds also. The maximum stress at the surface was nominally assumed as 35 ksi. The steady applied stress on the shroud is due to core differential pressure and its magnitude is small compared to the weld residual stress magnitude. Figure A-5 shows the assumed total stress profile used in the evaluation. Figure A-6 shows the calculated values of stress intensity factor (K) assuming a 360° circumferential crack. It is seen that the calculated value of K reaches a maximum of approximately 25 ksi√in. The average value of K was estimated as 20 ksi√in and was used in the crack growth rate calculations.

The weld residual stress magnitude is expected to decrease as a result of relaxation produced by irradiation-induced creep. Figure A-7 shows the stress relaxation behavior of Type 304 stainless steel due to irradiation at 550° F. Since most of the steady stress in the shroud comes from the weld residual stress, it was assumed that the K values shown in Figure A-6 decrease in the same proportion as indicated by the stress relaxation behavior of Figure A-7.

The second parameter needed in the evaluation is the EPR. In the model, the initial EPR value is assumed as 15 for the weld sensitized condition. Using Equation (A-2), the predicted increase in EPR value as a function of fluence is shown in Figure A-8.

The third parameter used in the GE predictive model is the water conductivity. A water conductivity of $0.1 \mu\text{S}/\text{cm}$ was used in this calculation which is a reasonable value for many plants. To demonstrate that the GE model conservatively reflects the effect of conductivity, Figure A-9 shows a comparison of the GE model predictions with the measured crack growth rates in the crack advance verification system (CAVS) units installed at several BWRs. The comparison with CAVS data in Figure A-9 also demonstrates the conservative nature of crack growth predictions by the GE model.

The last parameter needed in the GE prediction model is the ECP. Figure A-10 shows the measured values of ECP at two locations in the core. The ECP values at zero H_2 injection in Figure A-10 was used in this calculation. It is seen that the ECP values at zero H_2 injection rate range from 150 mV to 225 mV. Therefore, a value of 200 mV was used in the calculation.

A.3 Crack Growth Prediction

Based on the discussion in the preceding section, the crack growth rate calculations were conducted as a function of fluence assuming the following values of parameters:

Initial K	= 20 ksi $\sqrt{\text{in}}$
EPR ₀	= 15 C/cm ²
Cond.	= 0.1 $\mu\text{S}/\text{cm}^2$
ECP	= 200 mV

Figure A-11 shows the predicted crack growth rate as a function of fluence. It is seen that the predicted crack growth rate initially increases with the fluence value but decreases later as a result of significant reduction in the K value due to irradiation induced stress relaxation. The crack growth rate peaks at 4.5×10^{-5} in/hr at a fluence of 1×10^{20} n/cm². Thus, a value of 5×10^{-5} in/hr can be used in the structural integrity evaluation for the shroud.

This crack growth rate is quite conservative as can be shown in Figure A-12 from NUREG-0313, Rev. 2. It is seen that the crack growth rate of 5×10^{-5} in/hr at

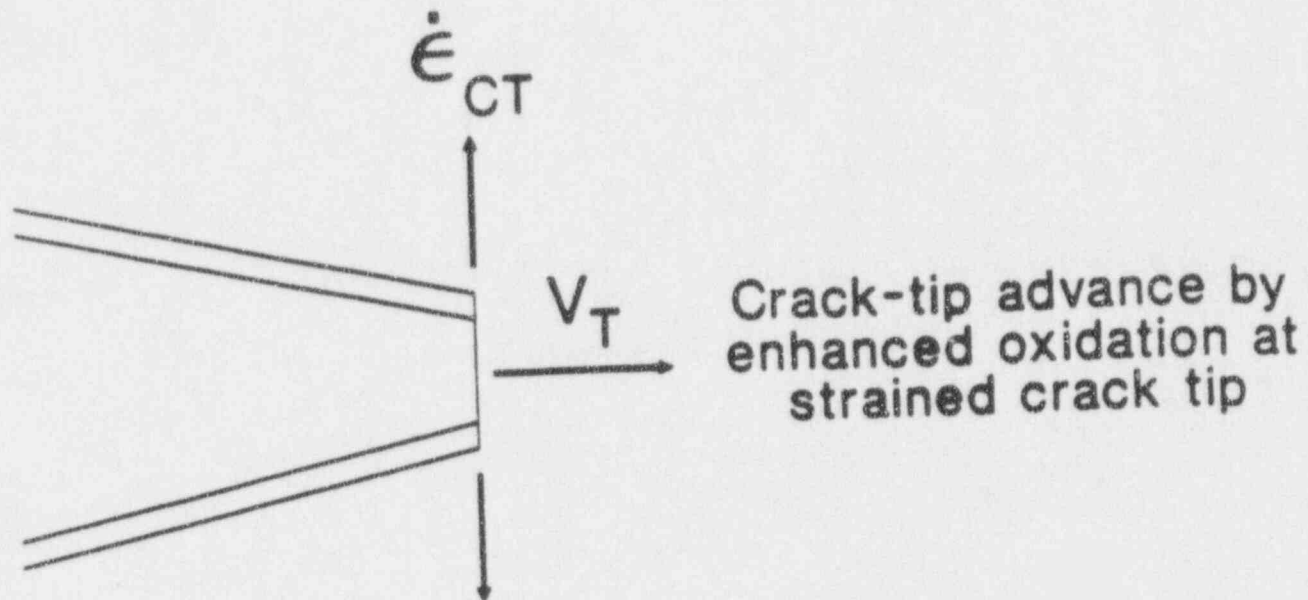
20 ksi/in is considerably higher than what would be predicted by using the NRC curve. This further demonstrates the conservatism inherent in the assumed bounding value of crack growth rate.

A.4 Conclusion

A crack growth rate calculation using the GE predictive model was conducted considering the steady state stress, EPR, conductivity and ECP values for a typical core shroud. The evaluation accounted for the effects of irradiation induced stress relaxation and the increase in effective EPR. The evaluation showed that a bounding crack growth rate of 5×10^{-5} in/hr may be conservatively used in the structural integrity evaluation of the core shroud.

A.5 Reference

- A-1 F.P. Ford et al, "Prediction and Control of Stress Corrosion Cracking in the Sensitized Stainless Steel/Water System," paper 352 presented at Corrosion 85, Boston, MA, NACE, March 1985
- A-2 F.P. Ford, D.F. Taylor, P.L. Andressen & R.G. Belanger, "Environmentally Controlled Cracking of Stainless Steel and Low Alloy Steels in LWR Environments," EPRI Report NP50064M, Contract RP2006-6, 1987.



$$V_T = A \dot{\epsilon}_{CT}^n$$

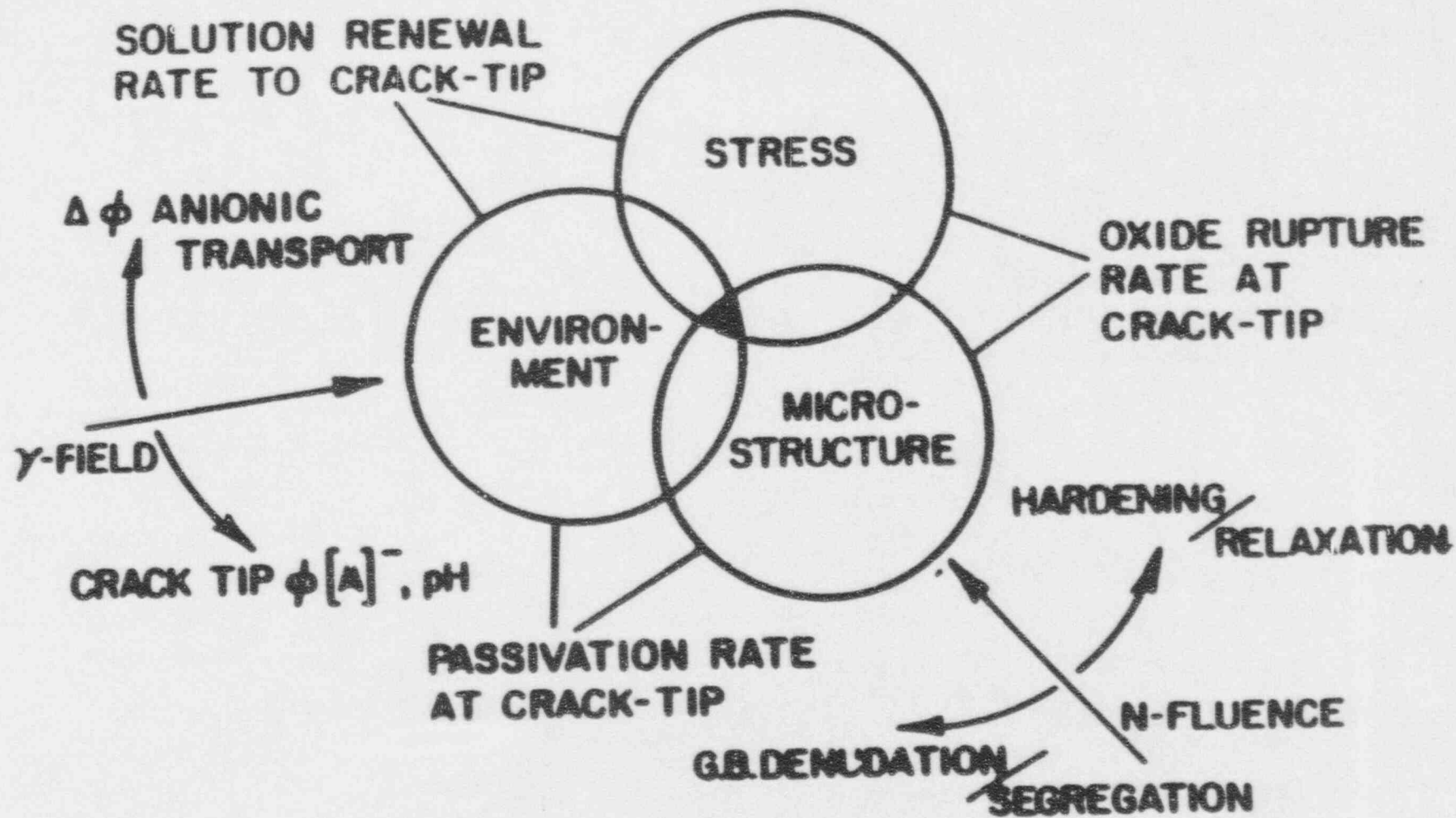
Where:

V_T = crack propagation rate

A, n = constants, dependent on material and environmental conditions

$\dot{\epsilon}_{CT}$ = crack-tip strain rate, formulated in terms of stress, loading frequency, etc.

Figure A-1 GE PLEDGE Slip Dissolution - Film Rupture Model of Crack Propagation



A-6

Figure A-2 Effects of Fast Fluence, flux & Gamma Field on parameters affecting IGSCC of Type 304 Stainless Steel

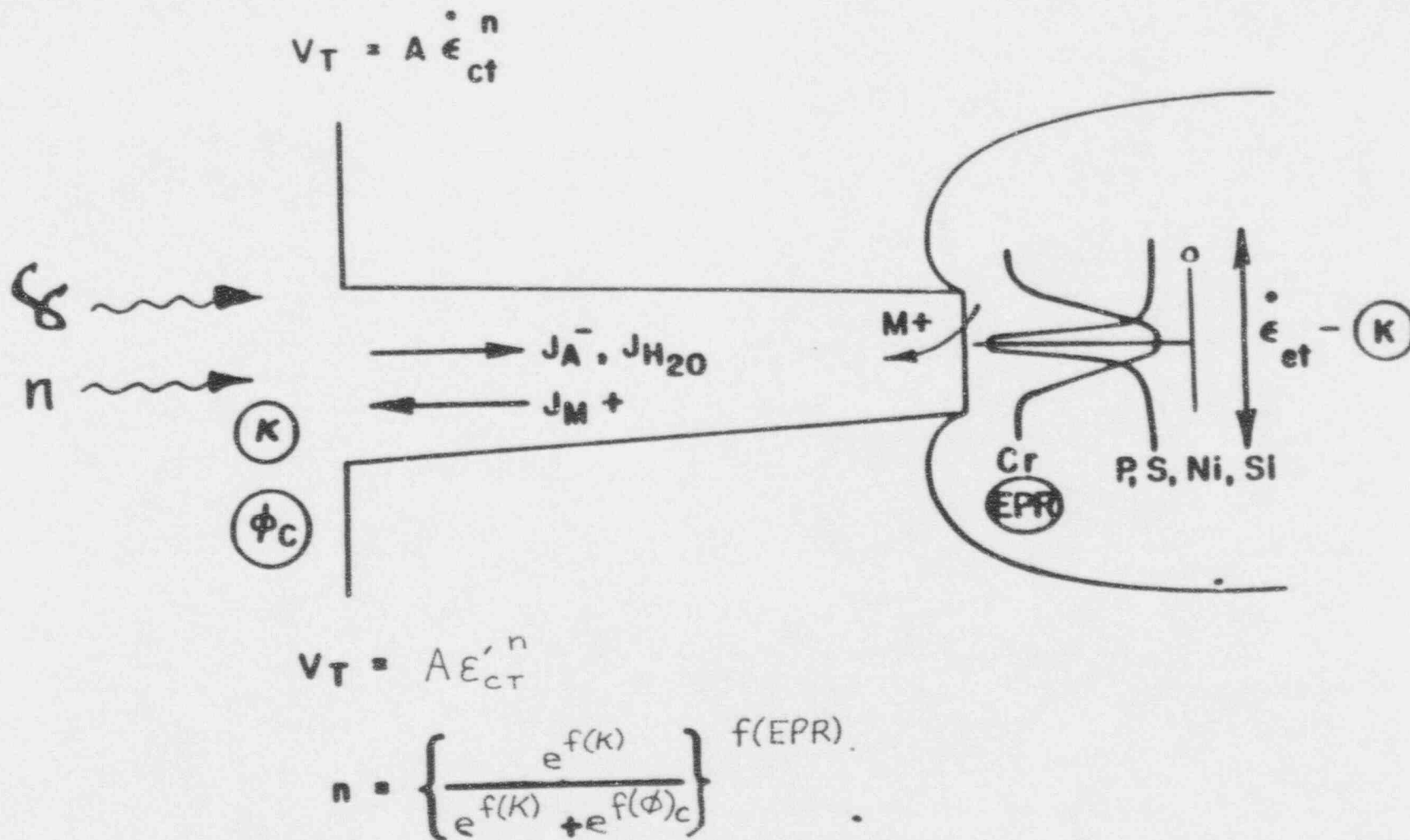


Figure A-3 Parameters of Fundamental Importance to Slip Dissolution Mechanism of IGSCC in Sensitized Austenitic Stainless Steel

**OBSERVED RESIDUAL STRESS PROFILES
IN HAZ OF 24"-28" DIA. SCH. 80 PIPING**

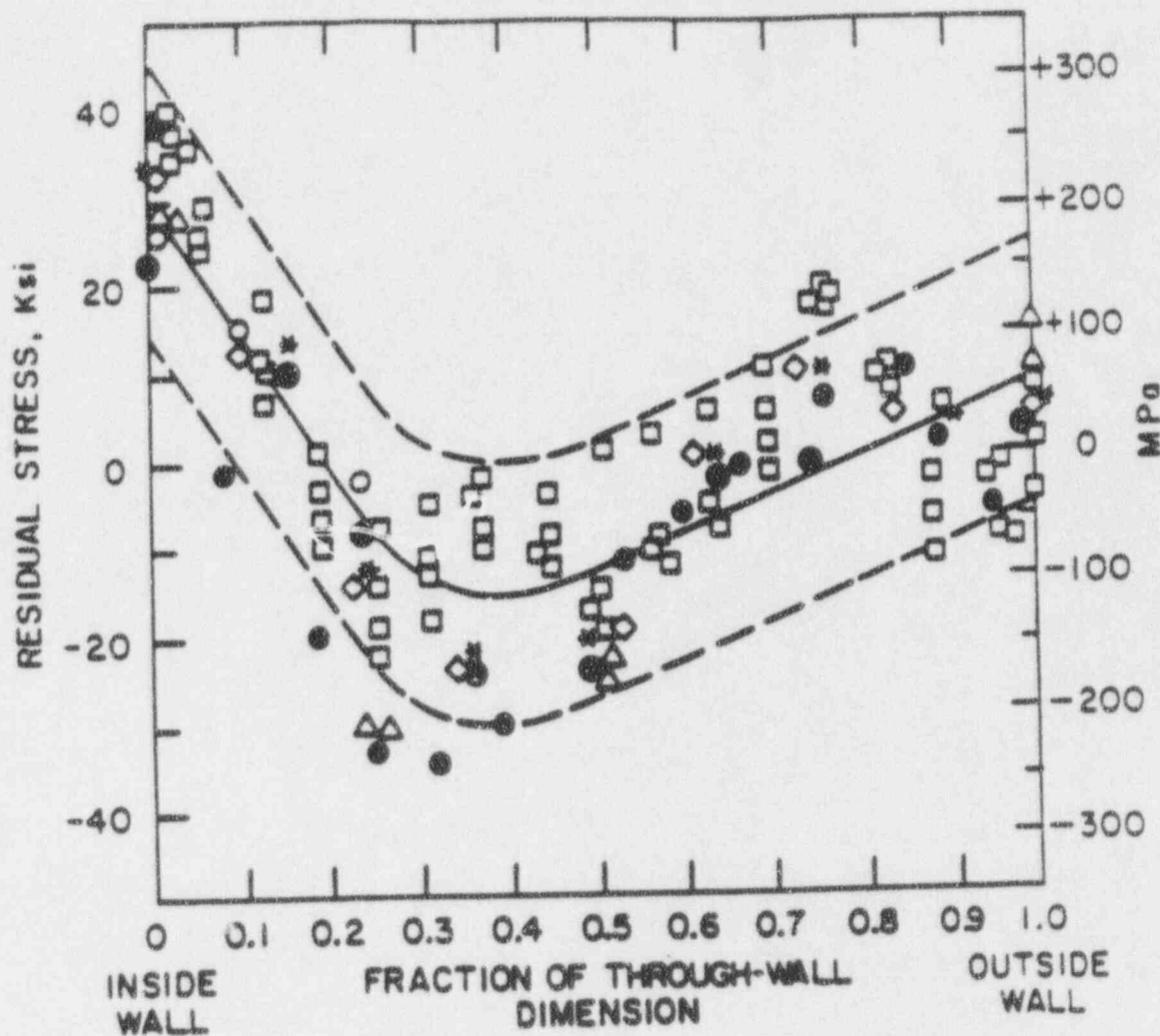


Figure A-4 Throughwall longitudinal residual stress data adjacent to welds in 12 to 28 inch diameter stainless steel piping

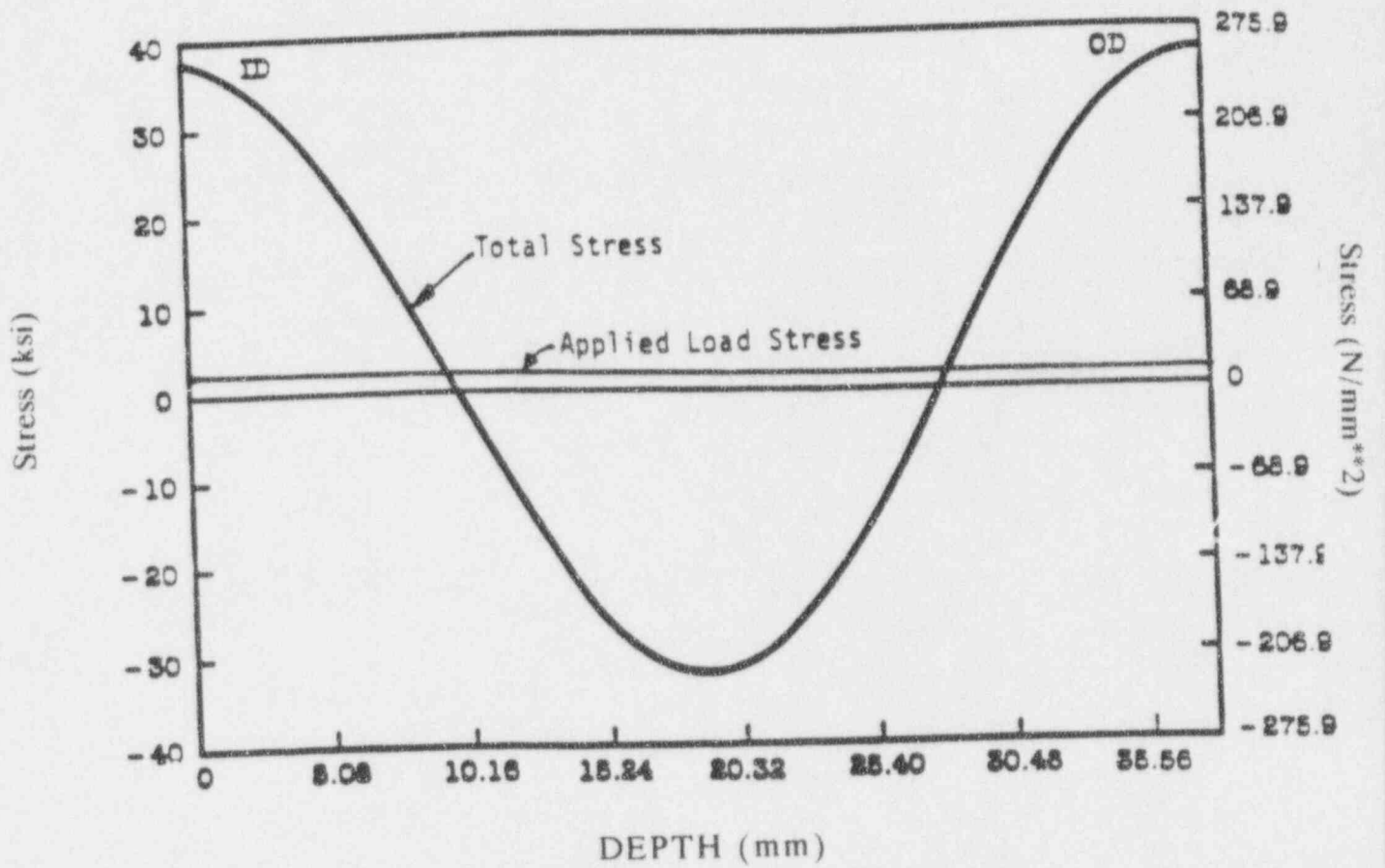


Figure A-5 Shroud Total Throughwall Stress Profile

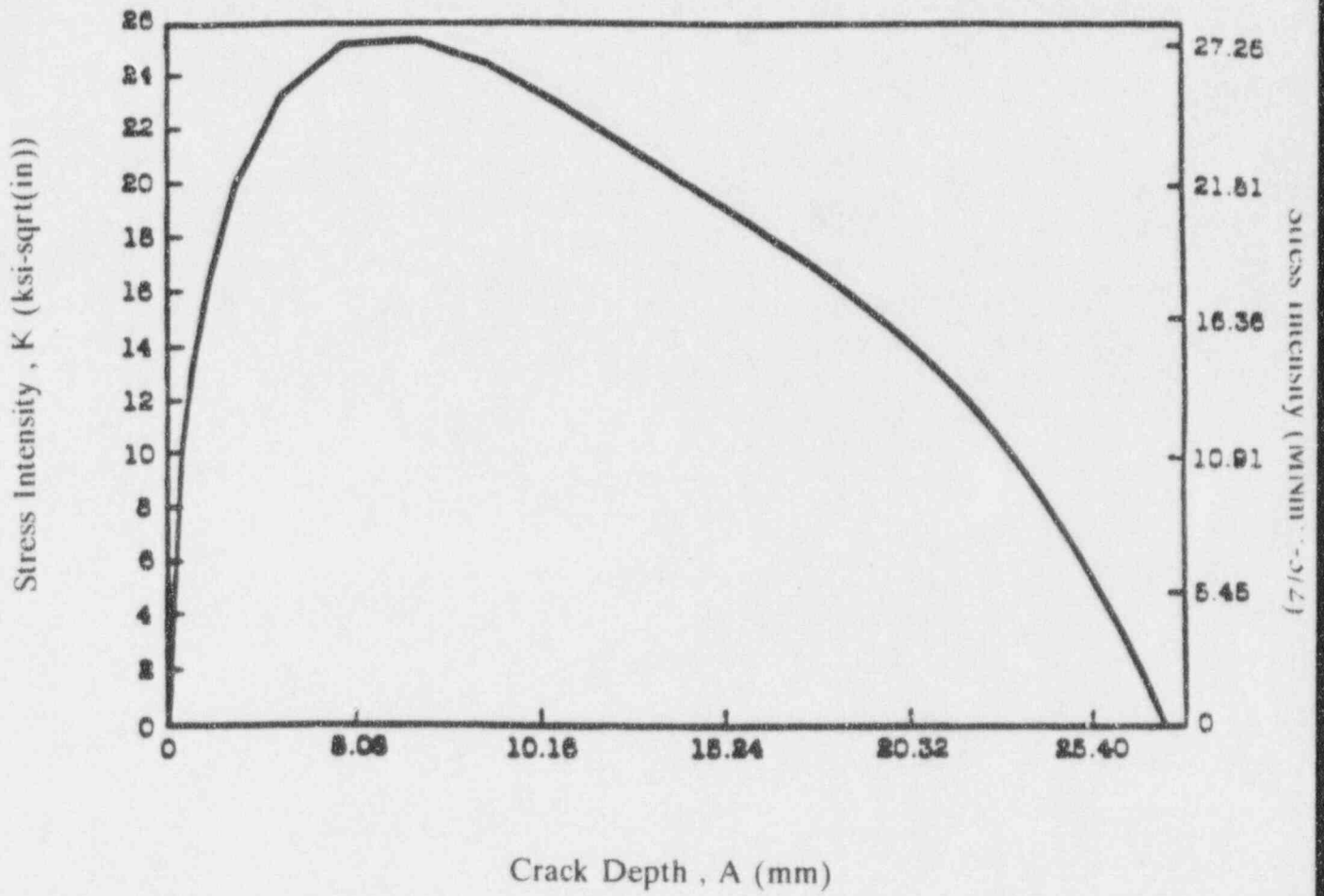


Figure A-6 Shroud Throughwall Stress Intensity Factor

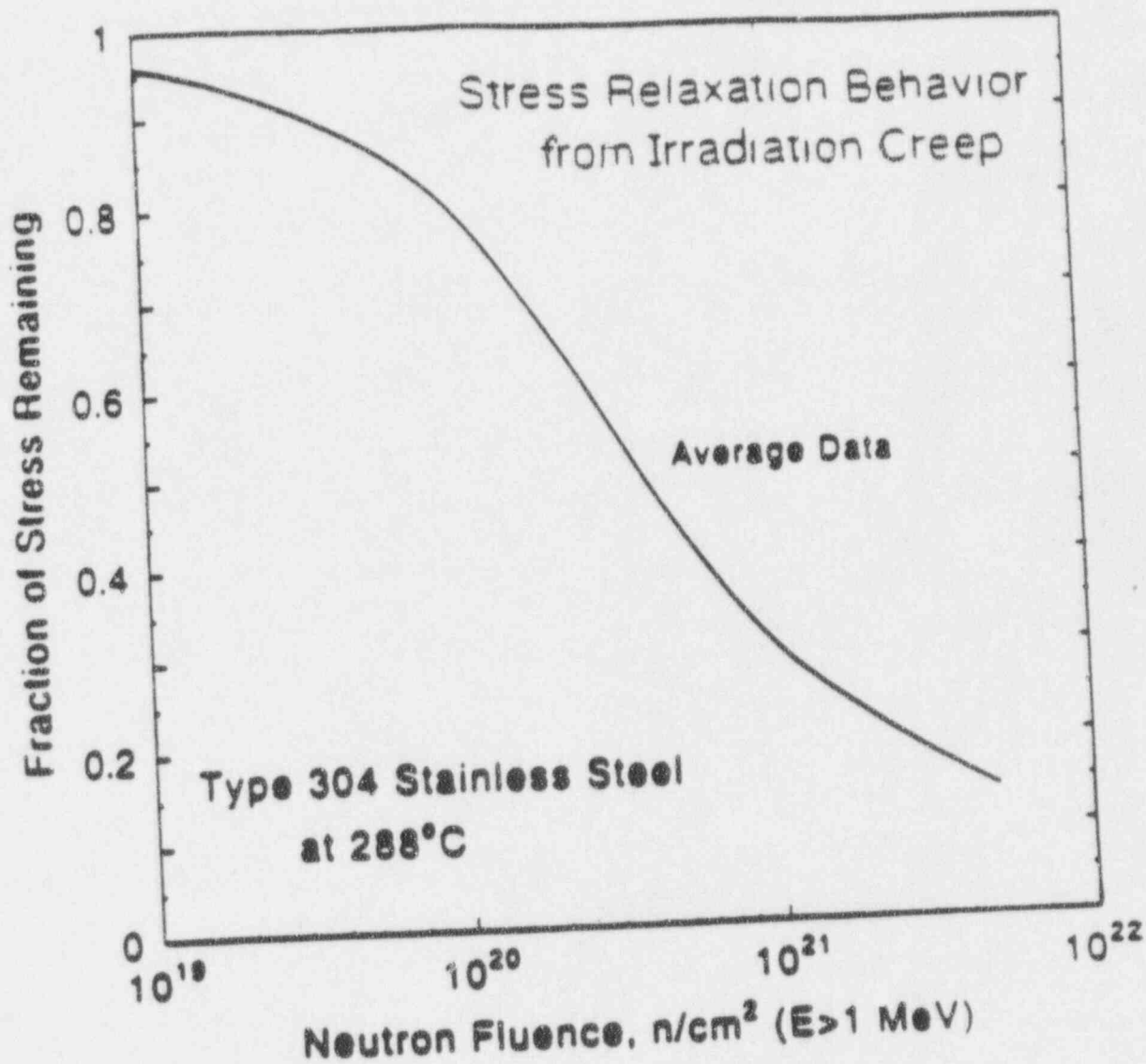
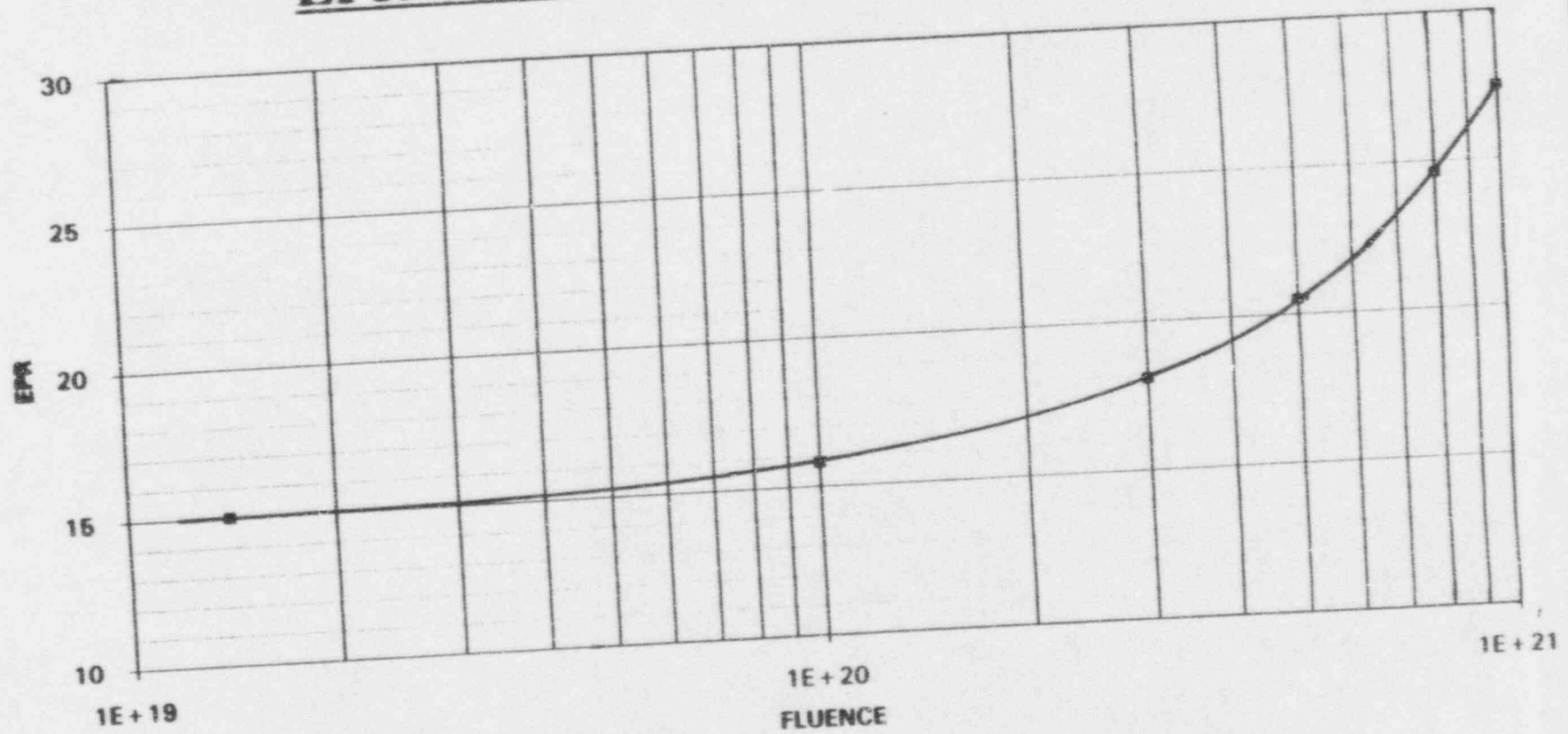


Figure A-7 Stress Relaxation Behavior of Type 304 Stainless Steel Due To Irradiation at 288C

EPR VERSUS NEUTRON FLUENCE

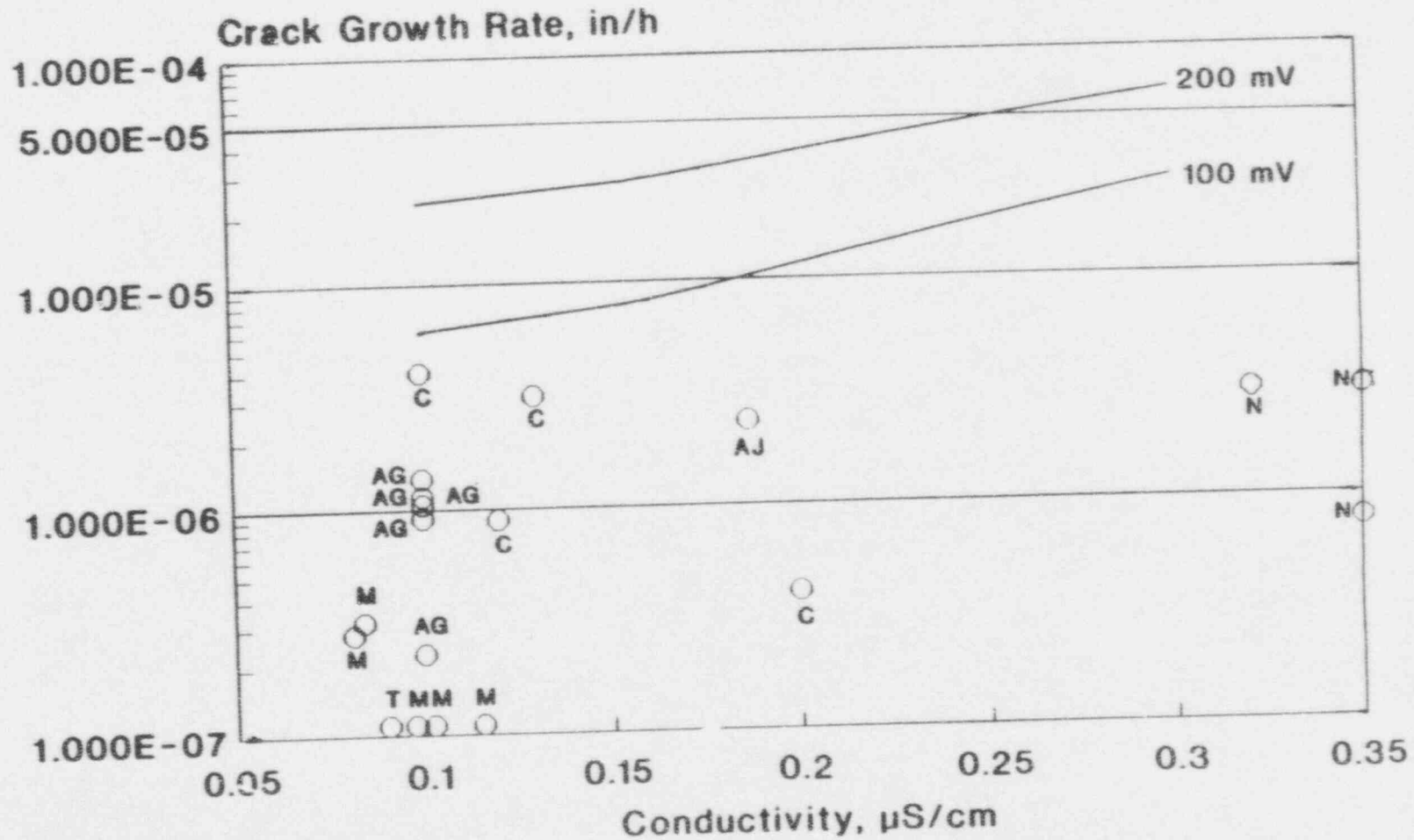


A-12

Figure A-8 - EPR Versus Neutron Fluence

Effect of Conductivity on Sensitized 304 Crack Growth Rate

GE Nuclear Energy



GENE-533-148-1193

PLEDGE: 20 ksi $\sqrt{\text{in}}$, 15 C/cm²
 CAV: 20-25 ksi $\sqrt{\text{in}}$, 13 C/cm², 100-160 mV

Figure A-9 Effect of Conductivity on Sensitized Type 304 Crack Growth Rate

A-13

In-Core Bypass ECP vs Feedwater Hydrogen for a BWR-4

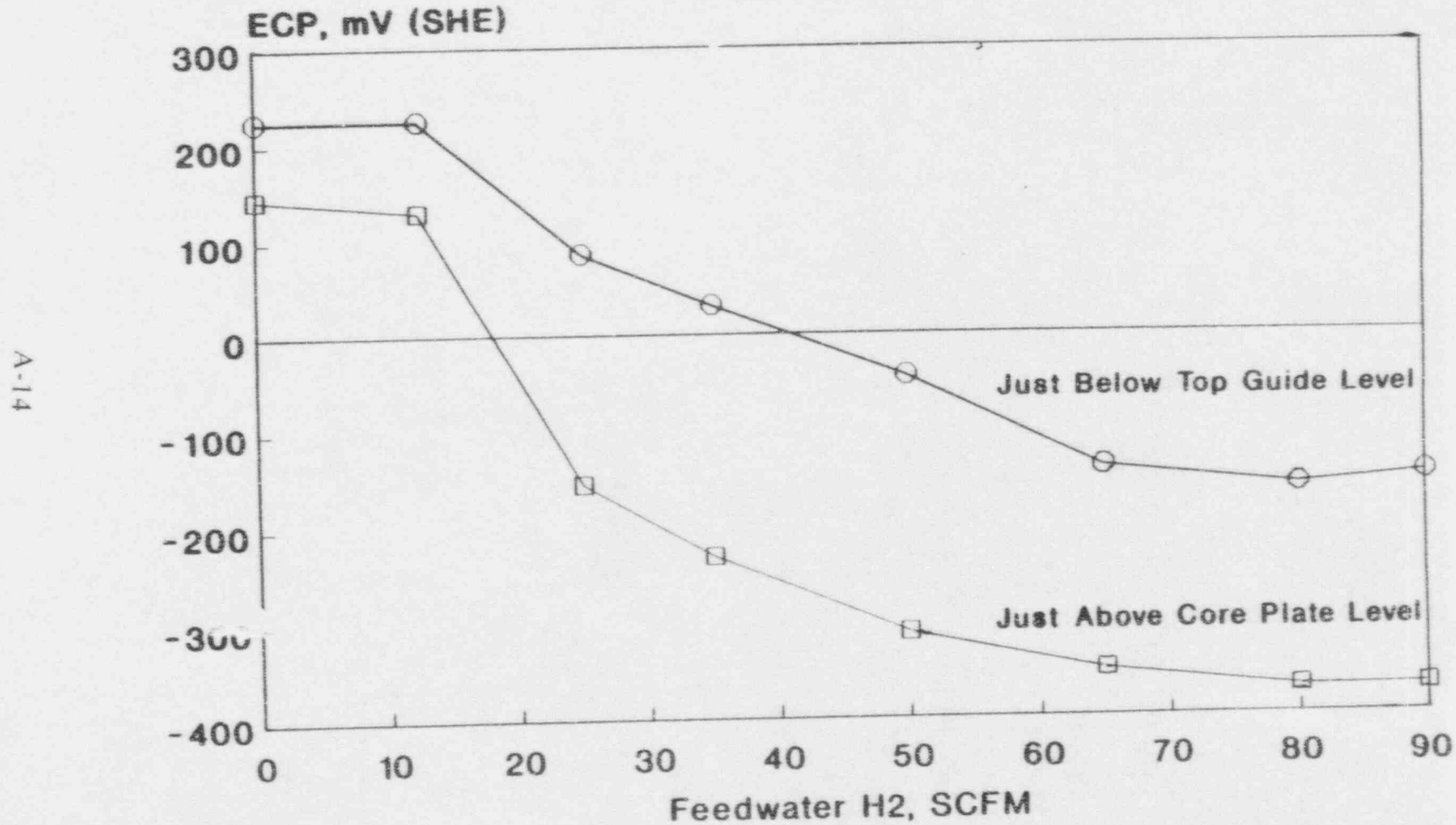
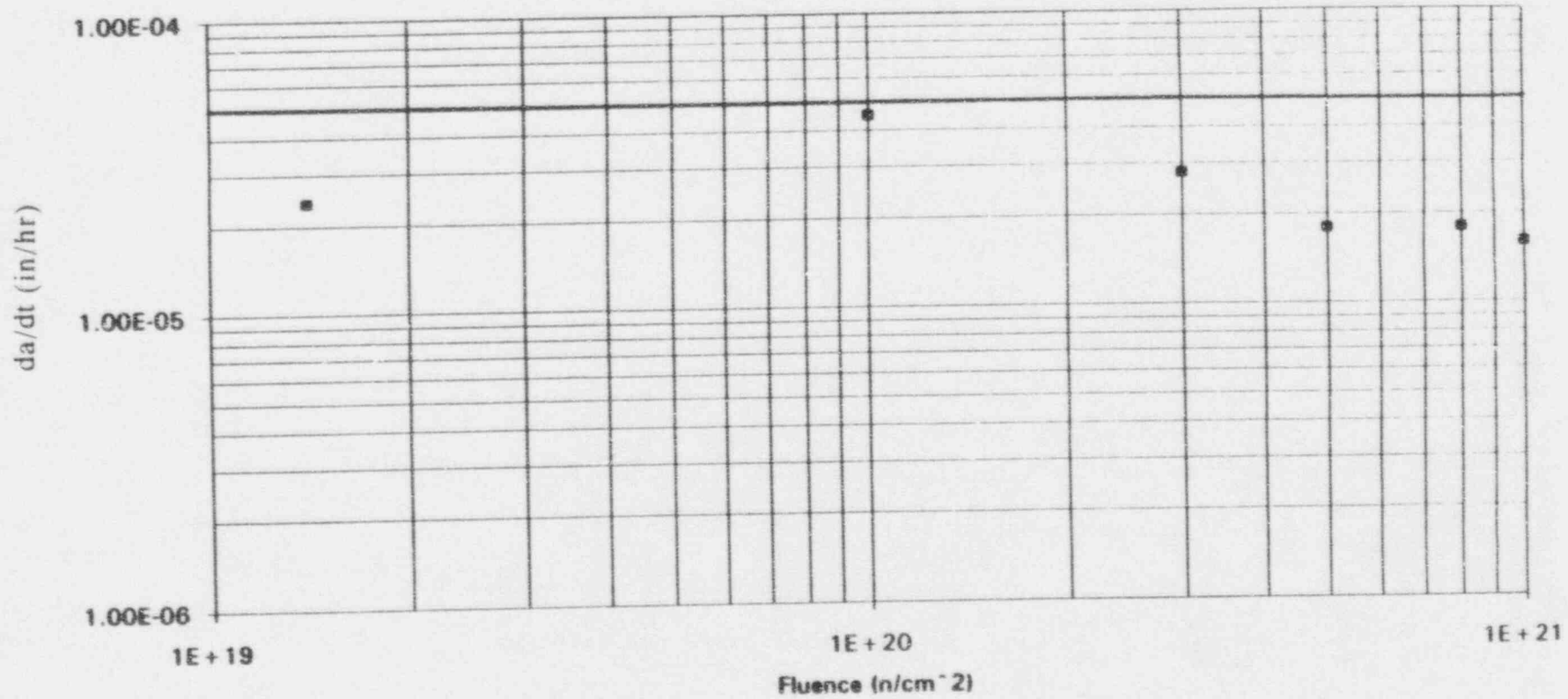


Figure A-10

In-Core Bypass ECP vs Feedwater Hydrogen for a BWR-4

Figure A-11

GROWTH RATE VERSUS FLUENCE



A-15

Stress Intensity = 20 Ksi/in, Initial EPR = 15 C/cm²

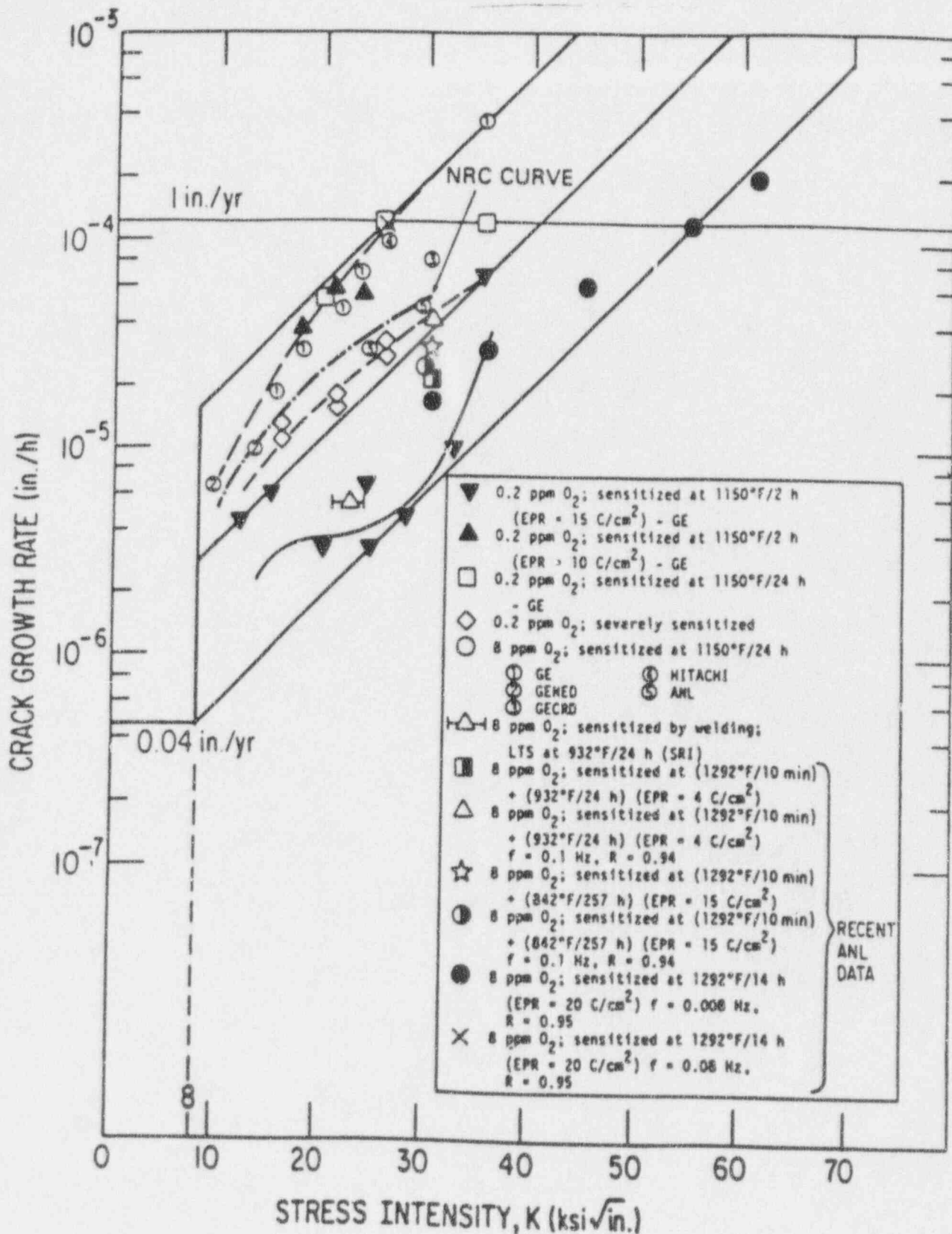


Figure A-12

Nureg 0313 Crack Growth Rate Data

APPENDIX B - LIST OF PARTICIPATING UTILITIES

The list of BWR Owners' Group utilities below have participated in submittal of this report:

Carolina Power & Light
Cleveland Electric Illuminating
Commonwealth Edison
Entergy Operations, Inc.
GPU Nuclear
IES Utilities Inc.
Niagara Mohawk Power
Northeast Utilities
Northern States Power
Pennsylvania Power & Light
PECO Energy
Public Service Electric & Gas
Southern Nuclear Operating Co.
Tennessee Valley Authority
Vermont Yankee
Washington Public Power Supply System

GE Nuclear Energy
175 Curtner Avenue
San Jose, CA 95125

BWR CORE SHROUD EVALUATION

April 1994

Prepared for the
BWR Owners' Group

Prepared by: *Marcos L. Herrera*
Marcos L. Herrera, Principal Engineer
Structural Mechanics Projects

Gene Eckert
Gene Eckert, Principal Engineer
Power Uprate Projects

Al Baker
for Al Baker, Project Manager
Shroud Inspections

Barry Gordon
Barry Gordon, Project Manager
Corrosion Technology

Approved by: *Dr. Sampath Ranganath*
Dr. Sampath Ranganath, Manager
Structural Mechanics Projects

Dr. Gerald Gordon
Dr. Gerald Gordon, Chief Technologist
BWR Technology

Steven J. Stark
Steven J. Stark, Projects Manager
BWR Owners' Group Projects

GE Nuclear Energy
San Jose, CA

~~9404080189~~

**IMPORTANT NOTICE REGARDING
CONTENTS OF THIS REPORT**

Please Read Carefully

The only undertaking of the General Electric Company (GE) respecting information in this document are contained in the Task Authorization (TA) between the participating utilities of the BWR Owners' Group (BWROG) and GE, and nothing contained in this document shall be construed as changing the TA. The use of this information by anyone other than the participating utilities of the BWROG, or for any purpose other than that for which it is intended under the TA is not authorized; and with respect to any unauthorized use, GE makes no representation or warranty, and assumes no liability as to the completeness, accuracy, or usefulness of the information contained in this document, or that its use may not infringe privately owned rights.

BWROG Core Shroud Evaluation

Table of Contents

EXECUTIVE SUMMARY

1.0 INTRODUCTION.....	1
2.0 CORE SHROUD DESIGN INFORMATION.....	6
3.0 SCREENING CRITERIA	10
4.0 MITIGATION OF CORE SHROUD IGSCC	48
5.0 OPERATIONAL SYMPTOMS.....	70
6.0 INSPECTION STRATEGY.....	80
7.0 SUMMARY	91

- APPENDIX A - BASIS FOR THE CRACK GROWTH RATE
- APPENDIX B - LIST OF PARTICIPATING UTILITIES

EXECUTIVE SUMMARY

Cracking has been observed in the vicinity of core shroud welds at six boiling water reactors (BWRs). Of the six BWRs where cracking was observed, three are domestic plants. Visual (VT) and ultrasonic (UT) test examinations of the shroud weld areas have shown both circumferential and axial indications, mostly associated with the heat affected zone of the shroud welds. This report contains a discussion of various aspects of the shroud cracking issue and provides the generic tool which utilities may use to address shroud cracking concerns. These issues include: screening criteria, mitigation actions, operational symptoms, and inspection strategy.

The screening criteria were developed to determine the acceptability of any indications. The criteria consist of a graded approach in screening indications. There are three major steps in the screening approach. These are:

- Acceptance Standard
- Visual Screening Criteria
- UT Screening Criteria

The acceptance standard is similar to the ASME Code Section XI IWB-3500 approach to acceptance of indications. Indications which meet this criteria do not require further evaluation. The visual screening criteria are used when an indication does not meet the acceptance standard criterion. The visual screening criteria include several significant conservatisms. These include using the maximum stress at any location in the shroud for all shroud locations, and assuming that all indications are positioned to result in lower allowable flaw sizes. In addition, the screening criteria include the consideration of potential growth of two neighboring indications into one indication, and the interaction of two neighboring indications with respect to linear elastic fracture mechanics (LEFM). If the indications meet the screening criteria, then the indications are considered to be acceptable for at least one additional fuel cycle without further evaluation. If the indications do not meet the screening criteria, guidance is presented for the performance of a more detailed evaluation assuming through-wall indications.

The UT screening criteria can be used when part through-wall characterization of indications has been obtained. With this criteria, the position of the indications in the

shroud (azimuthal) and remaining through-wall ligament can be used to obtain added structural margin.

Information regarding mitigation of core shroud cracking is presented. This includes discussion of hydrogen water chemistry, water conductivity control, and noble metal plasma spray coating. The recent incidences of cracking have demonstrated the advantage of taking early precautions to lessen the potential and extent of intergranular stress corrosion cracking (IGSCC). Water chemistry history, fabrication technique, and material have been identified as being significant contributors to the potential for cracking.

Operational symptoms are discussed to address the potential situation if unexpected significant crack growth occurs during plant operation. The potentially affected plant operational parameters are identified, as well as the modes of reactor operation that are most likely to show these symptoms if the shroud has degraded to the point that significant, through-wall leakage can occur.

Information for use by utilities to assess the shroud condition and level of inspection is also presented. The inspection strategy presented is designed to meet the intent of Service Information Letter (SIL) 572, Rev. 1 while responding to utility specific needs.

1.0 INTRODUCTION

Boiling water reactors (BWRs) are designed with a core shroud. The core shroud is a stepped cylinder which directs flow through the core. The core shroud rests on the shroud support legs (in most cases) and the shroud support plate. The steam separators, shroud head, top guide, and core plate rest on the shroud. The shroud does not support the weight of the fuel (except for a limited number of peripheral fuel bundles). The design configuration of the core shroud differs from plant to plant depending on the fabricator and BWR product line. The shroud is primarily made of Type 304 or Type 304L stainless steel of various carbon levels. The shroud support cylinder and flange is typically made from Alloy 600 material. The residual stresses due to welding, oxidizing core environment and fabrication practices create the potential for intergranular stress corrosion cracking (IGSCC). Figure 1-1 shows a schematic of a typical shroud.

In 1990, cracking was found near the circumferential seam weld at the core beltline area of the shroud in a GE BWR/4 located outside the United States. The crack indications, initially observed at three locations on the inside surface of the shroud, are confined to the heat-affected-zone (HAZ) of the circumferential seam weld.

GE RICSIL No. 054 provided interim recommendations. All owners of GE BWR plants were requested to review fabrication records for the type of material used in their plants' shroud and determine the weld locations. For plants with shrouds made of high carbon stainless steel, GE recommended visual examinations of the accessible areas of the seam welds and HAZs on the inside and outside surfaces of the shroud at the next scheduled outage.

Metallurgical samples removed from the overseas GE BWR/4 shroud revealed that the stress corrosion cracking (SCC) occurred in Type 304 stainless steel material from a relatively low carbon heat (0.045% carbon), and cracking was located in a region of high neutron fluence (8×10^{20} nvt, $E > 1$ MeV). The SCC mechanism appears to be irradiation assisted stress corrosion cracking (IASCC) with propagation promoted by residual stresses and likely helped by corrosion oxide wedging stresses.

As a result of In-Vessel Visual Inspection (IVVI) performed per RICSIL 054, cracking was subsequently observed at Brunswick Unit-1 in July 1993. Cracking was observed on

the inside diameter (ID) surface of the top guide support ring near the H3 weld. The cracking is 360° around the circumference, originating on the ID, in a material with carbon content of about 0.06%. The fluence at this location was estimated at 1.8×10^{20} nvt ($E > 1$ MeV).

A boat sample was taken from the H3 weld inside surface. A second sample containing a portion of a second outer shroud surface crack near the H4 weld was also removed for evaluation. This crack is axial in orientation and appears to initiate in the circumferential weld HAZ. Two additional boat samples were removed to verify UT sizing.

In addition to the initially observed cracking at the boat sample locations, additional crack-like indications (axial and circumferential) at the H1, H2, H4, H5, H6A weld (at core plate) and at the eccentric alignment pin, shroud head bolt lugs and the bottom of the top guide were observed.

As a result of the Brunswick Unit-1 shroud cracking, GENE SIL 572, Rev. 1 was issued which provided recommendations to address the potential for shroud cracking. The recommendations addressed the following areas:

- Plant fabrication and operational history
- Non-destructive examination (NDE) actions
- Destructive analysis
- Structural margin analysis
- Corrective action

As a result of inspections in response to SIL 572, Rev. 1, crack-like indications were observed at Peach Bottom Unit-3 in October 1993. Indications were seen on the shroud barrel inside surface in the plate side HAZ of the H3 weld; and at the H4 weld. The indications at the H3 weld differed from that at Brunswick Unit-1 because indications were not observed in the ring. It is believed that the ring did not crack due to the fact that it is a forged component.

This report provides the methodology and procedure for the evaluation of shroud indications which can be applied on a plant-specific basis. A graded approach is presented which includes comparison of the indications with an acceptance standard, visual screening criteria (assumed through-wall indications), and UT screening criteria (part through-wall indications). In addition, information is provided regarding potential mitigation actions, inspection program strategy, and operational symptoms if significant cracking were to occur.

1.1 Cause of Cracking

The extent and density of cracks associated with the H4 and H5 welds at Brunswick Unit-1 which were observed in September 1993, were found to have some correlation with regions of higher neutron fluence. On the basis of the results of the metallurgical evaluation of the boat sample, the current understanding of the root causes of cracking at the top guide support ring and higher flux H4 weld at the Brunswick plant are as follows:

1. The cracking in the HAZ on the top guide support ring side of the H3 weld was caused by IGSCC in the weld sensitized HAZ of high carbon stainless steel with apparent acceleration from:
 - Neutron fluence
 - Cold worked surface layer (approximately 0.01 inch deep) resulting from machining operations during fabrication
 - Possibly elongated inclusions or stringers because of exposure of surfaces oriented in the short transverse direction
 - Highly oxidizing environment at the weld location
2. The cracking in the H4 weld in the beltline region of the shroud at the outer surface was caused by IGSCC in weld sensitized material, with propagation by an IASCC mechanism, with:
 - Apparent acceleration of crack initiation caused by:
 - ◆ Circumferential weld HAZ
 - ◆ HAZ from apparent "repair weld"

- ♦ Possible localized high weld residual stresses, including the effect of "repair weld"
- Possible effects of localized surface grinding associated with the "repair weld"
 - ♦ Apparent promotion of crack propagation caused by:
 - Moderate sensitization associated with "repair weld"
 - Neutron fluence

On the basis of the pattern of observed cracking, it is believed that many of the conditions leading to the cracking observed in two boat samples are also present at the other observed crack locations in the core shroud. In addition, it is known that temporary welded attachments were used during both shroud fabrication and installation of the shroud in the vessel. Removal of these welded attachments could result in localized areas exhibiting heavy grinding as well as potential weld sensitization, and could lead to some SCC initiation in regions remote from the seam welds.

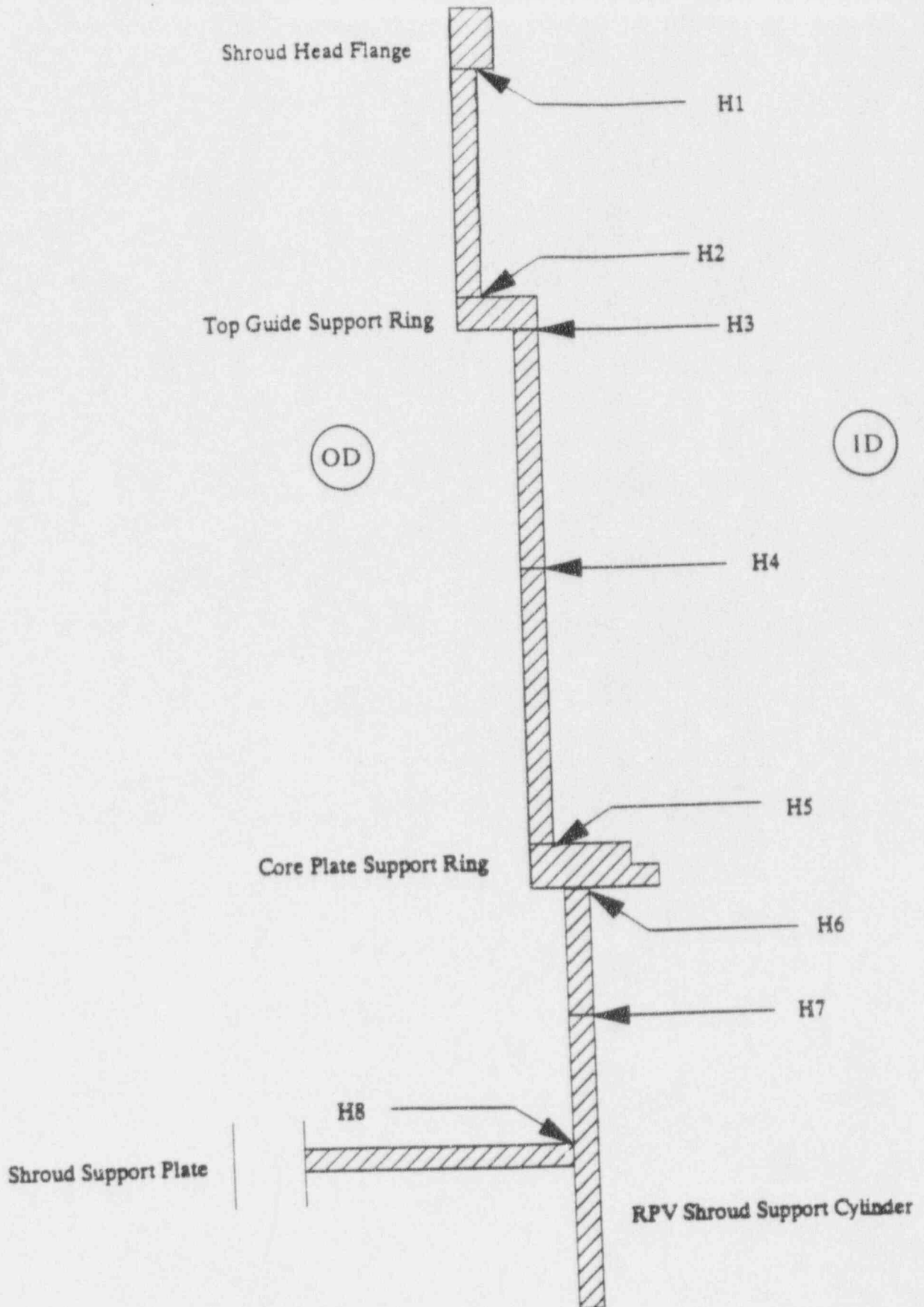


Figure 1-1 Example of Core Shroud (Design is plant specific)

2.0 CORE SHROUD DESIGN INFORMATION

The core shroud is typically composed of three cylindrical shell sections and three rings. The three rings are the shroud head flange, top guide support ring and core plate support ring. The top cylindrical shell connects the shroud head flange to the top guide support ring. The largest cylindrical portion connects the top guide support ring to the core plate support ring. The bottom cylindrical shell connects the core plate support ring to the shroud support cylinder which is typically made from Alloy 600 material. The shroud support legs are located at the bottom edge of the shroud support cylinder (a few plants do not have support legs).

Some of the significant differences between core shroud designs are:

- Diameter of shroud (diameter varies in some plants)
- Thickness of shroud wall (in some cases varying thickness along shroud height)
- Number of horizontal welds in the core beltline
- Number of vertical welds connecting the cylindrical shells
- Material (Type 304 vs. 304L)
- Carbon content
- Fabrication of rings (single piece forging vs. segmented welded plate pieces)
- Tapered lower cylindrical shell vs. straight lower cylindrical shell

Figure 2-1 and 2-2 illustrate two examples of the core shroud design. In Figure 2-1, there are two core beltline horizontal welds (H4 and H5). The thickness of the shroud wall is 1.5". In Figure 2-2, the shroud wall thickness is 2.0" and there is only one horizontal weld in the core beltline (H4). There are other variations to the two designs shown (e.g., BWR/2); however, the information provided in this report is applicable to all designs.

Based on a review of some plant records, in some plants the rings are made from single-piece forged material with low carbon ($\cong 0.035\%$). Carbon content for Type 304 shrouds varies from 0.045% to 0.074%. Hardness ranges vary from Rockwell B hardness of 90 for Type 304 and Rockwell B hardness of 92 for Type 304L.

The horizontal and vertical welds are typically submerged arc automatic welding. Weld filler material is Type 308 or Type 308L. The weld between the lower cylinder and the

RPV shroud support cylinder is typically Alloy 182. The weld prep is typically single beveled with or without a backing ring.

Typically, weld prep surfaces of the base metal were prepared by machining. The backside of the groove welding was prepared by grinding or gouging, followed by liquid penetrant inspection. Final surfaces of the welds were inspected by liquid penetrant examination.

The austenitic stainless steel material is typically purchased in solution annealed condition. No solution annealing is performed after welding of the various shroud parts.

General practices during assembly and shipment of the core shroud, bracing, jacks, temporary welds, and supports are used to help in meeting design geometric tolerances. Sometimes, there is no recorded documentation of these practices. However, it is likely that they did occur. These actions can result in local effects on material behavior and stress. For example, temporary welding results in local areas of high residual stress, and grinding results in local areas of cold working. If these local effects were to contribute to cracking, it is likely that the cracking would be of lesser concern than cracking at horizontal seam welds.

The design considerations discussed in this section are included in the development of the screening criteria. For example, the shroud thicknesses and diameter are considered in the determination of the stress, and a bounding crack growth rate is used which applies to all materials present in any of the shroud designs.

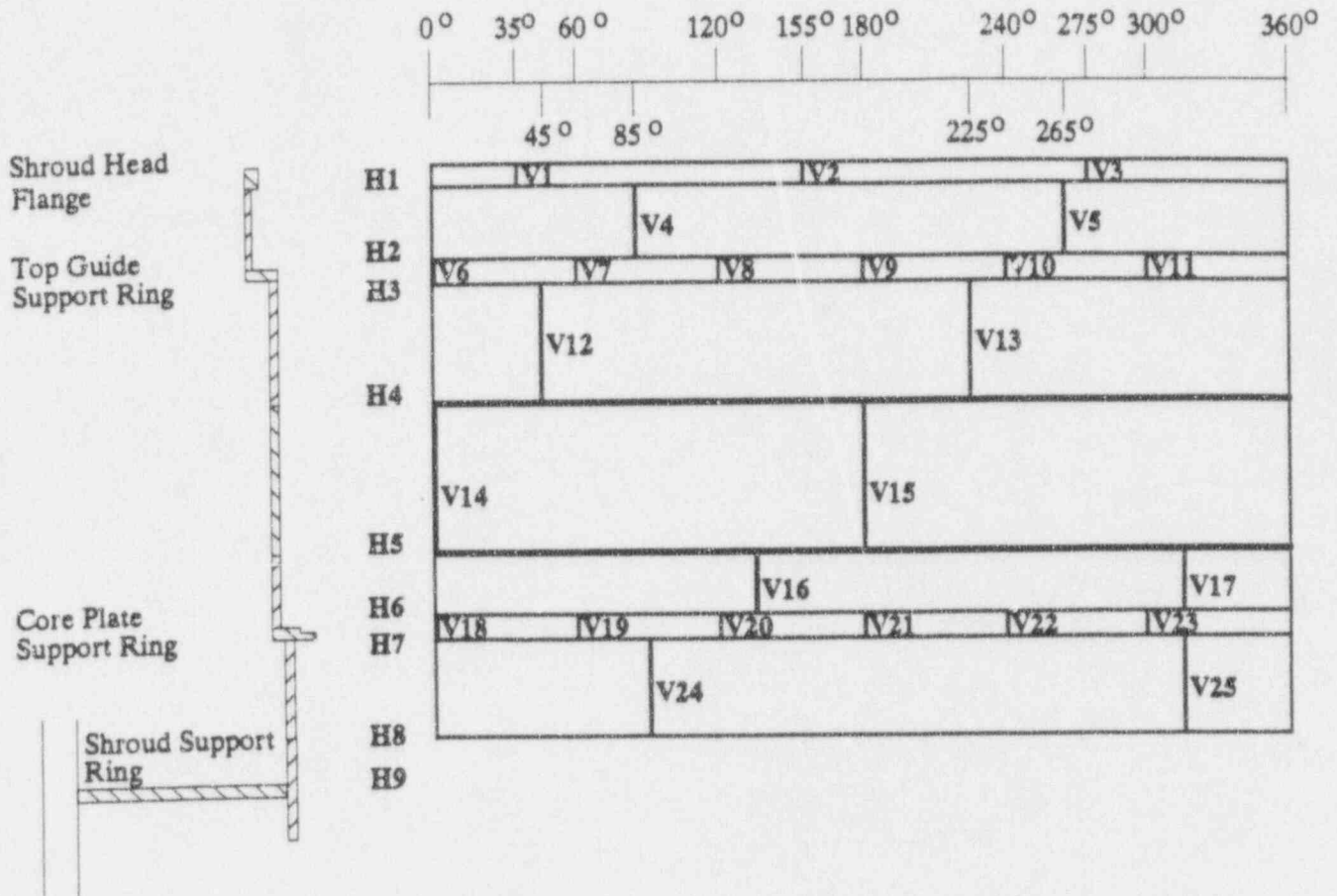


Figure 2-1 - Sketch Showing Typical Welds in Core Shroud (Example)

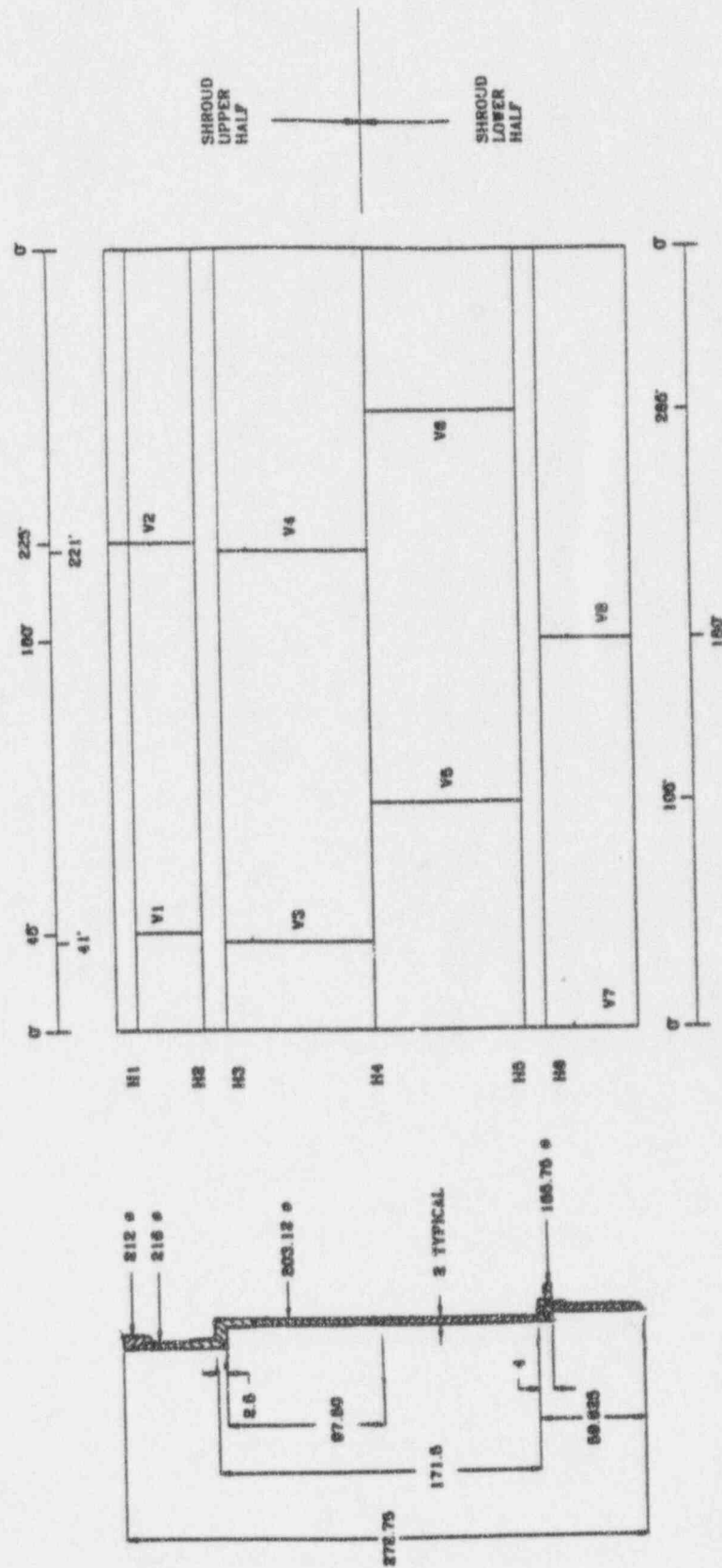


Figure 2-2 Schematic Showing Typical Welds in Core Shroud (Example 2)

3.0 SCREENING CRITERIA

This section provides the methodology and procedure which can be used to evaluate indications found by Non-Destructive Examination (NDE, e.g., ultrasonic testing (UT) or visual techniques (VT)). The screening criteria is presented as a graded procedure. The criteria is comprised of three major steps. These steps (in the order of application) are:

- Acceptance Standard
- Visual Screening Criteria
- UT Screening Criteria

The first step is to compare any indications with the acceptance standard. If the indications meet the acceptance standard, further evaluation of the indications is not required. Note that this approach is similar to that in ASME Code Section XI Subarticle IWB-3500.

The second step, performed if the indication does not meet the acceptance standard, is to compare the indication with the visual screening criteria. These criteria include several conservatisms and are intended to be a first-cut evaluation of the indications. The major assumption in this step is that all indications seen by IVVI are assumed to be through-wall. If UT is performed, this simpler method can be first applied (by assuming all flaws are through-wall) for rapid disposition of the indications.

The third step is to use UT through-wall characterization and the specific azimuthal location of the indications in the evaluation for structural acceptability. The evaluation is similar to that used for the visual screening criteria except for the through-wall and location aspects of the flaw mentioned above.

3.1 Acceptance Standard

This first step in the evaluation is to compare the observed indications to the acceptance standard. This approach is similar to that stated in ASME Code Section XI Subarticle IWB-3500 for acceptability of flaws without further evaluation. If the indications meet the acceptance standard, then further evaluation of the indications is not required.

3.1.1 Determination of Effective Flaw Length for Acceptance Standard

The ASME Code Section XI Subarticle IWA-3300 (1989 edition) proximity rules must be applied to the indications prior to comparing with the acceptance standard. Section IWA-3300 specifies how flaws are to be combined depending on the location and orientation of the indications found by volumetric examination. Briefly, the flaws are combined lengthwise if the distance between the crack tips is less than 2 times the depth of the deepest indication and the crack planes lie within 0.5 inches (perpendicular distance between the crack planes). However, for this acceptance standard, the Section XI proximity criteria are modified by increasing the 0.5 inches to 2 times the shroud wall thickness. Thus, two indications are combined lengthwise if,

$$S \leq 2B$$

where S = distance between indications
B = depth of deepest indication if depth of flaw known (for UT)
B = shroud thickness (for IVVI)

If UT data are available, the application of the proximity criteria should use the ASME Code Section IWA-3300 method based on the depth of the deepest indication. If IVVI information is the only information available, then the depth of the deepest indication should be taken as the thickness of the shroud. It can be seen that UT data may result in fewer flaw combinations due to the smaller required ligament between flaw tips.

3.1.2 Basis for Acceptance Standard

The acceptance standard was arrived at by evaluating information from several shroud analyses. In addition, an allowable length was desired which could also be related to the ASME Code margins. Based on shroud evaluations which represent a wide range of shroud designs and after application of a safety factor of 2.8 on stress, an acceptance standard was developed and is shown in the following table.

Acceptance Standard

Circumferential		Axial
<u>LEFM</u>	<u>Limit Load</u>	<u>LEFM and Limit Load</u>
15"	15" in any 90° quadrant	15"

Any flaw which meets the acceptance standard shown above is acceptable without further evaluation. It should be noted that the value of 15" is approximately one-tenth the length of a shroud quadrant.

3.2 Visual Screening Criteria

In the visual screening criteria, all indications are considered to be through-wall (consideration of UT sizing is discussed in Section 3.3). This screening criteria for evaluation of the shroud indications is based on the ASME Code Section XI procedures. This is considered conservative since most core shrouds were not originally designed using the ASME Code nor is it a primary pressure boundary component. In fact, the original design of the shroud included consideration of fabrication requirements. For example, the shroud thickness was made relatively thick (≥ 1.5 ") to avoid deformation during fabrication and shipping.

The limiting parameter is the allowable through-wall flaw size, which already includes the ASME Code Section XI safety factors. If all of the detected indications are assumed to be through-wall, then the longest flaws, or combination of flaws, would have the limiting margin against the allowable through-wall flaw size. In reality, the indications are likely not through-wall (which can be confirmed by UT), and therefore the criteria and methods presented in this report are conservative.

The result of this procedure will be the determination of the effective flaw lengths which will be compared against the allowable flaw size and selection of indications for more detailed evaluation. The determination of effective flaw length is based on ASME Code, Section XI, Subarticle IWA-3300 (1989 Edition) UT proximity criteria. These criteria provide the basis for the combination of neighboring indications depending on various geometric dimensions. Crack growth over a subsequent cycle is factored into the criteria.

The proximity rules described here also conservatively assume that there is interaction between two perpendicular flaws. It is assumed that circumferential and axial indications could increase the effective flaw length depending on the unflawed distance between them. This effective circumferential flaw length must be compared against the allowable circumferential flaw length. The axial flaw would be compared against the allowable axial flaw length.

Flaws are considered in the same plane if the perpendicular distance between the planes is within two times the shroud thickness or less ($2T$, where T =shroud thickness). Any flaws which lie at an angle to the horizontal plane should be separated into a circumferential and axial component. These components can then be used separately in the determination of effective flaw lengths.

The selection of indications for further investigation can be performed by evaluating the resulting effective flaw lengths. **Indications with effective flaw lengths greater than the allowable flaw sizes would require more detailed analysis or further characterization by NDE** (which is used as input to the UT screening criteria, Section 3.3). The procedure described here is conservative since all of the indications are assumed through-wall and are being compared against the allowable through-wall flaw size. More detailed evaluation of the indications can include using the location specific stress. Details of the more specific evaluation are described in Section 3.2.6.

This section describes the following steps:

- Determination of effective flaw length including proximity criteria for adjacent flaws.
- Determination of allowable flaw sizes based on both linear elastic fracture mechanics (LEFM) and limit load criteria.
- Visual screening criteria.

The procedure uses the limiting stresses for all the shroud welds. Therefore, the screening criteria developed here cover all shroud weld indications. A list of conservatisms used in this evaluation is summarized in Table 3-1.

Table 3-1 - Conservatisms Included in Visual Screening Criteria

1. All surface indications were assumed to be through-wall for analysis.
2. The visual screening criteria limit one-fourth of allowable circumferential flaw to any arbitrary 90° sector.
3. All indications are assumed to be grouped together for the limit load calculation and no credit is taken for the spacing between indications.
4. ASME Code Section XI primary pressure boundary safety margins were applied even though the shroud is not a primary pressure boundary.
5. ASME Code, Section XI proximity rules were applied.
6. An additional proximity rule which accounts for fracture mechanics interaction between adjacent flaws was used.
7. The highest stress computed for any single location was used for all locations.
8. Both LEFM and limit load analysis were applied, even though LEFM underestimates allowable flaw size for austenitic materials and is not required per ASME Code Section XI procedures.
9. The bounding crack growth estimated for the next fuel cycle was included in flaw lengths used for evaluation (See Appendix A).
10. A proximity rule to account for perpendicular flaws was applied, although not required by Section XI.

3.2.1 Determination of the Effective Flaw Length

The effective flaw lengths are based on ASME Code, Section XI proximity criteria as presented in Subarticle IWA-3300. The procedure addresses both circumferential and axial flaws. Indications are considered to be in the same plane if the perpendicular distance between the planes is less than two times the shroud thickness (2T). All flaws are considered to be through-wall. Therefore, indications on the inside and outside surface should be treated as if they are on the same surface. When two indications are close to each other, rules are established to combine them based on proximity. These rules are described here.

Proximity Rules

The flaw combination methodology used here is similar to the ASME Code, Section XI proximity rules concerning neighboring indications. Under the rules, if two surface indications are in the same plane (perpendicular distance between flaw planes <two times the shroud thickness, 2T) and are within two times the depth of the deepest indication, then the two indications must be considered as one indication.

In Figure 3-1, two adjacent flaws L1 and L2 are separated by a ligament S. Crack growth would cause the tips to be closer. Assuming a conservative crack growth rate (see Appendix A) of $g=5 \times 10^{-5}$ in/hr, crack extension at each tip is the crack growth rate multiplied by the number of hot operating hours above 200°F for the next fuel cycle. The crack growth at each tip is thus, gt . Therefore, combining the crack growth and proximity criteria, the flaws are assumed to be close enough to be considered as one continuous flaw if the ligament is less than $(2gt + 2T)$. If the ligament is less than $(2gt + 2T)$, the effective length is $(L1+L2+S+2gt)$. Note that the addition of $2gt$ is to include crack growth at the other (non-adjacent) end of each flaw (See Figure 3-2).

If the ligament is greater than $(2gt + 2T)$, then the effective flaw length is determined by adding the projected tip growth to each end of the flaw.

$$L1_{eff} = L1 + 2gt$$

$$L2_{eff} = L2 + 2gt$$

A similar approach is used to combine flaws when a circumferential flaw is close to an axial flaw (See Figure 3-3). If the ligament between the flaws is less than $(2T + gt)$, then the effective flaw length for the circumferential flaw is $L_{eff} = L1 + S + gt$ (the bounding ligament for these cases). If the ligament is greater than $(2T + gt)$, then the flaws are treated separately.

After the circumferential and axial flaws have been combined per the above criteria, a map of the effective flaws in the shroud can be made, and the effective flaw length can be used for subsequent fracture mechanics analysis.

To demonstrate the proximity criteria, three examples are shown in Table 3-2 and described below.

Table 3-2 Flaw Combinations Considered in Proximity Criteria

Case	Circumferential Flaw	Axial Flaw
A	Yes	No
B	Yes	Yes
C	No	Yes

Case A: Circumferential Flaw - No Axial Flaw

This case applies when two circumferential indications are considered. Figure 3-2a shows this condition. If the distance between the two surface flaw tips is less than $(2T + 2gt)$, the indications must be combined such that the effective length is (see Figure 3-2b):

$$L_{eff} = L1 + S + L2 + 2gt$$

where: L1 = length of first circumferential indication
 L2 = length of second circumferential indication
 S = distance between two indications

If the distance between the two tips is greater than $(2T + 2gt)$, the effective flaw lengths are (See Figure 3-2c):

$$\begin{aligned} L1_{\text{eff}} &= L1 + 2gt \\ L2_{\text{eff}} &= L2 + 2gt \end{aligned}$$

Case B: Circumferential Flaw - Axial Flaw

This case applies when both a circumferential and an axial flaw are being considered. Figure 3-3a demonstrates this condition. For this case, only growth of the circumferential flaw is considered. If the distance between the circumferential indication tip and the axial indication is less than $(2T + gt)$, then the effective circumferential flaw length is (see Figure 3-3b):

$$L_{\text{eff}} = L1 + S + gt$$

where: $L1$ = length of circumferential indication
 S = distance between the circumferential tip and axial flaw.

and the effective axial length is (Figure 3-3b):

$$L_{\text{eff}} = L2 + 2gt$$

where: $L2$ = length of axial indication

If the distance between the circumferential indication tip to the axial indication is greater than $(2T + gt)$, then the flaws are not combined (see Figure 3-3c) and the effective lengths are:

$$\begin{aligned} L1_{\text{eff}} &= L1 + 2gt \text{ (for circumferential flaw)} \\ L2_{\text{eff}} &= L2 + 2gt \text{ (for axial flaw)} \end{aligned}$$

Case C: No Circumferential Flaw - Axial Flaw

This case applies to when only axial flaws are being considered. The effective length is determined in a manner similar to that used for case A for circumferential flaws.

Application of Effective Flaw Length Criteria

The application of the effective length criteria is applied to two adjacent indications at a time. Figure 3-4 is a schematic which illustrates the process. For example, using the 0° azimuth as the starting location for a circumferential weld or plane, the general procedure would be as follows:

- Moving in the positive azimuthal direction, the first indication encountered is indication 1.
- The next indication is indication 2.
- Apply proximity rules to the pair of indications (indications 1 and 2). Combine the flaws if necessary (L_1+L_2+S). If the flaw is combined, the flaw becomes indication 2.
- Continue along positive azimuthal direction until the next indication is encountered. This becomes indication 3.
- Apply proximity rules to new indications 2 and 3.
- Continue proximity rule evaluation until all indications along the subject weld or plane have been considered.

3.2.2 Structural Analysis

The preceding section of this report described the determination of effective flaw lengths from the NDE results for use in the visual screening criteria. These effective flaw lengths have to be compared to the allowable flaw lengths to assess the structural integrity of the shroud. This section describes the details of the structural analysis to determine the allowable flaw lengths. The structural analysis consists of two steps: the determination of axial and circumferential stress magnitudes in the shroud, and the calculation of the allowable flaw lengths. Both the fracture mechanics and limit load methods are used in the calculation of allowable flaw lengths.

Applied Loads and Calculated Stresses

The applied loads on the shroud consist of internal differential pressure, weight and seismic. All other stresses are negligible in comparison. The seismic loads consist of a horizontal shear force at the top of the shroud and an overturning bending moment. The shear force produces a shear stress of insignificant magnitude, and is not considered. The bending moment stress at a shroud cross-section varies as a function of its vertical distance from the top of the shroud. Because of the inherent ductility of the material, residual stresses and other secondary stresses do not affect structural margin. Thus, they need not be considered in the analysis.

The magnitudes of the applied loads are obtained from the currently applicable seismic stress analysis and system information reports. The nominal shroud radius and thickness, R and T , are used to calculate the stresses from the applied loads. The stresses are essentially based on the strength of materials formulas. Since the bending stress due to seismic shear force varies with the elevation of a location, two conservative values of this stress can be calculated: one applicable to shroud sections above the core plate and the other for sections below the core plate. Figures 2-1 and 2-2 show the weld designation and relative locations for two of the shroud designs.

The seismic stress magnitudes for both the upset and faulted conditions must be calculated using the applied loads. The appropriate pressure differences for the normal and faulted conditions must also be obtained. The normal and faulted condition pressure drop across the shroud head and upper shroud, and core plate support ring and lower shroud are

required to obtain the appropriate stress due to pressure. Note that for below the core plate, the effective pressure difference for circumferential indications (axial stress) is:

$$\Delta P_{\text{below core plate}} = \Delta P_{\text{sh}} + \Delta P_{\text{cp}}$$

where: ΔP_{sh} = Pressure difference across shroud head + upper shroud

ΔP_{cp} = Pressure difference across core plate support ring and lower shroud

The structural analysis for the indications uses two methods: linear elastic fracture mechanics (LEFM) and limit load analysis. Both the limit load and the LEFM methods are used in determining the allowable flaw sizes in the shroud. Since the limit load is concerned with the gross failure of the section, the allowable flaw length based on this approach may be used for comparison with the sum of the lengths of all the flaws at a cross-section. On the other hand, the LEFM approach considers the flaw tip fracture toughness and thus, the allowable flaw length based on this approach may be used for comparison with the largest effective flaw length at a cross-section. The technical approach for the two methods is described below.

Fracture Mechanics Analysis

The shroud material (austenitic stainless steel) is inherently ductile and it can be argued that the structural integrity analysis can be performed entirely on the basis of limit load. In fact, J-R curve measurements (Figure 3-5) made on a core shroud sample taken from an overseas plant having a fluence of 8×10^{20} n/cm² showed stable crack extension and ductile failure when tested. The ASME Code recognizes this fact in using only limit load techniques in Section XI, Subsubarticle IWB-3640 analysis. Nevertheless, a conservative fracture mechanics evaluation can be performed using an equivalent K_{jC} corresponding to the material J_{IC} . The K_{jC} for the overseas plant shroud was approximately 150 ksi $\sqrt{\text{in}}$. Use of this equivalence is considered conservative since the J-R curves show J_{max} values well above the J_{IC} , confirming that there is load capability well beyond crack initiation (See Figure 3-5).

The allowable K_I is obtained by applying the appropriate safety factor for normal and upset or faulted conditions to the K_{jC} obtained from the test specimens described above. For the analysis presented here, the LEFM analysis is confined to the welds above the core

plate support ring (not including the core support plate ring welds). The fluence corresponding to welds at and below the core plate elevation is an order of magnitude lower and the associated fracture toughness is comparable to that of the unirradiated material. For those locations, only limit load analysis is used.

An additional consideration that applies only to the fracture mechanics analysis is the question, "When is a flaw independent of an adjacent flaw?". The ASME Code proximity rule described in Section 3.2.1 considers how flaws can link up and become a single flaw as a result of proximity. However, even when two flaws are separated by a ligament that exceeds $(2T + 2gt)$, they may not be considered totally independent of each other. That is, the flaw tip stress intensity factor may be affected by the presence of the adjacent flaw. This can be accounted for by using the finite width correction factor for a flaw in a finite plate. For a through-wall flaw in an "infinite" plate, the stress intensity factor is:

$$K = \sigma\sqrt{\pi a}$$

For a finite plate, the K value is higher as determined by the finite width correction factor, F. In this screening evaluation it is assumed that the plate is "infinite" if the correction factor F is less than 1.1. As seen in Figure 3-6, if the width of the plate exceeds 2.5L (or a/b less than 0.4), then there would be little interaction (less than 10% since $F \cong 1.1$) due to plate end edge effects. If this same condition is applied to two neighboring flaws, then there will be no interaction between the two indications if the tips are at least $0.75(L_1 + L_2)$ apart. If the distance between indications is greater than $0.75(L_1 + L_2)$, then they may be considered as two separate flaws. If however, they are closer, for the purpose of fracture analysis, the equivalent flaw length is the sum of the two individual flaws.

Limit Load Analysis

A through-wall circumferential flaw was assumed in this calculation. Limit load calculations were conducted using the approach outlined in Subsubarticle IWB-3640 and Appendix C of Section XI of the ASME Code. The flow stress was taken as $3S_m$. The S_m values for the shroud material are 16.9 ksi and 14.4 ksi for Type 304 and Type 304L, respectively, at the normal operating temperature of 550°F.

Safety factors similar to that used in the ASME Code (for normal and upset and emergency and faulted conditions) are used in the analysis. The highest seismic stress is used for the limit load calculations. Similarly, the highest axial pressure stress corresponding to the lower shroud is used. Thus, the analytical results are applicable for all welds since limiting values are used.

3.2.3 Allowable Through-Wall Flaws

Allowable through-wall flaw sizes are determined using both fracture mechanics and limit load techniques for both circumferential and axial flaws. It should be emphasized that the allowable through-wall flaws are based on many conservative assumptions (e.g., using the limiting stress for all welds) and are intended for use only in the visual screening criteria. More detailed analysis can be performed to justify larger flaws (both through-wall or part through when measured flaw depths are available). However, since the intent of the screening criteria is to determine when additional evaluation or NDE characterization is needed, a conservative bounding approach is utilized.

Allowable Through-Wall Circumferential Flaw Size

Both the LEFM and limit load methods are used to evaluate the allowable through-wall flaws. Above the core plate, the limiting location for through-wall cracking is the lowest weld above the core plate (e.g., H5 for the shroud design in Figure 2-1, and H4 for the shroud design in Figure 2-2). The weld between the lower shroud cylinder and core support cylinder involves Alloy 600, which has higher S_m values and therefore higher limit load capability, and is bounded by the allowable flaw size based on calculations assuming stainless steel.

Fracture Mechanics Analysis

The total axial pressure and seismic stress corresponding to the upset condition and faulted conditions are calculated based on simple strength of materials solutions. Using the ASME Code safety factors for fracture analysis, it must be determined which condition governs, faulted or normal and upset conditions. This is determined by multiplying the total normal plus upset stress by 2.8 and the faulted stress by 1.4. The condition with the highest resulting stress is considered the limiting condition.

To determine the allowable flaw size based on LEFM methods, the conservatively estimated irradiated material fracture toughness K_{Ic} value of 150 ksi $\sqrt{\text{in}}$ was used. Applying a safety factor of 2.8 for the upset condition or 1.4 for faulted conditions, the allowable K_I of 53.5 ksi $\sqrt{\text{in}}$ for normal and upset and 107 ksi $\sqrt{\text{in}}$ for faulted is obtained. The allowable flaw size is calculated using the following equation:

$$K_I = G_m * \sigma * \sqrt{(\pi a)}$$

where G_m is a curvature correction factor as defined in Figure 3-7 (Reference 3-1), σ is the axial stress, and 'a' is the half flaw length. The allowable through-wall circumferential flaw length (2a) is calculated by determining the crack length where the applied stress intensity factor equals the fracture toughness limit.

Limit Load Analysis

The stresses for the limit load analysis consist of an axial force stress and a bending moment stress. These stresses are calculated for both the normal and upset and faulted conditions. The allowable flaw length is then calculated using the approach in Subsubarticle IWB-3640 and Appendix C of Section XI of the ASME Code.

Allowable Through-Wall Axial Flaw Size

Fracture Mechanics Analysis

The allowable axial flaw size is governed entirely by the pressure hoop stress. Similar to the circumferential flaw case, the allowable axial flaw size is determined assuming a through-wall flaw. For a through-wall flaw of length 2a in the shroud, the applied stress intensity factor is given by:

$$K = M * \sigma_h * \sqrt{(\pi a)}$$

where M is the curvature correction factor as defined in Figure 3-8 (Reference 3-1). M is given by:

$$M = G_m + G_b$$

In the above expression, the allowable flaw length $2a$ can be determined by equating the calculated K to the fracture toughness divided by the safety factor of 3 or 1.5 depending on which condition is limiting, normal and upset or faulted. Comparison of the applied stress intensity factor with the allowable fracture toughness defines the allowable through-wall flaw length, $2a$.

Limit Load

An alternate approach to determining the allowable flaw size is to use limit load techniques. The allowable flaw length is given by the equation:

$$\sigma_h = \sigma_f / (M_1 * SF)$$

where M_1 is a curvature correction factor (which is a function of the flaw length (Reference 3-2)), $\sigma_f = 3S_m$ is the flow stress, SF is the safety factor of 3.0 for upset conditions or 1.5 for faulted, and σ_h = the hoop stress corresponding to the upset or faulted ΔP . The allowable flaw length is determined satisfying the equation shown above. The allowable flaw size is the limiting length determined from either the limit load or LEFM calculation.

3.2.4 Visual Screening Criteria

The determination of the allowable through-wall flaws has been described in Section 3.2.3. The objective was to use the allowable flaw size as the basis for the screening criteria. Since the screening rules represent the first step in the evaluation, they are by definition conservative. If the criteria are exceeded, the option of doing further detailed evaluation or performing additional NDE remains.

A conservative approach in developing the screening rule is to include both the LEFM and limit load analysis.

For circumferential flaws the LEFM based limit for a single flaw is not sufficient since there could be several flaws (each less than the allowable) in a circumferential plane that cumulatively add up to greater than the allowable circumferential flaw size based on limit load analysis. Thus, the cumulative flaw length should be less than that determined using

limit load analysis. While this fully assures the ASME Code margins, a significant conservatism has been included in the screening. **That is: the cumulative flaw length cannot be more than one-fourth of the limit load allowable flaw length in any 90° sector of the shroud.** This is a conservative restriction that assures that long continuous flaws are not admissible without additional inspection or analysis. With the provision that the cumulative flaw length cannot exceed one-fourth of the limit load allowable flaw length in any 90° sector of the shroud, this criterion may become more limiting than the fracture mechanics limitation. The approach used here for the one-fourth of the limit load allowable flaw length limitation for circumferential flaws is to assume a template with a moving window equal to the 90° sector. The cumulative length of flaws that appear in the window should be less than one-fourth of the limit load allowable flaw length. This is shown graphically in Figure 3-9. A similar restriction based on limit loads is not needed for axial flaws since they are associated only with circumferential welds and are unlikely to be aligned in the same plane.

The additional requirement of one-fourth of the limit load allowable flaw length can be revised if actual inspection demonstrates that there is significant uncracked ligament around the entire circumference of the shroud assuring the absence of long indications. This assures that all the indications are not concentrated in one part of the shroud section. If observed flaws are not long and continuous, a technical justification can be made to demonstrate structural integrity when the one-fourth limit is exceeded.

It should be noted that when considering LEFM based evaluations, the crack interaction criteria described in Section 3.2 must be applied in comparing against the allowable lengths. For example, for adjacent flaws where the spacing S is less than $0.75(L_1 + L_2)$, the length $L=L_1 + L_2$ is used for comparison with the LEFM based allowable flaw length.

3.2.5 Summary of Visual Screening Criteria

The visual screening criteria is schematically shown in Figure 3-10. The first step is to map the flaw indications observed by NDE. Next the proximity rules are applied to the flaw map to develop effective flaw lengths. The results of the effective flaw lengths are also mapped.

For axial flaws aligned in a vertical plane, two neighboring flaws must be summed if $S < 0.75(L_1 + L_2)$. If the longest resulting combined flaw is less than the limiting allowable axial through-wall flaw (LEFM), then the screening limit is met for axial flaws. Similarly, the effective flaw length for axial flaws must be compared against the limit load allowable for through-wall axial flaws.

For circumferential flaws, all flaws are summed in any 90° sector using a template. The total flaw length in the 90° window must be less than one-fourth of the limit load allowable through-wall flaw to meet the screening criteria. The next step is the LEFM based comparison using the interaction criteria. If $S < 0.75(L_1 + L_2)$, then the length $L = L_1 + L_2$ should be compared with the LEFM limit for circumferential flaws.

3.2.6 Detailed Evaluation of Indications

The visual screening criteria summarized in Section 3.2 is based on several conservative assumptions as noted in Table 3-1. If indications are found which exceed the visual screening criteria, more detailed analysis may be performed to evaluate the indication acceptability. Following are some of the modifications to the visual screening criteria which provide a more detailed evaluation for specific indication locations:

<u>Visual Screening Criteria</u>		<u>Detailed Analysis</u>
Use limiting stress for all locations.	⇒	Use location specific stress.
Assume all indications located to provide limiting results. Includes 90° limit applied to allowable circumferential flaw.	⇒	Knowing actual location of indications, reduce 90° limit if remaining ligament evenly distributed around circumference.
Limit load performed assuming flaws located in limiting configuration.	⇒	Perform limit load evaluation for known indication locations.
Use bounding crack growth rate.	⇒	Determine crack growth rate based on SCC predictive modeling.
Use LEFM and limit load analysis.	⇒	Perform elastic-plastic fracture mechanics analysis.
Assume through-wall indications.	⇒	Perform screening criteria with actual UT data to obtain contribution of remaining through-wall ligament. (See Section 3.3).

3.3 UT Screening Criteria

This section provides the methodology and procedure for the evaluation of indications based on UT information. In this procedure, the through-wall depth and location of the indication(s) (relative to the shroud) must be known. The visual screening criteria described in Section 3.2 uses the assumption that all indications are through-wall. This is a very conservative assumption and the use of flaw depth information provides a more realistic evaluation of the shroud structural margin.

Figure 3-11 can be used to demonstrate the difference in the flaw geometry assumed for the visual and UT screening criteria limit load analysis. The first figure shows an example flaw map of indications found during a UT inspection. The second figure shows how the flaw is modeled in the visual screening criteria. As can be seen, the flaw used to determine the allowable flaw size is assumed to be a single flaw located at the limiting location in terms of seismic overturning moment. The third figure shows how the flaw is treated in the UT screening criteria. The indications, once combined using the proximity criteria to determine effective flaw depth, are evaluated considering the actual location and flaw depth. Typically, significant added margin can be gained by considering the remaining ligament and actual location of the indication.

The methodology and procedure for the UT screening criteria is the same as that for the visual screening criteria described in Section 3.2 except for the following two major exceptions:

1. Flaw depth information regarding indications are used. Credit taken for the remaining ligament (after accounting for crack growth over one cycle).
2. Shroud azimuthal location of indications considered.

The result of this procedure is the determination of effective flaw lengths which, along with the flaw location and flaw depth, will be used to compare against the allowable flaw size. The determination of effective flaw length is based on the ASME Code, Section XI, Subarticle IWA-3300 (1989 Edition) proximity criteria. These criteria provide the basis for the combination of neighboring indications depending on various geometric dimensions. Crack growth over a subsequent cycle is factored into the criteria.

Flaws are considered in the same plane if the perpendicular distance between the planes is within two times the shroud thickness or less. Any flaws which lie at an angle to the horizontal plane should be separated into a circumferential and axial component. These components can then be used separately in the determination of effective flaw lengths.

Indications which do not satisfy the allowable flaw sizes based on the UT screening criteria would require further detailed analysis or repair of the shroud may be needed. More detailed evaluation of the indications can include using the location specific stress.

This section describes the following steps:

- Determination of effective flaw length including proximity criteria for adjacent flaws.
- Determination of allowable flaw length based on linear elastic fracture mechanics (LEFM) and determination of safety margin using limit load analysis.
- UT screening criteria

The UT screening criteria is similar to that used for the visual screening criteria. The conservatisms used in the visual screening criteria, except for the first three given in Table 3-1, are used in the UT screening criteria.

3.3.1 Determination of the Effective Flaw Length

The effective flaw lengths are based on ASME Code, Section XI proximity criteria as presented in Subarticle IWA-3300. Note that in the UT screening criteria, the position of the indication in the shroud (both through-wall depth and azimuthal location) is needed.

Similar to the visual screening criteria, rules are included to combine flaws based on proximity.

Proximity Rules

The flaw combination methodology is similar to that described in Section 3.2.1 for the visual screening criteria. The difference between the UT and visual criteria is that credit is taken for the part-through-wall flaw depth.

In Figure 3-1, two adjacent flaws, L1 and L2, are separated by a ligament S. Crack growth would cause the tips to be closer. Assuming a conservative crack growth rate of 5×10^{-5} in/hr (See Appendix A), crack extension at each tip is the crack growth rate multiplied by the number of hot operating hours above 200°F for the next cycle. The crack growth at each tip is thus, gt . Likewise, the flaw depth would become $a_1 = a_1 + gt$ and $a_2 = a_2 + gt$. Therefore, combining the crack growth and proximity criteria, the flaws are assumed to be close enough to be considered as one continuous flaw if the ligament is less than $(2gt + 2a')$, (where a' =deepest of the two indications considered). If the ligament is less than $(2gt + 2a')$, the effective length is $(L1+L2+S+2gt)$. Note that the addition of $2gt$ is to include crack growth at the other (non-adjacent) end of each flaw. Also, the crack depth of the combined flaw becomes $a_{eff} = a' + gt$ (a' =depth of deepest indication).

If the ligament is greater than $(2gt + 2a')$, then the effective flaw length is determined by adding the projected tip growth to each end of the flaw.

$$L1_{eff} = L1 + 2gt$$

$$L2_{eff} = L2 + 2gt$$

The crack depth is also modified to:

$$a1_{eff} = a1 + gt$$

$$a2_{eff} = a2 + gt$$

A similar approach is used to combine flaws when a circumferential flaw is close enough to an axial flaw (See Figure 3-3). If the ligament between the flaws is less than $(2a' + gt)$, then the effective flaw length for the circumferential flaw is $L_{eff} = L1 + S + gt$, and the crack depth is equal to the depth of the circumferential or axial flaw, whichever is greater. If the ligament is greater than $(2a' + gt)$, the flaws are treated separately.

After the circumferential and axial flaws have been combined per the above criteria, a map of the effective flaws in the shroud (which includes flaw depth and azimuthal location) can be made, and the effective flaw length can be used for subsequent fracture mechanics analysis.

Examples of the application of the combination of effective flaws for the UT screening criteria is similar to that for the visual screening criteria methods described in Section 3.2.1 except that the governing ligament is $(2a' + 2gt)$ instead of $(2T + 2gt)$.

Application of Effective Flaw Length Criteria

The application of the effective flaw length criteria is the same as that presented in Section 3.2.1 for the visual screening criteria. It should be noted that the flaw depths are now considered in this application.

3.3.2 Structural Analysis

The structural analysis of the shroud is similar to that used in the visual screening criteria described in Section 3.2. This section describes the analysis methodology and how it differs from that used in the visual screening criteria.

The methodology for the applied loads and resulting stresses and fracture mechanics analysis is identical to that described in Section 3.2. It should be noted that although part-through-wall credit is taken in the UT screening criteria, the interaction between crack tips (for LEFM analysis) still uses the shroud thickness instead of the depth of the deepest indication.

Limit Load Analysis

In the UT screening criteria limit load analysis, the part-through-wall depth, length and shroud azimuthal position are used to determine the acceptability of the flaws. Limit load calculations can be conducted using a similar approach to that outlined in Subsubarticle IWB-3640 and Appendix C of Section XI of the ASME Code. The flow stress was taken as $3S_m$. The S_m values for the shroud material are 16.9 ksi and 14.4 ksi for Type 304 and Type 304L, respectively, at the normal operating temperature of 550°F.

Safety factors similar to that used in the ASME Code are used in the analysis. The highest seismic stress is used for the limit load calculations. Similarly, the highest axial pressure stress corresponding to the lower shroud is used. Thus, the analytical results are applicable for all welds since limiting values are used. As an option, location specific stresses may be used in this evaluation.

3.3.3 Allowable Part Through-Wall Flaws

Allowable part through-wall flaws are determined using both fracture mechanics and limit load techniques for circumferential and axial flaws.

Allowable Part Through-Wall Circumferential Flaws

Both LEFM and limit load methods are used to evaluate the specific pattern of indications at a particular cross section. Above the core plate, the limiting location is the lowest weld above the core plate (e.g., H5 for the shroud design in Figure 2-1, and H4 for the shroud design in Figure 2-2). The weld between the lower shroud cylinder and core support cylinder involves Alloy 600, which has higher S_m values and therefore higher limit load capability, and is bounded by the allowable flaw size based on calculations assuming stainless steel.

Fracture Mechanics Analysis

The total axial pressure and seismic stress corresponding to the upset condition and faulted conditions are calculated based on simple strength of materials solutions. Using the ASME Code safety factors for fracture analysis, it must be determined which condition governs, faulted or normal and upset conditions. This is determined by multiplying the total normal and upset stress by 2.8 and the faulted stress by 1.4. The condition with the highest resulting stress is considered the limiting condition.

To determine the allowable flaw size based on LEFM methods, the conservatively estimated irradiated material fracture toughness K_{Ic} value of 150 ksi $\sqrt{\text{in}}$ was used. Applying a safety factor of 2.8 for the upset condition or 1.4 for faulted conditions, the allowable K_I of 53.5 ksi $\sqrt{\text{in}}$ for normal and upset and 107 ksi $\sqrt{\text{in}}$ for faulted is obtained. The allowable flaw size is calculated using the following equation from Section XI of the ASME Code:

$$K_I = \sigma_m M_m \sqrt{\pi} \sqrt{(a/Q)} + \sigma_b M_b \sqrt{\pi} \sqrt{(a/Q)}$$

Where σ_m = membrane stress

σ_b = bending stress

M_m = correction factor for membrane stress from Figure A-3300-3
from ASME Code, Section XI

M_b = correction factor for bending stress from Figure A-3300-5
from ASME Code, Section XI

a = crack depth

Q = flaw shape parameter from Figure A-3300-1 of ASME Code
Section XI.

Note that the flaw depth and length must include consideration for crack growth over the next cycle (gt for flaw depth, and $2gt$ for flaw length). Comparison of the applied stress intensity factor with the allowable fracture toughness determines if the flaw is acceptable.

Limit Load

Applying the limit load concept to the specific flaw configuration will result in a safety margin against collapse. Figure 3-12 shows an example of a flaw configuration. Similar to that performed in the visual screening criteria, the equations which can be used to determine the structural margin against collapse are derived by requiring equilibrium between an unflawed section of the shroud and the particular section of interest. Since the resulting equations are dependent on the particular crack configuration, a general expression cannot be determined prior to obtaining the actual UT results.

Prior to applying the equilibrium condition to a flaw pattern, the orientation of the axis (which defines the seismic moment direction) must be determined. This may be obtained on an iterative procedure until the limiting location is found.

Allowable Part Through-Wall Axial Flaws

Fracture Mechanics Analysis

The allowable axial flaw size is governed entirely by the pressure hoop stress. The applied stress intensity factor can be obtained using the same methodology presented for the

circumferential flaw LEFM determination. In this case, the axial stress (σ_b) is neglected. Comparison of the applied stress intensity factor with the allowable fracture toughness defines the allowable through-wall flaw length.

Limit Load

An alternate approach to determining the allowable flaw size is to use limit load techniques. The allowable flaw length is given by the equation:

$$\sigma_h = \sigma_f / (M_1 * SF)$$

where M_1 is a curvature correction factor (Reference 3-2), σ_f is the flow stress, SF is the safety factor of 3 for upset conditions or 1.5 for faulted, and σ_h = the hoop stress corresponding to the upset or faulted ΔP . The allowable flaw length is determined by satisfying the equation shown above.

3.3.4 UT Screening Criteria

The determination of flaw acceptability was described in Section 3.3.2. The UT screening criteria is summarized below.

For circumferential flaws, the effective flaw lengths (after application of proximity criteria) must be evaluated using the limit load method. In this method, a safety factor greater than 1.0 against the actual limit load must be shown to assure structural integrity. In addition to the limit load evaluation, the flaws must also be evaluated based on LEFM. This includes consideration of crack tip interaction, and subsequently compared with the allowable single flaw length for the given depth.

The effective axial flaw lengths can also be compared against the allowable LEFM length and the allowable limit load length.

It should be noted that when considering LEFM based evaluations, the crack tip interaction criteria must be applied in comparing against the allowable lengths. For example, for adjacent flaws where the spacing S is less than $0.75(L_1 + L_2)$, the length $L = L_1 + L_2$ is used for comparison with the LEFM based allowable flaw length.

3.4 References

- 3-1 Rooke, D.P. and Cartwright, D.J., "Compendium of Stress Intensity Factors," The Hillingdon Press (1976)
- 3-2 Ranganath, S., Mehta, H.S., and Norris, D.M., "Structural Evaluation of Flaws in Power Plant Piping," ASME PVP Volume No. 94 (1984)

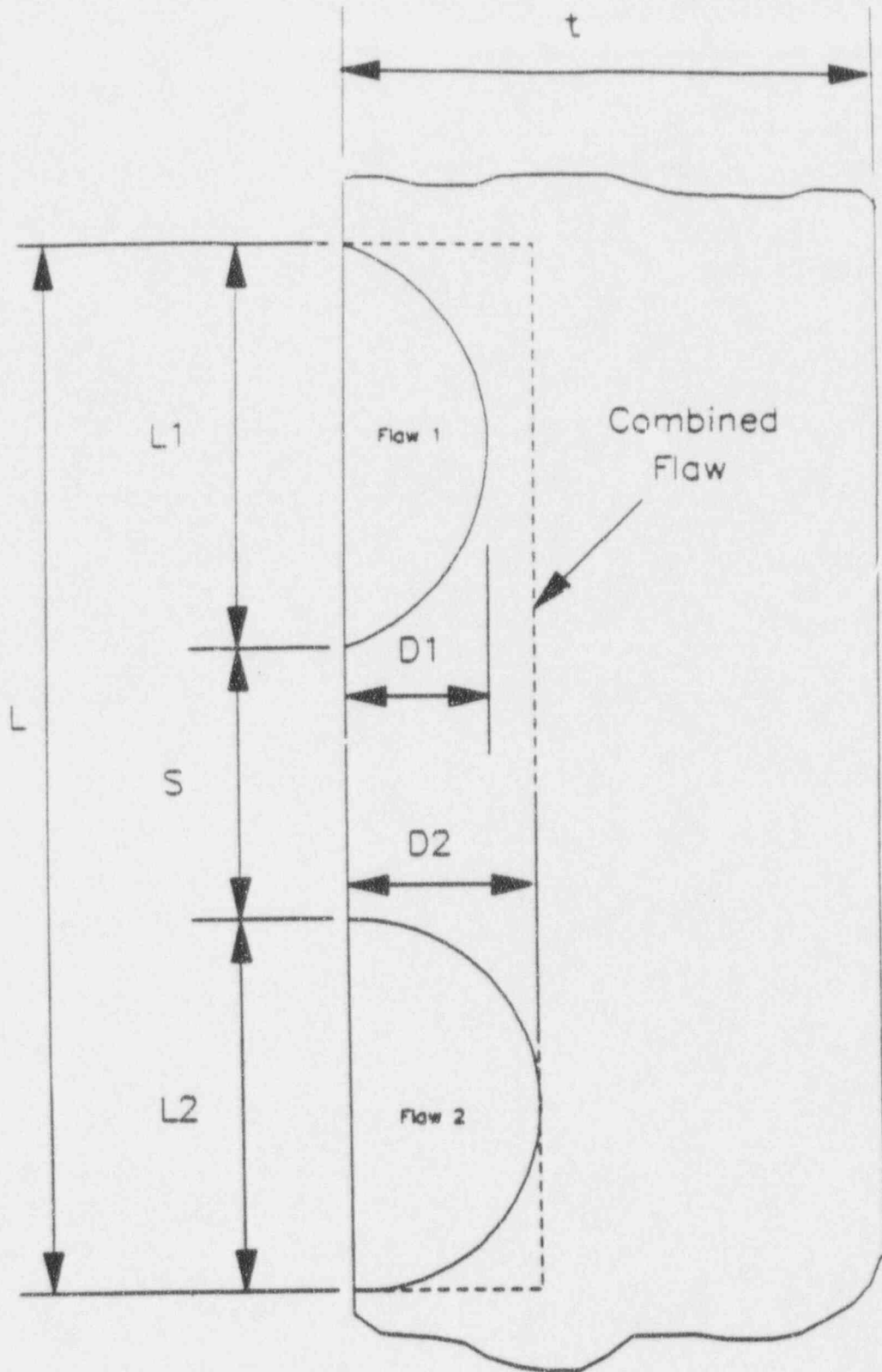


Figure 3-1 ASME Code Proximity Criteria

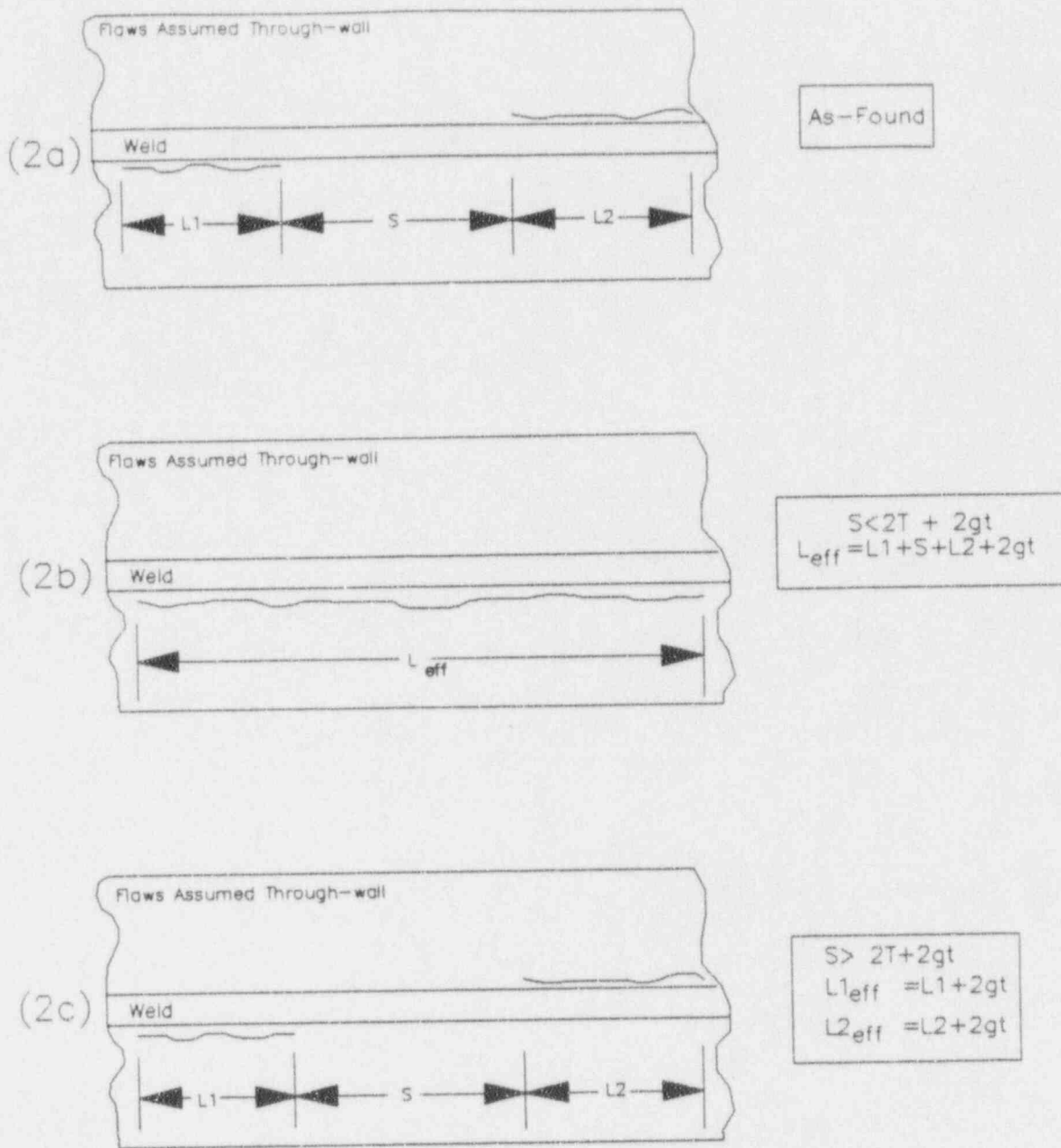


Figure 3-2 Application of Proximity Procedure to Neighboring Circumferential Flaws

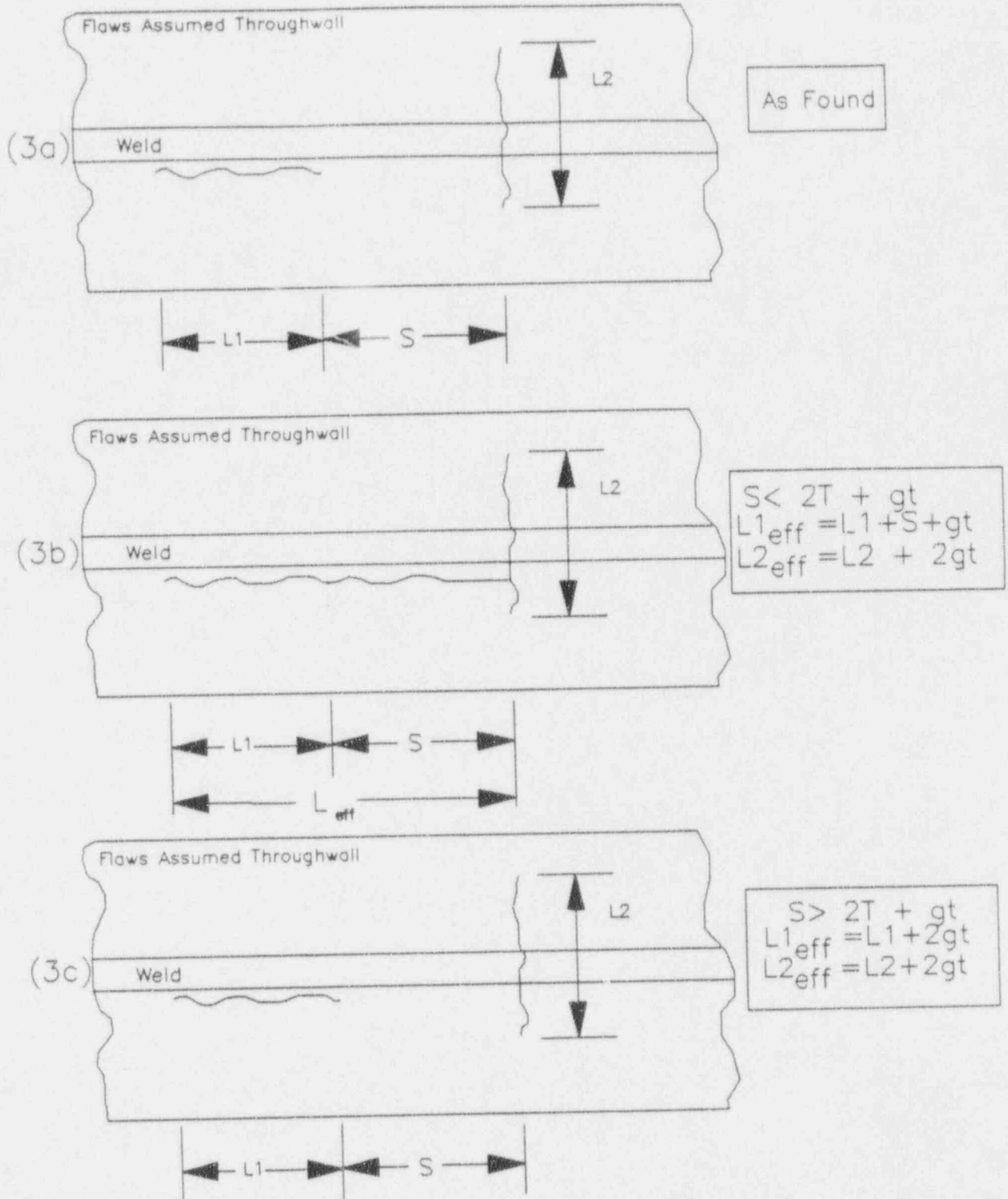


Figure 3-3 Application of Proximity Procedure to Neighboring Axial and Circumferential Flaws

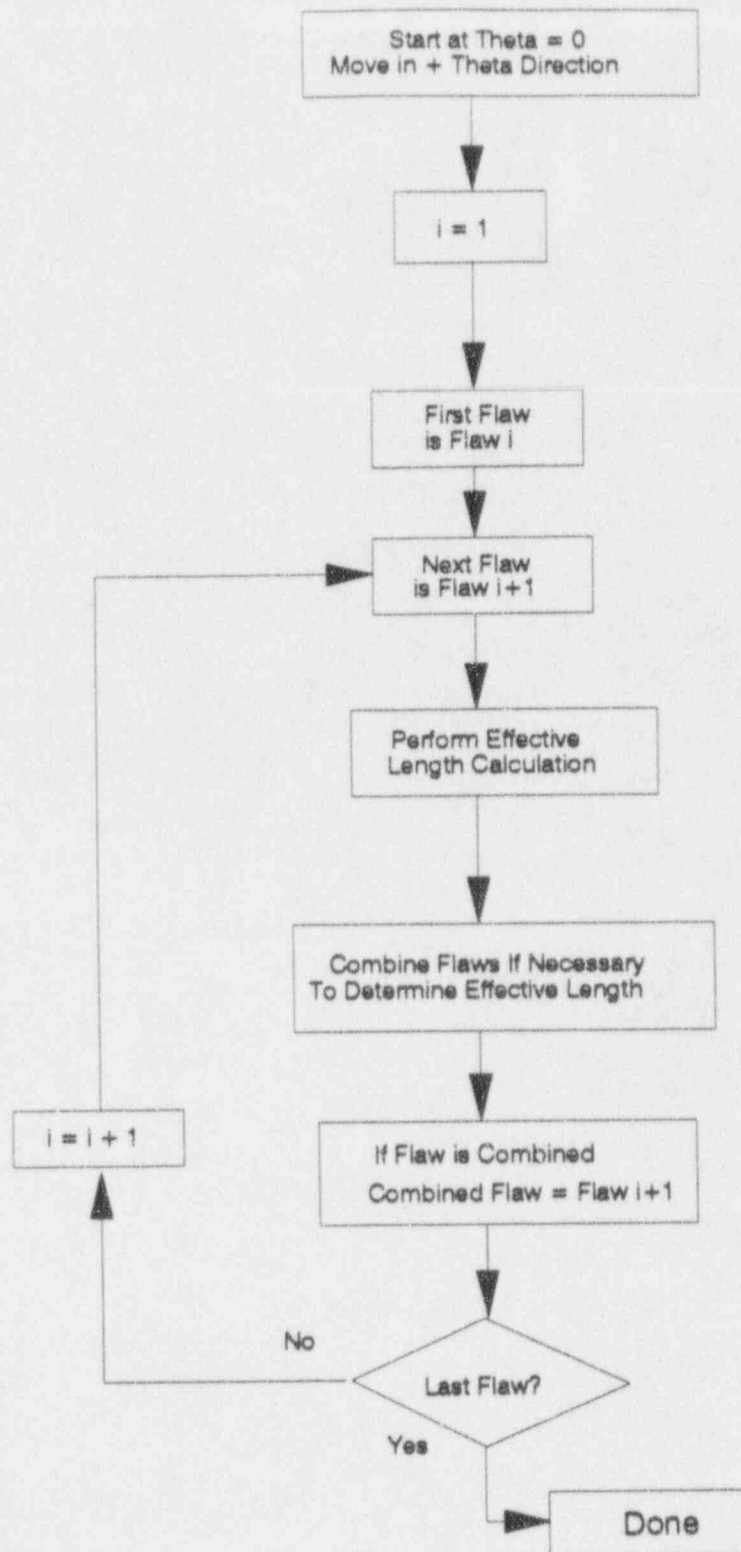


Figure 3-4 Process For Determining Effective Circumferential Flaw Length

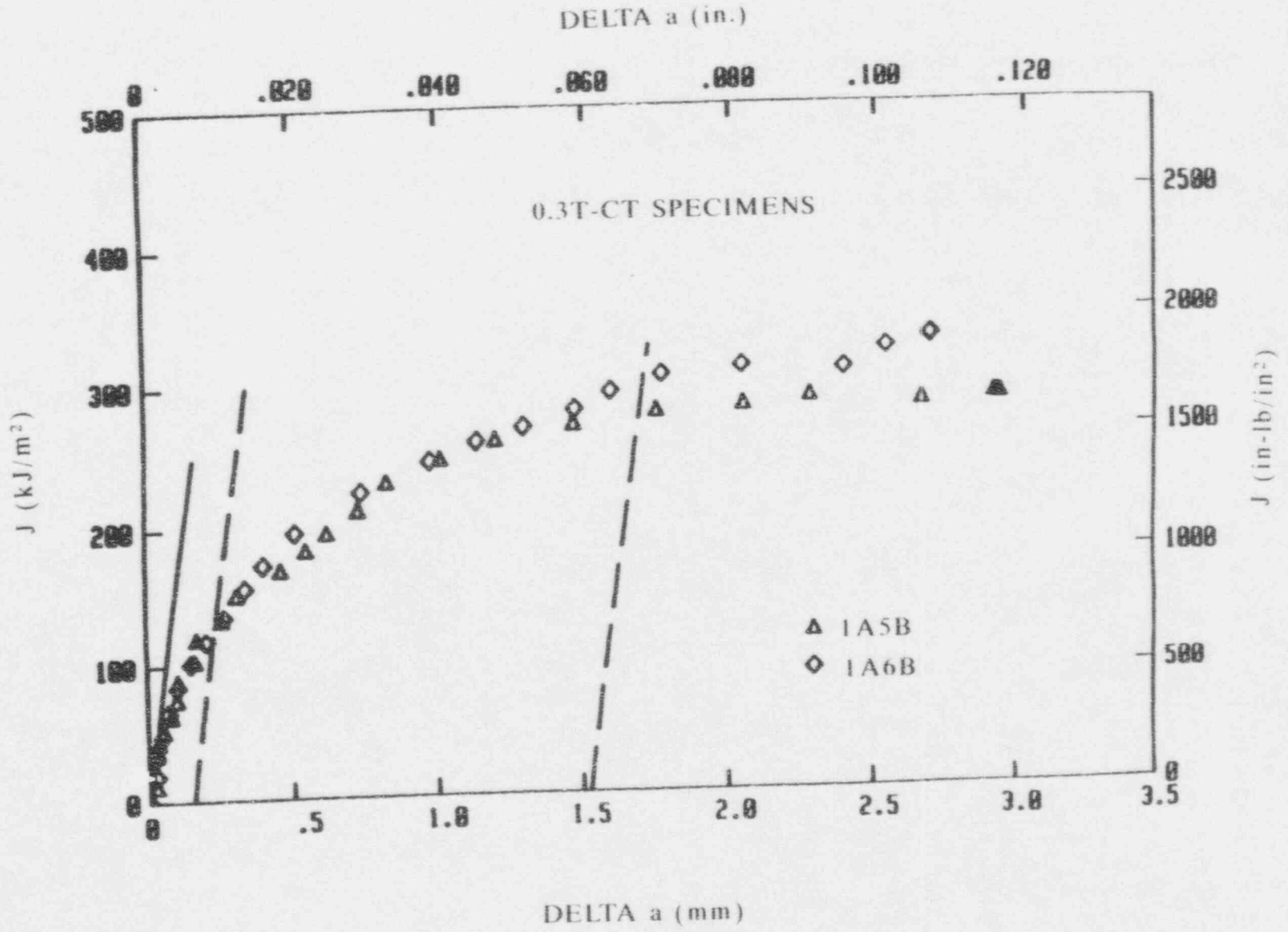


Figure 3-5 Comparison of J-R Curves For Two Irradiated Stainless Steel Specimens

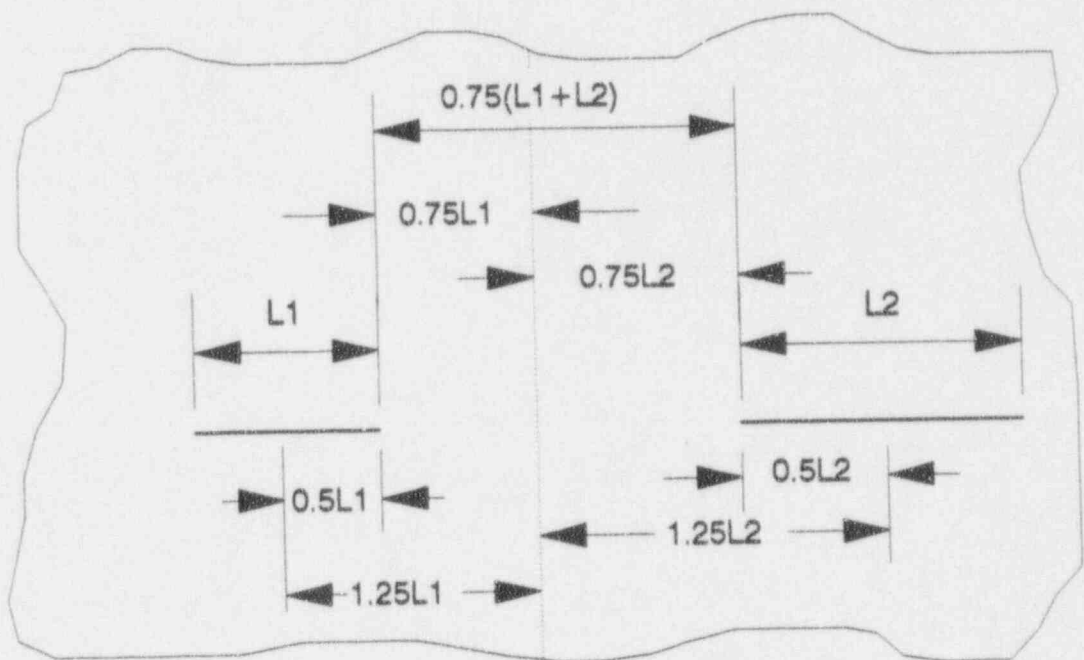
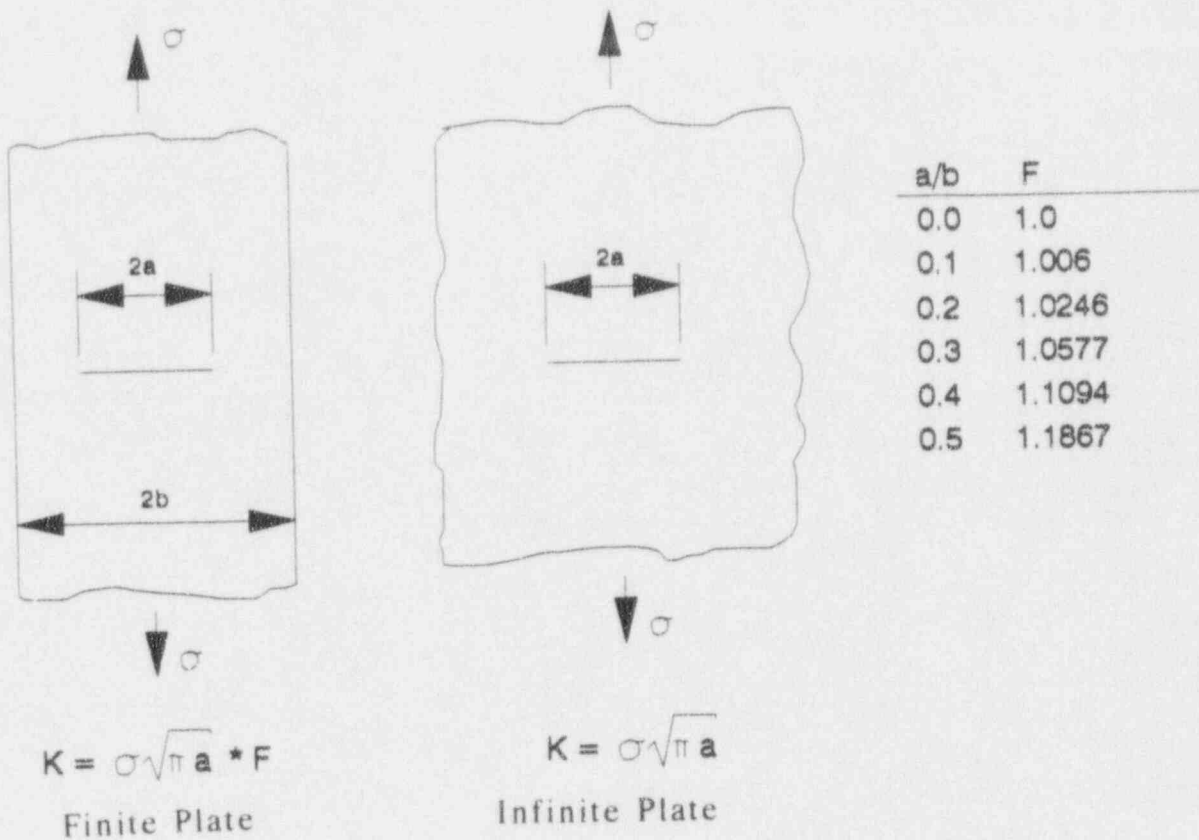


Figure 3-6 Schematic Illustrating Flaw Interaction

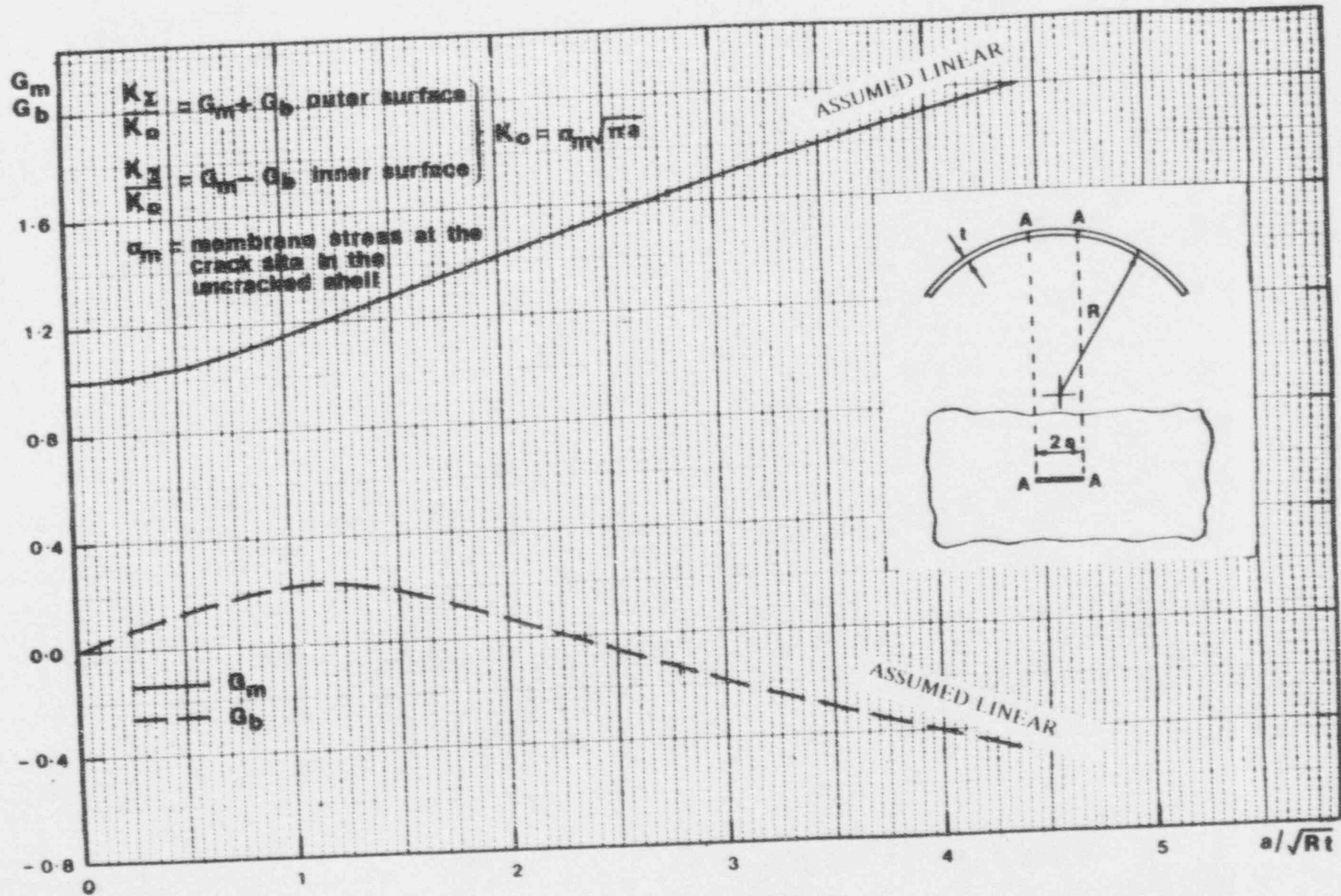


Figure 3-7 KI for Point A of a Circumferential Crack in a Cylindrical Shell Subjected to a Uniform Membrane Stress

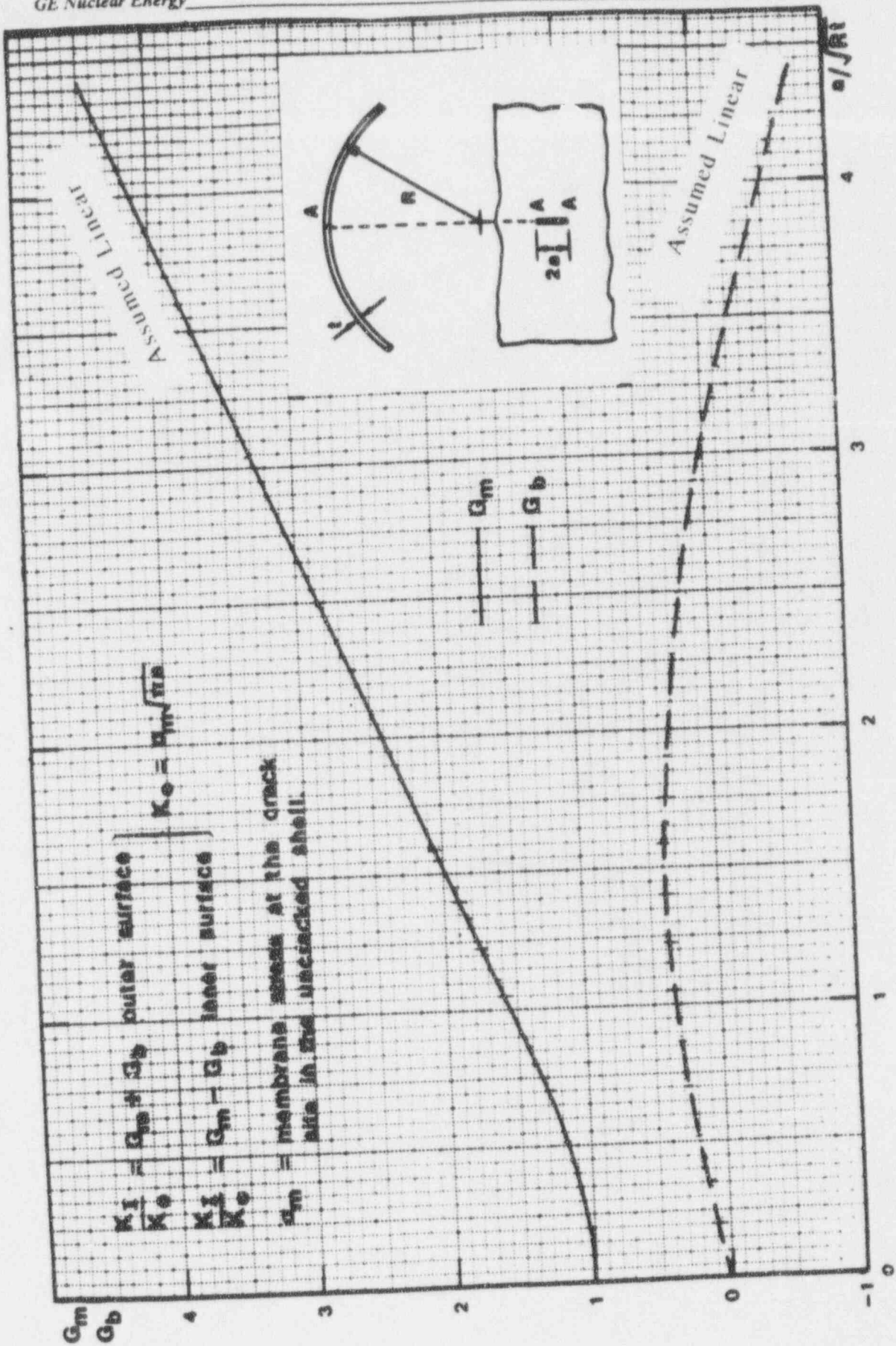
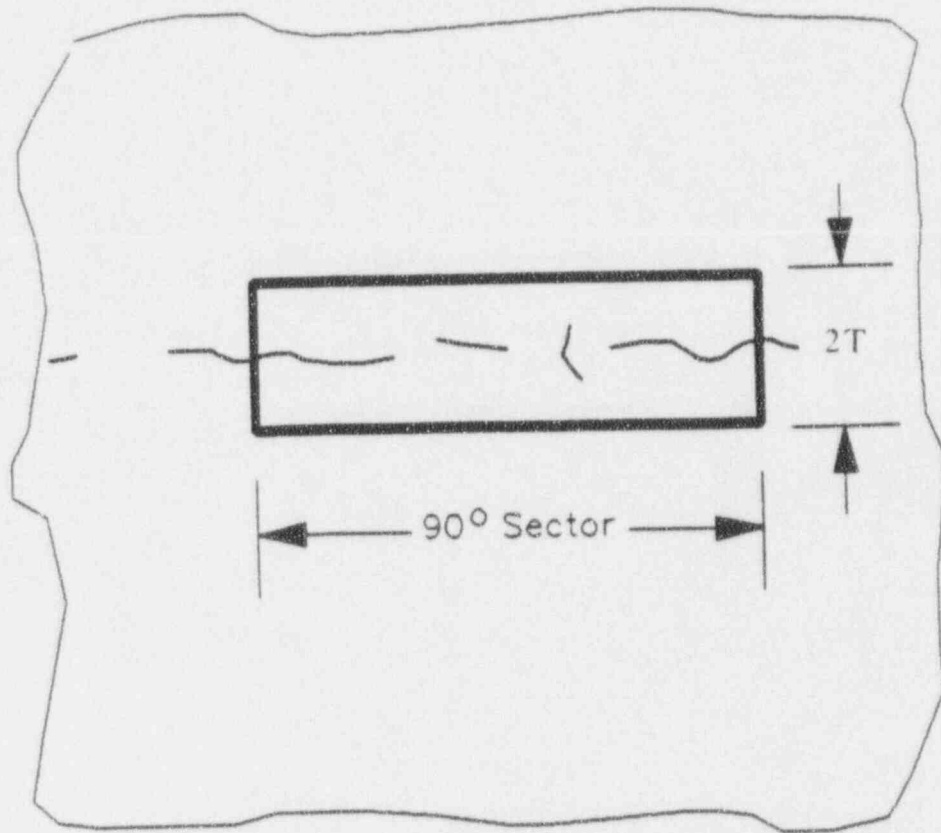


Figure 3-8 KI for Point A of a Longitudinal Crack in a Cylindrical Shell Subjected to a Uniform Membrane Stress



Not to Scale

Figure 3-9 Schematic Illustrating Cumulative Effective Flaw Criterion

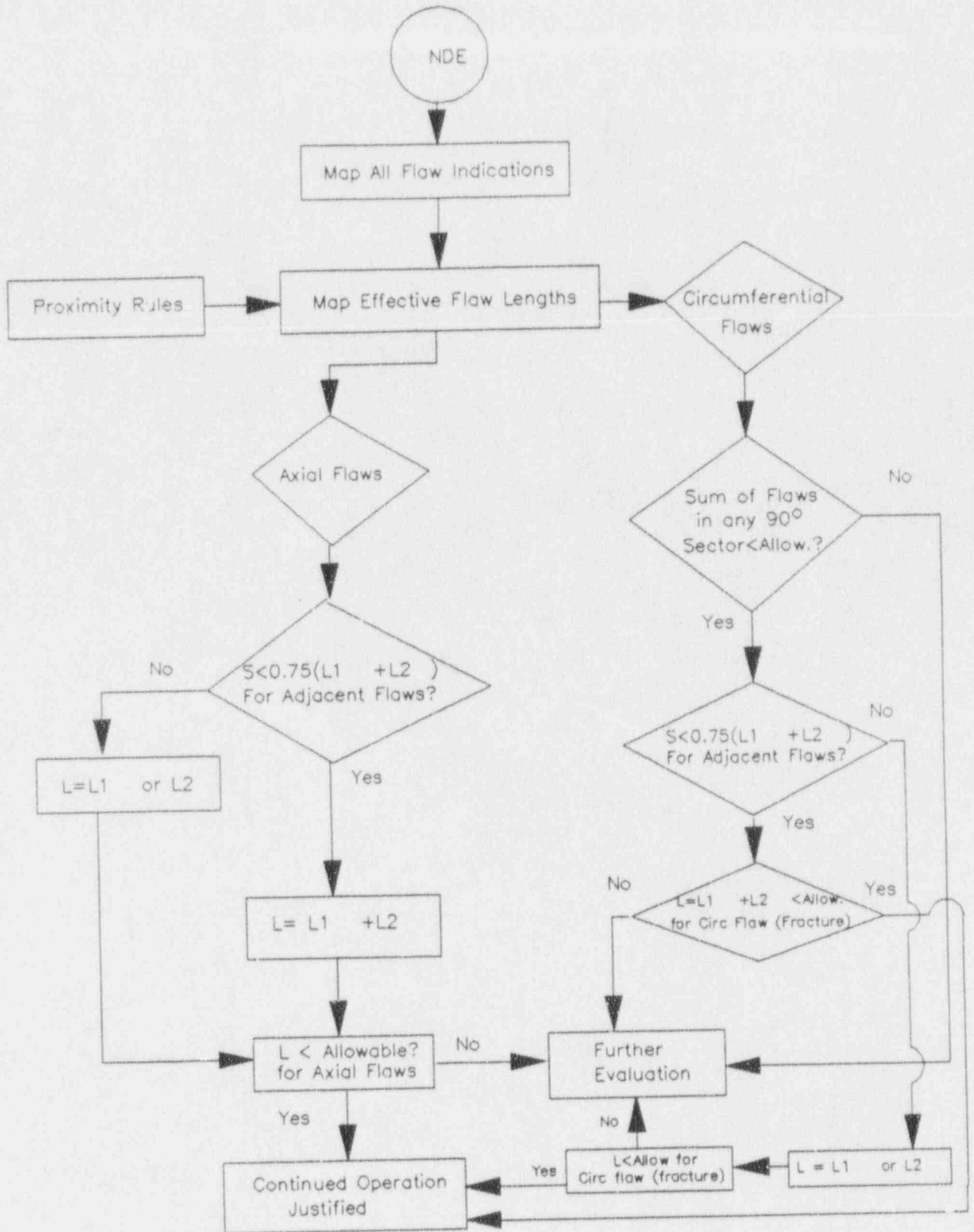


Figure 3-10 Schematic of Screening Criteria

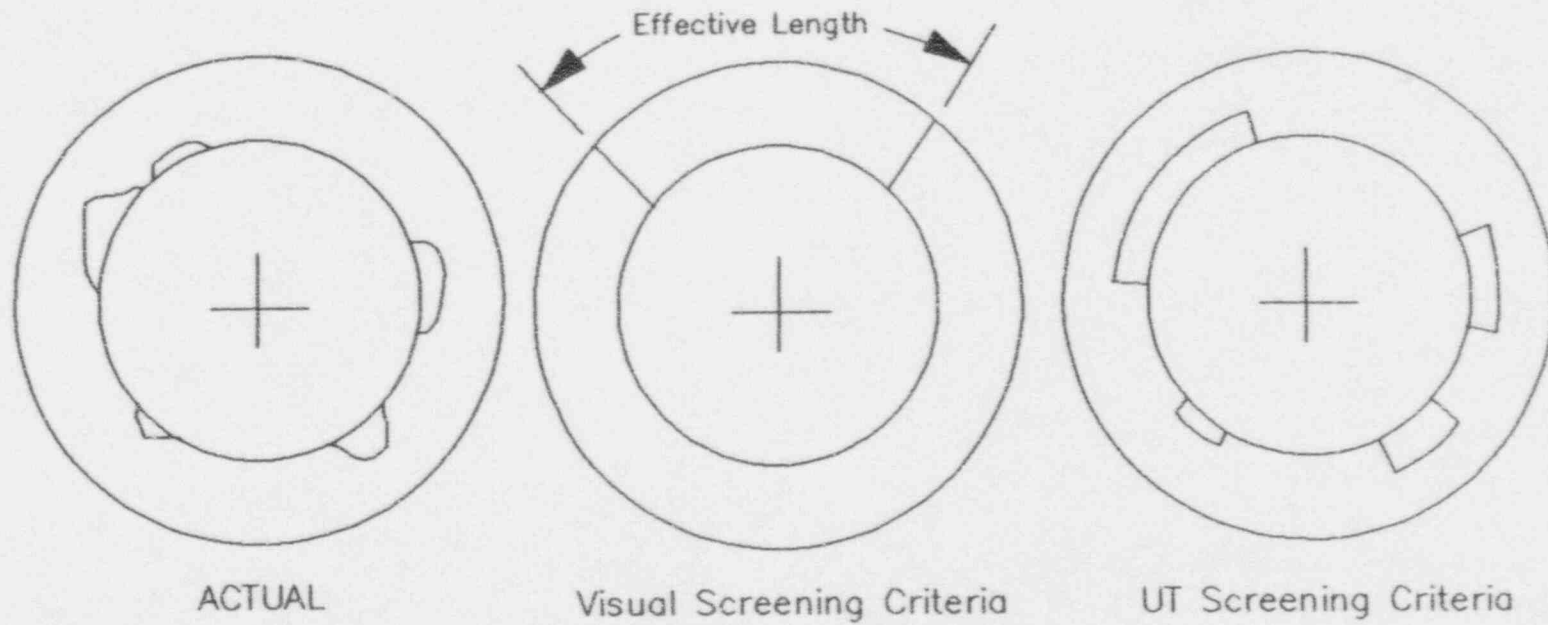


Figure 3-11 Flaw Geometry Assumption Used in Screening Criteria
(For Limit Load Evaluation)

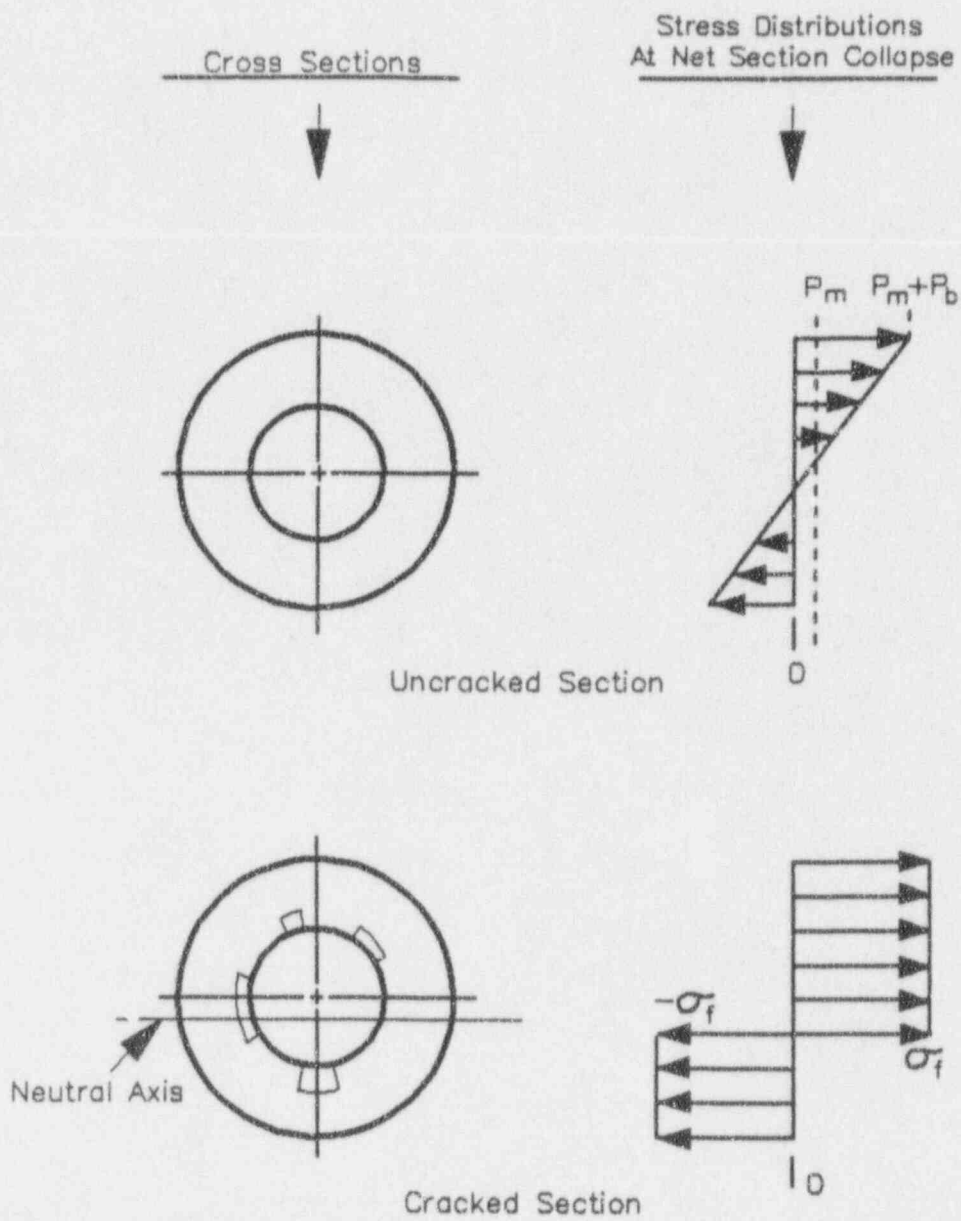


Figure 3-12 Limit Load Schematic for UT Screening Criteria

4.0 MITIGATION OF CORE SHROUD IGSCC AND IASCC

4.1 Introduction

This section provides information regarding mitigation of core shroud cracking. The recent incidences of cracking have demonstrated the advantage of taking early precautions to lessen the potential and extent of intergranular stress corrosion cracking (IGSCC) and irradiation assisted stress corrosion cracking (IASCC).

It is well documented that the BWR recirculation coolant's ≈ 200 ppb dissolved oxygen is more than sufficient to provide the electrochemical driving force for IGSCC of BWR structural materials. This concentration of dissolved oxygen (and other oxidizing species) generates an electrochemical potential (ECP) in the austenitic stainless steel piping system of ≈ 100 mV(SHE) that is above the ECP threshold for IGSCC of sensitized stainless steel and nickel based alloys. The more oxidizing core of the BWR is characterized by a higher ECP of $\approx +250$ mV(SHE). Finally, the conductivity of the BWR coolant is sufficiently high to allow these corrosion phenomena to occur.

Over a decade of laboratory and in-reactor investigations have revealed that lowering the ECP of sensitized stainless steel to < -230 mV(SHE) by injecting hydrogen gas into the BWR feedwater, and reducing coolant conductivity to < 0.3 μ S/cm by better BWR water chemistry operational practices, would mitigate IGSCC of BWR piping (Reference 4-1). For IASCC of non-thermally sensitized stainless steel, the threshold ECP is ≈ -140 mV(SHE) (Reference 4-2). Since this process, hydrogen water chemistry (HWC), reduces the "corrosiveness" of the entire BWR coolant, it is considered a potential "blanket" IGSCC/IASCC mitigation technique. The results of extensive testing have clearly demonstrated that HWC mitigates environmental cracking in numerous BWR structural materials and has no insuperable materials deleterious effects (Reference 4-1).

However, some BWRs may not be able to implement HWC on a timely basis. For this category of plants, the strict control of conductivity can still provide dramatic IGSCC benefits, albeit not total IGSCC/IASCC mitigation.

4.2 Core Shroud IGSCC Mitigation with HWC

Although IGSCC/IASCC of reactor internals to date has been limited due to their typically low tensile stress levels, and the impact has been manageable, IGSCC of reactor internals is an increasing concern as the BWR fleet ages. In the short term, continued operation of an overseas BWR-4 plant and Peach Bottom Unit-3 with core shroud indications are being supported by analysis. The Brunswick Unit-1 shroud has been repaired for the limiting locations and analysis is being used to disposition cracking at other weld locations.

Due to the complete lack of sensitization (chromium carbides at the grain boundaries) of the relatively low carbon (0.045%) stainless steel shroud, the cracking at the overseas BWR-4 appears to be strictly IASCC. For the Brunswick Unit-1 shroud, the nature of the cracking, (i.e., shroud ID surface with grain cracking envelopment, thicker oxides and extensive crack branching and OD surface with more pipe-like SCC characteristics) suggests that the total SCC phenomenon appears to be a synergistic combination of thermal sensitization IGSCC and IASCC.

Recent reactor internal cracking incidences suggest that the "blanket" IGSCC remedy, HWC, may be necessary to protect the reactor internals. However, to provide sufficient environmental protection in the highly oxidizing core region (O_2 plus H_2O_2) with HWC would require, in many instances, such large injection rates of hydrogen that burdensome radiation (increased N-16 during operation and increased shutdown radiation levels) penalties could occur. At most plants, this N-16 dose rate could be increased by factors of 4 to 6 or higher, and require additional shielding and modified operational practices to reduce personnel and site boundary exposures to acceptable levels.

Because of the highly oxidizing nature of the coolant within and above the core, even with HWC at moderate (1.0 to 1.6 ppm) to high (2.0 to 2.6 ppm) hydrogen addition levels, the upper shroud H1 and H2 welds are not protected on the outside diameter surface for plants with Type 304 stainless steel shrouds (Figure 4-1). In addition, at moderate levels, the inside of the shroud beltline welds H3, H4 and H5 (some plants only have H4 beltline weld) are not protected. Fortunately, as will be discussed in Section 4.3, the use of noble metal coatings (NMCs) in conjunction with HWC looks

promising for use in the future to provide SCC protection for these specific shroud welds.

4.3 "Low Impact" HWC and Internal Noble Metal Coatings/Alloys

A perhaps more timely shroud IGSCC/IASCC mitigation option for some plants that can make HWC more efficient while minimizing radiation penalties is the use of Noble Metal Coatings (NMCs). This technology is currently under development and qualification, and is being continuously evaluated by the BWROG. This approach would consist of depositing dilute NMCs on the shroud to lower the local ECP below the IGSCC/IASCC thresholds with near stoichiometric ratios of hydrogen and oxygen, i.e., with little excess hydrogen injection.

As noted above, due to the BWRs core's highly oxidizing nature ($\cong +250$ mV[SHE]), more hydrogen is required for an equivalent shift in ECP to provide protection against IGSCC/IASCC in the core region. However, since noble metals have long been recognized as recombination catalysts for oxygen and hydrogen dissolved in water, it is possible to use NMCs to assist in-core recombination. It has been determined that the ECP of a surface containing only small amounts of noble metals decreased to very low values when hydrogen was present in stoichiometric amounts (or greater), even in the absence of complete volume recombination of oxygen and hydrogen in the water (Reference 4-3).

Figure 4-2 presents the effect of Pd in 285°C (545°F) water containing 300 ppb oxygen and various hydrogen concentrations (Reference 4-3). While the nominal Type 316 stainless steel demonstrates little change in ECP, the palladinized electrode exhibits a dramatic drop in ECP from $\cong 100$ mV (SHE) to approximately -500 mV (SHE) below a molar ratio of 2. This hydrogen concentration ($\cong 24$ ppb) is less than stoichiometrically required for 300 ppb oxygen (37.5 ppb) due to the higher diffusivity (1.83x) of hydrogen versus oxygen in the water boundary layer. The above results clearly indicate that a catalyzed surface can reduce the ECP of stainless steel with significantly less hydrogen than is required in the absence of a catalyst. Subsequent studies have replicated these coating results and have also demonstrated identical beneficial results with Pd microalloyed stainless steel (Reference 4-4).

Constant extension rate tests (CERT) were conducted on welded plus low temperature sensitized (500°C/24h) Type 304 stainless steel to directly evaluate the effect of Pd coatings on IGSCC. The results are summarized in Table 4-1 and Figure 4-3 (Reference 4-3). As anticipated, the measured ECPs for Type 304 stainless steel were similar to those obtained for Type 316 stainless steel described above. It is uniformly observed that the stainless steel autoclave is characterized by ECPs above the protection potential since it was not palladinized.

The dissolved oxygen levels in all the CERT tests were maintained at significantly higher levels than would be observed in a HWC environment. In addition, the first two CERTs, which included the unpalladinized control specimen, were performed at high hydrogen-to-oxygen molar ratios. The remainder of the CERTs had hydrogen-to-oxygen molar ratios at the sample surface close to the stoichiometric value for the formation of water of 2:1, with consideration for the differences in diffusion coefficients. When the molar ratio exceeded 2.0, the ECPs of the palladinized specimens was considerably below the IGSCC protection potential even with coatings as thin as 0.03 μm . When the molar ratio was less than 2.0, the ECPs of the specimens were above the IGSCC (and in most cases the IASCC) protection ECP. Subsequent scanning electron microscopy (SEM) examinations of the fracture surfaces confirmed that only the unpalladinized specimens suffered IGSCC.

Since a few shrouds have SCC, crack propagation studies on Pd coated specimens are particularly relevant (Reference 4-5). Figure 4-4 presents the crack growth results of a furnace sensitized Type 304 stainless steel specimen that was noble metal coated under water with 0.42% Pd Type 309L stainless steel weld metal using the high velocity oxy-fuel (HVOF) technique. The high stress intensity (33 $\text{MPa}\sqrt{\text{m}}$ [30 $\text{ksi}\sqrt{\text{in}}$]) fracture mechanics specimen was exposed to both stoichiometrically excess oxygen (H_2/O_2 molar ratio < 2) and excess hydrogen environments (H_2/O_2 molar ratio > 2). When the specimen was exposed to the excess oxygen environment (180 ppb O_2 , 9.6 ppb H_2 , $\text{H}_2/\text{O}_2 = 0.85$), the crack propagation rate is 1.46 $\mu\text{m}/\text{h}$ (503 mpy). However, when the hydrogen concentration is increased to create a stoichiometrically excess hydrogen (150 ppb O_2 , 24 ppb H_2 , $\text{H}_2/\text{O}_2 = 2.56$) environment, the crack propagation rate dramatically decreases two orders of magnitude to only 0.01 $\mu\text{m}/\text{h}$ (3.5 mpy).

4.4 Conductivity Control to Reduce IGSCC Susceptibility

The benefit of good water purity in reducing IGSCC susceptibility has been recognized for several years, and the average water conductivity of the entire BWR fleet has improved dramatically in recent years.

An example of the effects of conductivity (sulfate) on crack initiation in uncreviced material is presented in Figure 4-5 (References 4-6 through 4-9). It is clear that an increase in sulfate/conductivity results in an acceleration in crack initiation as measured by CERT. A specific example of an acceleration in crack propagation rate on creviced material with sulfate is shown in Figure 4-6. Figure 4-6 displays June 1986 Peach Bottom 3 on-line reversing DC potential drop crack monitoring data for sensitized Type 304 stainless steel. The results clearly illustrate the change in crack growth observed after two closely linked water chemistry transients of 4-5 $\mu\text{S}/\text{cm}$, i.e., increases in water conductivity due to intrusions of demineralizer resin material (Reference 4-10). This figure demonstrates the dramatic increase in crack growth rate (2X) with conductivity. Similar on-line crack monitoring results with sulfate have also been documented in the laboratory, Figure 4-7 (Reference 4-11). Other anions such as chloride, fluoride, silicate, phosphate, etc., have similar kinetic effects on IGSCC initiation and propagation (References 4-12 and 4-13).

This high conductivity crack initiation and propagation acceleration factor is consistent with the relatively high incidence of IGSCC in creviced Alloy 600 shroud head bolts and access hole covers. Additional documentation on the strong correlation of IGSCC susceptibility with actual BWR plant water chemistry history for creviced BWR components has been published (Reference 4-14).

4.4.1 IGSCC Modeling

Finally, the effect of conductivity and ECP on crack propagation has also been quantified at the GE Research and Development Center based on a "first principles" model of crack advance known as the film rupture/slip dissolution model (Reference 4-15). Predictions from PLEDGE (Plant Life Extension Diagnosis by GE) model have been extensively compared with laboratory and field data and have provided validation of the technique. For example, PLEDGE predicts the crack growth rate in stainless steel and low alloy steel within a factor of approximately two for a 70% statistical

confidence over a range in observed crack growth rate of more than six orders of magnitude. Likewise, it provides a very reasonable mean value and can accurately bound the observed crack growth rate in stainless piping and other components. Aside from piping predictions, PLEDGE has been successfully used for predicting in-reactor on-line compact tension specimen crack growth monitoring data and incorporating this data into the model for refinement. In a more practical application, the PLEDGE modeling approach was used to avoid a mid-cycle plant shutdown safe end inspection. Non-sensitized (stabilized) stainless steels and reactor internals such as the core shroud, top guide, access hole cover and in-core monitor housing have also been successfully modeled with PLEDGE.

Finally, the PLEDGE Model of IGSCC and, more recently, IASCC (Reference 4-16) clearly indicate the strong effect of conductivity on crack growth rate and, by inference, crack initiation. Figure 4-8 presents a schematic estimation of Peach Bottom 2 and 3 sensitized Type 304 stainless steel crack growth rates as a function of conductivity using the PLEDGE model. Crack growth rates based on actual conductivity averages for the first ten years (Unit-2: 0.593 $\mu\text{S}/\text{cm}$, Unit-3: 0.752 $\mu\text{S}/\text{cm}$) were compared to those averages for the last two years. A value of 200 mV(SHE) was used for the ECP in these calculations. As noted in Figure 4-8, a factor of improvement (FOI) of approximately twenty (20) decrease in crack growth rate is obtained with Unit-2's decrease in conductivity. The FOI for Unit-3 is eleven (11).

4.5 Shroud IGSCC/IASCC Mitigation Factors of Improvement

Table 4-2 summarizes the estimated FOIs for reactor internals, based on relative crack propagation rates. The ECPs for the top of the core (Brunswick 1 shroud flange IGSCC) and bottom of the core (access hole cover) were estimated from FitzPatrick data, Figure 4-9 (Reference 4-17). The ECP of noble metals was derived from data from Duane Arnold, Figure 4-10 (Reference 4-18). The benefits of conductivity (only) improvement as based on PLEDGE model calculations are also included.

4.6 An Additional Potential IGSCC/IASCC Mitigation Technique

Although it has been demonstrated that there is a clear crack growth rate reduction benefit with zinc injection and HWC (References 4-19 and 4-20), the latest synergistic

depleted zinc oxide (DZO)/HWC laboratory studies indicate that the amount of crack growth reduction is highly variable with uncertain reproducibility, especially for Alloy 182. Since it has been observed that the material response time is much slower than that obtained with high hydrogen (HWC) levels alone, it requires considerably longer time to establish the lower bound crack growth rates. Although there is insufficient data to establish a BWR water chemistry specification with predictably reliable results, testing will continue to quantify the benefit at low DZO levels (10 ppb) since this may provide a future cost saving by allowing somewhat lower hydrogen addition rates to achieve HWC protection. The BWR Owners' Group will continue to monitor the progress of this activity.

4.7 Core Shroud IGSCC/IASCC Mitigation Options

The above discussion reveals the following options for addressing the degradation of the BWR core shroud:

1. HWC. This "blanket" IGSCC/IASCC remedy lowers the ECP of the core shroud and mandates a lower coolant conductivity. However, achieving such in-core protection can result in high radiation levels during operation and shutdown.
2. "Low Impact" HWC and NMCs. This technique utilizes the catalytic nature of noble metals to increase HWC efficiency and minimize radiation penalties. Although this concept has been clearly proven in the laboratory, technological application details are under development and qualification.
3. Conductivity Control. This universally sound approach would only delay the initiation of cracking and reduce crack propagation rates. It is not sufficient to mitigate SCC in the BWR.
4. DZO/HWC. This is a potential "low impact" HWC technique where an operating specification relationship could be developed between DZO and hydrogen additions to minimize SCC and radiation penalties. Additional testing of this technique is required.

It is obvious that the above SCC mitigation options are characterized by either detrimental side effects (HWC) or inadequacy (conductivity only), or they have not been fully qualified (HWC/NMCs and DZO/HWC). Therefore, the optimum core shroud SCC mitigation approach will vary from plant to plant and will require a complete specific evaluation of these and future options.

4.8 References

- 4.1. B. M. Gordon et al, "Hydrogen Water Chemistry for BWRs-Materials Behavior-Final Report," EPRI TR-100304, Palo Alto, CA, February 1992.
- 4.2. M. E. Indig et al, "Investigation of the Protection Potential Against IASCC," paper #71 presented at Corrosion 92, NACE, Nashville, April 1992.
- 4.3. L. W. Niedrach, "Effect of Palladium Coatings on the Corrosion Potential of Stainless Steel in High Temperature Water Containing Dissolved Hydrogen and Oxygen," *Corrosion*, Vol. 47, No. 3, p. 162, March 1991.
- 4.4. Y. Kim et al, "The Application of Noble Metals in Light-Water Reactors," *Journal of Metals*, p. 14, April 1992.
- 4.5. P. L. Andresen, "Effect of Pd-coating and Pd-alloying on the Stress Corrosion Cracking of Stainless Steel," PMWG-G-677, August 1992.
- 4.6. W. J. Shack, et al, "Environmentally Assisted Cracking in Light Water Reactors: Semiannual Report April - September 1985," NUREG/CR-4667, ANL-86-31, June 1986.
- 4.7. W. J. Shack, et al, "Environmentally Assisted Cracking in Light Water Reactors: Annual Report October 1983 - September 1984," NUREG/CR-4287, ANL-85-33, June 1985.
- 4.8. L. G. Ljungberg, D. Cubicciotti and M. Trolle, "Effects of Impurities on the IGSCC of Stainless Steel in High Temperature Water," *Corrosion*, Vol. 44, No. 2, February 1988.
- 4.9. W. E. Ruther, W. K. Soppet and T. F. Kassner, "Effect of Temperature and Ionic Impurities at Very Low Concentrations on Stress Corrosion Cracking of Type 304 Stainless Steel," paper 102 presented at Corrosion 85, Boston, MA, NACE, March 1985, published in *Corrosion*, Vol. 44, No. 11, November 1988.
- 4.10. D. A. Hale and C. G. Diehl, "Real Time Monitoring of Environmental Crack Growth in BWRs," paper 455 presented at Corrosion 88, St. Louis, MO, NACE, March 1988.
- 4.11. B. M. Gordon, "Corrosion and Corrosion Control in BWRs," NEDE-30637, p. 6-22, December 1984.

4.8. References (continued)

- 4.12. R. B. Davis and M. E. Indig, "The Effect of Aqueous Impurities on the Stress Corrosion Cracking of Austenitic Stainless Steel in High Temperature Water," paper 128 presented at Corrosion 83, Anaheim, CA, NACE, April 1983.
- 4.13. P. L. Andresen, "A Mechanism for the Effects of Ionic Impurities on SCC of Austenitic Iron and Nickel Base Alloys in High Temperature Water," paper 101 presented at Corrosion 85, Boston, MA, NACE, March 1985.
- 4.14. K. S. Brown and G. M. Gordon, "Effects of BWR Coolant Chemistry on the Propensity for IGSCC Initiation and Growth in Creviced Reactor Internals Components," paper presented at the Third Int. Symp. of Environmental Degradation of Materials in Nuclear Power Systems-Water Reactors, Traverse City, MI, August 1987, published in proceedings of same, TMS-AIME, Warrendale, PA, 1988.
- 4.15. F. P. Ford et al, "Prediction and Control of Stress Corrosion Cracking in the Sensitized Stainless Steel/Water System," paper 352 presented at Corrosion 85, Boston, MA, NACE, March 1985.
- 4.16. P. L. Andresen and F. P. Ford, "Modeling of Irradiation Effects on Stress Corrosion Cracking Growth Rates," paper 497 presented at Corrosion 89, New Orleans, LA, NACE, April 1989.
- 4.17. R. A. Head and M. Siegler, "In-Core Response to Hydrogen Water Chemistry at J. A. FitzPatrick," EP89-32, January 1992.
- 4.18. W. D. Miller, R. A. Head and M. E. Indig, "Measurement of In-Core and Recirculation Response to Hydrogen Water Chemistry at the Duane Arnold Energy Center," EPRI TR-102310 April 1993.
- 4.19. P.L. Andressen and T.P. Diaz, "Effects of Zinc Additions on the Crack Growth Rate of Sensitized Stainless Steel and Alloys 600 and 182 in 288°C Water," Paper #72 presented at the 6th International Conference on Water Chemistry of Nuclear Reactor Systems, October 1992.
- 4.20. W.J. Shack et al, "Environmentally Assisted Cracking in Light Water Reactors: Semiannual Report, April - September 1986," NUREG/CR-4667 Vol. III, ANL-87-37, September 1987

Table 4-1. Results of Constant Extension Rate Tests
Sensitized Type 304 Stainless Steel

CERT No.	Pd			Molar Ratio		ECP		Time to	
	Thick (μm)	H2 (ppb)	O2 (ppb)	H2:O2 (a)	(b)	CERT (mV)	Auto (mV)	Failure (h)	IGSCC (%)
1	0.00	161	95	27.1	49.6	-102	31	70	26
2	0.77	161	104	24.8	45.3	-535	-110	124	0
3	0.77	16	196	1.3	2.4	-515	-100	125	0
4	0.77	9	196	0.7	1.3	50	-102	76	33
5	0.07	19	251	1.2	2.2	-490	-150	118	0
6	0.03	20	263	1.2	2.2	-400	-110	126	0

Test Conditions:

287°C

0.3×10^{-6} M H₂SO₄

Conductivity: 0.3 $\mu\text{S}/\text{cm}$

Strain rate: $1 \times 10^{-6}/\text{s}$

(a) Molar ratio in water = 16 x ppb H₂/O₂

(b) Molar ratio at surface = 1.83 Molar ratio in water
where 1.83 is the ratio of the diffusion coefficients
for H₂ and O₂ in water

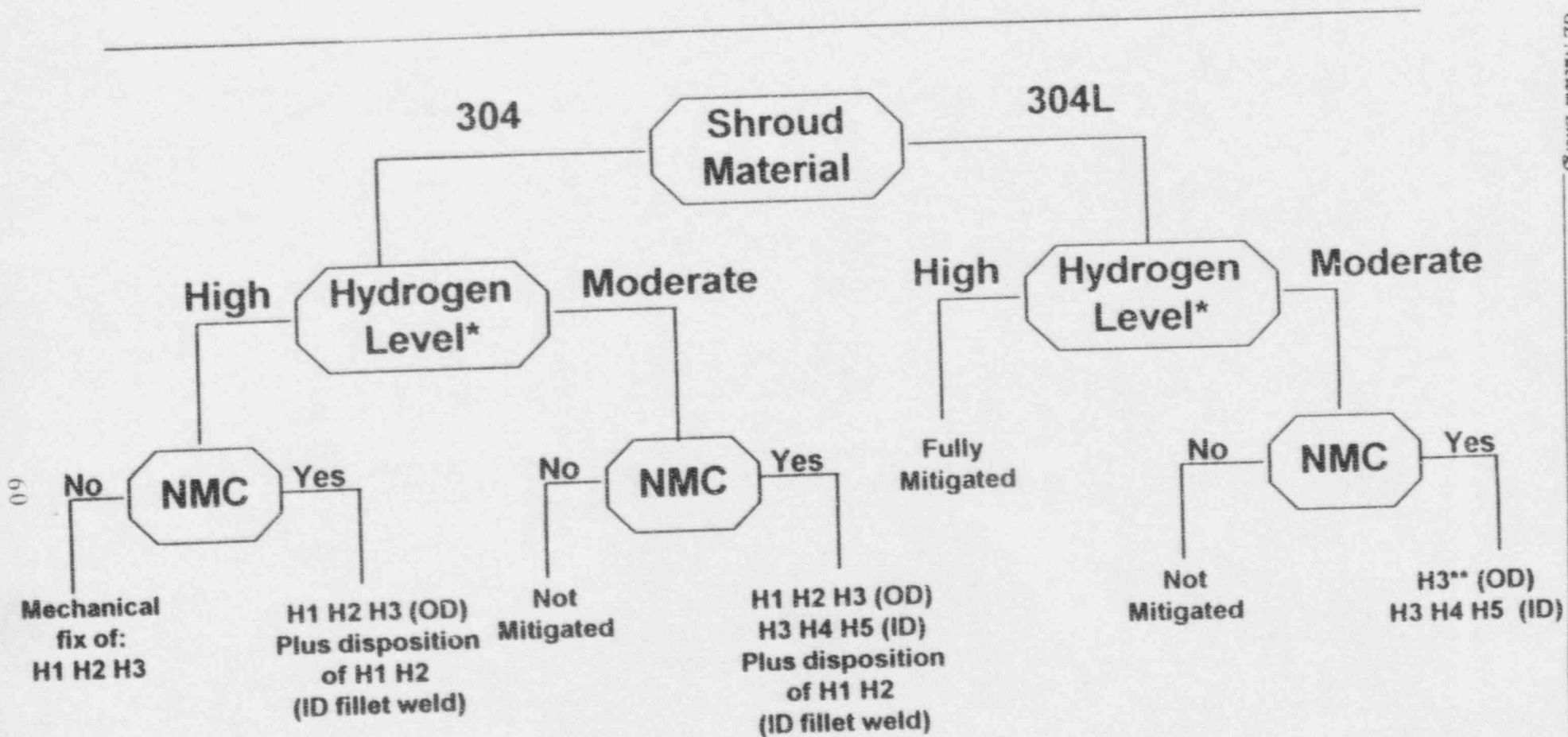
Auto = autoclave

Table 4-2. Shroud Estimated IGSCC Factors of Improvement (FOI)¹

	<u>Top of Core</u>			<u>Bottom of Core</u>		
H2 SCFM	0	12	20	0	12	20
T 304 ECP	225	200	140	140	75	-40
Pd ECP	225	-220	-310	140	-345	-435
HWC FOI	1	1.5	3	1	2	8
Pd FOI	1	100	60	1	30	7
Conductivity 0.3 to 0.06 $\mu\text{S}/\text{cm}$ (only)	5			5		

1. Assumes that all FOIs are multiplicative. Separate conductivity FOI.

Figure 4-1 Shroud SCC Mitigation Options



* High H₂ range is 2.0 to 2.7 ppm in feedwater. BOP flow assisted corrosion evaluation and fuel surveillance recommended by EPRI/BWROG Water Chemistry Guidelines (currently under revision).
Moderate H₂ range is 1.0 to 1.6 ppm in feedwater.

** NMC if end of life fluence exceeds 5x10²⁰ nvt
NMC (Noble Metal Coating)

61

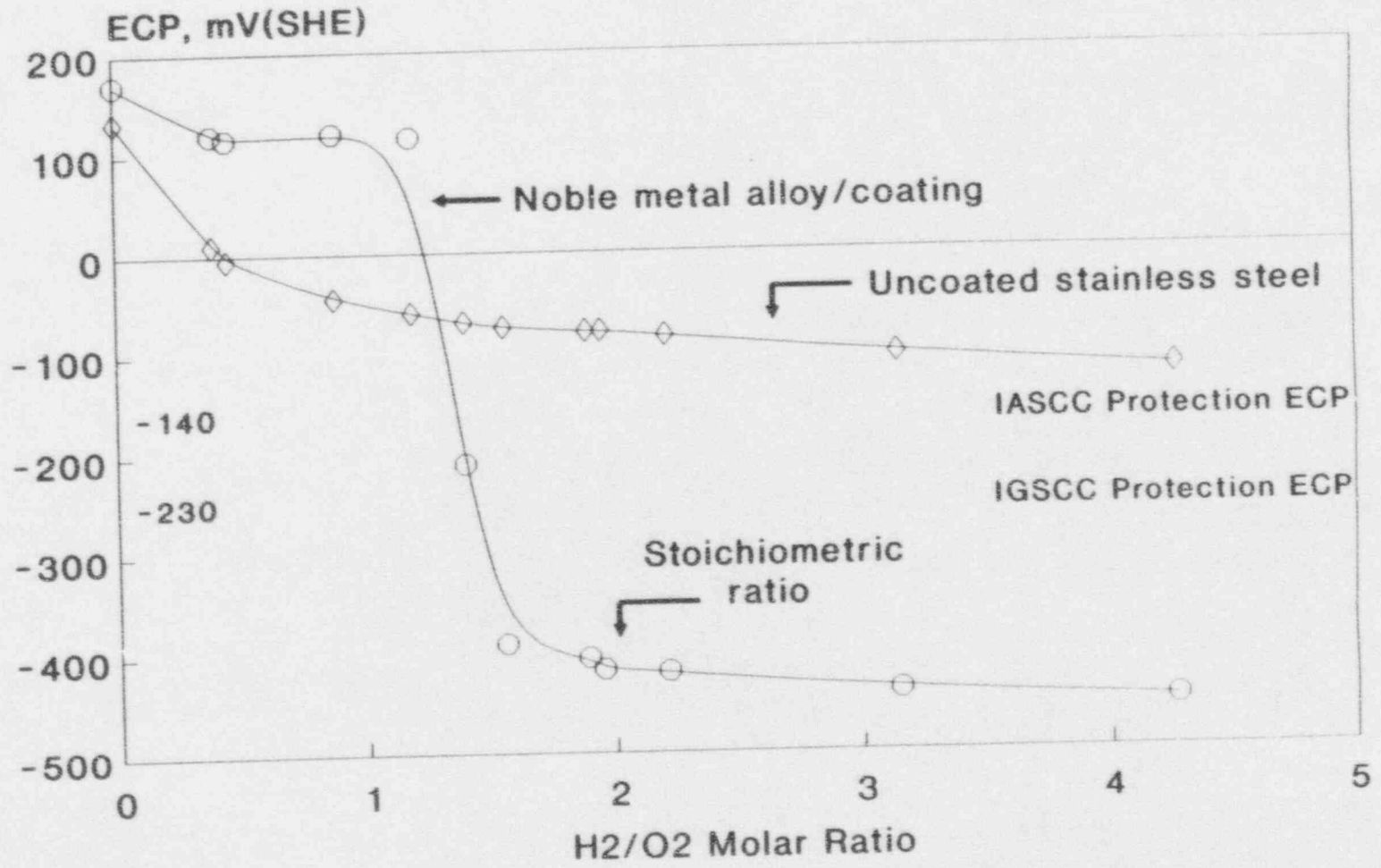


Figure 4-2 - ECPs of Pd-coated Type 316 SS in 300 ppb Oxygenated Water at 282C

62

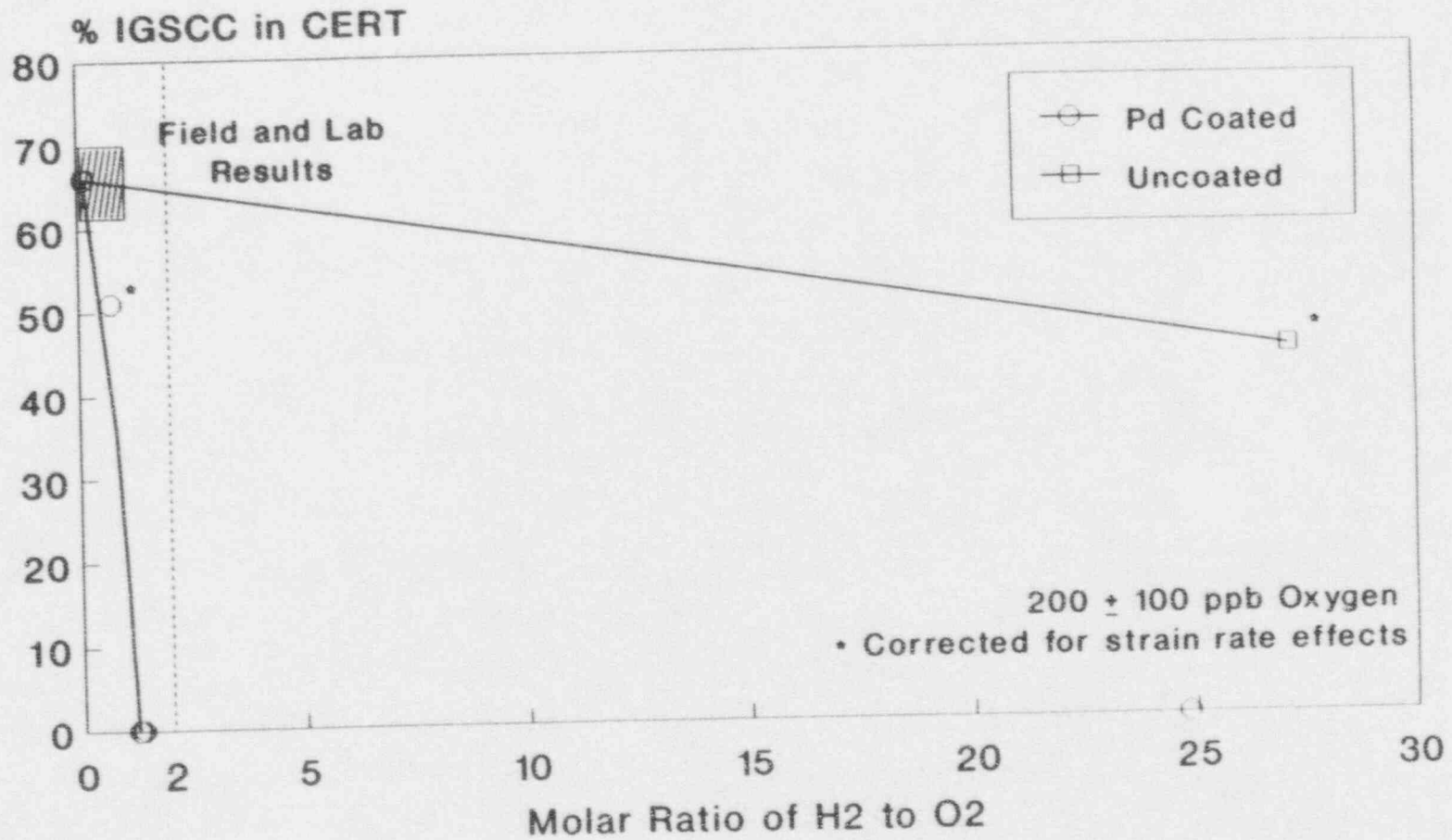
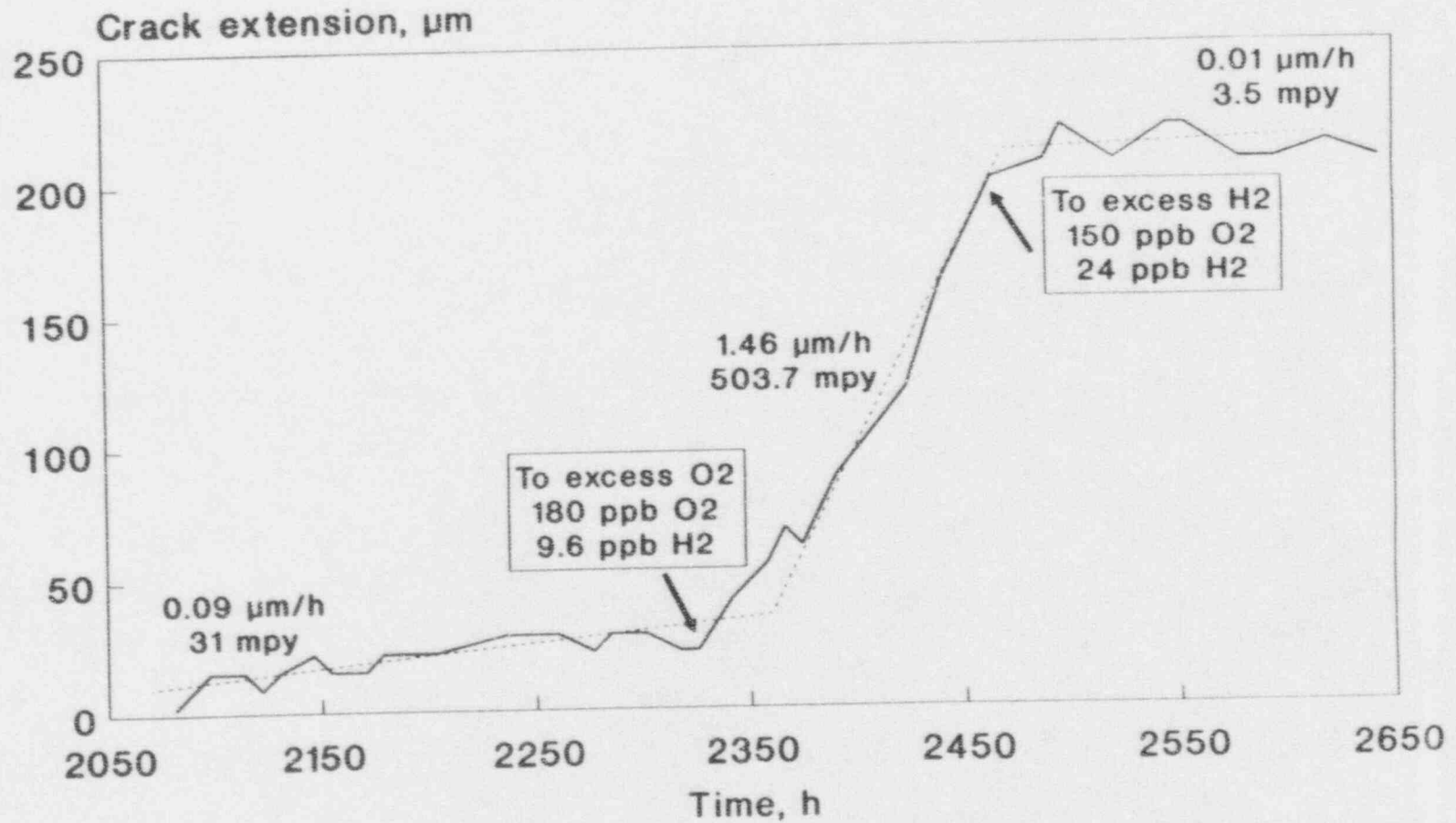


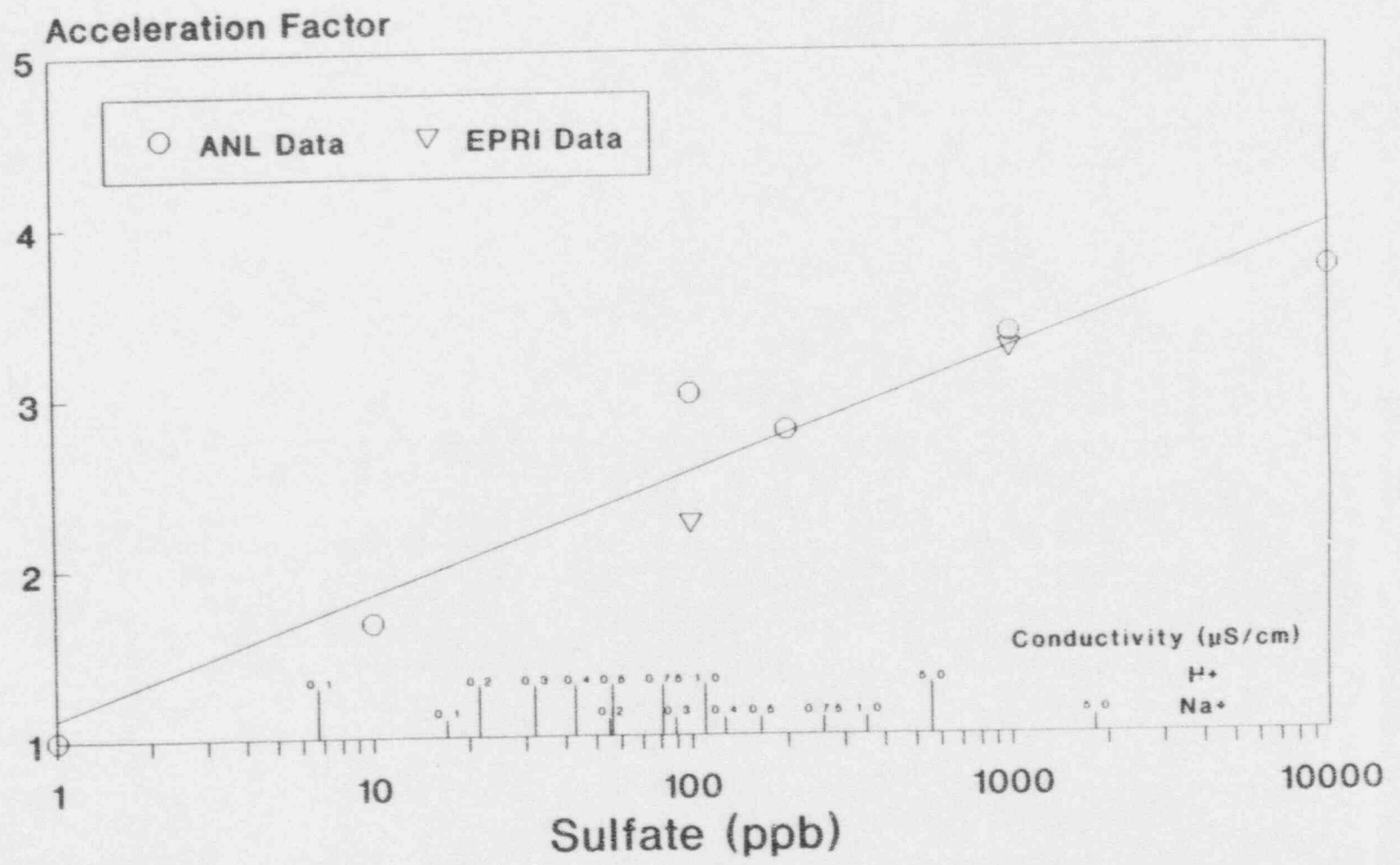
Figure 4-3 - Effect of Hydrogen/Oxygen Molar Ratio on IGSCC of Pd Coated and Uncoated FS Type 304 in CERT at 288C

63



Coated in shallow water by HVOF/T309L SS
K = 33MPa $\sqrt{\text{m}}$, R = 0.7, 0.01 Hz after 200s
0.435 $\mu\text{S/cm}$ H₂SO₄

Figure 4-4 - Effect of 0.42% Pd Coating on Crack Propagation in FS Type 304



Crack initiation data based on CERT

Figure 4-5 - Effect of Concentration and Conductivity on FS Type 304 IGSCC Initiation

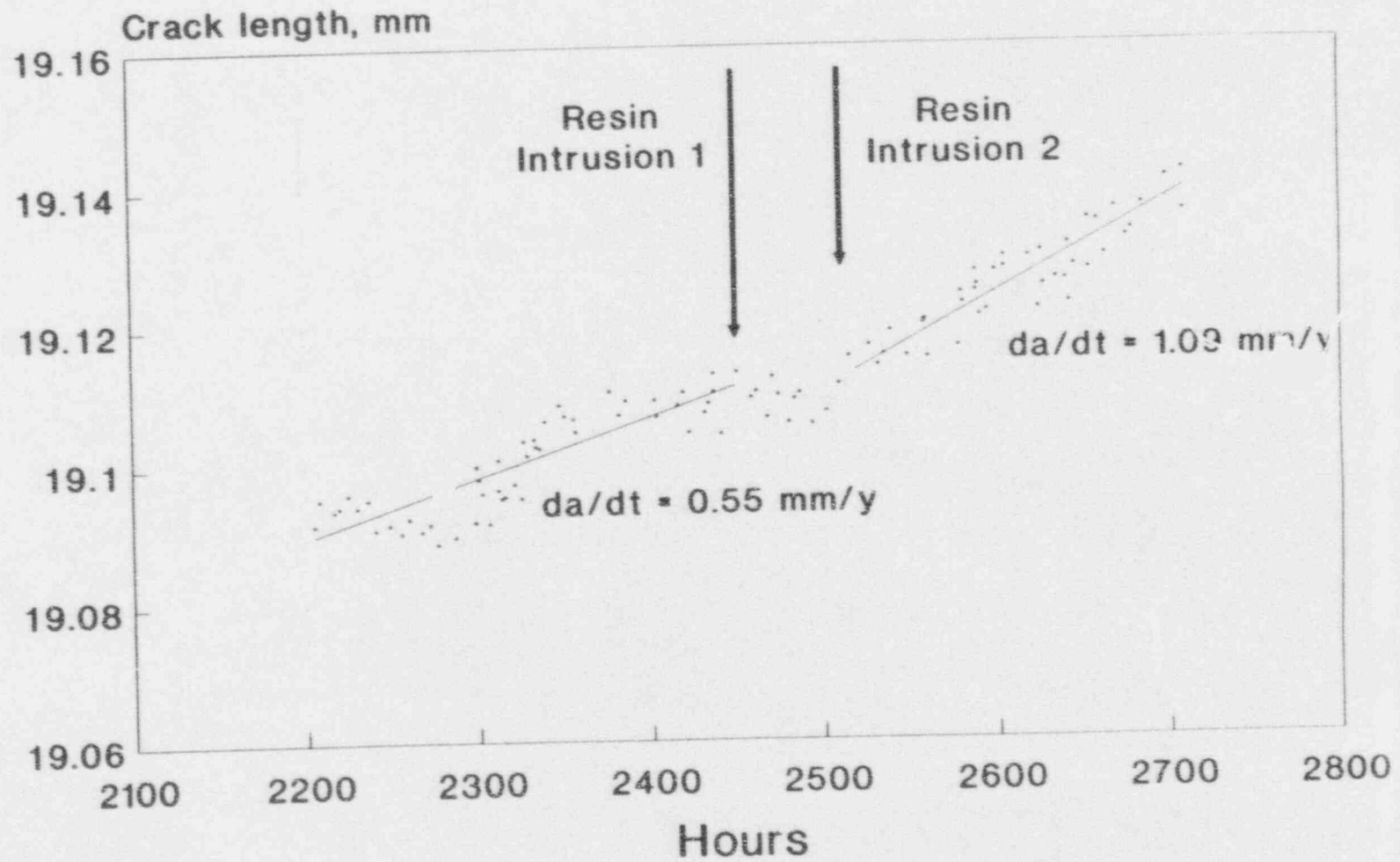


Figure 4-6 - Peach Bottom 3 Response to June 1986 Water Chemistry Transient

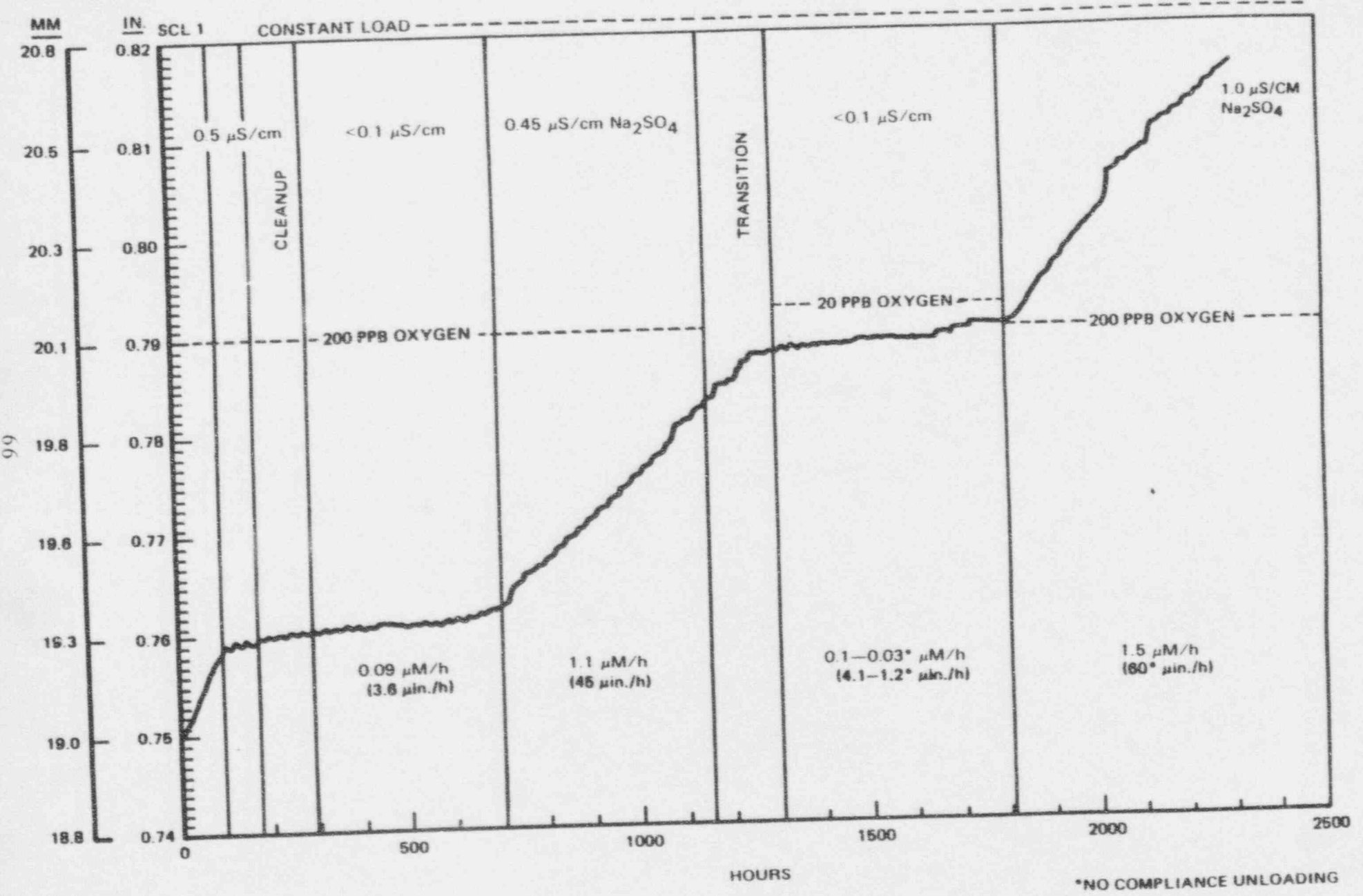
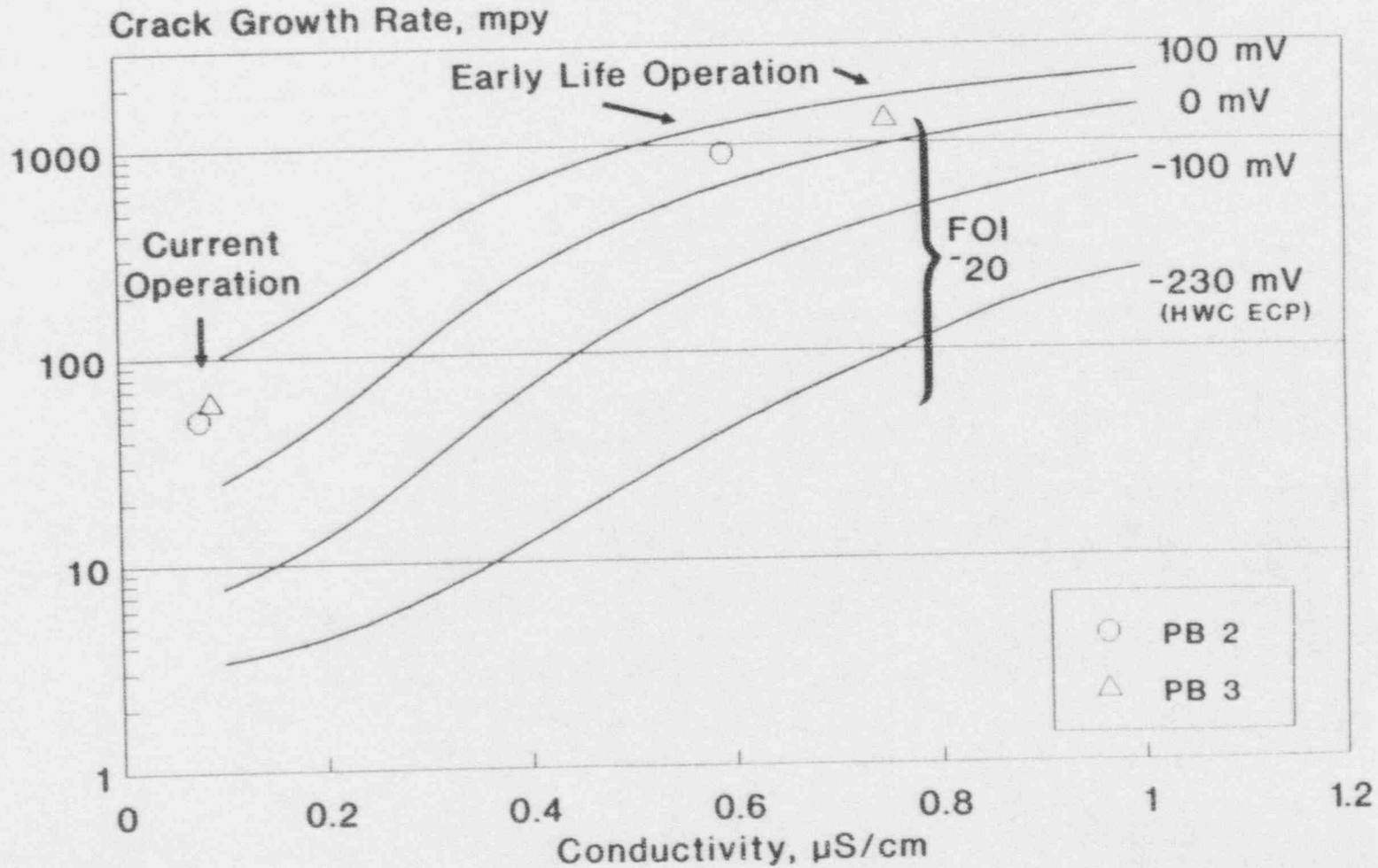


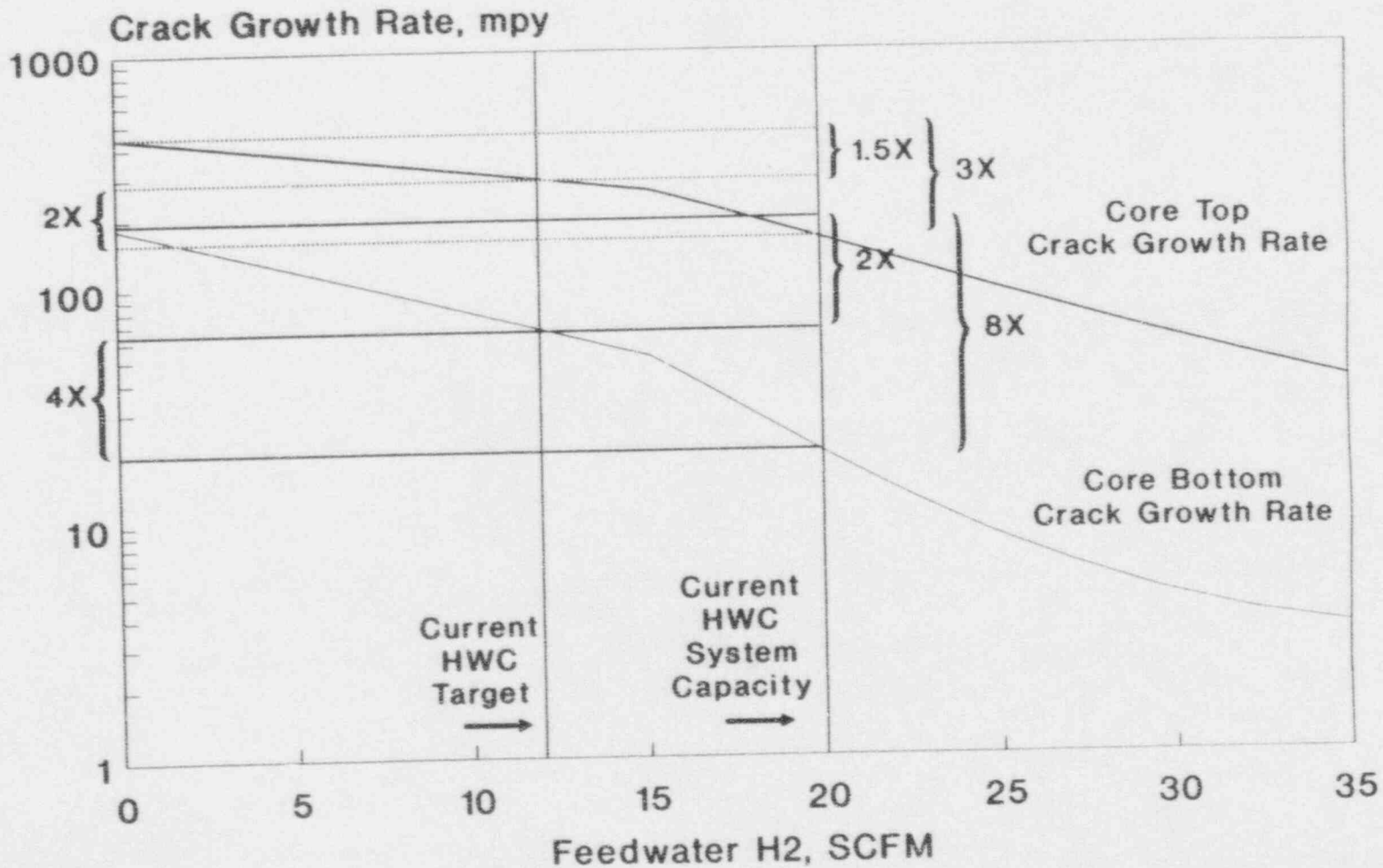
Figure 4-7 Crack Length vs. Time, Sensitized Type 304 Stainless Steel 286C Oxygenated Water Environment
K = 28.5 to 30.5 MPa \sqrt{m} (26-28 ksi \sqrt{in})



Estimated CGRs for ECP 0-100 mV[SHE]

PLEDGE: 15 C/cm², 25ksi/in

Figure 4-8 - GENE PLEDGE Model Prediction for Peach Bottom Type 304 Crack Growth

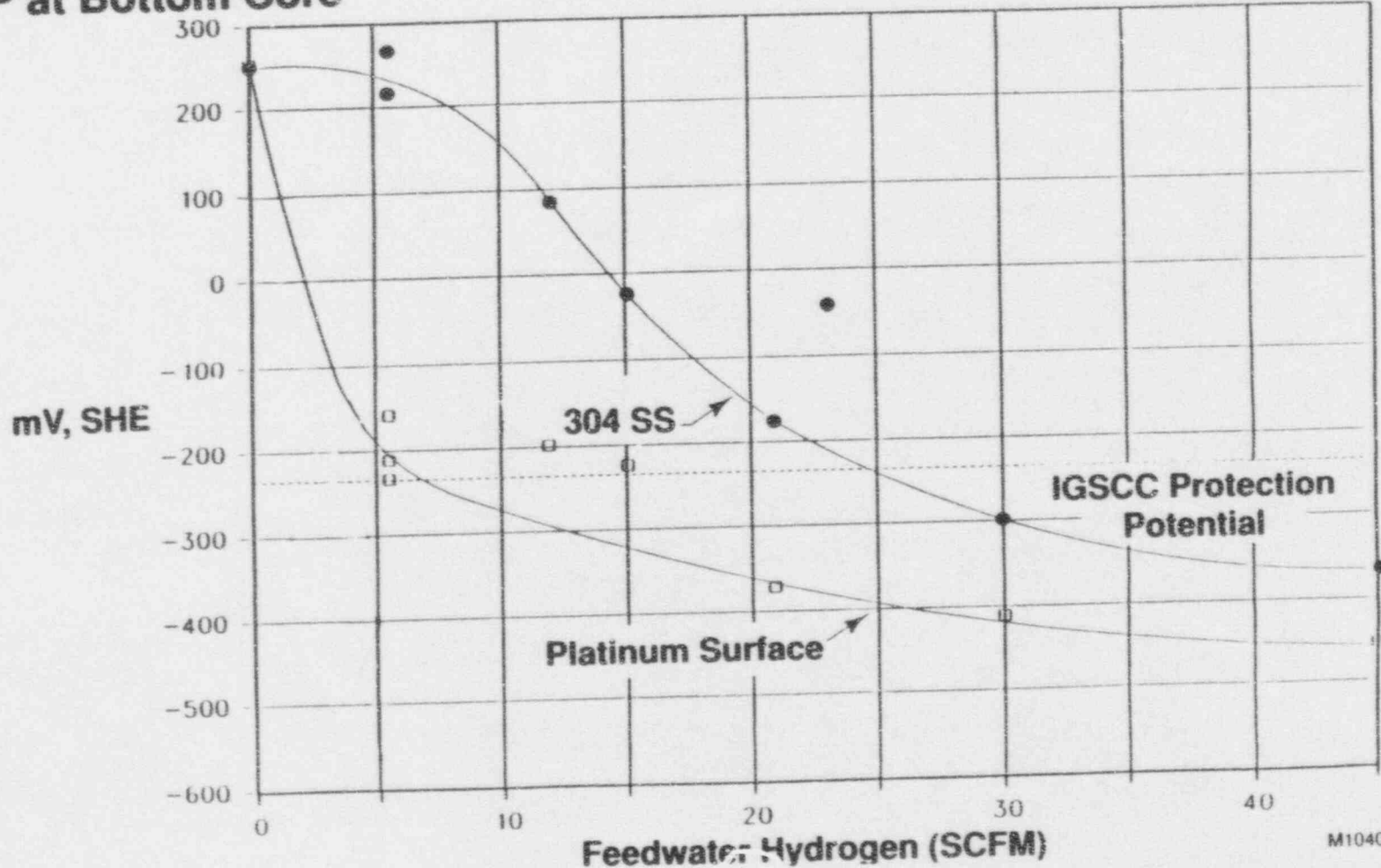


PLEDGE: 25 ksi√in, 15 C/cm², 0.12 μS/cm

ECP based on FitzPatrick

Figure 4-9 - Effect of H₂ Injection Rate on Calculated IGSCC Rate for Brunswick 1

ECP at Bottom Core



69

M10407-13

Figure 4-10 - Comparison of ECP for 304 SS and Platinum Surfaces vs. Hydrogen Addition Rate for BWR 4

5.0 OPERATIONAL SYMPTOMS

This section on operational symptoms is included to address the potential situation if unexpected significant crack growth occurs during plant operation. The potentially affected plant operational parameters are identified, as well as the modes of reactor operation that are most likely to show these symptoms if the shroud has degraded to the point that significant, through-wall leakage can occur.

5.1 Functional Effects of Significant Leakage in the Upper Shroud

The primary abnormal effect of significant leakage through the top portion of the core shroud assembly is that a portion of the steam-liquid flow leaving the core will bypass the steam separators. The bypass leakage will instead flow directly into the vessel annulus region.

The left side of Figure 5-1 shows the normal flow and fluid enthalpy pattern for a typical BWR unit. A postulated situation with some shroud leakage is shown on the right side of Figure 5-1. Several fluid paths are mixing in this bulkwater/annulus region of the vessel. The normal mixing process involves the combination of the following flow paths (typical full power values are given for a BWR/4 218 inch vessel plant):

- Downward liquid flow from the separators (66.2×10^6 lbm/hr)
- Carryunder steam flow ($.0025 \times \text{sep. liquid flow} = 0.17 \times 10^6$ lbm/hr)
- Drain flow (liquid) from the dryers ($\sim 1\%$ of steam flow = 0.1×10^6 lbm/hr)
- Feedwater flow (10.5×10^6 lbm/hr)

The subcooled feedwater flow (420°F, 398 Btu/lbm) mixes with the other, saturated flow paths, normally producing a downcomer enthalpy that is about 527 Btu/lbm (below saturation [subcooled] by about 18.7 Btu/lbm).

The right side of Figure 5-1 shows the same parameters, but assumes, for example, that significant leakage is occurring equivalent to 6% of the total core flow. This is approximately the amount of leakage that would occur with an equivalent crack height (Leakage area / Circumference of the shroud) of about 1/2 inch.

An initial calculation was made assuming that the power and core flow remained at the rated values. Subsequent calculational iterations were performed to adjust the power/flow for the new parameters. The results for the different flow paths are:

- Downward liquid flow from the separators (63.8×10^6 lbm/hr)
- Carryunder steam flow ($0.0025 \times \text{sep. liquid flow} = 0.148 \times 10^6$ lbm/hr)
- Drain flow (liquid) from the dryers (~1% of steam flow = 0.1×10^6 lbm/hr)
- Feedwater flow (9.45×10^6 lbm/hr)
- Liquid leakage flow (4.1×10^6 lbm/hr)
- Leakage steam flow (0.15 quality in plenum above core gives 0.6×10^6 lbm/hr)

The subcooled feedwater flow (417°F, 395 Btu/lbm) still mixes with the saturated flow paths from the separators and dryers. However, the leakage flow increases the effective carryunder fraction to about 5 times normal. This raises the downcomer, recirculation loop, and core enthalpy to about 532 Btu/lbm, however, it remains below saturation [subcooled] by about 11.8 Btu/lb.

The change in subcooling (from about 19 to 12 Btu/lbm in this example) would not impact the recirculation system significantly because the net pump suction head (NPSH) margins remain adequate. However, the shroud leakage does change four other basic reactor parameters:

- The warmer recirculation water will become evident in the recirculation loop temperature monitors. For this example, the temperatures would be about 4°F above normal.
- The reduced core inlet subcooling will reduce reactor power. For this example, a power reduction of about 11% is expected.
- The leakage path essentially reduces the pressure drop in the flow path from the core upper plenum to the downcomer. This effect will produce a slight increase in the total core flow (assuming that the recirculation drive loop flow remains constant). For this example, a core flow increase of only about 1.5% is expected.
- The core flow effect will raise power about 1%, so that the overall power reduction will be from 100% to about 90%. Clearly this is the strongest indicator of the presence of leakage

For reasonable ranges of hypothesized effective crack size and resulting leakage, the power level signal is the strongest indication of an abnormal condition of the shroud. Figure 5-1 (right side) shows the approximate operating conditions with the 10% power decrease and the slight core flow increase.

The example case only produced a small change in the recirculation loop temperature. Close monitoring would be needed to identify this change. The temperature difference between the loops and the vessel dome (saturation) temperature is reduced to about 11°F, very close to the setpoint of the subcooling monitors on those units that have them.

If leakage develops on one side more than another, the symptoms may also include indications of non-symmetry: greater changes for one recirculation loop than the other(s). This asymmetry may also be seen in local core power (one side reduced more than the other).

If a larger leakage flow path is postulated, the downcomer subcooling could be reduced to the point where recirculation system cavitation is experienced. At about four times more leakage (leakage about ten times the normal amount of steam carryunder from the separators), the recirculation pump NPSH margin approaches zero. Plants with jet pumps would also approach cavitation at the jet pump suction and nozzle areas. Under these conditions, the recirculation system efficiency is reduced rapidly, and significant indications of low recirculation drive loop flow, low core flow, and additionally reduced power can be experienced. These signals may also show noisy and erratic behavior.

One other characteristic would be observed if a through shroud wall crack developed abruptly while the unit was at high power, steady state conditions. The rapid creation of leakage flow into the annulus region of the vessel could potentially cause an observable increase in the water level. This sequence of events could even raise the water level so that a high water level trip could be initiated. In the more probable case that the water level transient is not enough to reach the trip points, reactor operation will change to conditions displaying the other symptoms previously identified.

5.2 Specific Operational Parameters for Upper Shroud Leakage

The following monitored parameters will provide indication of abnormal conditions to the reactor operating staff. They are presented in the approximate order in which the indication would become significant as upper shroud leakage developed.

- (1) Reactor thermal power will be suppressed below its normal value for the selected rod pattern and core flow. A good way to observe this anomaly is to compare the power ascension trajectory versus core flow (as in Figure 5-2).

The process computer trend output information will clearly be helpful in these comparisons to normal. It is recommended that a baseline trajectory for these parameters should be established (if it does not already exist) in a useful format. This will enable utilities to perform this type of comparison to expected performance at each reactor startup.

The experiences observed at two BWRs (in 1984 and in 1991) used this type of comparison (between expected and observed power versus core flow) to discover problems associated with loose shroud head bolts. In those cases, physical motion of the shroud head occurred as the pressure drop became large enough to lift the upper shroud/separator assembly. At that power-flow condition (about 80% power and 85% core flow), leakage began. In these cases, the motion of the shroud head and induced leakage was restricted by the bolts that were in place.

For upper shroud leakage without significant shroud motion, there will not be such a distinct characteristic change at a particular power-flow condition. Power will be suppressed over the whole power versus flow range. If some motion is postulated (e.g., only one side is intact, and the other tends to open further when the power-flow conditions exceed the point of lifting pressure drop), then some of the distinctive characteristics of the loose bolts case may be experienced. This case (shroud lifting) is quite remote because it takes such a small amount of remaining ligament (even on one side) to maintain shroud integrity and geometry.

- (2) Those plants that have recirculation loop cavitation instrumentation could reach those setpoints if large leakage flow occurs from the upper shroud. All plants would be able to observe the increase in recirculation drive loop temperature

above normal. If cavitation conditions are actually encountered, the loop flow, jet pump diffuser flow, pump head, and vibration monitoring instruments may display noisy, erratic signals.

It is recommended that baseline characteristics of normal recirculation loop temperature versus power and flow conditions be established so that an abnormal pattern can be detected. Figure 5-3 shows a typical pattern for recirculation loop temperature during the upper portion of the ascension to full power. The differences calculated for the example case of shroud leakage are also shown.

- (3) The characteristic that a slight increase in core flow may be observed due to the reduced pressure loss in the shroud/separator region can also be monitored. This anomaly can be discovered by comparing the core flow to drive loop flow (in a jet pump plant), or by comparing core flow to coupler scoop tube position or pump speed (for all MG set plants). Figure 5-4 shows a typical relationship between core flow and drive flow, and the type of anomaly that may be observed. This sensitivity is not very strong for potential equivalent crack sizes up to the 1/2 inch upper shroud leakage example shown here.

The baseline relationship of these parameters along the rated flow control rod line should be established for use in detecting abnormal operation.

- (4) If bypass leakage develops on one side of the upper shroud more than another, some symptoms may also include indications of non-symmetry in the core power (one side reduced more than the other), or greater changes for one recirculation loop than the other(s).
- (5) In the unlikely case that upper shroud leakage develops abruptly during normal steady state operation, a rising water level transient would be created. Such a transient could reach the high water level trip setpoints. If the unit does not trip on high water level, it will shift to operating conditions with the characteristics described in the previous items.
- (6) The discussion of these symptoms is most applicable to the upper shroud area associated with weld areas H1 and H2. These areas see the full, two-phase mixture being discharged from the core. The H3 weld area is below the fuel top

guide. It is primarily exposed to the bypass region flow which is heated, but the mixture quality is lower than the core exit. A significant leak in this area would draw some two-phase flow from the plenum above the core in addition to the heated water. However, the symptoms would be smaller than if the cracking developed higher in the shroud.

5.3 Functional Effects of Leakage in Beltline or Lower Shroud Areas

If large cracking occurs lower on the shroud, in the beltline zone or lower, it does not produce observable symptoms. The fluid that would leak through the shroud wall would be partially heated water from the outer bypass region outside the fuel bundles. It would only produce a very small change in the temperature of the recirculation and core inlet flow, and no detectable change in power or loop temperature is expected. At the bottom of the shroud, the bypass region water is the same temperature as the recirculation flow in the vessel annulus and recirculation loops.

It is concluded that no detectable symptoms would accompany larger than expected cracking in the middle and lower shroud. All indications found so far are well below the allowable criteria, and no leakage has occurred through the shroud (in the upper, middle, or lower region of the shroud). Safe operation is assured for all areas by regular inspection of the shroud.

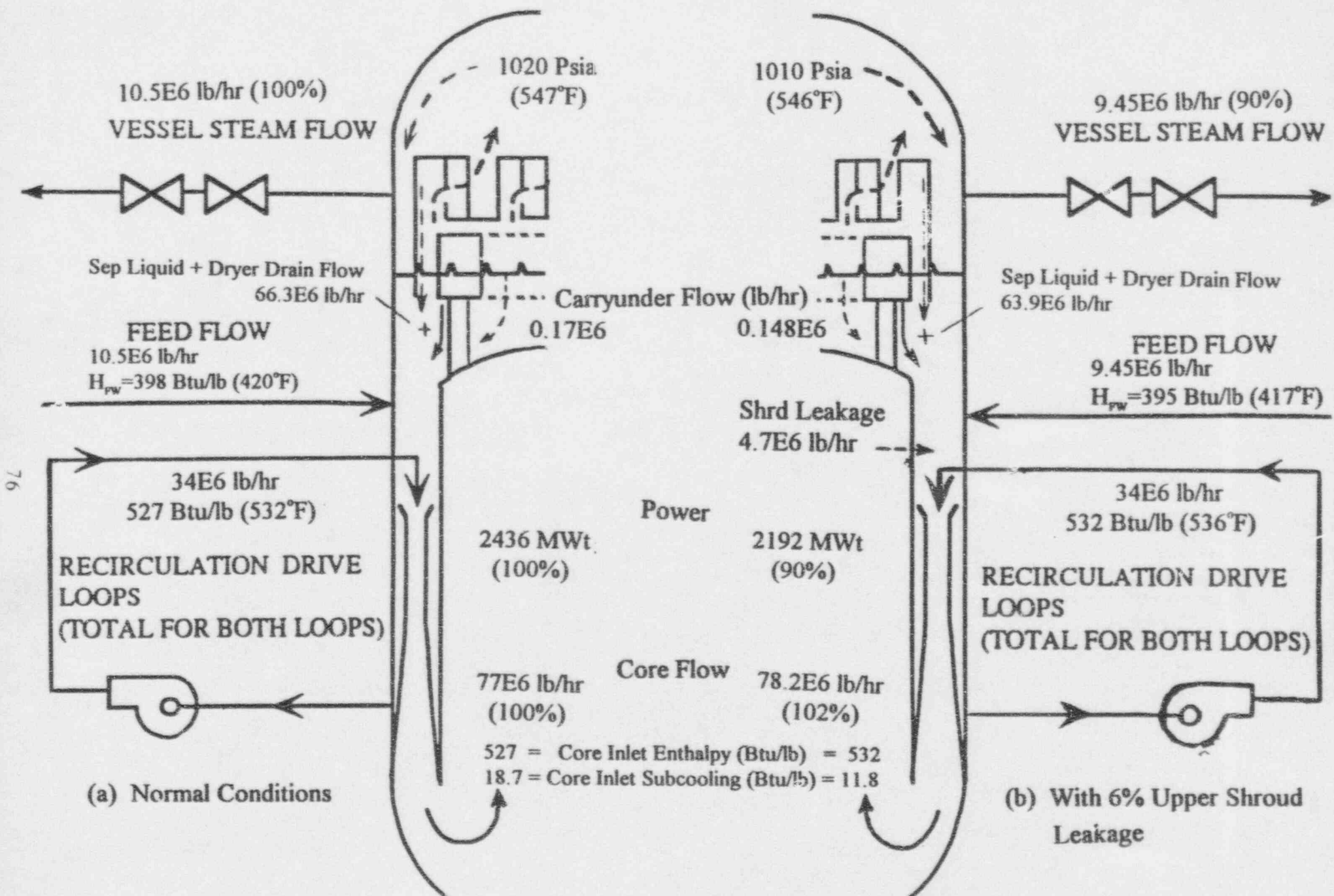


Figure 5-1 Typical Reactor Flow and Enthalpy Conditions Normal (Left) and With 6% Upper Shroud Leakage (Right)

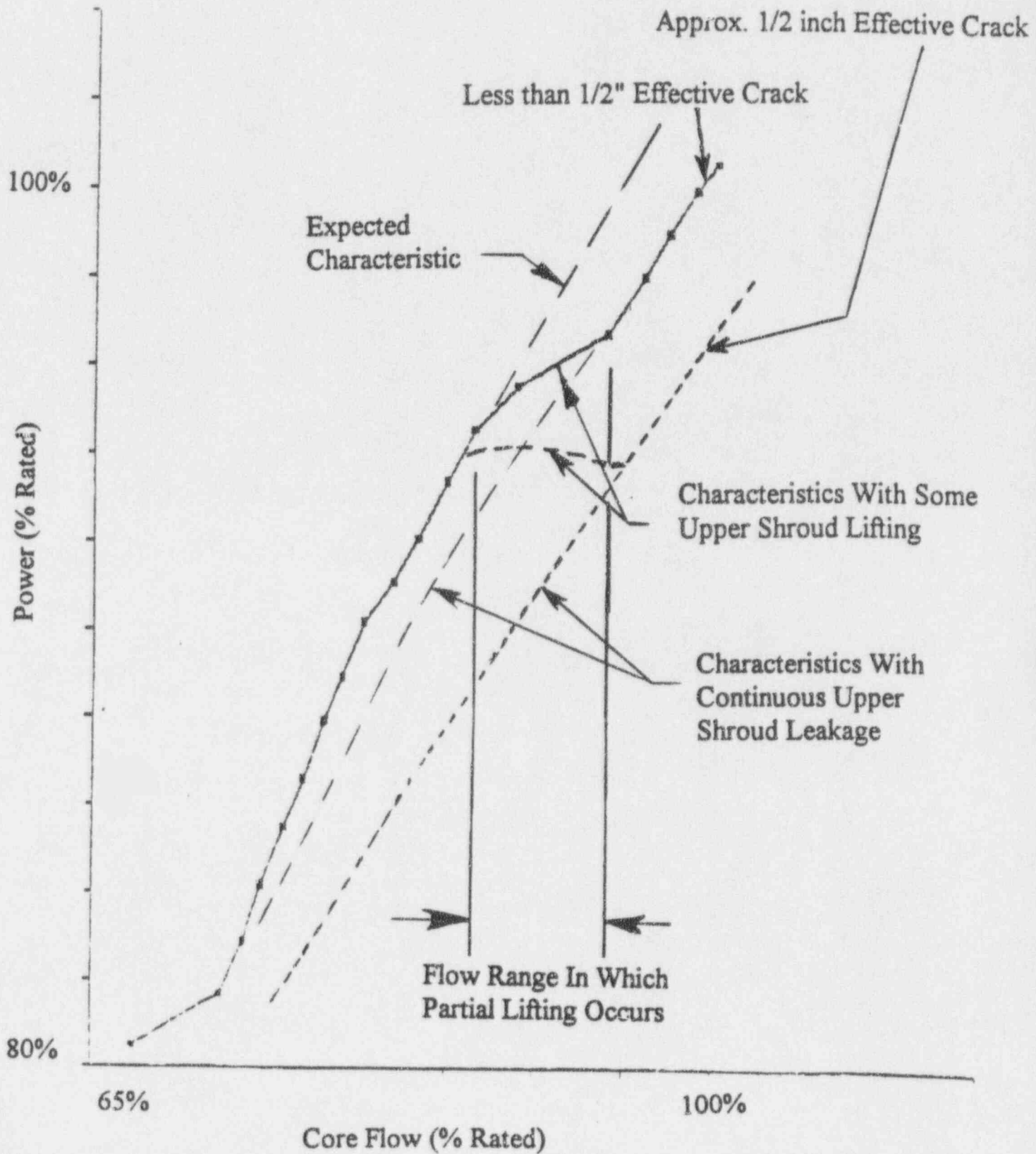


Figure 5-2 Typical Plant - Core Power vs Core Flow

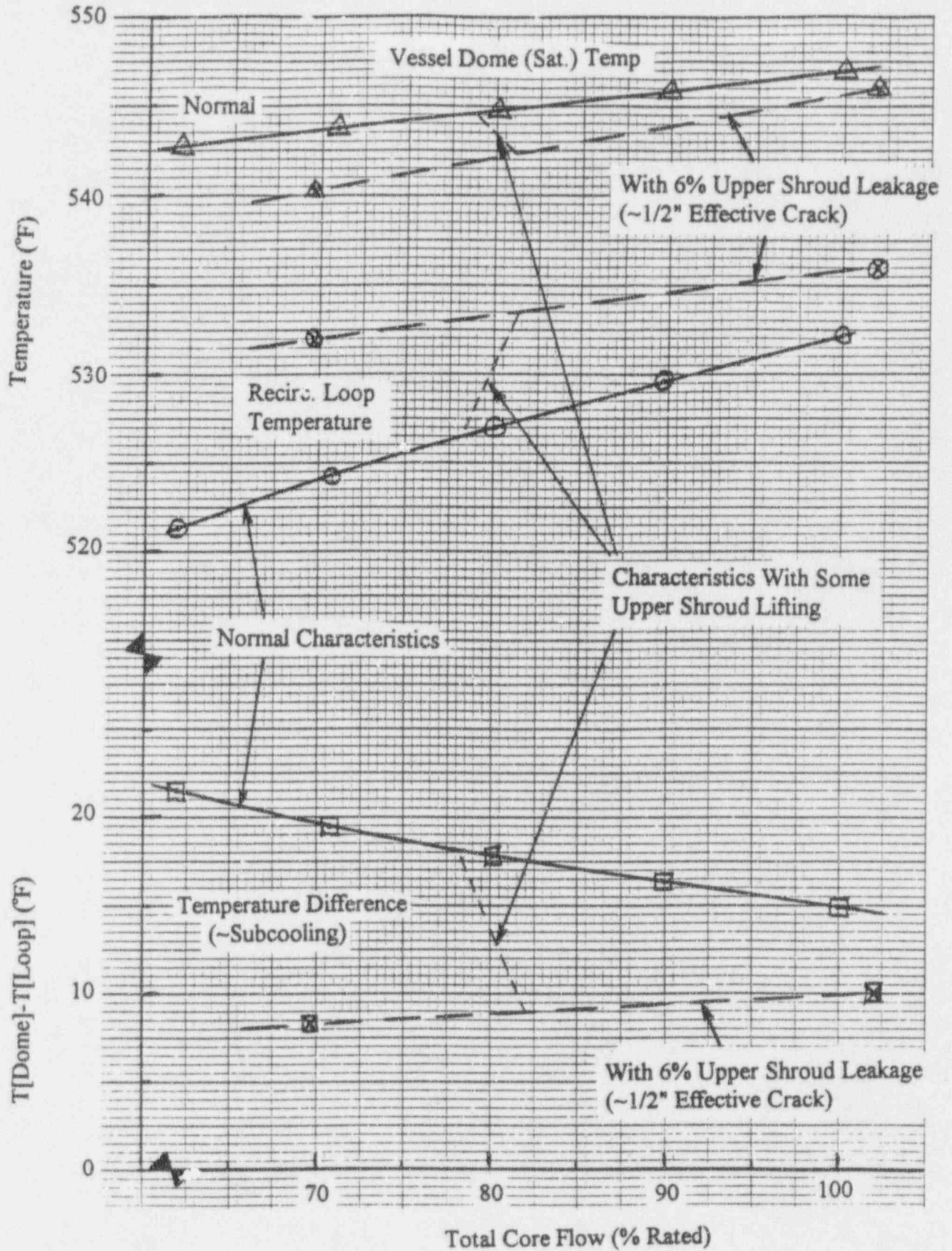


Figure 5-3 Typical Plant - Recirculation Loop Temperature and Vessel Dome (Saturation) Temperature vs Total Core Flow (100% Flow Control/Rod Line)

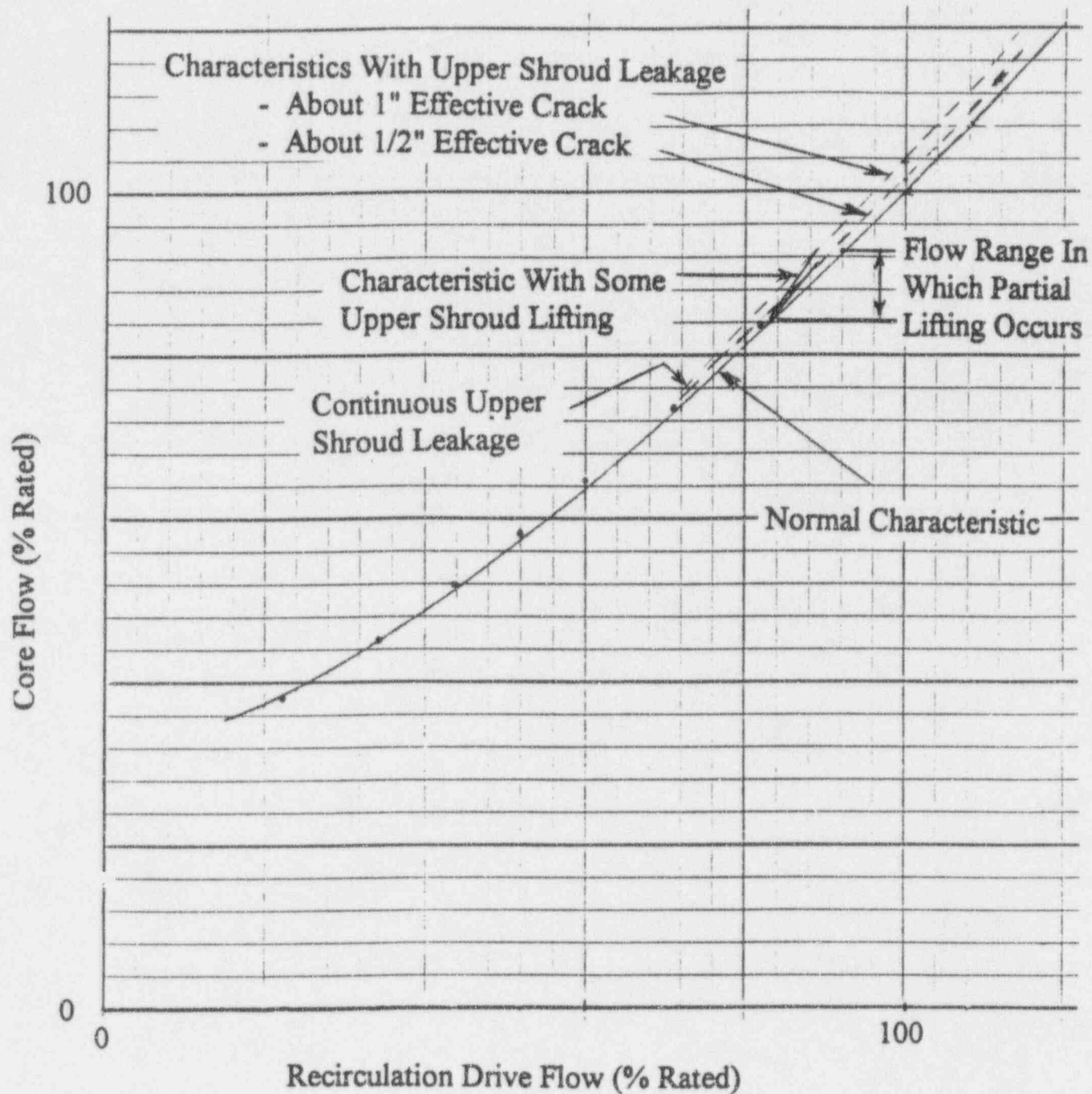


Figure 5-4 Typical Plant - Total Core Flow versus Recirculation Drive Flow (100% Flow Control/Rod Line)

6.0 INSPECTION STRATEGY

This section describes a strategy and integrated plan for shroud inspections. This program is designed to meet the intent of SIL 572 Rev. 1 while responding to utility specific needs. This discussion is based on shroud inspections to date and current available inspection equipment. The information in this section may require modification as new inspection equipment becomes available.

This strategy and recommendations are provided based on current knowledge of the shroud issue and experience at various plants. As more inspections are performed, some of these recommendations may change. The recommendations provided here are not mandatory, but provided to utilities as a guide in developing their plant-specific inspection plans. For example, the selection of VT or UT and consideration of inspecting for sufficient material to confirm structural margin could result in a modified inspection plan. Thus, the plant specific inspection plans may vary from those provided in this section.

The inspection recommendations provided here are considered applicable to all BWR's and exceed the requirements of ASME Code Section XI (where applicable, e.g., for BWR/6).

The specific goals of this inspection plan are to:

- Provide an integrated shroud inspection philosophy that:
 1. Meets the intent of the inspection recommendations in SIL 572 Rev. 1
 2. Meets utility requirements
 3. Contains a defensible basis, and
 4. Can be applied uniformly and consistently from plant to plant
- Provide a strategy to minimize the impact of the shroud inspections on the overall outage.

6.1 Susceptibility Factors

SIL 572 Rev. 1 recommends a review of shroud fabrication records and operating history for each plant. The purpose of this review is to determine the relative degree of shroud susceptibility to cracking. This will affect the decision process to determine what types

and to what extent inspections should be performed. In some situations a repair contingency package may be applicable.

The susceptibility evaluations involve a combination of absolute and relative comparisons to other information and data and can be quite subjective. As new information becomes available the perceived susceptibility of the plant to shroud cracking may change.

In considering the relative susceptibility of one BWR plant versus another, there are several key parameters that must be evaluated. These include materials, fabrication, water chemistry, neutron fluence, and IGSCC/IASCC history of other in-reactor components.

1. Materials: Material composition, in general, and carbon content more specifically, can have a major affect on shroud IGSCC susceptibility. Bimetallic welds utilizing Ni-Cr-Fe material (Alloy 182) have higher susceptibility than stainless materials. Laboratory tests and field experience conclude that components with a higher carbon content are more susceptible to cracking than a lower carbon equivalent.

The primary effect of carbon content is to increase the degree of sensitization in the as-welded condition, which is related to the minimum chromium content of the chromium depleted regions at the material grain boundaries, and thus the IGSCC susceptibility. A series of time to failure tests versus percent carbon have been performed in the GE pipe test labs for 304 stainless steel in 288°C oxygenated water. In general, based upon the results of the pipe tests and field experience, it appears that those plants with materials containing above 0.05% carbon are in the highest susceptibility category, those with 0.04% to 0.049% are in the intermediate category, and those with less than 0.04% are in the most resistant category.

2. Fabrication: The fabrication processes and weld designs affect IGSCC susceptibility. Examples of higher susceptible fabrication techniques include designs containing crevices, welds utilizing backing rings, high weld residual stress from fitup, and the orientation of plate materials that result in the laminations exposure to the oxidizing environment (presence of surface cold work, cool down rate from solution heat treatment temperature, weld repair, fit-up stresses, etc.).
3. Water chemistry: Water chemistry can be divided into steady state and transients. Steady state involves maintaining/sustaining proper chemistry such as low conductivity. Transients are short term events such as seawater and resin intrusions. Transients and poor water chemistry have been shown to increase IGSCC susceptibility. A significant contributor to shroud condition is plant conductivity

history (early life vs. overall operation, presence of severe potentially damaging transients, etc.).

GE has performed a considerable amount of laboratory testing and analytical modeling of material susceptibility to IGSCC as a function of conductivity. Based upon this data, it was observed that a plant operated early in life with a conductivity of about $0.5\mu\text{S}/\text{cm}$ has about a five to tenfold increase in IGSCC propensity when compared to a plant that has operated at $0.1\text{-}0.2\mu\text{S}/\text{cm}$. Field data has, in general, supported this conclusion. As a measure of ranking, the most susceptible category would be for those plants that have operated for the first five operating cycles with conductivity above $0.5\mu\text{S}/\text{cm}$. The next most susceptible category would be those plants that have operated between 0.3 and $0.5\mu\text{S}/\text{cm}$, and the least susceptible category would be those plants that operated below $0.3\mu\text{S}/\text{cm}$ consistent with the EPRI Water Chemistry Guidelines Action Level 1 values.

4. **Fluence:** The shroud fluence distribution is a function of core design/configuration and operating power history. The threshold fast neutron fluence ($E > 1\text{mev}$) for initiation of IASCC (Irradiated Assisted Stress Corrosion Cracking) is approximately $5 \times 10^{20}\text{ n}/\text{cm}^2$ based upon test data. IASCC has been observed to occur below the predicted initiation threshold if classic IGSCC is also present. This observation is based upon metallurgical evaluations of a boat sample of a core shroud whose fluence was approximate $3 \times 10^{20}\text{ n}/\text{cm}^2$. Based upon this data, plants with shrouds having fluences above $5 \times 10^{20}\text{ n}/\text{cm}^2$ are considered susceptible to IASCC. Plants with fluences below $3 \times 10^{20}\text{ n}/\text{cm}^2$ are not considered susceptible to IASCC.

In addition, the plant specific cracking history is an indicator of shroud susceptibility. The presence of previous cracking in other components of a plant such as shroud head bolts, access hole covers, recirculation piping, and core spray spargers/piping would suggest a greater susceptibility for shroud cracking. It is also useful to review/compare inspection results from other plants with similar shroud susceptibility factors when known.

6.2 Inspection Plan

Figure 6-1 is a graphic representation showing the relationship between SIL 572 Rev. 1 (top level document containing the bases for the inspection recommendations) and the site specific inspection strategy, tools and procedures.

The first step to generating a plant specific inspection plan consists of reviewing SIL 572 Rev. 1 for applicability. The factors affecting shroud susceptibility to cracking are then

evaluated. The inspection plan is developed by utilizing the susceptibility factors in combination with the utility specific input. The utility specific input includes outage and inspection specific goals as well as the integration of the shroud inspection with other site activities.

6.2.1 Inspection Strategy

Inspection Recommendation Summary

The following is a summary of the key inspection recommendations:

- Inspect at the appropriate refueling outage as indicated by SIL 572, Rev. 1 criteria, susceptibility factors, etc.,
- Perform either an Enhanced VT-1 or UT inspection. Decision of UT vs. VT is dependent on a plant specific evaluation (i.e., time cost/benefit, history, susceptibility)
- Determine the extent of cleaning required, and perform as appropriate,
- Perform inspection on a significant statistical sampling based upon perceived susceptibility to cracking, and
- Re-examine every second outage if no cracking is observed.

The strategy invoked to accomplish this is to perform a susceptibility evaluation of the shroud and to characterize its susceptibility to cracking as either low, medium, or high. Then, each utility should compare the benefits of each type of exam (UT or VT) such as minimum sample size prior to selecting the exam technique.

Inspection Philosophy

The inspection philosophy is to start with the smallest data set that will provide justification for continued operation in the absence of cracking. If the inspections were performed visually on a limited data set, then the data set must be expanded if cracking is observed. One domestic utility inspected for 8 weeks with a combination of VT and UT to fully map out the cracking. An alternative is to use UT to simultaneously detect and characterize the cracking. This may be very cost effective as a proactive inspection alternative if substantial cracking is anticipated.

The two welds initially targeted for the inspection are the H3 and H4 welds. The H3 weld (shroud to top guide support ring) is susceptible to IGSCC due to the highly oxidizing environment. Some plants additionally have shrouds with top guide support rings that have been fabricated in a manner that may make it more susceptible to IGSCC. The H4 or beltline weld is the most susceptible to IASCC since it is located in the high flux region and thus has the highest fluence.

It is believed that the H3 and H4 weld are the most susceptible welds to IGSCC and IASCC, respectively. Therefore, the initial examination data set should be based upon these two welds. The recommended initial UT inspection for all risk plants (High, Medium, Low) is full inspection of the H3 and H4 welds.

Inspection Plan 1: Low Risk Plants

A low risk plant is not expected to experience shroud cracking at this time. Therefore, the strategy is for a minimum visual inspection. In general, low risk plants have had good water chemistry, low fluence, have shrouds made of low carbon materials and do not have substantial fabrication anomalies (e.g., weld repairs) and have no reported IGSCC of other in-reactor components. A recommended strategy involves:

- Limited enhanced VT-1 inspection. Surface preparation is considered by comparing cleaned and non cleaned surface resolutions.
- Minimum number of weld locations selected.
- OD or ID depending on weld location.

A typical inspection plan for a low risk plant would include:

- Weld H3 - Examine 4 cell locations, preferably at highest neutron flux azimuths.
- Mid plane weld - Examine 4 cell locations, preferably at highest neutron flux azimuths.
- Shroud to shroud support weld - Examine 10% of weld length on OD at azimuths where access hole covers are located.

Alternative Plan 1 inspection: Use UT approach to establish baseline for future inspections. A complete UT with no findings may support a longer cycle prior to a reinspection.

Inspection Plan 2: Medium Risk Plants

A medium risk plant may have some limited shroud cracking. The screening criteria (flaw evaluation) can be utilized with other information to determine in advance the amount of inspection required for each weld. Identified shroud anomalies, such as weld repairs, areas with ground off lifting lugs, etc., should be inspected. Significant indications may result in "crack chasing" and/or UT for crack characterization. Performing UT initially in lieu of VT may be cost effective option. The inspection strategy for a medium risk plant is similar to the low risk plant.

A typical inspection plan for a medium risk plant would include:

- Weld H3 - Examine 8 cell locations, preferably at highest neutron flux azimuths
- Mid plane weld - Examine 4 cell locations, preferably at highest neutron flux azimuths
- Vertical weld - Examine 1 weld if cell already vacated
- Shroud to shroud support weld - Examine 10% of weld length on OD at azimuths where access hole covers are located
- Expand sample set if cracking is observed

Alternative Plan 2 inspection: Use UT approach to establish baseline for future inspections. A complete UT with no findings may support a longer cycle prior to a reinspection.

Inspection Plan 3: High Risk Plants

In general, high risk plants have had below average water chemistry, high fluence, have shrouds made of high carbon materials and may have some fabrication anomalies. Shroud cracking is expected for a high risk plant. The inspection strategy for a high risk plant should consider UT in lieu of VT as an alternative.

To summarize, for high risk plants:

- Weld H3 - Examine 8 cell locations, preferably at highest neutron flux azimuths

- Mid plane weld - Examine 8 cell locations, preferably at highest neutron flux azimuths
- Vertical weld - Examine 1 weld if cell already vacated
- Shroud to shroud support weld - Examine 10% of weld length on OD at azimuths where access hole covers are located
- Expand sample set if cracks are found

Alternative Plan 3 inspection: One plant with shroud cracking spent 8 weeks mapping and characterizing the cracks. Another domestic BWR took about 3 weeks to perform enhanced VT-1 on the original and expanded data set. UT is suggested for consideration as a proactive cost beneficial alternative to visual inspections. One overseas utility inspected 180 degrees of the shroud beltline weld in 8 hours using UT. The inspection was performed from the shroud OD, thus requiring no cell disassembly, and the cracking was detected and characterized simultaneously.

6.3 Inspection Techniques

The following is a brief discussion of the available shroud inspection techniques.

6.3.1 Visual Inspection

The enhanced VT-1 examination is the recommended technique for visual inspections. Visual examinations are typically performed from the refueling bridge. As a result, no other refuel activities are performed in parallel since the bridge cannot be moved. The following four major steps are involved:

1. Vacate fuel cells as applicable
2. Clean examination areas, if required
3. Inspect areas (ID and OD)
4. Evaluate results against screening criteria, then depending on results
 - No action required,
 - Expand VT sample set, or
 - Perform UT sizing

If no indications are observed, then the examination is complete and no further actions are required. If indications are present, then the sample set may need to be increased. In

addition, an ultrasonic examination may also be required (depending on results of screening criteria application) as a visual examination cannot fully characterize the crack.

6.3.2 Ultrasonic Examinations

Ultrasonic inspections have been performed on the shroud from the OD and ID at two plants.

A localized UT scanner was utilized on an overseas plant to characterize cracking on the beltline weld from the shroud ID. A second examination using a more sophisticated device was performed on a 180° segment of the beltline weld from the shroud OD. In this instance no fuel was removed since the inspection was performed from the OD. The ID and OD measurements were compared at the applicable area with good correlation.

A domestic utility performed ultrasonic measurements of some shroud cracking from the ID and the OD depending on location. Two boat samples were obtained from the H2 weld and the crack depth was physically measured which validated the UT technique.

6.3.3 UT/VT Comparison

This section is a comparison of VT and UT shroud examination. This is based on current available inspection equipment, and shroud inspection experience to date. This comparison should be reviewed and modified if needed as new inspection equipment becomes available.

VT and UT: Advantages & Disadvantages

Visual

Ultrasonic

Advantages

Equipment readily available
Large experience base
Utilized for ID and OD
Images can be digitized and enhanced

Most exams from OD
No surface preparation
No cell disassembly
Detection/sizing performed simultaneously
Minimum impact on other in vessel work
Faster than VT
Consistent and repeatable

Disadvantages

Surfaces may need cleaning
Indications may be missed
Fuel cells must be disassembled (ID)
Welds difficult to locate
Refuel bridge required
No through wall sizing
Frequent camera changeouts
Low repeatability
Subjective evaluation

More personnel required
New technology
Higher equipment costs

6.4 Recommendations

The following is a summary of BWROG recommendations relative to shroud:

- Susceptibility Investigation; Each utility should determine its relative susceptibility to shroud cracking.
- Screening criteria; The utility should perform flaw size evaluations in advance of the inspection to establish acceptance criteria.
- Plant specific objectives; The inspection goals must be established to determine the most effective inspection technique; short term and long term goals and philosophies should be considered.
- Integrate inspection plan into refuel floor activities; the shroud inspection should be incorporated into the refuel floor activities to optimize productivity and minimize outage length.
- Contingency repair package as appropriate; in cases where the shroud has been evaluated as having high susceptibility factors for cracking, the utility should have a contingency repair package in place.

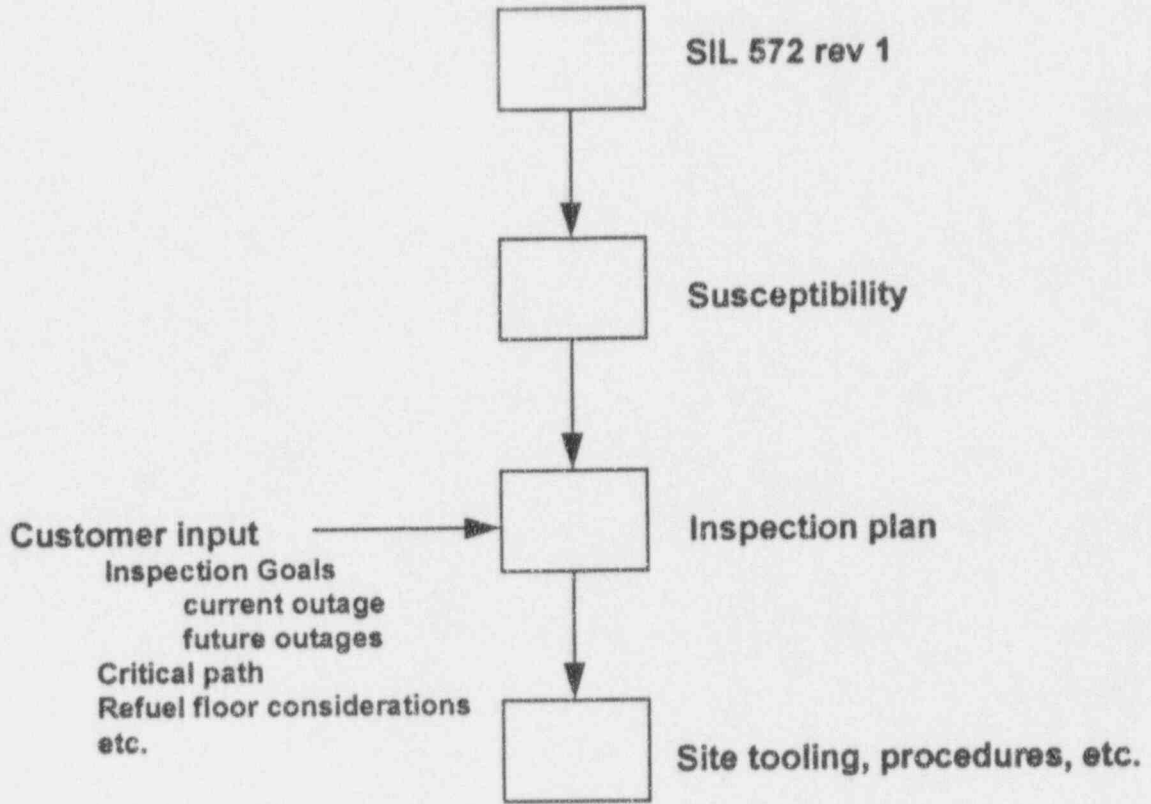


Figure 6-1 Shroud Inspection Plan Approach

7.0 SUMMARY

This report was prepared in response to recent cracking observed in the vicinity of core shroud welds at four boiling water reactors (BWRs). This report contains a discussion of various aspects of the shroud cracking issue and provides the generic tool which utilities may use to address shroud cracking concerns. These issues include: screening criteria, mitigation actions, operational symptoms, and inspection strategy.

The graded screening criteria was developed to provide the procedure for the evaluation of any indications. The screening criteria includes three steps, 1) acceptance standard, 2) visual screening criteria, and 3) UT screening criteria. If the indications meet the screening criteria, then the indications are considered to be acceptable for at least one fuel cycle without further evaluation. If the indications do not pass a particular level of the graded approach, the next level may be applied. For example, if the indications do not meet the acceptance standard, then the visual screening criteria may be applied. If the indications do not meet the UT screening criteria, then repair of the shroud may be required.

Information regarding mitigation of core shroud cracking was presented. This includes discussion of hydrogen water chemistry, water conductivity control, and noble metal plasma spray coating. The recent incidences of cracking have demonstrated the advantage of taking early precautions to lessen the potential and extent of IGSCC. Water chemistry, fabrication techniques, and material have been identified as being significant contributors to the potential for cracking.

Operational symptoms were discussed to address the potential situation if unexpected significant crack growth occurs during plant operation. The potentially affected plant operational parameters are identified, as well as the modes of reactor operation that are most likely to show these symptoms if the shroud has degraded to the point that significant, through-wall leakage can occur.

An integrated plan and strategy for shroud inspections was also presented. This program was designed to meet all the recommendations of SIL 572 Rev. 1 while responding to utility specific needs. The purpose of the inspection plan is to provide the link between SIL 572, Rev. 1 and the plant specific shroud inspection.

APPENDIX A - BASIS FOR THE CRACK GROWTH RATE

The basis for the crack growth rate used in the screening criteria is provided in this section. The shroud cylinder was fabricated from roll formed Type 304 or Type 304L stainless steel plate. Therefore, the weld heat-affected-zone (HAZ) is likely sensitized. The shroud is also subjected to neutron fluence during the reactor operation which further increases the effective degree of sensitization. The other side effect of neutron fluence induced irradiation is the relaxation of weld residual stresses. The slip-dissolution model developed by GE quantitatively considers the degree of sensitization, the stress state and the water environment parameters, in predicting a stress corrosion cracking (SCC) growth rate. The crack growth rate predictions of this model have shown good correlation with laboratory and field measured values.

A.1 Slip-Dissolution Model

Figure A-1 schematically shows the GE slip-dissolution film-rupture model (Reference A-1) for crack propagation. The crack propagation rate V_t is defined as a function of two constants (A and n) and the crack tip strain rate, ϵ'_{ct} .

$$V_t = A \epsilon'_{ct}{}^n \quad (\text{A-1})$$

$$\begin{aligned} \text{where } \epsilon'_{ct} &= CK^4 \quad (\text{for constant load}) \\ A &= 7.8 \times 10^{-3} n^{3.5} \quad (\text{from Reference A-2}) \\ n &\text{ is defined in Reference A-2} \\ K &= \text{stress intensity factor (units of MPa}\sqrt{\text{m)}} \end{aligned}$$

The constants are dependent on material and environmental conditions. The crack tip strain rate is formulated in terms of stress, loading frequency, etc. When a radiation field, such as the case for the shroud, is present, there is additional interaction between the gamma field and the fundamental parameters which affect intergranular stress corrosion cracking (IGSCC) of Type 304 stainless steel (see Figures A-2 and A-3).

The increase in sensitization (i.e., Electrochemical Potentiokinematic Reactivation, EPR) and the changes in the value of constant A as a function of neutron fluence (>1MeV) is given as the following:

$$\text{EPR} = \text{EPR}_0 + 3.36 \times 10^{-24} (\text{fluence})^{1.17} \quad (\text{A-2})$$

where, EPR is in units of C/cm², fluence is in units of n/cm² and the calculated value of EPR has an upper limit of 30.

The constant C is defined as the following:

$$\text{for fluence} \leq 1.4 \times 10^{19} \text{ n/cm}^2: C = 4.1 \times 10^{-14} \quad (\text{A-3a})$$

$$\begin{aligned} \text{for fluence} > 1.4 \times 10^{19} \text{ n/cm}^2 \text{ but } \leq 3 \times 10^{21} \text{ n/cm}^2, \\ C = 1.14 \times 10^{-13} \ln(\text{fluence}) - 4.98 \times 10^{-12} \end{aligned} \quad (\text{A-3b})$$

$$\text{for fluence} \leq 3.0 \times 10^{21} \text{ n/cm}^2 \quad C = 6.59 \times 10^{-13} \quad (\text{A-3c})$$

A.2 Calculation of Parameters

The parameters needed for the crack growth calculation by the GE model are: stress state and stress intensity factor, effective EPR, water conductivity, and electro-chemical corrosion potential (ECP).

The stress state relevant to IGSCC growth rate is the steady state stress which consists of weld residual stress and the steady applied stress. Figure A-4 shows observed through-wall weld residual stress distribution for large diameter pipes. This distribution is expected to be representative for the shroud welds also. The maximum stress at the surface was nominally assumed as 35 ksi. The steady applied stress on the shroud is due to core differential pressure and its magnitude is small compared to the weld residual stress magnitude. Figure A-5 shows the assumed total stress profile used in the evaluation. Figure A-6 shows the calculated values of stress intensity factor (K) assuming a 360° circumferential crack. It is seen that the calculated value of K reaches a maximum of approximately 25 ksi√in. The average value of K was estimated as 20 ksi√in and was used in the crack growth rate calculations.

The weld residual stress magnitude is expected to decrease as a result of relaxation produced by irradiation-induced creep. Figure A-7 shows the stress relaxation behavior of Type 304 stainless steel due to irradiation at 550° F. Since most of the steady stress in the shroud comes from the weld residual stress, it was assumed that the K values shown in Figure A-6 decrease in the same proportion as indicated by the stress relaxation behavior of Figure A-7.

The second parameter needed in the evaluation is the EPR. In the model, the initial EPR value is assumed as 15 for the weld sensitized condition. Using Equation (A-2), the predicted increase in EPR value as a function of fluence is shown in Figure A-8.

The third parameter used in the GE predictive model is the water conductivity. A water conductivity of $0.1 \mu\text{S}/\text{cm}$ was used in this calculation which is a reasonable value for many plants. To demonstrate that the GE model conservatively reflects the effect of conductivity, Figure A-9 shows a comparison of the GE model predictions with the measured crack growth rates in the crack advance verification system (CAVS) units installed at several BWRs. The comparison with CAVS data in Figure A-9 also demonstrates the conservative nature of crack growth predictions by the GE model.

The last parameter needed in the GE prediction model is the ECP. Figure A-10 shows the measured values of ECP at two locations in the core. The ECP values at zero H_2 injection in Figure A-10 was used in this calculation. It is seen that the ECP values at zero H_2 injection rate range from 150 mV to 225 mV. Therefore, a value of 200 mV was used in the calculation.

A.3 Crack Growth Prediction

Based on the discussion in the preceding section, the crack growth rate calculations were conducted as a function of fluence assuming the following values of parameters:

Initial K	= $20 \text{ ksi}\sqrt{\text{in}}$
EPR ₀	= $15 \text{ C}/\text{cm}^2$
Cond.	= $0.1 \mu\text{S}/\text{cm}^2$
ECP	= 200 mV

Figure A-11 shows the predicted crack growth rate as a function of fluence. It is seen that the predicted crack growth rate initially increases with the fluence value but decreases later as a result of significant reduction in the K value due to irradiation induced stress relaxation. The crack growth rate peaks at $4.5 \times 10^{-5} \text{ in/hr}$ at a fluence of $1 \times 10^{20} \text{ n}/\text{cm}^2$. Thus, a value of $5 \times 10^{-5} \text{ in/hr}$ can be used in the structural integrity evaluation for the shroud.

This crack growth rate is quite conservative as can be shown in Figure A-12 from NUREG-0313, Rev. 2. It is seen that the crack growth rate of $5 \times 10^{-5} \text{ in/hr}$ at

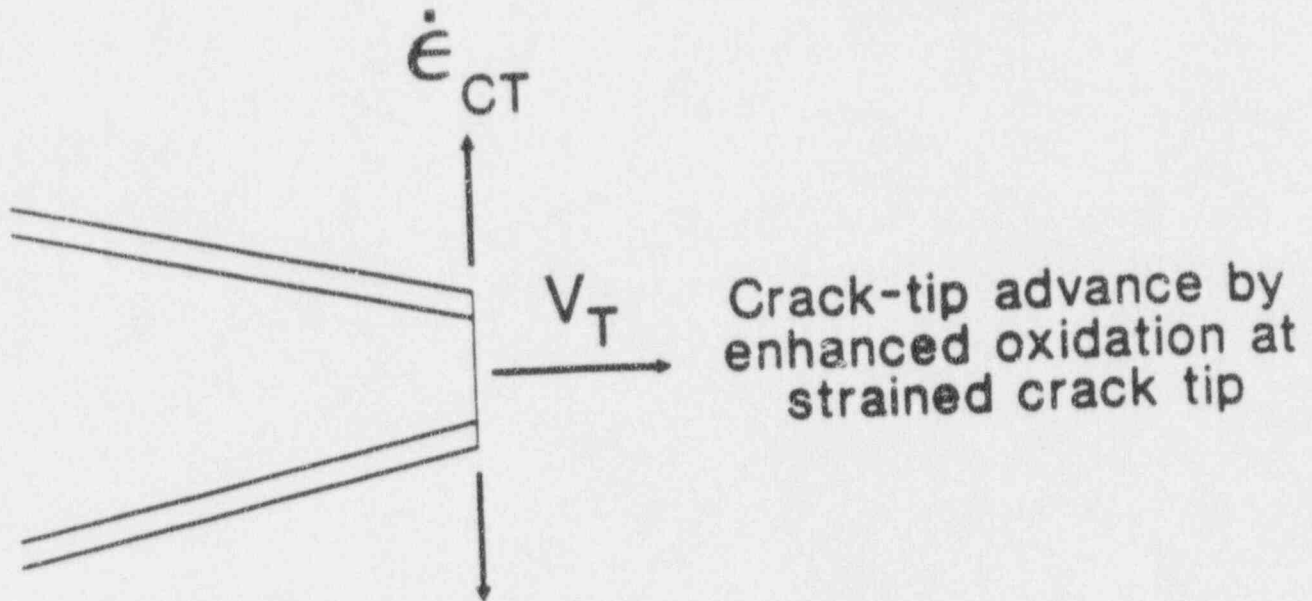
20 ksi $\sqrt{\text{in}}$ is considerably higher than what would be predicted by using the NRC curve. This further demonstrates the conservatism inherent in the assumed bounding value of crack growth rate.

A.4 Conclusion

A crack growth rate calculation using the GE predictive model was conducted considering the steady state stress, EPR, conductivity and ECP values for a typical core shroud. The evaluation accounted for the effects of irradiation induced stress relaxation and the increase in effective EPR. The evaluation showed that a bounding crack growth rate of 5×10^{-5} in/hr may be conservatively used in the structural integrity evaluation of the core shroud.

A.5 Reference

- A-1 F.P. Ford et al, "Prediction and Control of Stress Corrosion Cracking in the Sensitized Stainless Steel/Water System," paper 352 presented at Corrosion 85, Boston, MA, NACE, March 1985
- A-2 F.P. Ford, D.F. Taylor, P.L. Andressen & R.G. Belanger, "Environmentally Controlled Cracking of Stainless Steel and Low Alloy Steels in LWR Environments," EPRI Report NP50064M, Contract RP2006-6, 1987.



$$V_T = A \dot{\epsilon}_{CT}^n$$

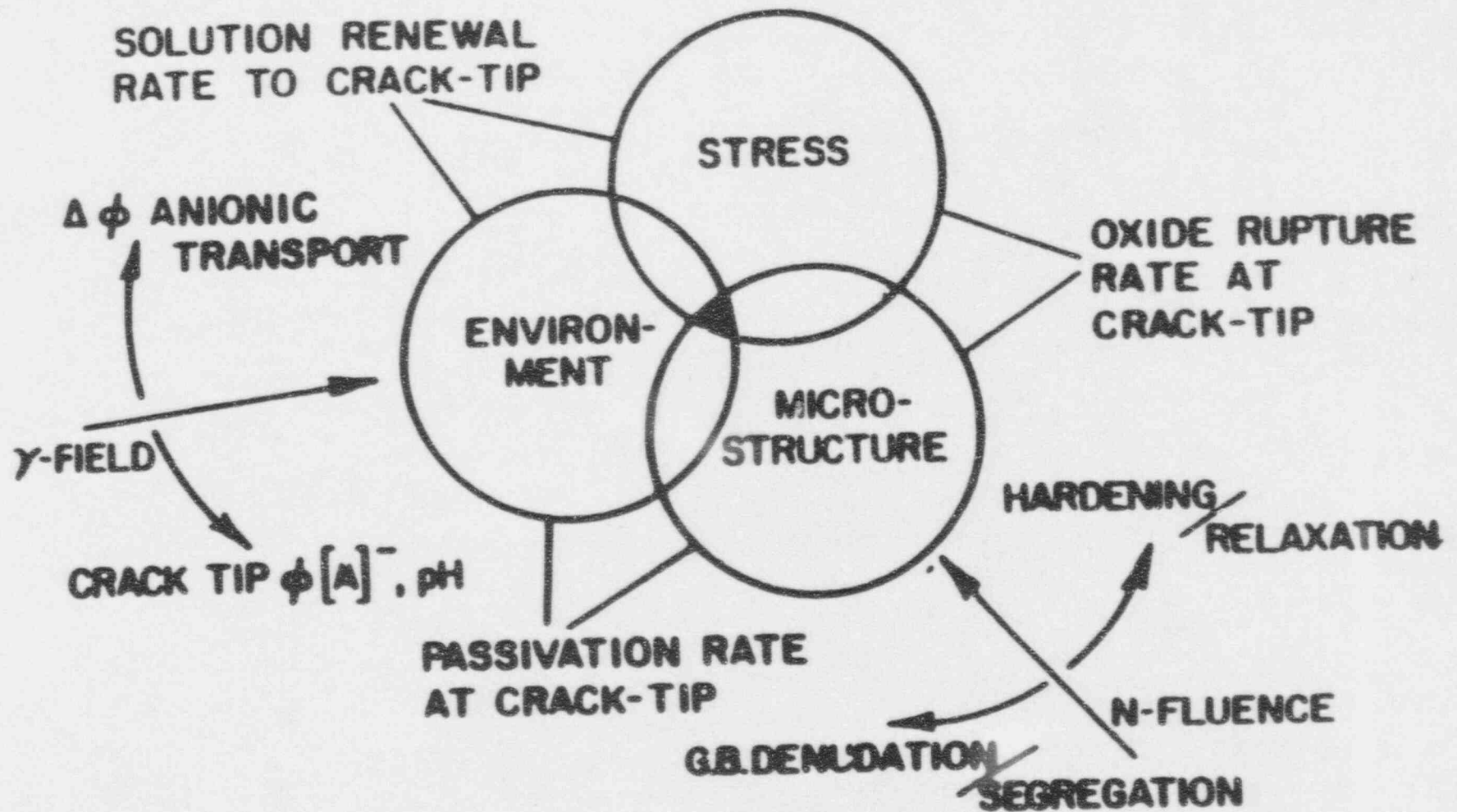
Where:

V_T = crack propagation rate

A, n = constants, dependent on material and environmental conditions

$\dot{\epsilon}_{CT}$ = crack-tip strain rate, formulated in terms of stress, loading frequency, etc.

Figure A-1 GE PLEDGE Slip Dissolution - Film Rupture Model of Crack Propagation



A-6

Figure A-2 Effects of Fast Fluence, flux & Gamma Field on parameters affecting IGSCC of Type 304 Stainless Steel

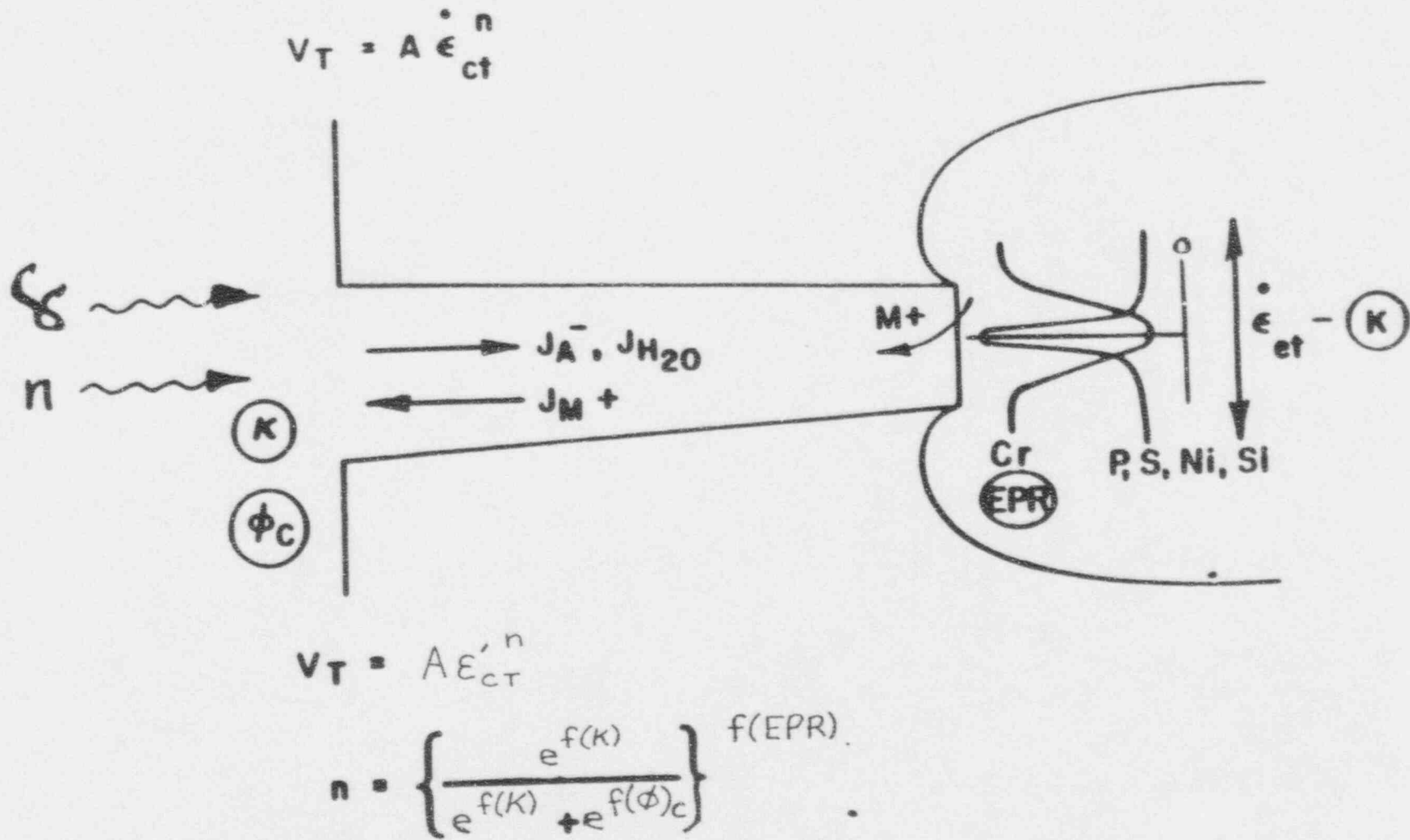


Figure A-3

Parameters of Fundamental Importance to Slip Dissolution Mechanism of IGSCC in Sensitized Austenitic Stainless Steel

**OBSERVED RESIDUAL STRESS PROFILES
IN HAZ OF 24"-28" DIA. SCH. 80 PIPING**

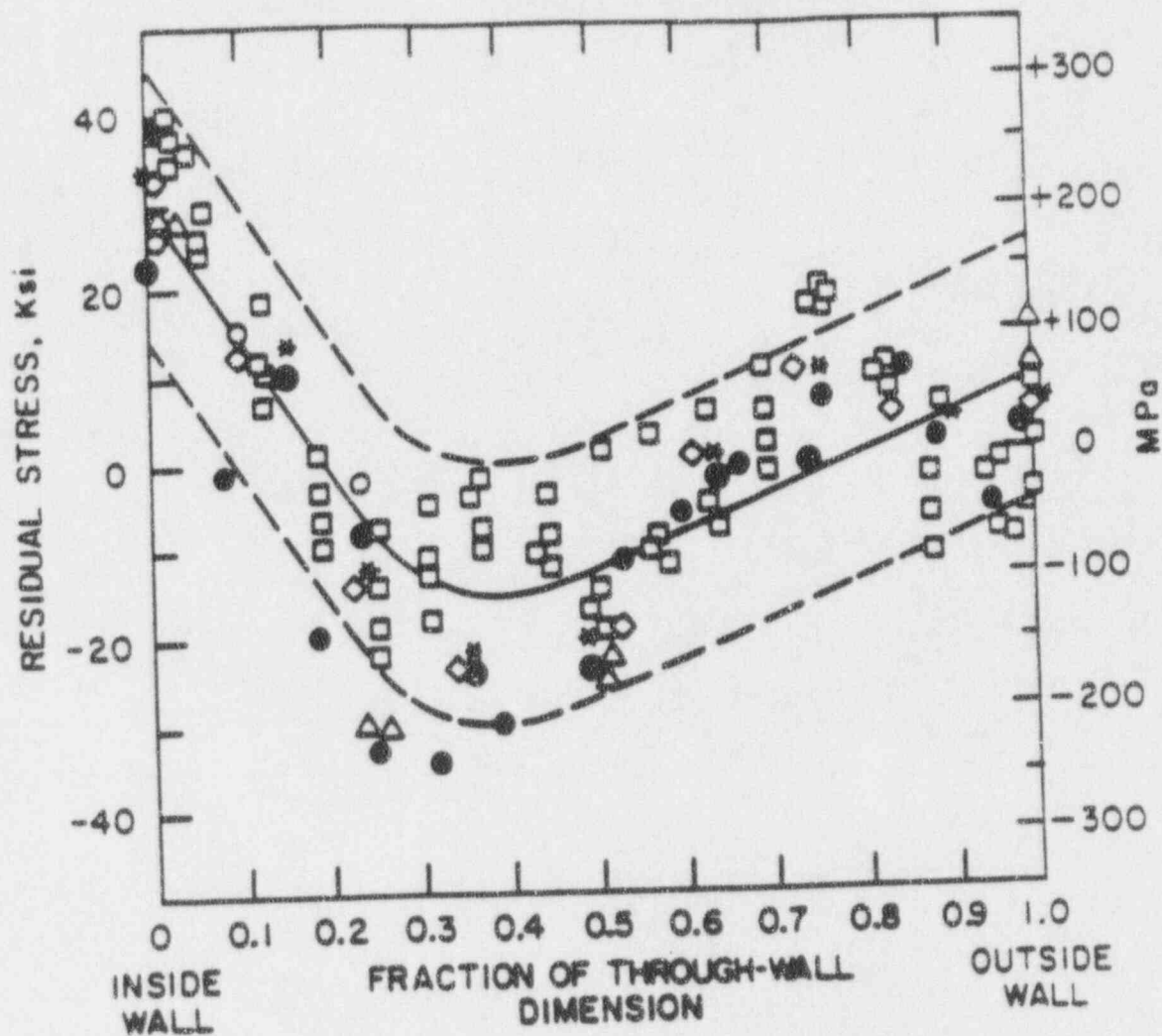


Figure A-4 Throughwall longitudinal residual stress data adjacent to welds in 12 to 28 inch diameter stainless steel piping

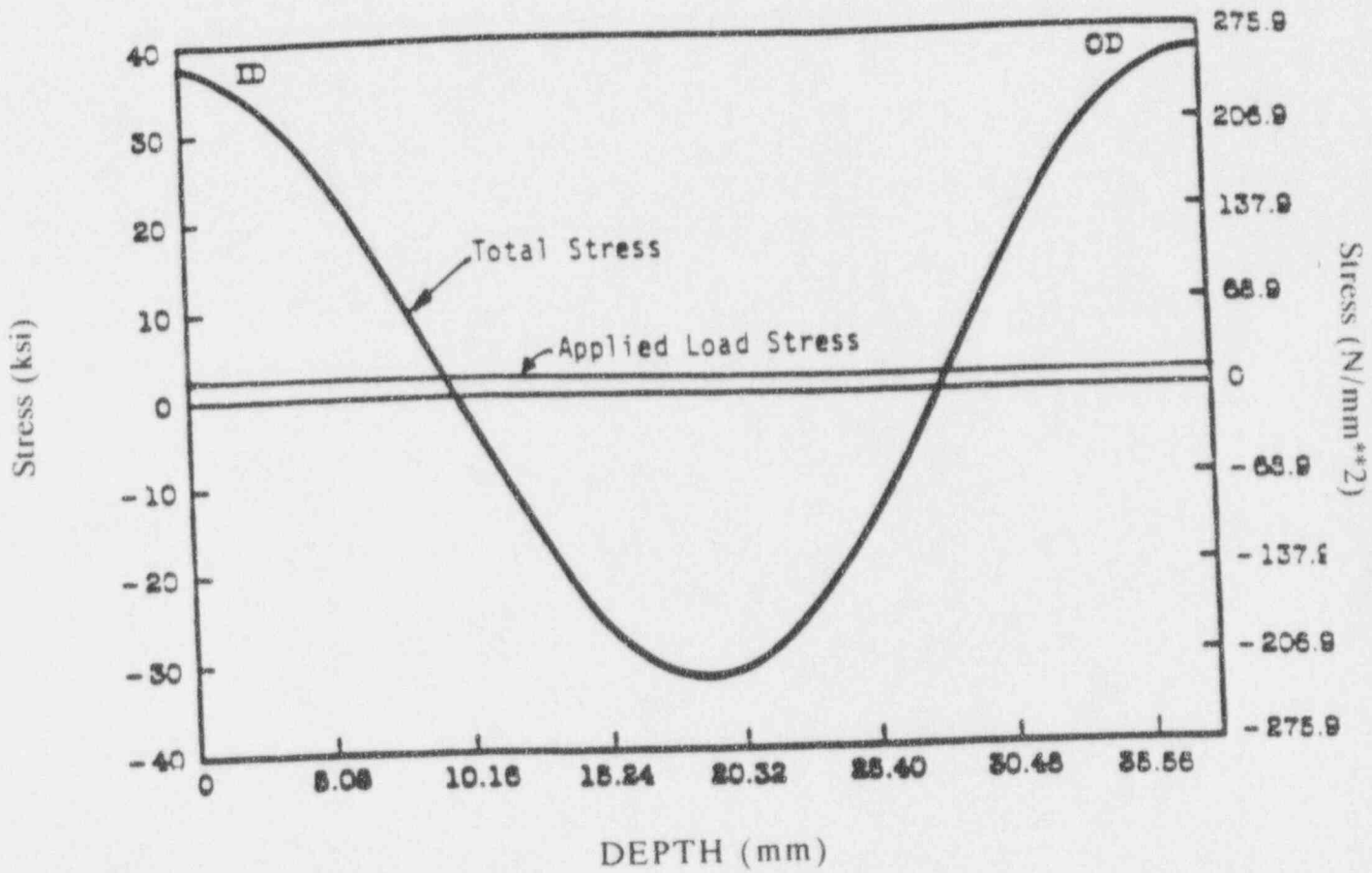


Figure A-5 Shroud Total Throughwall Stress Profile

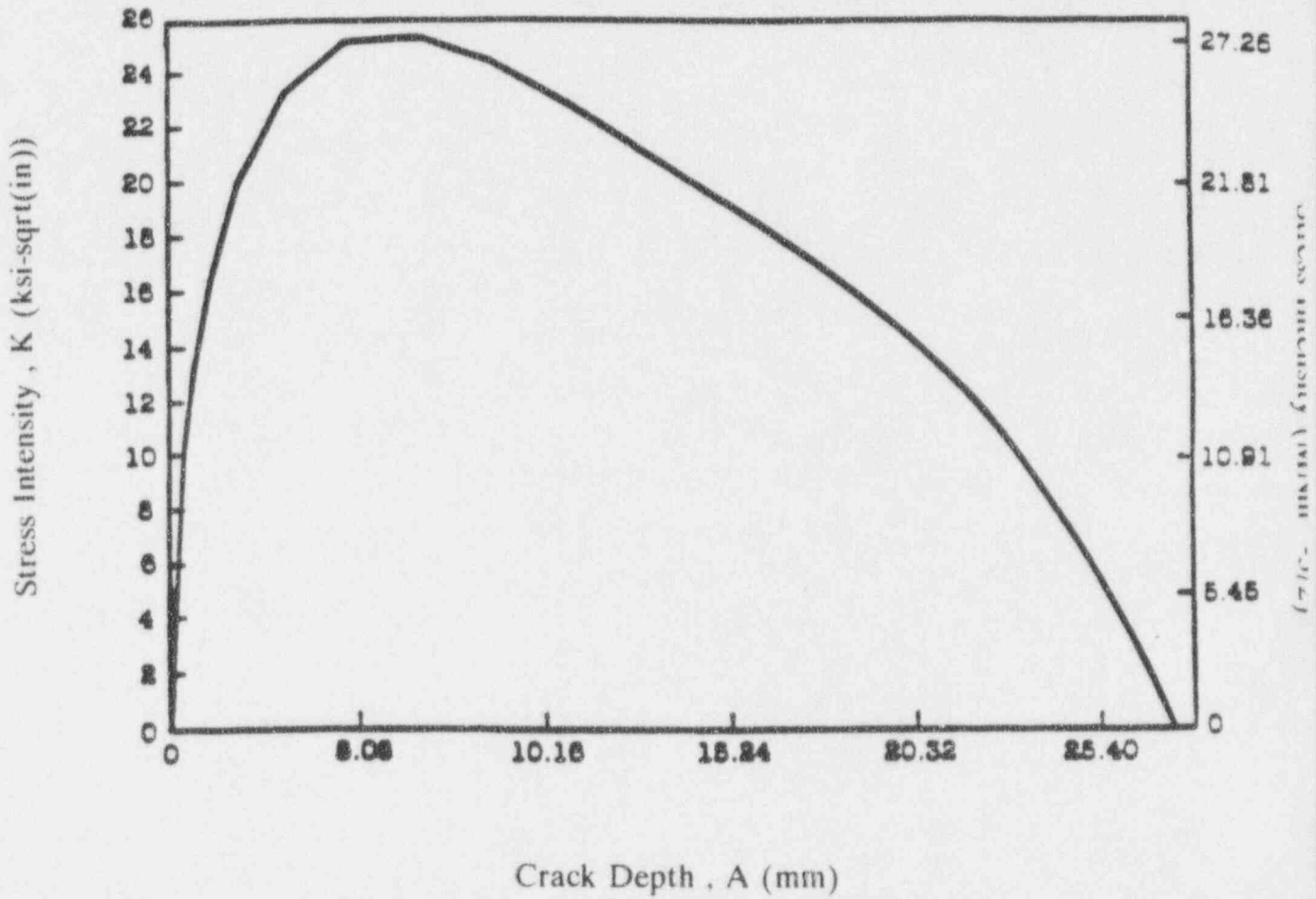


Figure A-6 Shroud Throughwall Stress Intensity Factor

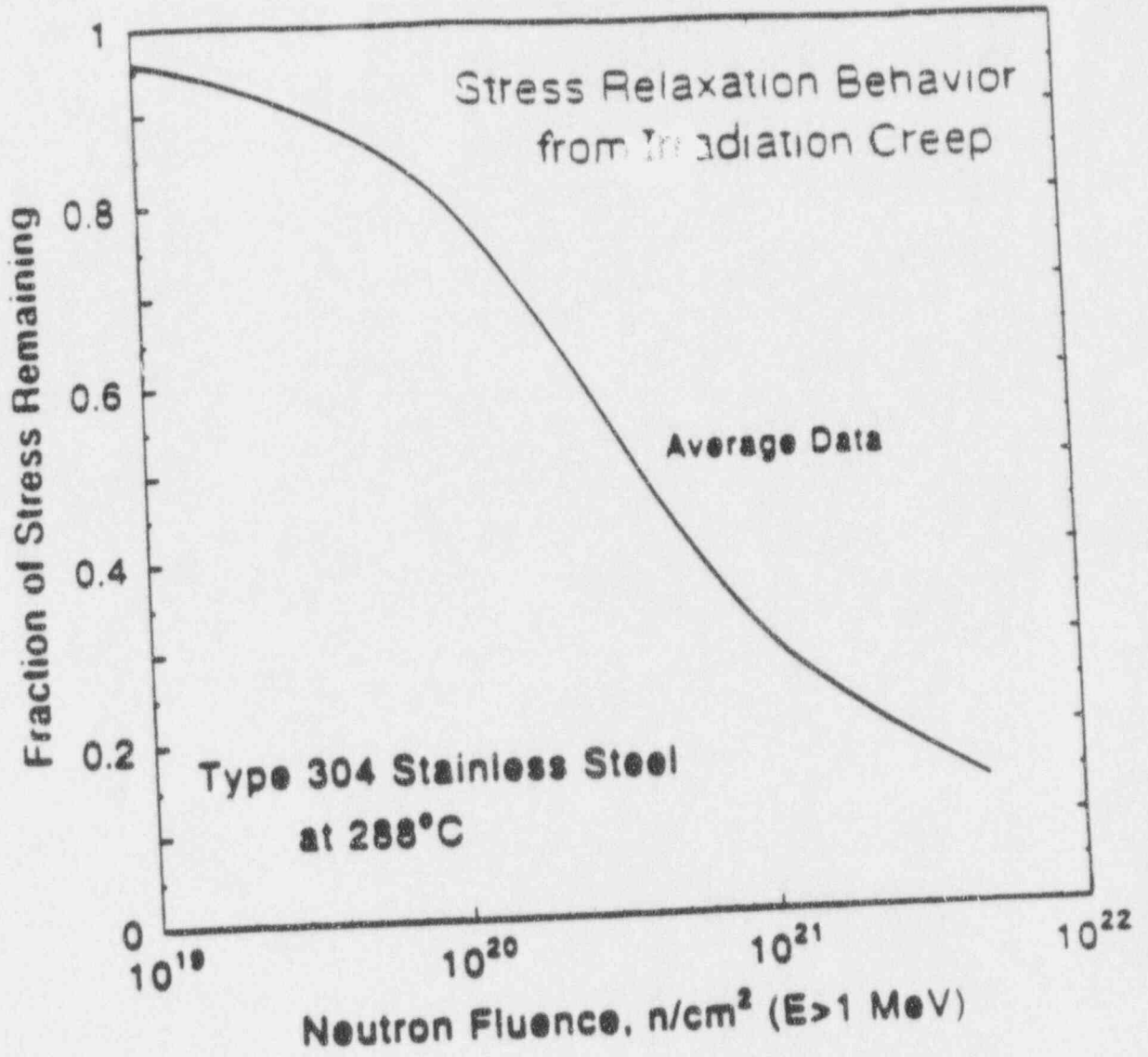
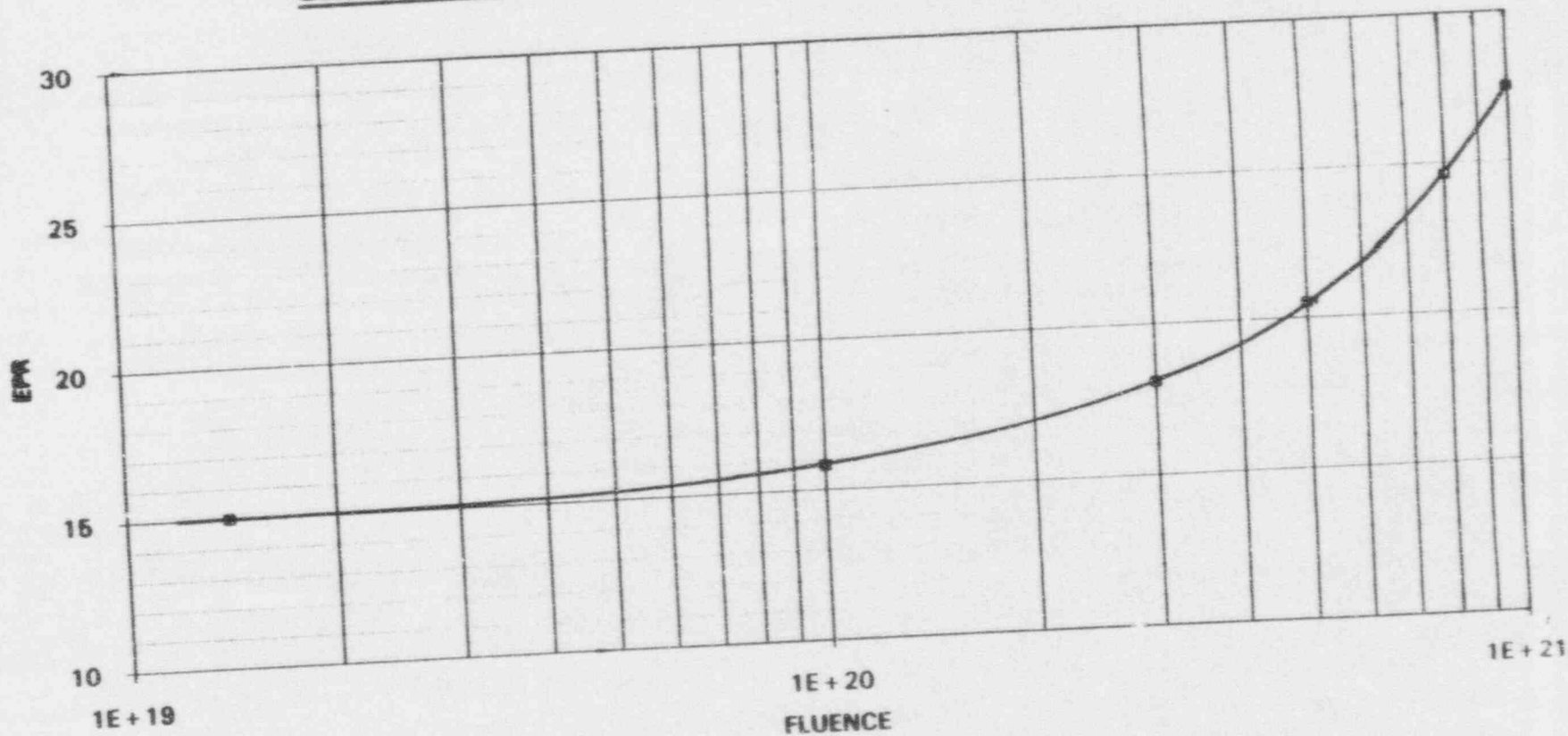


Figure A-7 Stress Relaxation Behavior of Type 304 Stainless Steel Due To Irradiation at 288C

EPR VERSUS NEUTRON FLUENCE

GE Nuclear Energy

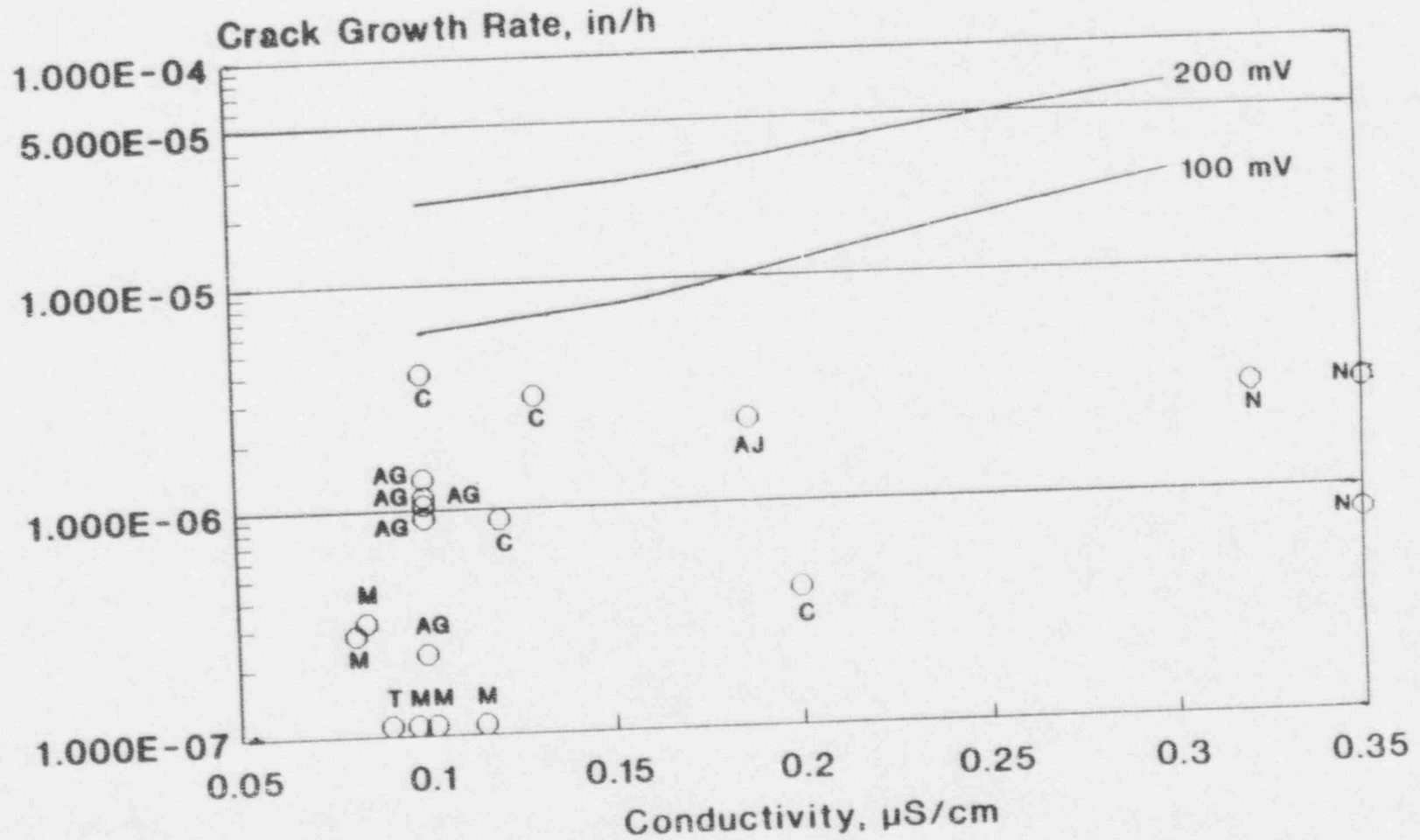


A-12

GENE-523-148-1193

Figure A-8 - EPR Versus Neutron Fluence

Effect of Conductivity on Sensitized 304 Crack Growth Rate



PLEDGE: 20 ksi/in, 15 C/cm²
 CAV: 20-25 ksi/in, 13 C/cm², 100-160 mV

Figure A-9 Effect of Conductivity on Sensitized Type 304 Crack Growth Rate

In-Core Bypass ECP vs Feedwater Hydrogen for a BWR-4

A-14

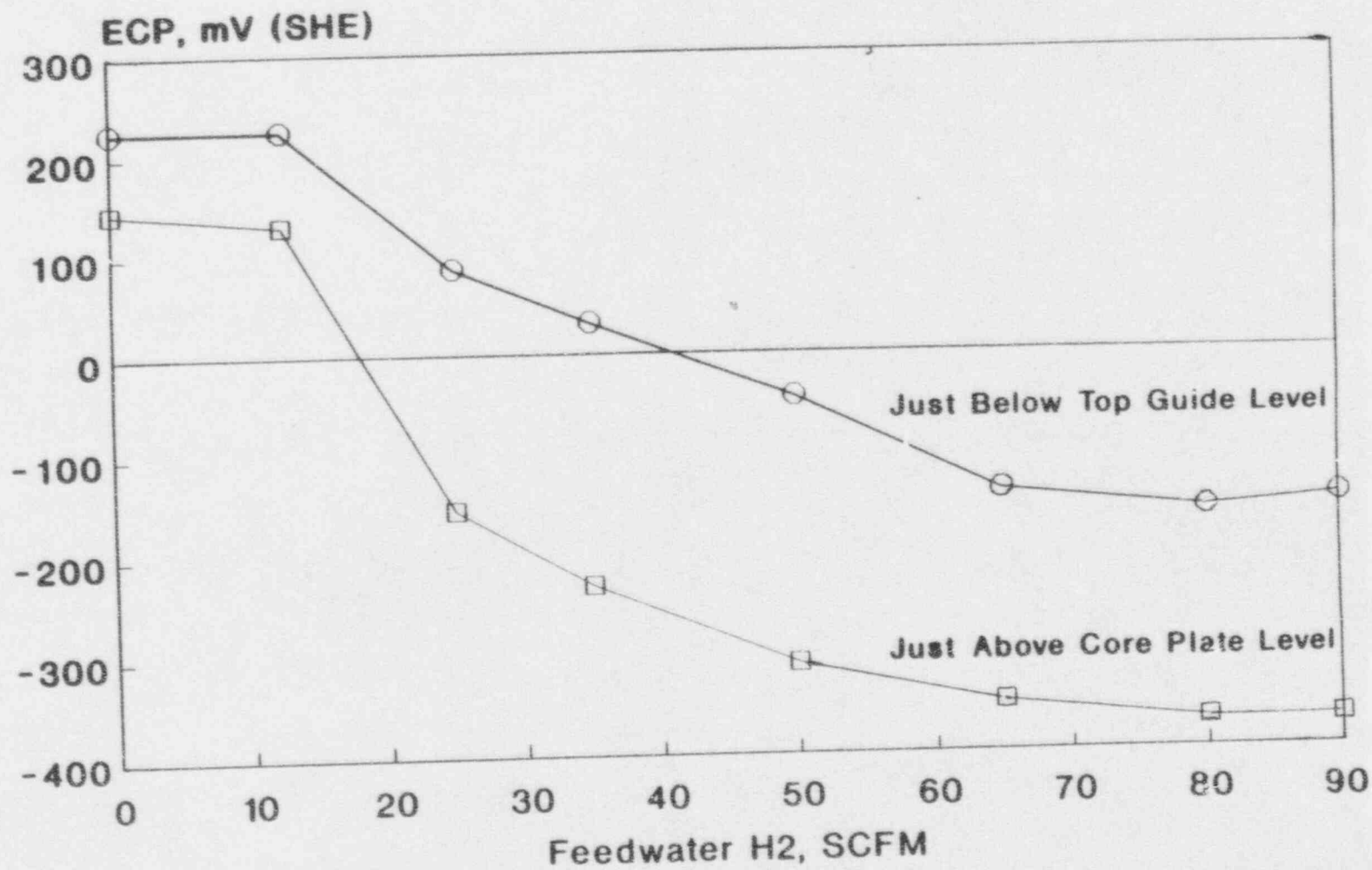
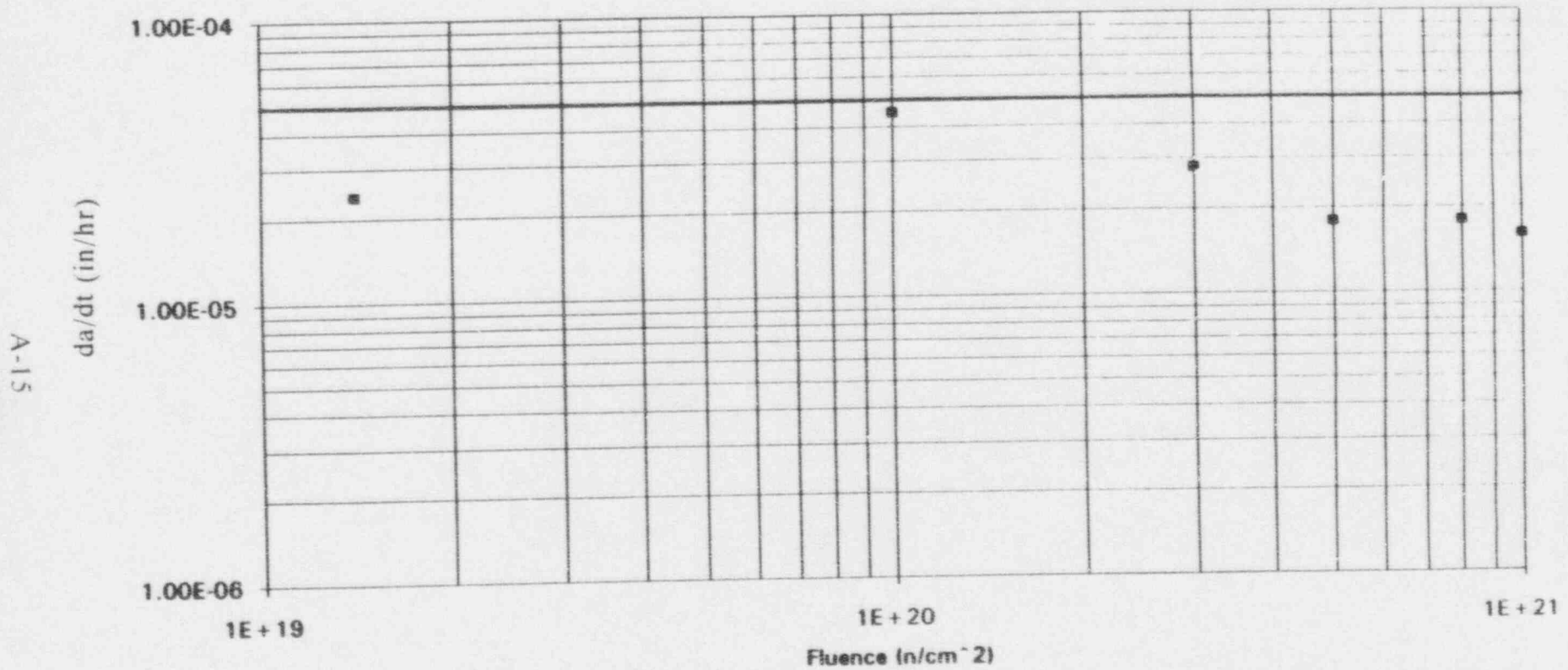


Figure A-10 In-Core Bypass ECP vs Feedwater Hydrogen for a BWR-4

Figure A-11

GROWTH RATE VERSUS FLUENCE



Stress Intensity = 20 Ksi/in, Initial EPR = 15 C/cm²

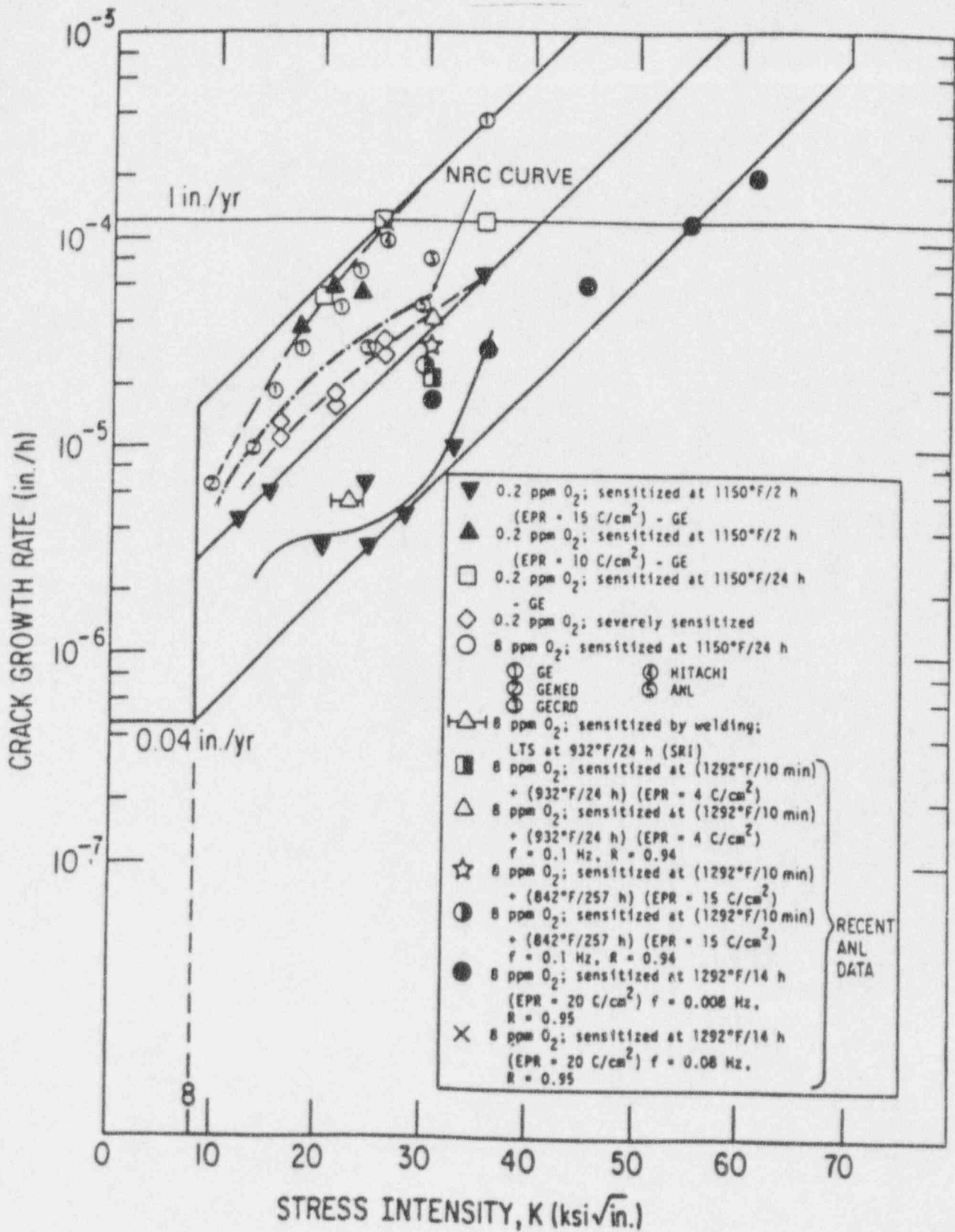


Figure A-12

Nureg 0313 Crack Growth Rate Data

APPENDIX B - LIST OF PARTICIPATING UTILITIES

The list of BWR Owners' Group utilities below have participated in submittal of this report:

Carolina Power & Light
Cleveland Electric Illuminating
Commonwealth Edison
Entergy Operations, Inc.
GPU Nuclear
IES Utilities Inc.
Niagara Mohawk Power
Northeast Utilities
Northern States Power
Pennsylvania Power & Light
PECO Energy
Public Service Electric & Gas
Southern Nuclear Operating Co.
Tennessee Valley Authority
Vermont Yankee
Washington Public Power Supply System